THE DEVELOPMENT OF A LABORATORY SYSTEM TO INVESTIGATE THE INTERACTIONS OF TROPOSPHERIC AEROSOL AND HO_x RADICALS

by

KATHLEEN HELEN FALOON

A thesis submitted to
The University of Birmingham
for the degree of
DOCTOR OF PHILOSOPHY

School of Geography, Earth and Environmental Sciences
College of Life and Environmental Sciences
The University of Birmingham
August 2011

Abstract

This thesis describes the development and application of a laboratory system to investigate the loss of peroxy radicals to aerosol. The laboratory system consisted of an aerosol flow tube coupled to a custom-built PEroxy Radical Chemical Amplifier (PERCA). Aerosol was generated using an atomiser and their distribution measured using a SMPS.

New values of the HO_2 uptake coefficient, γ, were obtained for dry sodium chloride aerosol (0.021 ± 0.006) and dry ammonium sulphate aerosol (0.047 ± 0.015). The mass accommodation coefficient, α, was also determined for NaCl (0.009 ± 0.02). A box model was used to determine the implications of the new uptake coefficient of HO_2 loss to NaCl aerosol for tropospheric chemistry in the marine boundary layer.

For my Mother

ACKNOWLEDGEMENTS

I always thought that I would produce some witty and heartfelt acknowledgments, but now the time has come no clever phrases come to mind, so this will have to do instead.

First I would like to thank my supervisor, Bill Bloss, who has been a model boss - helpful when I needed help, confidence boosting when I felt I knew nothing, strict when I needed deadlines and understanding when I broke another piece of glassware. It wasn't all work though - Bill has jovially put up with the madness that surrounds our office, he's provided drinks in the pub, been likened to Highlander and been taken in by my 'humorous' practical jokes. Thanks Bill!

Next I'd like to thank everyone down in the Wolfson Lab. Thanks to everyone who helped me with various practical issues with my experiment: Gillian, Richard, Mel, Shana, Juan, Johanna and Suad. Thanks especially to the random people I persuaded to help me move my glass tube when they had no idea who I was! Special thanks to Ray and Alan in Stores who went out rain or shine every week to get me a new cylinder - I'm sorry for always running out of gas when there was a downpour. Thanks to the guys in the workshop, and to Steve the glass blower, who all built and fixed many things for use in my experiments.

Thanks also need to go to the School of Geography, Earth and Environment who provided a School Scholarship which allowed me to undertake this project.

Then there are all those other people who helped me along the way throughout my PhD. The ever-changing crew at Park Hill Road: Gemma, Helen, Alison, Jill, Nick, Claire, Chloe, Emma, Alex and Liz. Thanks go to Mr Duffill for putting a roof over our heads! Next thanks to everyone in the Wolfson Lab who entertained me when I was bored and fed me tea when I needed it: Matt, Chris, Jill and Richard come to mind mostly, but there were many more too! Thanks to those in my office who made my time there so memorable: Adam, Sue, Jessie, Salim and Paula - lunchtimes, tea breaks and cakes were the backdrop of our lives in the office, but were punctuated by practical jokes, Samantha the ghost and Salim's many excuses. Thanks to you all for making me laugh so much!

Thanks also go to Bailey. Thanks for understanding my need for constant pots of Ben & Jerry's and my nightly buckets of whisky. Thanks for being my sounding board and for listening to the constant stream of chemistry that emerged from me while practising for my viva and finally - thanks just for being here.

Finally there are five people who need extra special thanks: Helen & Michael, Naomi, Rob and Paula - they have been the most supportive friends anyone could ever ask for.

CONTENTS

LIST OF FIGURES

LIST OF TABLES

LIST OF ABBREVIATIONS

A/D Analogue / Digital

AFT Aerosol Flow Tube

AIM Aerosol Instrument Manager

CIMS Chemical Ionization Mass Spectrometer

CL Chain Length

CPC Condensation Particle Counter

DMA Differential Mobility Analyser

EC Electrostatic Classifier

EPR Electron Paramagnetic Resonance

ESR Electron Spin Resonance

FAGE Fluoresence Assay Gas Expansion

IUPAC International Union of Pure and Applied Chemists

JPL Jet Propulsion Laboratory

LIF LASER Induced Fluoresence

MCM Master Chemical Mechanism

MFC Mass Flow Controller

NAMBLEX North Atlantic Marine Boundary Layer EXperiment

PBL Planetary Boundary Layer

PERCA PEroxy Radical Chemical Amplifier

PMT Photo-Multiplier Tube

ppb parts per billion (by volume)

ppm parts per million (by volume)

ppt parts per trillion (by volume)

ROXMAS RO_x Mass Spectrometer

sccm standard cubic centimeters per minute

slm standard litres per minute

SMPS Scanning Mobility Particle Sizer

VOC Volatile Organic Compound

CHAPTER 1

INTRODUCTION

1.1 Introduction

This thesis describes the development of a new experimental system which has been used to determine the uptake coefficient of hydroperoxy radicals (HO_2) to aerosol particles. Heterogeneous loss of HO_2 to aerosol has been shown to account for a decrease in the concentration of HO_x (OH and HO_2) radicals within the troposphere (Jacob, 2000; Martin et al., 2003). This study aimed to determine the uptake coefficients for HO_2 to sodium chloride (NaCl) and ammonium sulphate ($(NH_4)_2SO_4$) aerosol at ambient tropospheric conditions.

Oxidants in the troposphere react with pollutants, breaking them into simpler chemical species (degradation) which eventually leads to their removal from the troposphere. The hydroxyl radical OH (along with ozone, O_3) is an important daytime tropospheric oxidant, while the nitrate radical, NO_3, is an important night- time oxidant (Wayne, 2002). Understanding the processes which affect the concentration of OH in the troposphere leads to a better understanding of the rate of removal of pollutants, which is important for understanding and predicting the composition and air quality in the lower troposphere. Changes in the concentration of HO_x could also affect the concentration of O_3 in the troposphere, leading to changes in radiative forcing due to tropospheric ozone (Forster et al., 2007).

This chapter gives some background to this study. The atmosphere of the Earth is briefly described, with particular mention given to the troposphere. The tropospheric chemistry of HO_x radicals is summarised and the importance of understanding the concentration of OH in the troposphere with relation to its oxidising capacity is explained in detail. A brief description of aerosol within the troposphere is also given.

Heterogeneous chemistry, in particular between aerosol particles and gas molecules, is explained with important terms, such as the uptake coefficient, being rigorously defined. Following this a discussion on the current state of knowledge of uptake coefficients of gases to aerosol particles is presented. Finally a review of current uptake coefficients for heterogeneous loss of HO_2, along with a review of the experimental procedures used to determine them, is given.

1.2 The Troposphere

The atmosphere is a thin layer of gases which surround the Earth; it is crucial in making the planet habitable by keeping the surface temperature suitable for life. The overall composition of the dry atmosphere consists of nitrogen (78 %), oxygen (21 %) and argon (0.9 %). The final 0.1 % consists of trace gases, such as carbon dioxide and methane. Water vapour is also an important trace gas, however its percentage in the troposphere varies widely, at times reaching as high as 0.1 %. Trace gases are very important as they are responsible for the chemistry occurring in the atmosphere, which determines its various properties (e.g. its ability to absorb radiation or remove pollutants).

The atmosphere is separated into various altitude layers with respect to its temperature profile (see Figure 1.1). The troposphere is the lowest part of the atmosphere and extends to the tropopause between 10 –15 km (dependent on latitude and time of year). Here temperature decreases with height and the air is well mixed due to heating from the surface, which leads to turbulence. Above the tropopause lies the stratosphere which is capped around 50 km by the stratopause. The stratosphere is heated by the formation of

O_3 and the absorption of ultraviolet light by O_3; a peak in the heating from stratospheric O_3 chemistry causes the temperature gradient in the stratosphere and forms a stable layer of air. The troposphere and stratosphere together account for 99.9 % of the atmospheric mass and are the most important areas for atmospheric chemistry studies. Above the stratosphere is the mesosphere, thermosphere and ionosphere.

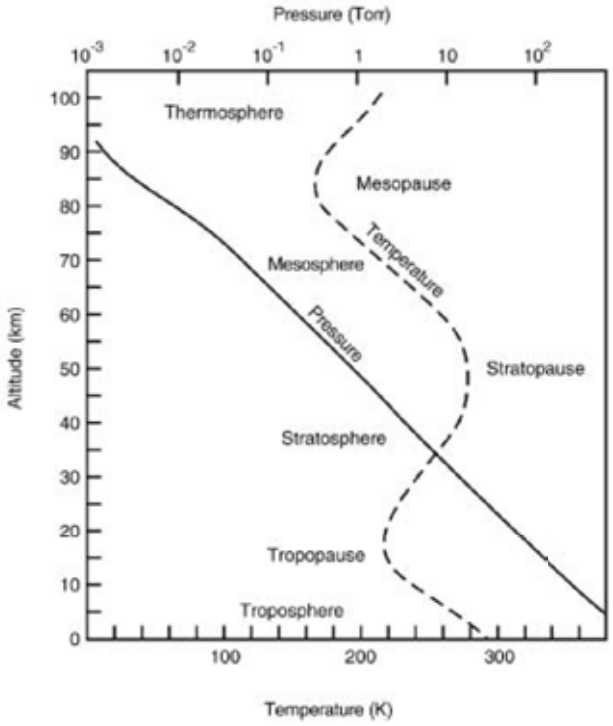

Figure 1.1: The pressure and temperature profiles of the atmosphere. (Finlayson-Pitts and Pitts, 2000)

This study focuses on the troposphere and in particular the lowest part of the troposphere - the Planetary Boundary Layer (PBL). The PBL is defined as the lowest part of the troposphere and is characterised by its highly turbulent nature, which is caused by frictional drag at the surface of the planet. The PBL extends from the Earth's surface up to approximately 1 km whilst the rest of the troposphere is referred to as the free troposphere (Seinfeld and Pandis, 1998). Pollutants (both natural and anthropogenic) are emitted into the boundary layer from the Earth's surface and can be removed by physical (e.g. deposition) or chemical (e.g. oxidation) processes in the atmosphere. Oxidation by the OH radical is an important process for the removal of pollutants from the troposphere

and is discussed in detail in the next section. This chemical degradation of pollutants can lead to the production of ozone in the troposphere. Tropospheric ozone is a greenhouse gas because it traps infrared radiation emitted from the Earth. Greenhouse gases can effect the radiative balance of the atmosphere. The radiative balance of the atmosphere is the balance between the incoming and outgoing infrared radiation and determines the temperature at the Earth's surface. Factors which can change this balance have a radiative forcing. Tropospheric ozone has a positive radiative forcing which will alter the balance to increase the temperature of the Earth's surface (Forster et al., 2007).

1.2.1 Tropospheric Chemistry of HO_x Radicals

HO_x is defined as the sum of OH and HO_2 radicals. Figure 1.2 shows a summary of the tropospheric chemistry of HO_x radicals, which are discussed in more detail in this chapter.

The Production of OH and HO_2 in the Troposphere

The main route of tropospheric production of OH radicals is through the tropospheric photolysis of O_3. At wavelengths shorter than approximately 310 nm O_3 photolyses to produce $O(^1D)$ atoms, which react with water vapour to produce two OH radicals (Reactions R 1.1 and R 1.2) (Jacob, 1999; Wayne, 2002; Seinfeld and Pandis, 1998).

$$O_3 + h\nu \; - \quad O(^1D) + O_2 \tag{R 1.1}$$

$$O(^1D) + H_2O - \quad OH + OH \tag{R 1.2}$$

Reaction R 1.2 is the minor route for $O(^1D)$: the majority of $O(^1D)$ atoms are quenched to their ground state and react with oxygen to reform O_3 (Reactions R 1.3 and R 1.4, where M is N_2 or O_2). However, due to the high water vapour concentration within the troposphere Reaction R 1.2 is sufficiently important to provide the major source of OH in the free troposphere.

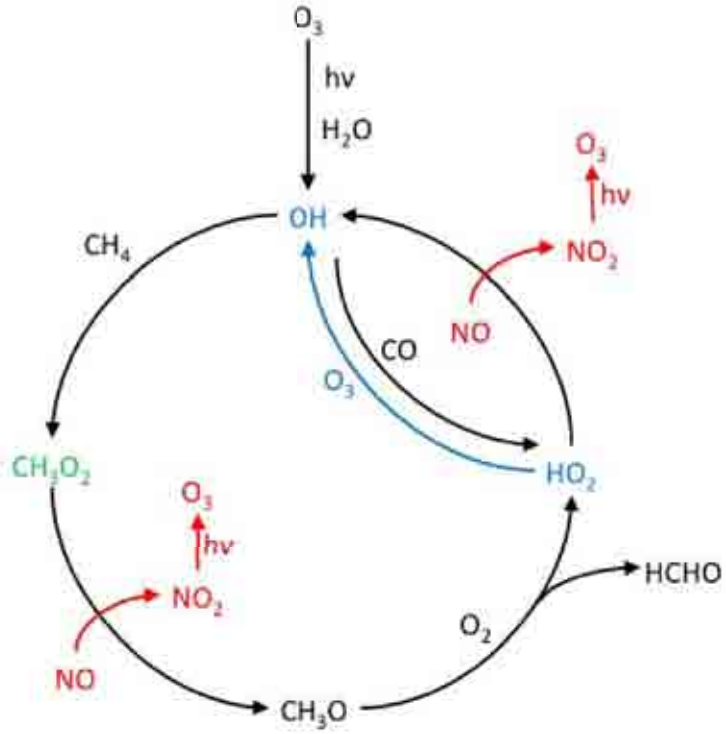

Figure 1.2: The main reaction processes involved in HO_x chemistry in the troposphere. The reactions coloured in blue show the dominant reactions in a clean (low NO_x) tropospheric environment, with an overall loss of O_3. The reactions coloured in red are the dominant reactions in a polluted (high NO_x) tropospheric environment. The production of NO_2 leads to an overall production of O_3 by photolysis. The reactions coloured in green are not well understood and are the focus of this thesis.

$$O(^1D) + M - \quad O + M \tag{R 1.3}$$

$$O + O_2 + M - \quad O_3 + M \tag{R 1.4}$$

Another route of formation of OH within the troposphere is the dissociation of formaldehyde (HCHO) by sunlight to form HO_2 (Reactions R 1.5 and R 1.6), which is rapidly converted to OH by O_3 (Reaction R 1.7).

$$HCHO + h\nu \; - \quad HCO + H \tag{R 1.5}$$

$$HCO + O_2 - \quad CO + HO_2 \tag{R 1.6}$$

$$HO_2 + O_3 - \quad OH + 2\,O_2 \tag{R 1.7}$$

It can be seen from Reactions R 1.1 – R 1.7 that the production of OH in the troposphere depends on O_3 being present. Ozone has a long lifetime (a few years) in the lower stratosphere and so is transported down to the troposphere. Ozone is also produced within the troposphere - this is discussed in detail later in this chapter.

Oxidation by OH Radicals in the Troposphere

The OH radical can react with trace species in the troposphere in a number of ways. In the clean troposphere about 70 % of OH radicals are converted to HO_2 radicals by reaction with carbon monoxide (Reactions R 1.8 and R 1.9). Competing reactions with NO_x (in a polluted environment) are discussed in the next section.

$$OH + CO - \quad CO_2 + H \tag{R 1.8}$$

$$H + O_2 + M - \quad HO_2 + M \tag{R 1.9}$$

The remaining 30 % of OH radicals are converted to HO_2 via more complex reactions with methane (CH_4) or other hydrocarbons (Reactions R 1.10 – R 1.16).

$$OH + CH_4 - \quad H_2O + CH_3 \tag{R 1.10}$$

$$CH_3 + O_2 + M - \quad CH_3O_2 + M \tag{R 1.11}$$

The main sink of the CH_3O_2 radical (in an unpolluted environment) is through reaction with HO_2 (Reaction R 1.12).

$$CH_3O_2 + HO_2 - \quad CH_3OOH + O_2 \tag{R 1.12}$$

The resulting CH_3OOH radical can dissolve in rainwater and be washed out or it can react further either by photolysis (Reaction R 1.13) or by reaction with OH (Reaction R 1.14 or R 1.15).

$$CH_3OOH + h\nu \; - \quad CH_3O + OH \tag{R 1.13}$$

$$CH_3OOH + OH - \quad CH_3O + OH + H_2O \tag{R 1.14}$$

$$CH_3OOH + OH - \quad CH_3O_2 + H_2O \tag{R 1.15}$$

The resulting CH_3O radical reacts rapidly with O_2 to produce formaldehyde (HCHO) and reform HO_2 (Reaction R 1.16).

$$CH_3O + O_2 - \quad HCHO + HO_2 \tag{R 1.16}$$

The net result of these reactions, in the unpolluted environment, is the destruction of methane by OH and HO_2. This is shown as the main circle of the reactions shown in Figure 1.2. Volatile Organic Compounds (VOCs), which are pollutants emitted into the troposphere, are oxidised by similar catalytic chemical processes as shown for methane. The next section shows how this reaction cycle is perturbed by nitrogen oxides and other pollutants, such as VOCs, emitted into the troposphere. The concentration of OH in the atmosphere is used as a measure of how oxidising the atmosphere is, and thus, how

quickly pollutants are removed from it.

Tropospheric Chemistry of NO_x

Nitrogen oxides (NO_x, the sum of NO and NO_2) are emitted into the troposphere from both anthropogenic and natural sources. By day NO_2 is photolysed to NO and O, the resulting O atom reacts quickly with O_2 to form O_3, which in turn reacts with NO (created from the photolysis of NO_2) to reform NO_2 (Reactions R 1.17 – R 1.19).

$$NO_2 + h\nu \; - \quad O + NO \tag{R 1.17}$$

$$O + O_2 + M - \quad O_3 + M \tag{R 1.18}$$

$$NO + O_3 - \quad NO_2 + O_2 \tag{R 1.19}$$

These reactions lead to a photostationary state within the troposphere, with O_3 being determined by the Leighton Equation (Equation 1.1, where $k_{R1.19}$ is the rate constant for Reaction R 1.19).

$$[O_3] = \frac{J_{NO_2}[NO_2]}{k_{R1.19}[NO]} \tag{1.1}$$

At night the photostationary state relaxes and, because O_3 is usually in excess, NO concentrations drop to zero.

As well as reacting with O_3, NO can also react with HO_2, as well as other organic peroxy radicals (RO_2) emitted into the troposphere as pollutants, to produce OH (Reactions R 1.20 – R 1.22, where R is a hydrocarbon and R' is R with one less CH_2 group).

$$HO_2 + NO - \quad OH + NO_2 \tag{R 1.20}$$

$$RO_2 + NO - \quad RO + NO_2 \tag{R 1.21}$$

$$RO + O_2 - \quad R\,CHO + HO_2 \tag{R 1.22}$$

The NO_2 produced in Reactions R 1.20 and R 1.21 can be photolysed (Reaction R 1.17), which leads to a net production of O_3 (Reactions R 1.18 and R 1.19).

These reactions show that in the presence of NO (i.e. a polluted environment, with NO typically above 14 ppt (Salisbury et al., 2002)) the oxidative destruction of organic compounds in the troposphere is a source of O_3 (Jenkin and Clemitshaw, 2000). NO_xlevels of greater than 0.5 ppb are typically found in urban sites and polluted sites, and corresponding increased levels of O_3 are also recorded (Sillman, 1999). These reactions are shown in Figure 1.2: the reactions shown in red are the dominating NO_x reactions in a polluted environment, while the reactions shown in blue are the dominating reactions in a clean environment.

Overview of Tropospheric HO_x Chemistry

The chemical processes shown in the previous sections give an overview of the HO_x chemistry in the troposphere. The concentration of OH in the troposphere is indicative of its oxidising capacity due to the oxidation reactions of OH with organic species. Oxidising agents degrade organic compounds, leading to their removal from the troposphere - therefore the oxidising capacity of the troposphere determines the lifetime of these compounds, of which many are pollutants (Wayne, 2002; Bloss et al., 2005b).

The oxidation of pollutants in environments with high NO_x levels can lead to the production of ozone. Ozone is normally present in the troposphere at levels of 20 – 40 ppb but following emissions of NO_x and VOCs, and in the presence of sunlight, photochemical pollution events can occur and can increase ozone levels up to 150 – 400 ppb (Jenkin and Clemitshaw, 2000). Notable examples of these photochemical events were first seen in Los Angeles, in California, in the late 1940s. More recently notable events have occurred in the UK (e.g. during the summer of 2003 (Stedman, 2004)). The high levels of O_3 have been linked to effects on human health and to low crop yields and damage to plants. Another effect of the increased ozone is a change in the radiative balance of the atmosphere, as discussed previously - an increase in tropospheric ozone is thought to have a positive

radiative forcing, indicating that it will increase the temperature at the surface of the Earth.

The HO_x reactions discussed so far in this section are largely well understood (Finlayson-Pitts and Pitts, 2000; Wayne, 2002; Seinfeld and Pandis, 1998), however measurements of HO_x within the troposphere tend to over-predict modelled concentrations of OH. One suggestion for the overestimation of HO_x in tropospheric models is the loss of HO_2 to aerosol (Jacob, 2000; Carslaw et al., 2002; Sommariva et al., 2006). Equivalent loss reactions are thought to happen with RO_2 (see Figure 1.2). The reaction of HO_2 and RO_2 with aerosol will lead to a lower concentration of both radical species. The loss of these species will affect the HO_x chemistry within the troposphere - for example, a reduction in the concentration of OH will occur, which will lead to a reduction in the oxidising capacity of the troposphere. This thesis aims to quantify the loss of HO_2 to aerosol in order to better understand how this process effects HO_x chemistry in the troposphere.

1.2.2 Aerosol within the Troposphere

The term aerosol is technically the combination of both a gas and the particles suspended in that gas. However, the term is often used loosely, as it is within this thesis, to mean the particles within the gas, with the gas assumed to be air (in the atmosphere).

Aerosol particles can be solid or liquid droplets and their composition is wide ranging, with both natural and anthropogenic sources. Particles range in size from 1 nm – 100 µm, but larger particles (such as raindrops and hail) fall out of the atmosphere rapidly, so are not considered aerosol particles (Finlayson-Pitts and Pitts, 2000). Primary aerosol is emitted directly into the atmosphere, while secondary aerosol is formed within the atmosphere from chemical processes. Examples of natural sources of primary aerosol are evaporation of sea-spray from oceans, volcanic emissions and suspensions of natural soil and rock erosion. Anthropogenic sources of primary aerosol are black carbon from incomplete combustion. The main anthropogenic source of primary aerosol is combustion, which produces black carbon from incomplete combustion. Other sources are from agriculture

(e.g. pesticide spraying), mining processes (e.g. rock cutting), and mechanical processes (e.g. grinding of brake pads on vehicles). Gaseous sulphur dioxide is also produced from combustion sources and can form secondary aerosol in the troposphere following oxidation. Another source of secondary aerosol is the oxidation of nitrogen oxides and most recently it is thought that diiodomethane (produced from seaweed) is photolysed to produce iodine oxides, which can also form secondary particles in the troposphere (Kolb, 2002).

Aerosol particles are characterised by their mass, size, chemical composition and optical and aerodynamical properties. The size of the particle is often determined by a diameter measurement (the effective diameter), which assumes the particle to be spherical in shape; this is often erroneous as many particles are not spherical, but it is a useful term to help define and compare particles. The effective diameter of the particle is important as it can give information on the source of the particle, its possible lifetime in the atmosphere and its effect on human health (e.g. the extent of penetration of the particle into the pulmonary system). The effective diameter corresponds to a particular property of the particle (e.g. its optical properties or electrical mobility). The most commonly used definition of the effective diameter is the aerodynamic diameter, which is defined as the diameter of a sphere of density $1\,\mathrm{g\,cm^{-3}}$ which has the same gravitational settling velocity as the particle under consideration (Baron and Willeke, 2001).

The number of particles in the troposphere can be be determined by simply counting them (e.g. by using a Condensation Particle Counter (Hinds, 1999)); while this gives a good indication of the total number concentration of aerosols within the troposphere it does not give any information on the diameter, surface area, or volume of the particle - all which are important to understand the effect of aerosol on the chemical processes within the troposphere.

Ambient aerosol is polydisperse, which means the aerosol particles have a range of sizes (e.g. a range of effective diameters). Aerosol distributions are measured which record the number of particles over a range of diameters, which gives more information about the

aerosol than a simple total count. The surface area or volume distribution can be found mathematically from the number distribution by assuming the particles are spherical. A log-normal distribution is usually used for ambient aerosol.

Ambient aerosol can be categorised into three groups: the coarse particle mode, the accumulation mode and the nucleation mode (Hinds, 1999; Seinfeld and Pandis, 1998; Finlayson-Pitts and Pitts, 2000; Baron and Willeke, 2001). These modes are shown in Figure 1.3.

Coarse particles have aerodynamic diameters greater than about 2.5 µm. These particles are created from mechanical processes such as grinding, wind and erosion. The particles are large so settle out quickly by sedimentation or washout, except on windy days when the sedimentation rate can match the re-entrainment rate (re-entrainment is the lifting of large particles from the ground by wind). Coarse particles can be transported over long distances if they are lofted to high altitudes by wind. They mostly consist of inorganic matter such as sand and sea-salt but can also consist of organic matter such as pollens and spores. Figure 1.3(a) shows that the number of these particles in ambient aerosol is low, but their volume (and thus mass) makes up nearly half of the total volume of ambient aerosol (Figure 1.3(b)).

The accumulation mode covers particles with aerodynamic diameters from about 1 µm to about 2 µm. These particles are created by the condensation of low volatility vapours or by the coagulation of smaller particles. They contain water, sulphate, nitrate, ammonium, organic compounds and black carbon. This mode is small in number of particles (Figure 1.3(a)), but makes up more than half of the total volume of ambient aerosol (Figure 1.3(b)). Accumulation mode particles are removed from the atmosphere by washout or incorporated into rainclouds and rained out. Particle removal mechanisms in this mode are the least efficient, so particles tend to accumulate in this mode.

The nucleation mode consists of particles with aerodynamic diameters from about 10 nm to 100 nm and arises from recent gas to particle conversion or from combustion processes which produce low volatility vapours. They have a short lifetime due to rapid

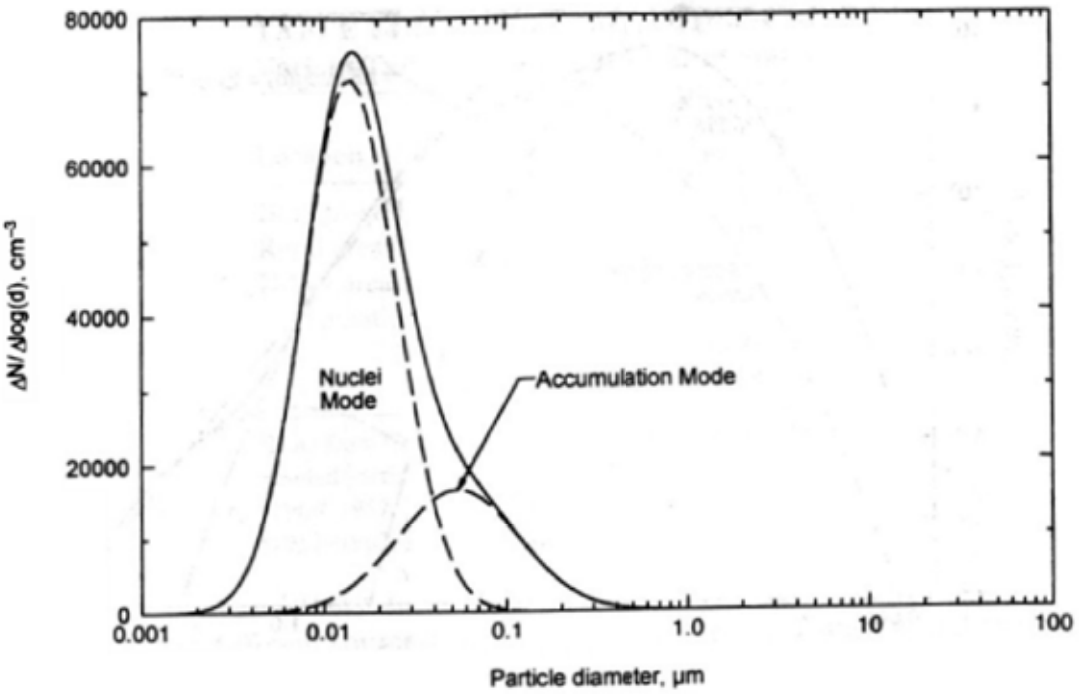

(a) Number Distribution

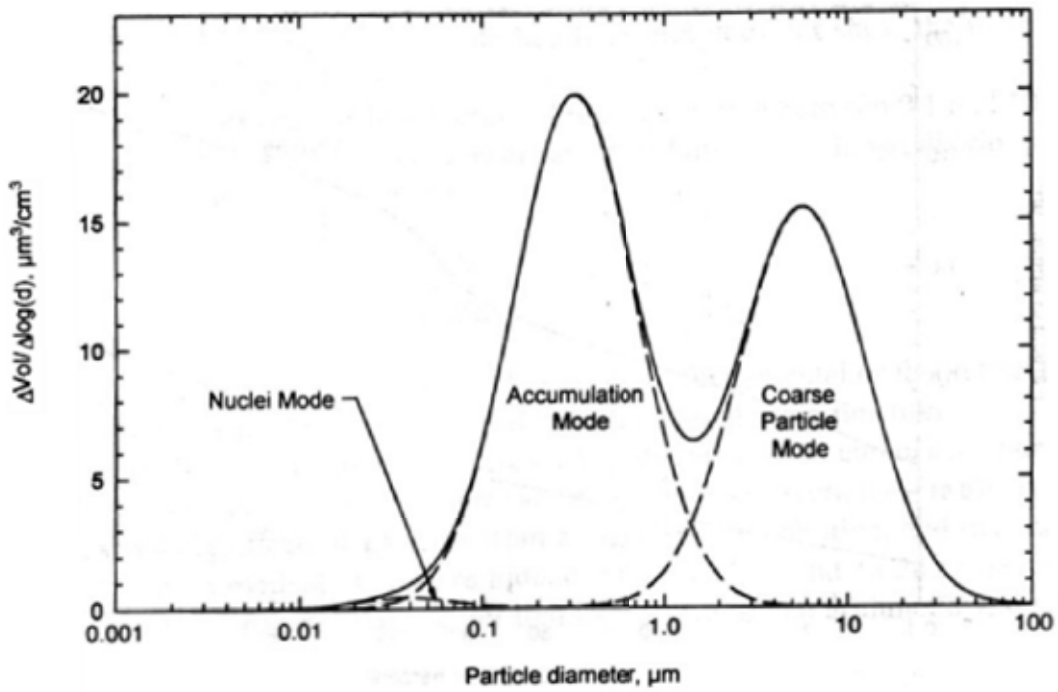

(b) Volume Distribution

Figure 1.3: A typical number and volume distribution for an urban aerosol. The distribution shows the three categorisations of urban aerosol (coarse, accumulation and nuclei modes) (Hinds, 1999)

coagulation, forming accumulation mode particles.

1.3 Heterogeneous Chemistry

Heterogeneous reactions are reactions which occur between different physical phases. The heterogeneous reactions within this study are specifically those between gases and solid or liquid particles in the atmosphere. Heterogeneous chemistry has been recognised as an important factor in the understanding of atmospheric chemistry. For example oxidation of SO_2 to sulphuric acid occurs via cloudwater interactions, causing acid rain, and the chemistry of the Antarctic ozone hole has been linked to polar stratospheric clouds, which provide a surface for reactions to occur which would not be possible in the gas-phase (Wayne, 2002).

When a gas molecule collides with an aerosol particle a number of potential processes may follow:

- bouncing off the particle
- reaction at the surface
- uptake to the bulk

The net rate of irreversible loss of the gas molecule to the particle (normalised to the rate of gas-particle collisions) is known as the uptake coefficient, γ. For a solid particle the only process through which gas molecules can be lost to the particle is by reaction at the surface. For an aqueous particle the reaction process are more complicated - the gas molecule can be absorbed into the bulk of the particle, whereupon it can diffuse into the bulk, react within the bulk or evaporate out of the particle. These processes are explained in more detail shortly. The maximum rate at which a gas molecule can be lost to an aerosol particle is called the mass (or bulk) accommodation coefficient, α, and is defined as the fraction of gas-particle collisions that result in uptake to the bulk of the particle. γ and α are therefore dimensionless quantities with values between 0 and 1. It

should be noted that α does not include reverse processes, such as the evaporation from the bulk.

If a gas molecule collides with an aqueous particle a number of steps can occur, as shown in Figure 1.4. The molecule could simply bounce off the particle or a reaction could occur at the surface of the particle, which will lead to loss of the molecule from the gas phase. Alternatively the collision could result in uptake of the gas molecule to the particle, the likelihood of which is determined by α. Once the gas molecule is in the bulk of the particle it can diffuse through the bulk of the aerosol; the rate of which is determined by the diffusion coefficient in the liquid phase. The molecule can also react within the bulk of the particle - reactions can occur both close to the surface and throughout the bulk. Where the reactions occur depends on the rate of diffusion through the bulk relative to the rate of the reaction. Whether the molecule reacts at the surface of the particle or within the bulk of the particle has important implications for kinetic studies. If the reaction is at the surface it will depend on the surface area of the aerosol, but if it is in the bulk it will depend on the volume of the aerosol.

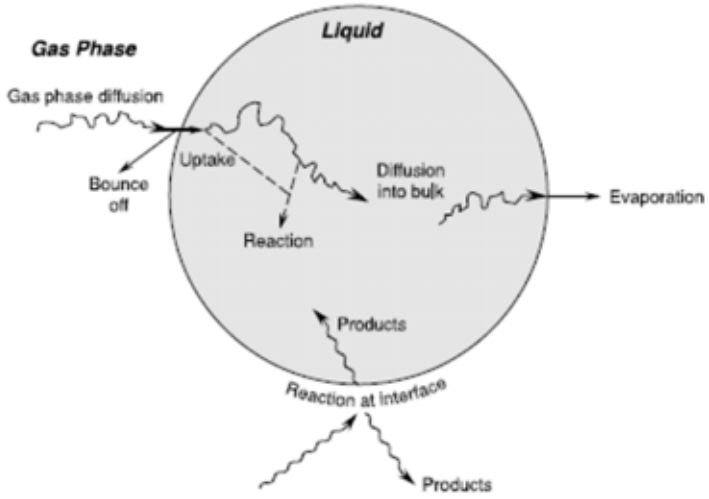

Figure 1.4: Schematic diagram of uptake and reaction of gases in liquids. (Finlayson-Pitts and Pitts, 2000)

The effect on HO_x tropospheric chemistry due to the heterogeneous reaction between HO_2 and aerosol is thought to be significant. This is because the lifetime of HO_x with

respect to aerosol loss is of the order of minutes, assuming γ is its maximum of 1, (Jacob, 2000), which is comparable to the lifetime of HO_2 with respect to gas phase reactions (a few minutes). Heterogeneous loss of OH radicals, on the other hand, is not thought to affect tropospheric HO_x chemistry, as the lifetime of OH with respect to gas phase reactions in the troposphere is less than 1 s. The rate of loss (i.e. the uptake coefficient) of HO_2 to aerosol has not yet been determined and the mechanism of the loss process is not fully understood (Jacob, 2000; Thornton et al., 2008; Loukhovitskaya et al., 2009; Kolb et al., 2010; Macintyre and Evans, 2011).

1.3.1 Mechanisms for Loss of HO_2 to Wet and Dry Aerosol

As mentioned at the end of the last section the mechanism for loss of HO_2 to aerosol is not fully understood. This section gives an outline of the possible reactions of HO_2 with wet and dry aerosol particles.

Dry Aerosol

Jacob (2000) suggests Reactions R 1.23 and R 1.24 as a set of possible surface reactions. Note that these reactions are dependent on H_2O, so the relative humidity of the aerosol could play a part in this reaction scheme.

$$HO_{2\,(g)} - \quad HO_2{\cdot}H_2O_{(surface)} \tag{R 1.23}$$

$$HO_2{\cdot}H_2O_{(surface)} + HO_{2\,(g)} - \quad H_2O_{2\,(g)} + O_{2\,(g)} + H_2O_{(g)} \tag{R 1.24}$$

A similar reaction process at the surface has been suggested by Loukhovitskaya et al. (2009) (Reactions R 1.25 and R 1.26, where S is a surface site). Their suggestion was backed up by experimental measurements of gaseous hydrogen peroxide, H_2O_2, while looking at the uptake of HO_2 to solid surfaces, with NaBr as the active surface. Loukhovitskaya et al. (2009) determined a H_2O_2 yield of nearly 0.5, which is consistent with the reaction scheme shown.

$$S_{(surface)} + HO_{2\,(g)} - \quad S{\cdot}O{-}OH_{(surface)} \tag{R 1.25}$$

$$S{\cdot}O{-}OH_{(surface)} + HO_{2\,(g)} - \quad S_{(surface)} + O_{2\,(g)} + H_2O_{2\,(g)} \tag{R 1.26}$$

Remorov et al. (2002) suggested that the reaction of dry NaCl aerosol uptake is due to the surface reaction between HO_2 and NaCl (Reaction R 1.27). This reaction is not elementary, but follows a complex mechanism. However, it shows a similar overall reaction scheme to that suggested by both Jacob (2000) and Loukhovitskaya et al. (2009):

$$HO_{2\,(g)} + NaCl_{(s)} - \quad \tfrac{1}{2}(H_2O_2)_{(g)} + NaCl_{(s)} + \tfrac{1}{2}(O_2) \tag{R 1.27}$$

Despite differences in the reaction schemes suggested by Jacob (2000), Loukhovitskaya et al. (2009) and Remorov et al. (2002) there is general agreement that a surface reaction occurs which aids in the self reaction of HO_2 to produce gas-phase H_2O_2.

Wet Aerosol

HO_2 can react with aqueous aerosol in two different ways; by reaction on the surface as described in the previous section, or by absorption into the bulk of the particle followed by reaction within the bulk (described in this section).

Jacob (2000) suggested the reaction of HO_2 with aqueous aerosol to be via an acid-base dissociation process within the bulk of the particle, as shown in Reactions R 1.28 – R 1.30. It should be noted that the aqueous H_2O_2 produced within the bulk of the particle could evaporate from the particle and revert to the gaseous phase.

$$HO_{2\,(g)} \rightleftharpoons HO_{2\,(aq)} \tag{R 1.28}$$

$$HO_{2\,(aq)} \rightleftharpoons O^-_{2(aq)} + H^+_{(aq)} \tag{R 1.29}$$

$$HO_{2\,(aq)} + O^-_{2(aq)} \xrightarrow{H_2O_{(aq)}} H_2O_{2\,(aq)} + O_{2\,(aq)} + OH^-_{(aq)} \tag{R 1.30}$$

Thornton et al. (2008) added to these reactions by suggesting a further reaction of HO_2 which could compete with Reaction R 1.30, which is shown by Reactions R 1.31.

$$HO_{2\,(aq)} + HO_{2\,(aq)} - \quad H_2O_{2\,(aq)} + O_{2\,(aq)} \tag{R 1.31}$$

Cooper and Abbatt (1996) also suggested a reaction of HO_2 with acid sulphate (Reaction R 1.32).

$$HO_{2\,(aq)} + HSO^-_{4(aq)} - \quad SO^-_{5(aq)} + H_2O_{(aq)} \tag{R 1.32}$$

The reaction with sulphate to produce a non-H_2O_2 product has also been cited by Mao et al. (2010), who compared a model output with observation from the ARCTAS (Arctic Research of the Composition of the Troposphere from Aircraft and Satellites) field campaign. They found that if the product of HO_2 reactions on aerosol was H_2O_2 their model would overestimate observed H_2O_2 levels, but if the product was not H_2O_2 (e.g. if HO_2 loss occurred via Reaction R 1.32) the model would underestimate the observed H_2O_2 levels in the upper troposphere. Mao et al. (2010) suggest a mixture of HO_2 reactions with aerosol, some of which produce H_2O_2 (e.g. Reaction R 1.32) and some which do not (e.g. Reactions R 1.28 – R 1.31).

HO_2 is also thought to react with transition metals. Transition metals, such as Cu(II) or Fe(II), are emitted into the troposphere by combustion and crustal erosion processes. These metals are thought to catalyse the conversion of HO_2 to H_2O_2 in the aqueous particle bulk (Mozurkewich et al., 1987; Cooper and Abbatt, 1996; Jacob, 2000; Thornton and Abbatt, 2005a). The aqueous catalytic reactions of HO_2 with Cu(II) are shown in Reactions R 1.33 – R 1.36.

$$HO_{2\,(aq)} + Cu^{2+}_{(aq)} - \quad H^+_{(aq)} + Cu^+_{(aq)} + O_{2\,(aq)} \tag{R 1.33}$$

$$O^-_{2(aq)} + Cu^{2+}_{(aq)} - \quad Cu^+_{(aq)} + O_{2\,(aq)} \tag{R 1.34}$$

$$HO_{2\,(aq)} + Cu^{+}_{(aq)} \xrightarrow{H_2O_{(l)}} H_2O_{2\,(aq)} + Cu^{2+}_{(aq)} + OH^{-}_{(aq)} \quad \text{(R 1.35)}$$

$$O^{-}_{2(aq)} + Cu^{+}_{(aq)} \xrightarrow{2\,H_2O_{(l)}} H_2O_2 + Cu^{2+}_{(aq)} + 2\,OH^{-}_{(aq)} \quad \text{(R 1.36)}$$

Typical atmospheric aerosol is unlikely to contain enough aqueous Cu(II) (or Fe(II), which has analogous reactions) to significantly affect the loss of HO_2 in the troposphere. However these reactions can be used in the laboratory to determine lower limits to the mass accommodation coefficient, α, by providing a fast sink of HO_2 in the aqueous phase and thus making the mass accommodation the rate limiting step (Mozurkewich et al., 1987; Thornton and Abbatt, 2005a; Taketani et al., 2008).

As with HO_2 reactions with dry aerosol, the reactions of HO_2 with aqueous aerosol are not well understood. There is a general agreement of H_2O_2 being the product of the reactions of wet aerosol with HO_2, but with other products suggested too (e.g. SO_5^-). More laboratory work needs to be undertaken to fully understand these process (Mao et al., 2010).

1.3.2 Modelled Effects of Heterogeneous HO_2 Loss on Tropospheric Chemistry

Model predictions of HO_2 and OH tend to overestimate ambient concentrations of the radicals. Heterogeneous loss of HO_2 to aerosol, which is not currently included in most models, has been cited as a possible reason for this overestimation (Jacob, 2000; Carslaw et al., 2002; Sommariva et al., 2006; Kanaya et al., 2007). As discussed previously a loss of HO_2 will lead to a reduction in OH and thus the oxidising capacity of the troposphere. A number of models have been used to investigate the possible affects of heterogeneous loss of HO_2 on the HO_x chemistry of the troposphere (and thus its oxidation capacity).

Models have used various ways to estimate the heterogeneous loss of HO_2 to aerosol, estimating first order rate constants or using uptake coefficients (γ). When incorporating heterogeneous chemistry into HO_x chemistry models (e.g. ozone budget models) Jacob (2000) suggests a simple reaction probability parameterisation to describe the reactive

uptake of various species, including HO_2 (Equation 1.2, where a is the radius of the aerosol, A is the aerosol surface area per unit volume of air, v is the mean molecular speed of species in the gas phase, D_g is the gas-phase molecular diffusion coefficient of a species in air, k is the first order rate constant for heterogeneous reaction of a species with an aerosol and γ is the uptake coefficient of the gas phase species to the liquid phase).

$$k = \left(\frac{a}{D_g} + \frac{4}{v\gamma} \right)^{-1} A \tag{1.2}$$

The first term in Equation 1.2 deals with the gas phase diffusion of the gas molecule to the particle, while the second term deals with the uptake of the gas to the particle. This parameterisation is chosen because of the limited knowledge of heterogeneous chemistry, so a more detailed treatment cannot currently be justified. Note that γ is still the critical parameter used in this treatment. $\gamma = 0.2$ is the currently recommended value (Jacob, 2000) for HO_2 uptake to all aerosol types. The chemistry of these reactions need better quantifying so they can be included more accurately in model calculations.

Two modelling studies of HO_x chemistry are outlined below in order to illustrate the potential importance of heterogeneous loss of HO_2 in the modelling of the troposphere.

Smith et al. (2006) compared steady state calculations of OH and HO_2 with measurements observed during the NAMBLEX (North Atlantic Marine Boundary Layer EXperiment) field campaign. Measurements of OH were made with a Fluorescence Assay by Gas Expansion (FAGE) technique, with HO_2 measured in the same way after chemical conversion to OH. The steady state calculations of OH were constrained to production by photolysis of O_3 and destruction by CO and CH_4 only. A second set of calculations were performed which included sources of OH by $HO_2 + NO$ and $HO_2 + O_3$ and extra sinks due to reaction with organic VOCs. These steady state calculations were compared to observed measurements as shown in Figure 1.5. It can be seen that the observations are generally slightly lower than the steady state calculations with the ratio of calculated values to observed values calculated as 1.04 ± 0.36. This study shows that the sources and sinks of OH in the atmosphere is fairly well understood.

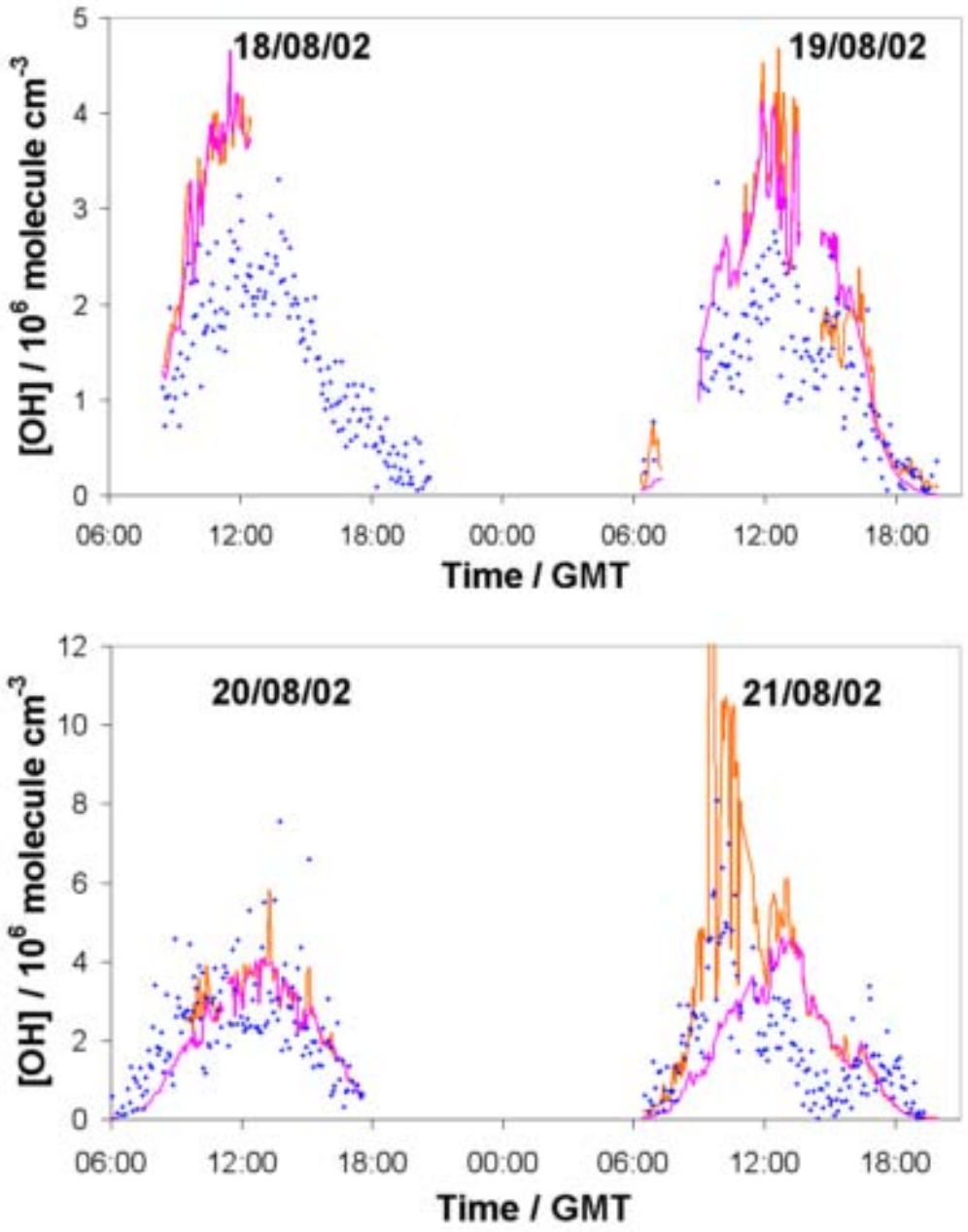

Figure 1.5: Diurnal profiles of measured OH (blue diamonds), OH calculated using a simple steady state expression, which includes primary production from O_2 photolysis; and loss by reaction of CO and CH_4 only (pink line) and OH calculated by a more complex steady state expression which also includes $HO_2 + NO$ and $HO_2 + O_3$ as OH sources and also OH loss by reaction with organic-VOCs (orange line) for representative 2-day periods (Smith et al., 2006).

HO_2 steady state calculations and observed concentrations were also compared during this study (Figure 1.6). The steady state calculations were more complicated than those for OH due to the need to account for second order rate loss (the self reaction of HO_2 and its reaction with RO_2) and the need to account for the fast interconversion with OH. An expression developed by Carslaw et al. (2002) (which used the Master Chemical Mechanism to derive constants appropriate for the observed conditions) was invoked to calculate the HO_2 steady state concentration.

It can be seen in Figure 1.6 that the model measurements consistently over-predicted the observed measurements of HO_2 - the simplest steady state calculations overestimated the measurements by an average factor of 4.2±1.6. Two other losses of HO_2 were considered - loss by reaction with halogen and loss to aerosol.

Steady state calculations accounting for halogen chemistry were added to the original calculations: these new calculations overestimated the concentration of HO_2 by an average of 2.8±0.6. Calculations to account for the HO_2 loss to aerosol (with γ at its maximum, i.e. 1) were added to the original steady state calculations and reduced the average factor for overestimation to 2.0±0.7. These calculations show that neither halogen chemistry, nor heterogeneous chemistry alone can explain the overestimation in HO_2 chemistry. Calculations accounting for both halogen and heterogeneous chemistry were also performed, resulting in an overestimation of HO_2 by an average factor of 1.09±0.42.

These model calculations show the need to account for loss of HO_2 to aerosol when using models to calculate the concentration of HO_2 in the troposphere. These calculations use the maximum value for γ indicating the need to determine an experimental value for the uptake coefficient.

Martin et al. (2003) used a coupling of a 3D model of tropospheric chemistry (Goddard Earth Observing System - Chemistry (GEOS-Chem)) with a 3D aerosol model (Goddard Chemistry Aerosol Radiation and Transport (GOCART)) to look at the global effect on HO_x due to heterogeneous aerosol reactions. For this model the value of $\gamma = 0.2$ was used for HO_2 uptake to all aerosol (sulphate, mineral dust, sea salt, black carbon and

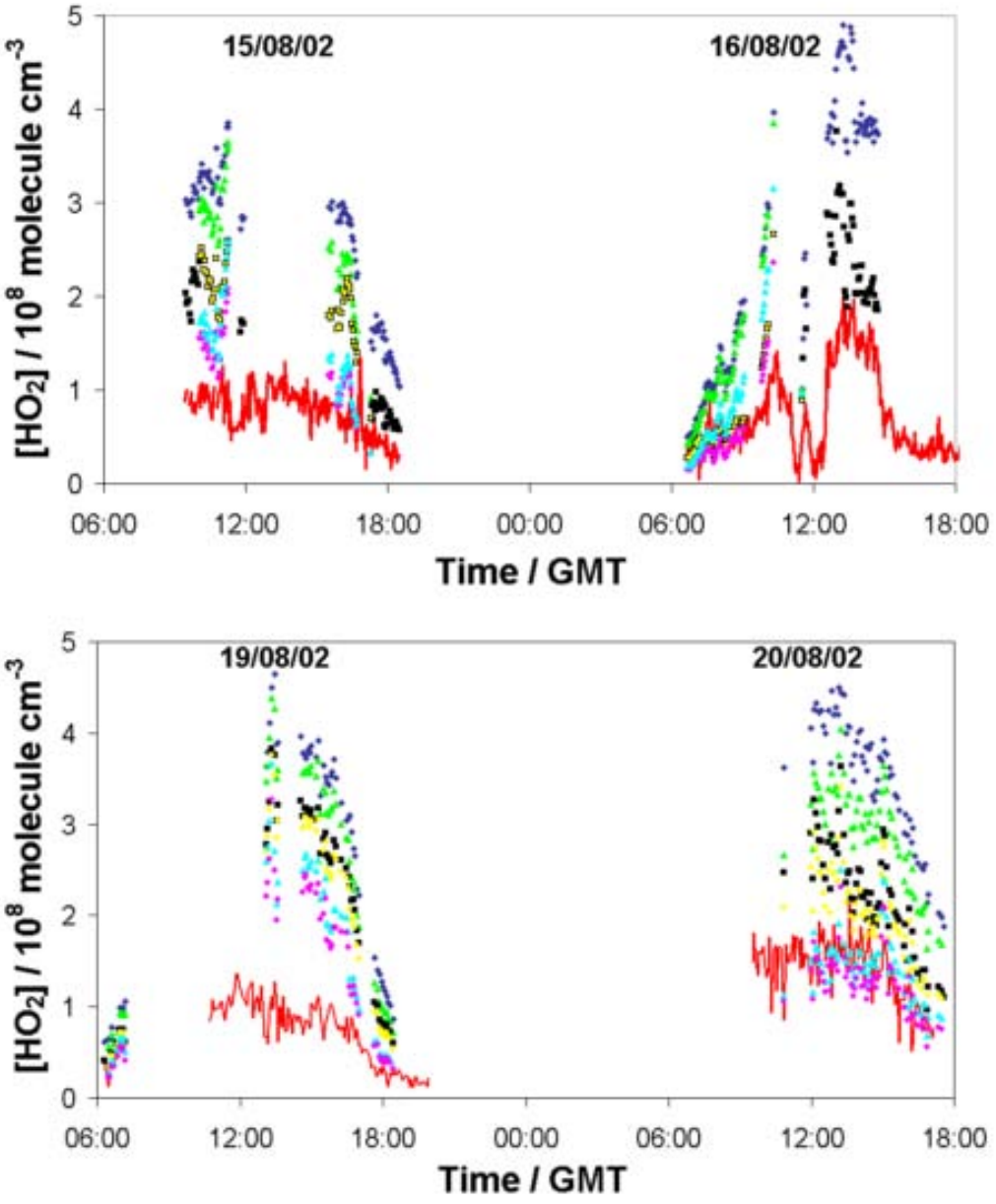

Figure 1.6: Diurnal profiles of measured HO_2 (red line), and a simple steady state calculation of HO_2 (navy blue diamonds), and several modifications which also include: loss by reaction of HO_2 with measured IO (green triangles), loss by reaction of HO_2 with measured IO times 10 (light blue triangles), uptake of HO_2 onto aerosol (black squares), both loss of HO_2 by reaction with IO and by uptake onto aerosol (yellow circles with or without black border) and both loss of HO_2 by reaction of IO times 10 and uptake onto aerosols (pink circles) (Smith et al., 2006).

organic carbon). The heterogeneous loss of HO_2 to aerosol was shown to account for 10 – 40 % of the total HO_2 loss in the polluted continental boundary layer and for more than 70 % over tropical biomass burning regions (Figure 1.7). A more pronounced effect is seen with high concentrations of fine aerosol which provide a large surface area for gas-particle collisions. Figure 1.7 shows the HO_x loss in the lower troposphere due to the uptake of HO_2 to aerosol. The model results also showed an increase in the global lifetime of CH_3Cl_3 against oxidation by tropospheric OH (consistent with observations), which indicated a decrease of 9 % in the concentration of OH. The decrease in OH indicates a decrease in the oxidative capacity.

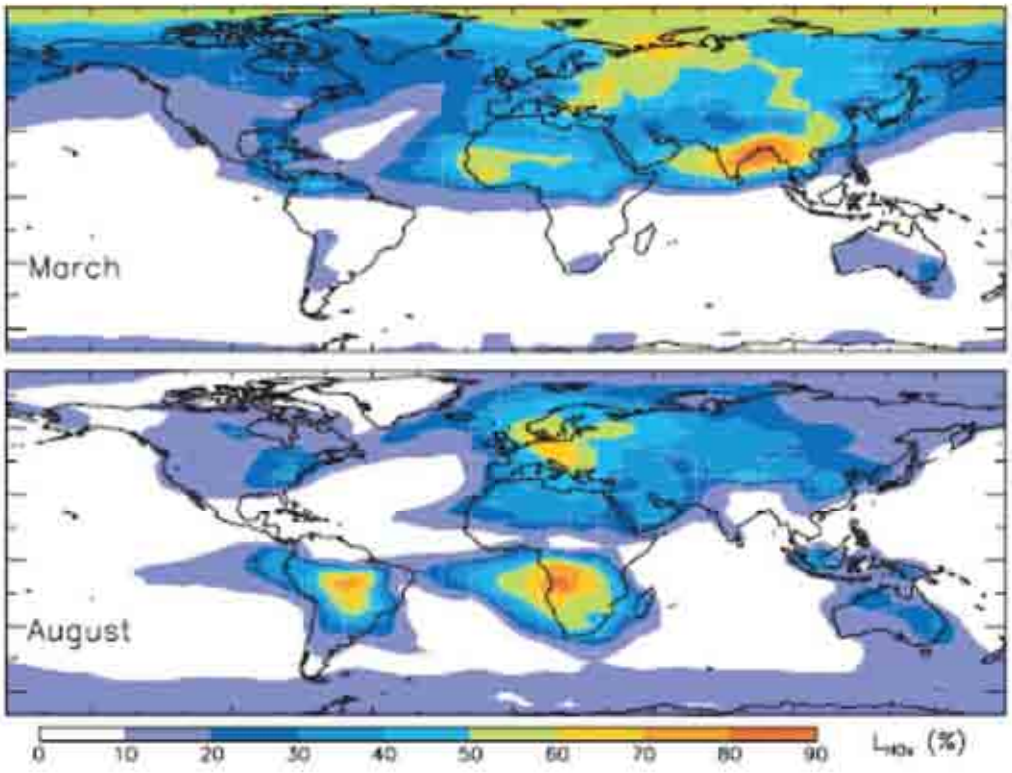

Figure 1.7: Modelled results from Martin et al. (2003) showing the fraction of total HO_x loss in the lower troposphere (below 600m) due to uptake of HO_2 to aerosol. (Martin et al., 2003)

1.3.3 Review of Current Uptake Coefficients for HO_2 to Aerosol

The heterogeneous uptake of trace gases within the atmosphere has recently been discussed in some detail in the review by Kolb et al. (2010). This paper draws attention to the need to understand uptake processes as there is evidence they can affect the concentration of trace gases within the atmosphere leading to changes in the tropospheric oxidative capacity and ozone depletion in the stratosphere. There is also evidence that uptake to aerosol particles will change the properties of the aerosol, leading to changes in their size or optical properties. These property changes could lead to a change in the radiation that is reflected or absorbed by the particles, thus leading to changes in radiation reaching the Earth's surface. Amongst other recommendations Kolb et al. recommended future studies of the uptake of HO_2, including the study of the uptake coefficient to various particles and the mechanism of the loss process.

Previous laboratory studies have investigated the uptake of HO_2 to aerosol, in particular work by Mozurkewich et al. (1987), Gershenzon et al. (1995), Thornton and Abbatt (2005a), Taketani et al. (2008), Loukhovitskaya et al. (2009) and George et al. (2010). Each study is examined briefly below. Table 1.1 gives a summary of the uptake coefficients measured for uptake to NaCl and $(NH_4)_2SO_4$ during those studies.

There are various laboratory approaches in use to study heterogeneous reactions; flow tube studies are the most common, although other systems, such as the Knudsen cell or an aerosol chamber are also used (Finlayson-Pitts and Pitts, 2000). The general approach is to expose the trace gas of interest (in this case HO_2) to the heterogeneous surface of interest (in this case a surface mimicking atmospheric aerosol particles). The trace gas is monitored and how it changes when exposed to the surface can be used to determine the rate of loss of the trace gas to the surface. The flow tube system can be used in two ways - as an aerosol flow tube system (in which aerosol particles are the reactive species) or a coated wall flow tube system (in which the flow tube surface is coated with the reactive species).

Mozurkewich et al. (1987) measured the mass accommodation coefficient for HO_2 on

Table 1.1: A summary of previous measurements of γ and α for uptake of HO_2 to NaCl and $(NH_4)_2SO_4$ aerosol. All measurements were recorded at atmospheric pressure. Measurements of uptake to other aerosol (e.g. KCl, $(NH_4)HSO_4$ and $LiNO_3$) have been measured, details of which are included in the text, but not in this summary table.

γ	α	Relative Humidity	Temperature	Aerosol	Reference
0.016±0.003			295 K	$NaCl_{(s)}$	Gershenzon et al. (1995)
0.011			295 K	$(NH_4)_2SO_{4\,(s)}$	
0.012±0.002				$NaCl_{(s)}$	Remorov et al. (2002)
	0.5±0.1	40 – 45 %	295 K	$(NH_4)_2SO_{4\,(aq)}$	Thornton and Abbatt (2005a)
< 0.01		20 %	296 K	$NaCl_{(s)}$	Taketani et al. (2008)
0.02±0.01		53 %	296 K	$NaCl_{(s)}$	
0.09 – 0.11	0.65	53 – 75 %	296 K	$NaCl_{(aq)}$	
0.04±0.02		20 %	296 K	$(NH_4)_2SO_{4\,(s)}$	
0.05±0.02		45 %	296 K	$(NH_4)_2SO_{4\,(s)}$	
0.011 – 0.19	0.53	45 – 75 %	296 K	$(NH_4)_2SO_{4\,(aq)}$	
0.0018			240 – 310 K	$NaCl_{(s)}$	Loukhovitskaya et al. (2009)
0.0023			240 – 310 K	Solid synthetic sea-salt	
< 0.002		15 – 60 %		$(NH_4)_2SO_{4\,(s)}$	George et al. (2010)
0.024± 0.01	0.08± 0.02	51 %		$(NH_4)_2SO_{4\,(aq)}$	
< 0.002		7 – 50 %		$NaCl_{(s)}$	
0.032±0.008		50 %		$NaCl_{(aq)}$	

aqueous particles of $LiNO_3$ (which has good deliquescence properties and low chemical reactivity) and NH_4HSO_4 (representative of atmospheric aerosol) aerosol using an aerosol flow tube and a PEeroxy Radical Chemical Amplification (PERCA) technique. Radicals were produced using a hot wire technique to produce H atoms, which reacted with oxygen to produce HO_2 radicals. The PERCA was not calibrated to determine the absolute concentration of HO_2 as relative concentrations were used during the analysis procedure. However, using assumptions based on the work of Cantrell et al. (1984), Mozurkewich et al. estimated that the concentration of HO_2 was about 1×10^8 – 1×10^9 molecules cm^{-3}. Cu(II) was added to the aerosol as a catalyst to obtain α values. This was the first laboratory use of this technique, which has been used in various studies since. Measured values of α were 0.94±0.50 for $LiNO_3$ and 0.40±0.21 for NH_4HSO_4; the experiments were conducted at 75 % relative humidity.

Gershenzon et al. (1995) measured HO_2 uptake by dry NaCl, KCl, NH_4NO_3, $(NH_4)_2SO_4$ and aqueous H_2SO_4, using a matrix isolation Electron Paramagnetic Resonance (EPR) to detect the radicals, coupled with a coaxial reactor for the heterogeneous reactions. The central rod of the reactor was coated with the surface of interest. Radicals were generated using a microwave discharge of He containing a small amount of H_2. The discharge created H atoms, which reacted with oxygen to produce HO_2. Initial concentrations of HO_2 varied from 3×10^9 – 3×10^{11} molecules cm^{-3}. Values for γ for HO_2 loss on dry salts ranged from 0.01 – 0.02, while values for loss to H_2SO_4 were close to unity. Remorov et al. (2002) used the same apparatus as Gershenzon et al. to further study the mechanism of loss of HO_2 radicals to solid NaCl.

Thornton and Abbatt (2005a) measured HO_2 loss to H_2SO_4 (35 – 40 % relative humidity), a highly acidic aqueous aerosol and $(NH_4)_2SO_4$ (40 – 45 % RH), a neutral aqueous aerosol. These values were obtained using an aerosol flow tube coupled to a Chemical Ionisation Mass Spectrometer (CIMS). HO_2 measurements used relative concentrations rather than determining absolute concentrations. Radicals were produced using a microwave discharge technique similar to Gershenzon et al. The initial concentration of HO_2

was estimated by assuming the non-aerosol loss of the radical was due to its self-reaction. A second order rate analysis was then performed to determine initial concentrations of HO_2 to be $\approx 1 \times 10^{10}$ molecules cm^{-3}. Aerosols were produced using a constant output atomiser and a Scanning Mobility Particle Sizer (SMPS) was used to measured the aerosol distribution. The typical total surface area used during these experiments varied from 3×10^{-5} – $1 \times 10^{-3}\,cm^2\,cm^{-3}$. Values of $\alpha = 0.8 \pm 0.3$ for H_2SO_4 and $\alpha = 0.5 \pm 0.1$ for $(NH_4)_2SO_4$ were measured. A low reactivity of HO_2 to H_2SO_4 aerosol prevented a clear value for γ being obtained but an upper limit of 0.01 was determined. For $(NH_4)_2SO_4$ aerosol $\gamma \approx 0.1$ was determined, but this value is thought to only be appropriate for the concentration of HO_2 used during the experiments, which is two orders of magnitude higher than ambient tropospheric concentrations. The high concentration of the HO_2 radicals is a major limitation because at these concentrations the gas phase HO_2 self-reaction will be a significant loss, espically under humid conditions, thus the uptake coefficent measured may be an overestimate of the real value.

Taketani et al. (2008) studied the uptake coefficient for HO_2 for wet and dry aerosol of $(NH_4)_2SO_4$ (a proxy for an urban type aerosol) and NaCl (a proxy for a sea-salt aerosol) at ambient temperature and pressure and for various relative humidities. An aerosol flow tube was used for the radical/aerosol reactions coupled to a chemical conversion Laser Induced Fluorescence (LIF) instrument. The LIF instrument detects OH radicals, therefore in order to use this instrument for the detection of HO_2 the radicals must first be converted to OH. This conversion is performed by adding NO to the HO_2 radicals just before detection by the LIF instrument ($HO_2 + NO - \quad OH + NO_2$). Radicals were produced by photolysis of H_2O followed by reaction with oxygen. The concentration of HO_2 radicals used during this study was approximately atmospheric ($[HO_2] \approx 1 \times 10^8$ molecules cm^{-3}). A constant output atomiser was used to produce $(NH_4)_2SO_4$ and NaCl aerosol. Both wet and dry aerosol was studied with dry particles obtained using a diffusion dryer. An SMPS was used to detect the aerosol distribution, with the total surface area of the particles in the region of $1 \times 10^{-4}\,cm^2\,cm^{-3}$. Dry particles were found to have

a significantly lower measured γ value (< 0.05) than wet particles (0.10 and 0.15 for NaCl and $(NH_4)_2SO_4$ respectively), suggesting the loss mechanism of HO_2 is enhanced in aqueous aerosol.

Loukhovitskaya et al. (2009) used a low pressure coated wall flow tube technique to study the uptake of HO_2 to dry salt surfaces. The radicals were created using a microwave discharge technique using either chlorine and methanol or fluorine and hydrogen peroxide. Typical initial concentrations of HO_2 were $2 - 9 \times 10^{11}$ molecules cm^{-3}. The HO_2 radicals were detected using a mass spectrometer (either by direct detection or by conversion to NO_2 followed by detection). Loukhovitskaya et al. studied the uptake to dry NaCl ($\gamma = 0.0018$) and NaBr ($\gamma = 0.0022$) as well as to synthetic sea salt ($\gamma = 0.0023$). Loukhovitskaya et al. also studied the product of the heterogeneous reaction and determined the production of H_2O_2, indicating the self-reaction of HO_2 as a possible mechanism for heterogeneous loss of HO_2.

Most recently there has been a study by George et al. (2010). This study used an aerosol flow tube coupled to a FAGE instrument (along with the chemical conversion of HO_2 to OH). HO_2 radicals were produced by photolysis of water vapour and subsequent reaction with oxygen; the initial concentration of HO_2 used was in the range $1 \times 10^8 - 1 \times 10^9$ molecules cm^{-3}. An atomiser was used to generate the aerosol particles and an SMPS was used to measure the aerosol distribution. The total surface area of the aerosol distributions used was of the order of $1 - 6 \times 10^{-5}\,cm^2\,cm^{-3}$. The study investigated loss to wet and dry NaCl, $(NH_4)_2SO_4$ and organic acid aerosol.

These studies show that a variety of laboratory systems have been used to study the heterogeneous loss of HO_2 to various aerosol particles. However there is no general agreement for the measured uptake coefficients. For aqueous NaCl γ has been measured only by Taketani et al. and George et al. Their values disagree, with Taketani et al. quoting a value three times larger than that determined by George et al. γ determined for dry NaCl particles agree better, with Gershenzon et al., Remorov et al. and Taketani et al. determining γ between approximately 0.01 and 0.02. However there is also disagreement

here with Taketani et al., Loukhovitskaya et al. and George et al. determining γ less than 0.001 for uptake to dry NaCl, which is an order of magnitude smaller. The difference in this coefficient determined by Taketani et al. could be due to its determination at a lower relative humidity, which may also explain the difference in measurements by Loukhovitskaya et al. and George et al. The disagreement in these measurements (and similar disagreement with other types of aerosol) show the need for further studies to determine these uptake coefficients.

The International Union of Pure and Applied Chemistry (IUPAC) evaluates data and produces suitable recommendations for the chemical community including evaluations specifically aimed at atmospheric studies. IUPAC have not been able to recommend a value for the uptake of HO_2 to ice particles, mineral dust surfaces and other surfaces, although work is currently being undertaken to look at uptake of trace species to water, salt solutions and semi-volatile organics (Crowley et al., 2010). The Jet Propulsion Lab (JPL) also provide an evaluation of chemical data for use in atmospheric studies. Their most recent evaluation notes the lack of available data for heterogeneous reactions relevant in the atmosphere, especially for tropospheric reactions. With respect to heterogeneous uptake of HO_2 they recommend values for water ice, sulphuric acid, sodium chloride and potassium chloride. The uptake for sodium chloride is taken from the study by Gershenzon et al. only (Sander et al., 2006).

$\gamma =$ is 0.2, as recommended by Jacob, is the most frequently used value for modelling studies which include the heterogeneous loss of HO_2. This value was determined from the laboratory studies available at the time as well as some model calculations which attempted to account for heterogeneous loss of HO_2. It should be noted that although Jacob recommends the value of 0.2 a range for this value is also given, which is 0.1 - 1. This large range shows the uncertainity of the magnitude of the uptake of HO_2 to aerosol.

This study aimed to build a system which can be used quantify the uptake of HO_2 to aerosol. The study aimed to investigate the uptake of HO_2 to aerosol relevant to the troposphere. NaCl aerosol was used as a proxy for marine aerosol and $(NH_4)_2SO_4$

aerosol used as a proxy for urban aerosol. The system aimed to study the uptake at tropospherically relevant conditions i.e. atmospheric pressure and temperature and with ambient HO_2 concentrations. An aerosol flow tube, rather than a wall coated flow tube, provided aerosol particles in their ambient form. Absolute concentrations of HO_2, rather than relative concentrations, were determined using a PERCA system - knowing the absolute concentration of HO_2 within the flow tube system ensured ambient conditions were met and thus that the self-reaction of HO_2 was negligible within the system. The next two chapters discuss in detail the methodology used in this study, while Chapter 4 details the analysis used to determine the uptake coefficients of HO_2 to aerosol.

1.4 Summary

This chapter introduced the background to this thesis. The atmosphere of the Earth was briefly described, followed by some of its characteristics which are relevant to this study. The chemistry of the troposphere was discussed in detail, with Figure 1.2 showing a summary of the most important reactions regarding HO_x chemistry in the troposphere. Aerosols were then introduced and their characteristics and importance in the atmosphere described.

Heterogeneous chemistry was also discussed, with important terms rigorously defined. Some possible mechanisms for loss of HO_2 to particles were shown, but overall the mechanism is not well understood. Model studies were described in order to demonstrate the potential importance of HO_2 loss within the troposphere - trace gas concentrations, such as OH, are shown to change due to the uptake of HO_2 to aerosol. A change in the concentration of OH can lead to a decrease in the oxidising capacity of the troposphere, allowing pollutants to remain in the troposphere for longer.

Finally this chapter gives a review of previous studies investigating the loss of HO_2 to aerosol. A summary table, giving previously determined values of γ for HO_2 is shown and details of the experimental set-up used to to obtain these values is given in the text.

This study aimed to produce a system that could measure γ for various aerosol using an aerosol flow tube system mimicking ambient conditions.

This chapter gives an overview of the importance of this work within the study of atmospheric chemistry. The heterogeneous loss of HO_2 has been shown to affect the chemistry of HO_x in the troposphere, leading to changes in the oxidising capacity of the atmosphere which has a direct effect on pollutants at the Earth's surface.

1.5 Aims and Objectives of This Study

The overall aim of this study was to design and build an experimental system which could be used to determine the mass accommodation coefficient and the uptake coefficient of HO_2 radicals to aerosols. The objectives of this study are shown below.

- Build an aerosol flow tube system to investigate the rate of loss of HO_2 radicals to aerosol particles
- Build a peroxy radical chemical amplifier to detect HO_2 radicals
- Produce and characterise wet and dry aerosol particles
- Determine mass accommodation and uptake coefficient values for NaCl and $(NH_4)_2SO_4$ aerosol at atmospherically relevant conditions
- Validate the aerosol flow tube system by comparing determined uptake coefficients to values determined in other studies
- Understand the implications of new uptake coefficients for HOx chemistry in the troposphere

CHAPTER 2

EXPERIMENTAL METHODOLOGY

2.1 Introduction

Flow tube systems were first developed for determining gas-phase rate constants (Finlayson-Pitts and Pitts, 2000; Howard, 1979) but were soon used to study heterogeneous reactions too (e.g. the uptake of ammonia gas to sulphuric acid droplets which is important in understanding the acidity of atmospheric aerosol (McMurry et al., 1983)). A basic flow tube system consists of two tubes - a main flow tube and an injector tube. A carrier gas is flowed through both tubes to maintain a constant flow of gas through the system. The main flow tube has a reactant present in it (typically in excess); this reactant could be a gas, an aerosol or a coating on the walls of the flow tube. The injector will have a second reactant present within the carrier gas flow. The reaction occurs when the two flows start to mix. A detector at the exit of the main tube will monitor the concentration of a reactant. The injector tube can be moved parallel to the main tube which changes the contact distance and hence the reaction time of the species under consideration. If a laminar plug flow is assumed in the main tube then the velocity of the flow in this tube can be determined by dividing the total flow rate by the cross-sectional area of the tube. The reaction time can then be determined by dividing the distance between the injector and the detector by the velocity of the flow in the main tube. In this way the reaction between the two species can be monitored over time and a rate constant for the reaction

can be determined by assuming a pseudo-first order reaction and then using simple kinetic analysis (i.e. Equation 2.1).

$$\frac{d[A]}{dt} = -k[A] \tag{2.1}$$

One issue that arises during kinetic analysis is that reactants are usually lost to the walls of the flow tube as well as undergoing the reaction under investigation. This means that the rate constant for loss of the measured reactant to the walls must be determined. This is performed experimentally in the same manner described above, but without the second reactant present. The rate of loss of the reactant to the walls of the tube may be quite large compared to its rate of reaction with the other reactant. The rate constant for loss of the reactant to the walls is often reduced by coating the walls of the tube with an unreactive substance such as Teflon or halocarbon wax.

Variations of the simple flow tube system have been used to study heterogeneous reactions relevant to the atmosphere, but they can be broadly split into two categories - coated wall flow tube reactors and aerosol flow tube reactors (Kolb et al., 2010).

Coated wall flow tube reactors have the reactant surface of interest coated onto the walls of the flow tube. The reactant gas is then injected into the system in the same way as described above and the analysis can be completed as above. The wall coating can be a solid surface: Cooper and Abbatt (1996) studied the uptake of OH and HO_2 radicals to water ice, NH_4HSO_4 and $(NH_4)_2SO_4$ by coating the walls of a flow reactor with the reactant of interest. Alternatively the coating could be a liquid film flowing continuously on the sides of the flow tube: Hanson and Ravishankara (1991) used a wetted-wall flow tube to study the uptake of $ClONO_2$ and N_2O_5 to sulphuric acid (a reaction thought to be important to understand the chlorine budget in the atmosphere).

In the aerosol flow tube reactor the reactant surface of interest is in the form of aerosol particles. Typically an artificial aerosol is created and flowed into the main tube of the reactor and the gaseous molecules of interest enter the reactor tube through the injector tube. There are many examples of this type of flow tube, for example both Thornton

and Abbatt (2005b) and Badger et al. (2006) used this technique to look at the uptake of N_2O_5 (an important sink of NO_x) to various aerosol particles. Thornton and Abbatt (2005a) and Taketani et al. (2008) used this technique to study the uptake of HO_2 to aerosol particles, which is also the aim of this study.

2.2 Experimental Overview

This study uses an aerosol flow tube system to investigate the mass accommodation coefficient and the net uptake coefficient of HO_2 radicals to NaCl and $(NH_4)_2SO_4$ aerosol. Figure 2.1 shows a block diagram of the experiment.

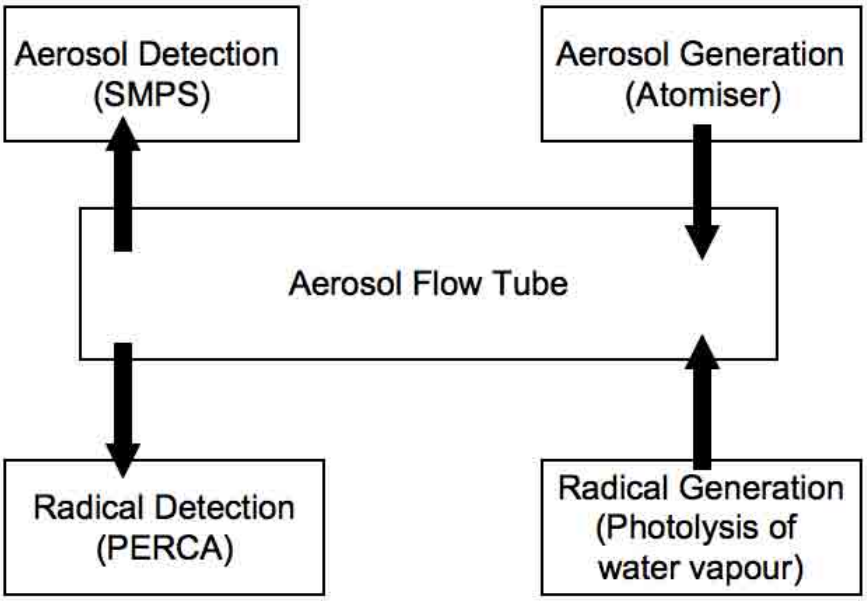

Figure 2.1: A block diagram showing an overview of the experimental system.

The relevant aerosol was created using an atomiser, the flow from the atomiser entered the main tube and mixed with a carrier gas. The aerosol distribution was characterised by a Scanning Mobility Particle Sizer (SMPS).

HO_2 radicals were created *in situ* by photolysis of water vapour and were injected into the main tube, where some were lost to aerosol particles. The position of the injector was varied to change the reaction time between the aerosol particles and the radicals in order to study the progression of the reaction. The concentration of HO_2 was monitored

throughout the experiment using a PEroxy Radical Chemical Amplifier (PERCA) and the rate of loss of HO_2 was determined using a pseudo-first order kinetic analysis.

Radicals were lost to the walls of the flow tube as well as to the aerosol, therefore two experiments were performed to determine the rate of loss of radicals to the aerosol. The first experiment was performed without any aerosol present. The radicals were injected into the flow tube, through which only the carrier gas was flowing. The loss of HO_2 was monitored and the rate constant for the observed loss of radicals to the walls of the flow tube, k_{walls}^{obs}, was determined. These experiments are termed *wall loss* experiments. The second experiment performed was to determine the rate constant for the total observed loss of radicals to the walls of the flow tube and to the aerosol particles, k_{total}^{obs}. The aerosol was mixed with the carrier flow in the main tube and radicals were injected into the main tube as before. k_{total}^{obs} could then be determined as a pseudo first order rate constant equal to the sum of the rate constant for loss of radicals to the walls of the tube, k_{walls}^{obs} and the rate constant for loss of radicals to aerosol particles, k_{aero} (i.e. k_{total}^{obs}= k_{walls}^{obs}+ k_{aero}). Experiments performed to determine k_{total}^{obs} (and thus k_{aero}) are termed *aerosol loss* experiments.

Once the rate constant for the loss of HO_2 to aerosol particles was determined the observed uptake coefficient, γ_{obs}, could be calculated using Equation 2.2 (where S_a is the total surface area of the aerosol particles and ω_{HO2} is the mean molecular speed of HO_2 molecules). Alternatively multiple experiments were performed to determined k_{aero} for varying values of the total surface area of the aerosol particles and γ_{obs} obtained from a regression analysis of a plot of k_{aero} against S_a.

$$\gamma_{obs} = \frac{4k_{aero}}{S_a \omega_{HO2}} \tag{2.2}$$

2.3 Aerosol Flow Tube

2.3.1 Description of the AFT

The Aerosol Flow Tube (AFT) consisted of a glass tube with inner diameter 6.5 cm and length 120 cm. A sliding Pyrex injector tube (2.5 cm diameter, 140 cm length) was held in the centre of the main tube by a supporting disc made of nylon. Figure 2.2 shows the flow tube setup.

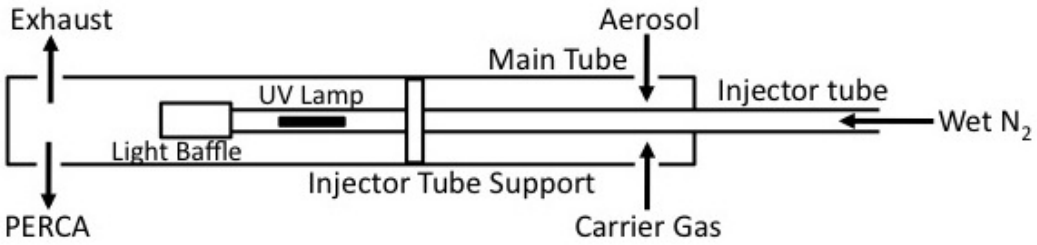

Figure 2.2: The aerosol flow tube (AFT). Aerosol particles are present in the main tube and radicals are injected into the main tube via the injector tube.

A UV pen-ray lamp (Ultra-Violet Products Ltd., $\lambda = 184.9$ nm) was positioned inside the injector tube and was used to produce radicals by photolysis of water vapour (see Section 2.4 for details). Pyrex glass blocks the transmission of UV light below approximately 280 nm (Moore et al., 2003) therefore light below this wavelength was not transmitted from the lamp into the main tube through the sides of the injector tube. A light baffle was placed on the open end of the injector tube, a number of offset holes in the light baffle allowed gas to escape from the injector tube, but blocked the light from doing so. The prevention of light entering the main tube prevents ozone from being created within the flow tube system.

The position of the injector was changed in order to vary the reaction time of the radicals and the aerosol within the AFT. Figure 2.3 shows the key distances in the AFT. The reaction distance, x, along with the velocity of the flow in the tube, was used to

determine the reaction time. The distance the injector protrudes into the main tube, y, was recorded throughout experiments; regular measurement marks were etched onto the injector tube to ease this process. A measurement of y was recorded rather than a direct measurement of x as it was a more accurately reproducible measurement. The reaction distance, x, was determined by subtracting the measured distance, y, from the distance from the entry point of the injector tube into the main tube to the PERCA inlet, z, which was usually a distance of 130 cm - this was the maximum distance the injector could protrude into the main tube i.e. $x = 0$. Note that this distance is longer than the length of the tube because there were Teflon supports holding the tube, which made the flow system slightly longer than the tube itself. The minimum distance the injector could protrude into the main tube was determined by the injector tube support. This was fixed to the injector tube at a distance of 30 cm, giving the longest possible reaction distance as 100 cm.

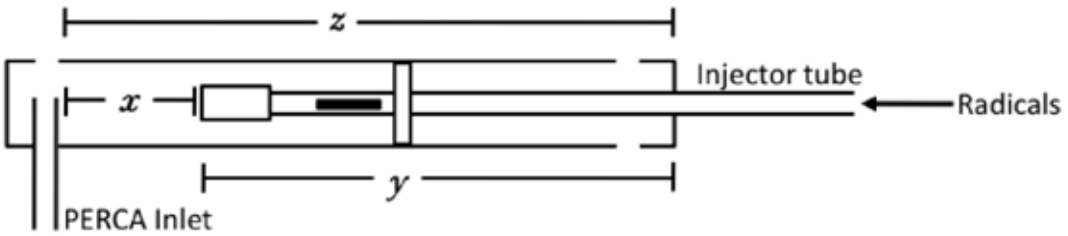

Figure 2.3: Key distances within the AFT. The injector position was changed to vary the reaction distance, x, within the AFT. The distance the injector protruded into the AFT, y, was measured and x was determined by subtracting this measurement from the total possible distance, z.

During the later part of this study the walls of the AFT were coated with halocarbon wax (Chemical Raw Materials Ltd, Halocarbon Wax 600) in order to reduce the loss of radicals to the walls of the AFT (Finlayson-Pitts and Pitts, 2000). Halocarbon wax is an unreactive material made from polymers of chlorotrifluoroethylene (PCTFE). The wax has a melting point of 57 °C so was melted using a heat gun. The melted wax was poured down the inside of the AFT and a heat gun was used to keep the wax liquid as the tube was slowly turned, producing a thin layer of wax on the walls of the AFT.

2.3.2 Flows within the AFT

Gas flows entered the AFT through 6 mm Teflon tubing, except the aerosol flow for which anti-static tubing was used to reduce the loss of aerosol. Nitrogen (BOC Gases, 99.9 % stated purity) was used as the carrier gas for the injector tube and air (BOC Gases) was used as the carrier gases for the main tube. Charcoal traps were used to remove hydrocarbon impurities from both gases and a silica trap was used on the nitrogen line to remove traces of water so that no radicals were created unless the water bubbler was in use (see Section 2.4 for details). Flows in this system were controlled using Mass Flow Controllers (MFCs) (Brooks Instruments; Model 5850S). The units used for flows were standard litres per minute (slm) or standard cubic centimetres per minute (sccm).

The AFT typically had a total flow of 11 slm which consisted of the carrier flow (a mixture of wet and dry air, total flow 4 slm), the injector flow (a mixture of wet and dry nitrogen, total flow 4 slm) and, during an *aerosol loss* experiment, the aerosol flow (air with entrained aerosol particles, 3 slm). During a *wall loss* experiment the carrier flow was increased to a total flow of 7 slm and there was no aerosol flow from the atomiser. Wet air and nitrogen were produced by bubbling the relevant gas through distilled water. The relative humidity of the system was varied by changing the ratio of wet and dry air making up the carrier flow in the main tube. The relative humidity was measured using a HygroPalm 2 monitor (Rotronic). Figure 2.4 shows the gas flows in and out of the AFT.

Laminar Flow within the AFT

The flow of the gases within the AFT must be properly understood in order to be able to analyse the experimental conditions correctly. As discussed previously (Section 2.1) laminar plug flow is assumed in order to analyse the flow tube data. A plug flow is a model for a flow with a constant velocity, in this case within a cylindrical tube. There is no mixing within plug flow so every parcel of gas entering the tube will be resident within it for the same amount of time. For a plug flow it is assumed that the velocity of the gas flow is constant across the diameter of the pipe. This is not the case in reality as

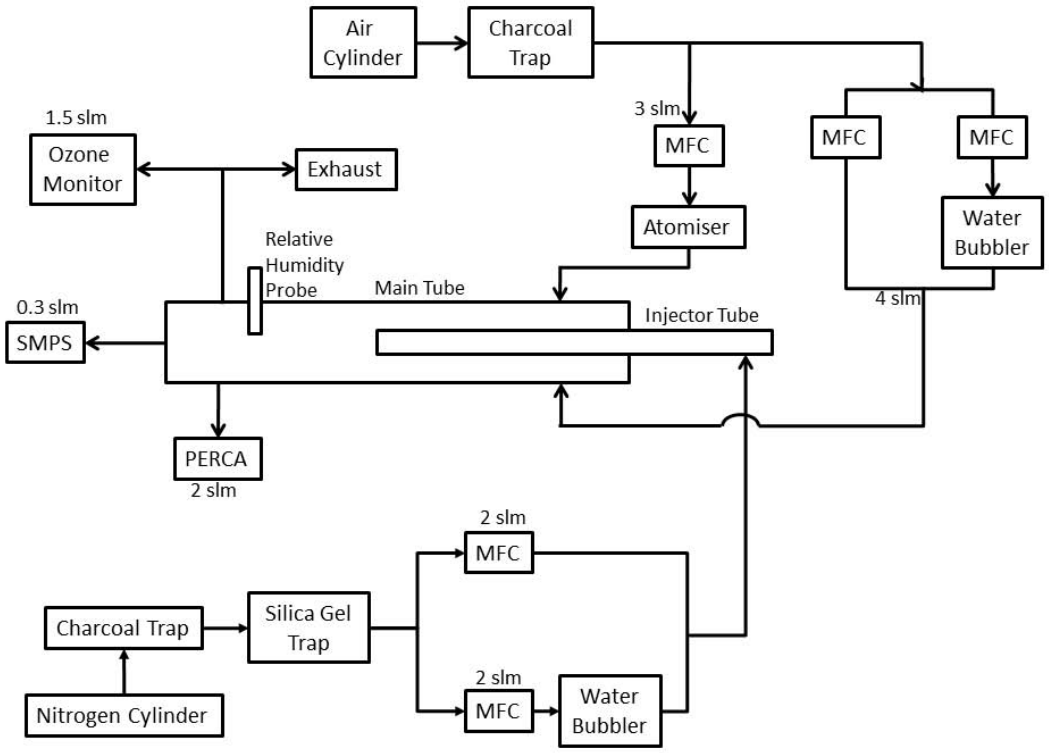

Figure 2.4: This diagram shows the gas flows in and out of the AFT. Flow rates are shown next to each MFC or, in the case of the air MFCs, the total flow into the tube from a group of MFCs is shown.

the friction on the walls of the tube slows the flow at the boundary between the gas and the tube walls, resulting in a parabolic velocity profile with the flow in the middle of the tube moving faster than the flow at the sides of the tube i.e. laminar flow. To determine whether a flow is laminar or turbulent (i.e. well mixed) the Reynolds number is used. The Reynolds number, Re, is a dimensionless quantity that gives a ratio of the inertial forces and the viscous forces of the system in question. For the flow of fluids within circular tubes it may be determined using Equation 2.3, where r is the radius of the tube and v is the velocity, ρ is the density and η is the viscosity of the gas flow (Bird et al., 2002).

$$Re = \frac{2rv\rho}{\eta} \tag{2.3}$$

If Re is less than 2100 (for a circular pipe, Bird et al. (2002)) then the flow is considered to be laminar. In this system the flow velocity was $5.52\,\mathrm{cm\,s^{-1}}$, the radius was

3.25 cm, the density of air is 1.195 kg m^{-3} and the viscosity of air is 18.2 µPa s (both at atmospheric pressure and 20 °C, Kaye and Laby (1986)), giving a Reynolds number of 236 and putting the flow firmly into the laminar region. This Reynolds number calculation neglects entrance and exit effects of the flow from the tube. Once the gas flow enters the tube it will travel a distance along the tube before laminar flow conditions are achieved; this distance is defined by the entrance length, Le, and is calculated by Equation 2.4 (Bird et al., 2002) using the diameter, D and the Reynolds number, Re. In this flow tube Le is determined as 54 cm.

$$Le = 0.035DRe \tag{2.4}$$

Mixing of the Flows within the AFT

The injector flow and the main tube flow take a finite time to mix, known as the mixing time, t_{mix}. If the mixing of the injector flow (containing the HO_2 radicals) into the main tube flow was due just to diffusion then the time taken for the HO_2 molecules to be evenly distributed across the radius of the main tube can be determined using Equation 2.5 (Keyser, 1984), where r is the radius of the main tube and D_g is the diffusion constant for HO_2 (0.25 cm s^{-1}, Mozurkewich et al. (1987)).

$$t_{mix} = \frac{r^2}{5D_g} \tag{2.5}$$

In this case t_{mix} was calculated as 8.45 s, which is equivalent to a distance of 46 cm in the AFT. In reality the mixing distance was less than this as the flow from the injector had a high velocity due to its exit from the injector into the main tube through a small hole in the light baffle. The high velocity entering the main tube created a turbulent region and lead to a faster mixing time than expected through diffusion alone. The mixing time was experimentally found to be approximately 5 s (see Chapter 4 for more details).

In order to balance the mixing of the flows, the entrance length for the flow to become

laminar and the sensitivity of the PERCA (which limited the longest usable reaction time), measurements of the HO_2 decay were performed at reaction distances between 25 cm and 90 cm, which lead to reaction times between the aerosol and the radicals of 5 s to 16 s.

2.4 Generation and Characterisation of HO_2 Radicals

2.4.1 Generation of HO_2

In this study radicals were created *in situ* in the injector tube. A UV mercury lamp (Ultra-Violet Products Ltd., 184.9 nm) was placed within the injector tube 20 cm away from the injection point into the AFT. 2 slm of nitrogen was bubbled through water to produce water vapour; an additional flow of dry nitrogen (2 slm) was also added to the injector tube to give a total flow in the injector of 4 slm. The ratio of the flows kept the injector tube relative humidity around 50 %. Nitrogen was used as the carrier gas for the injector tube instead of air (as used in the main tube) because oxygen in the air photolyses to form ozone at the same wavelength as water vapour is photolysed; ozone was not wanted within the AFT as it would perturb the HO_2 decay. The injector tube was made of Pyrex and a light baffle was added to the end of it to prevent any UV light from penetrating to the AFT (and thus producing ozone). The water vapour was photolysed by the UV light as it flowed through the injector tube (Reaction R 2.1) to produce H atoms and OH radicals. The H atoms were injected into the centre of the AFT tube where they mixed with oxygen (present in the air carrier gas in the AFT) to produce HO_2 *in situ* in the main tube (Reaction R 2.2).

$$H_2O + h\nu - \quad OH + H \tag{R 2.1}$$

$$H + O_2 + M - \quad HO_2 + M \tag{R 2.2}$$

The aim of this study was to investigate the loss of HO_2 radicals to aerosol, so it was important to ensure that only HO_2, rather than a mixture of OH and HO_2, was present in the AFT. The PERCA detects both HO_2 and OH, so if there was a mixture of radicals the concentration of both would be detected, giving an incorrect loss rate for HO_2 to aerosol. It was thought that the H atoms escaped the injector tube to react with oxygen in the main tube to produce HO_2, whereas the OH radicals were lost to the walls of the injector and so did not enter the AFT. To demonstrate that this was the case excess CO was added to the injector tube as CO converts OH to H via Reaction R 2.3.

$$OH + CO - \quad H + CO_2 \tag{R 2.3}$$

Once CO was added to the injector tube three possible outcomes could occur; the concentration of HO_x radicals detected by the PERCA would increase, decrease or stay the same with respect to the concentration of radicals detected when CO is not present. If the concentration detected by the PERCA increased it would imply that the conversion of OH to H allowed more radicals to exit the injector tube and so OH radicals were lost to the walls of the tube faster than H radicals. If the concentration decreased it would imply that the conversion of OH to H allowed less radicals to exit the injector tube and so H atoms were lost to the walls of the tube faster than OH radicals. Finally, if the concentration stayed the same then it would imply that both are lost to the walls equally. The results of an experiment to determine this are shown in Figure 2.5. 0.01 slm CO was added to the injector tube for 10 min, with the PERCA sampling the AFT. After 10 min the CO was removed and the PERCA sampled the AFT as before. This process was repeated three times. It can be seen in Figure 2.5 that the first time CO was added a large increase in HO_x was detected by the PERCA - indicating that more H atoms had escaped the injector tube and entered the AFT. The second time that CO was added a smaller increase in HO_x was seen (relative to the HO_2 detected without CO present). However, there was a large increase in HO_x detected between the first experiment and the next two, so perhaps the CO was not all flushed out of the injector tube within the

10 min that it was not flowing, thus causing an increase in HO_2. This experiment suggests that CO does increase the concentration of HO_x detected by the PERCA, which in turn suggests that OH radicals are lost before it reaches the main tube, but H atoms are not.

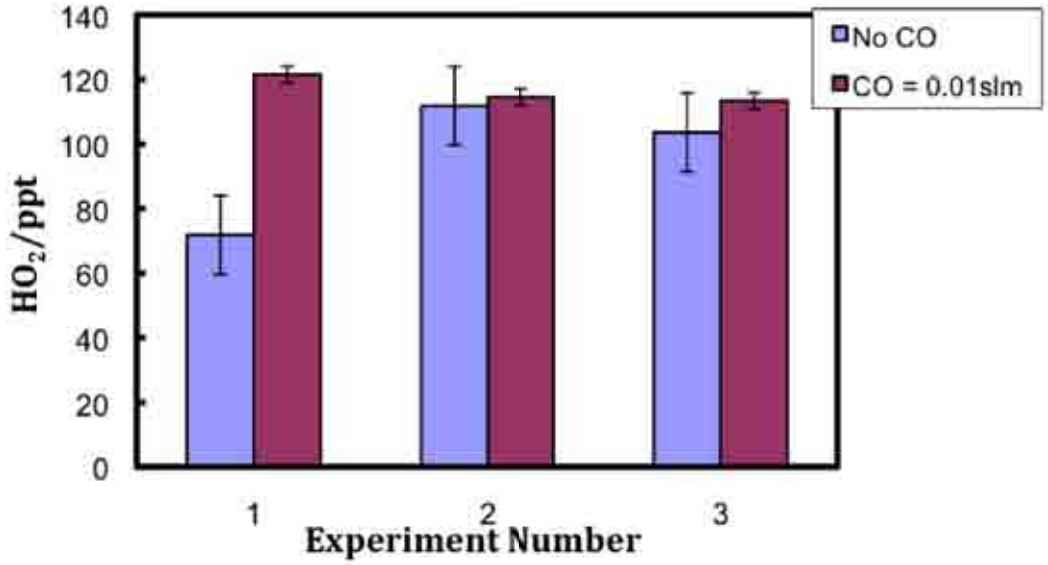

Figure 2.5: This graph shows the results of adding CO to the injector tube. Slightly more HO_x radicals were detected by the PERCA when CO was added to the injector tube.

2.4.2 Initial HO_2 Concentration

The concentration of HO_2 in the boundary layer troposphere is approximately 1×10^8 molecules cm^{-3} (4 ppt) (Heard and Pilling, 2003). This study attempted to work at these concentration levels in order to mimic atmospheric conditions as closely as possible. It is good laboratory practice to mimic atmospheric conditions because the results can then be easily applied to explain observations and model predictions.

Another consideration for choosing the initial concentration of HO_2 was the self-reaction of HO_2. The self-reaction of HO_2 occurs via both a bimolecular (Reaction R 2.4) and a termolecular (Reaction R 2.5) process at temperatures around 298 K.

$$HO_2 + HO_2 - \quad H_2O_2 \qquad \text{(R 2.4)}$$

$$HO_2 + HO_2 + M - \quad H_2O_2 + M \qquad \text{(R 2.5)}$$

The recommended rates of reactions are $k_{R2.4} = 1.6 \times 10^{-12}\,\mathrm{cm^3\ molecule^{-1}\ s^{-1}}$ and $k_{R2.5} = 5.2 \times 10^{-32}\ [\mathrm{N_2}]\,\mathrm{cm^3\ molecule^{-1}\ s^{-1}}$ at 298 K (Atkinson et al., 2004).

The rate of the self reaction is dependent on the concentration of water vapour present (Atkinson et al., 2004). This dependence is thought to be due to a HO_2-H_2O complex (Lii et al., 1981; Kircher and Sander, 1984; Cox and Burrows, 1979). The complex stabilises the intermediate formed during the self reaction of HO_2, shifting the equilibrium of the reaction towards the products of the reaction. To account for the self reaction $k_{R2.4}$ and $k_{R2.5}$ must be multiplied by the factor $(1+1.4 \times 10^{-21}[\mathrm{H_2O}]\exp(2200/T))$ (Atkinson et al., 2004).

At high concentrations (1×10^{10} molecules $\mathrm{cm^{-3}}$) the rate of loss of HO_2 due to its self-reaction is $0.0530\,\mathrm{s^{-1}}$ (Atkinson et al., 2004) (at 50% relative humidity), whereas at atmospheric concentrations (1×10^{8} molecules $\mathrm{cm^{-3}}$) the rate of loss due to the self reaction is $0.0005\,\mathrm{s^{-1}}$ (at the same relative humidity). The expected rate of loss of HO_2 to aerosol particles of NaCl and $(NH_4)_2SO_4$ is between 0.01 and $0.3\,\mathrm{s^{-1}}$ (Taketani et al., 2008) at approximately the same relative humidity and total surface area of aerosol particles of the order of $1 \times 10^{-4}\,\mathrm{cm^2\,cm^{-3}}$. The rate of the self-reaction when the concentration of HO_2 is 1×10^{10} molecules $\mathrm{cm^{-3}}$ is 20 % of the total loss of HO_2 (i.e. the loss of HO_2 due to both the self-reaction and the loss to aerosol) when aerosol is present, whereas at atmospheric concentrations the self-reaction is only 0.002 % of the total reaction.

Most previous studies that investigated heterogeneous reactions of HO_2 to atmospheric aerosol used high concentrations of HO_2. Gershenzon et al. (1995) used approximately 1×10^{11} molecules $\mathrm{cm^{-3}}$ to study the uptake of HO_2 to an NaCl coated reactor and Thornton and Abbatt (2005a) used $2.5 - 5 \times 10^{10}$ molecules $\mathrm{cm^{-3}}$ to study the uptake of HO_2 to particles of H_2SO_4 and $(NH_4)_2SO_4$. However Taketani et al. (2008) used boundary layer tropospheric concentrations of 1×10^{8} molecules $\mathrm{cm^{-3}}$ when determining the uptake of HO_2 to NaCl and $(NH_4)_2SO_4$ aerosol particles.

The initial concentration of HO_2 radicals within the AFT depended on the concentration of water vapour within the injector tube, the radiant power of light used for the

photolysis and the residence time in the illuminated region. The concentration of water vapour was controlled by changing the ratio of the wet and dry nitrogen flow within the injector tube, the flows were usually kept equal, giving a relative humidity within the injector tube of approximately 50 %.

The radiant power of light used for the photolysis of the water vapour was varied either by changing the operating current of the lamp or by partially covering the lamp with aluminium foil. Throughout this study the initial concentration of HO_2 in the AFT varied from 1×10^9 molecules cm^{-3} to 5×10^9 molecules cm^{-3} with an average of approximately 4×10^9 molecules cm^{-3}. This concentration is one order of magnitude larger than atmospheric concentrations of HO_2 but was used because it was found to give the best balance between keeping the concentration as close to atmospheric conditions as possible, while still being able to detect the decay of radicals reliably.

2.5 Detection of HO_2 Radicals: PERCA

HO_2 was detected using a PEroxy Radical Chemical Amplifier (PERCA). The instrument was built during this study and its design and characterisation is detailed in Chapter 3.

2.6 Generation of Aerosol

Artificial aerosol were used in this study. Sodium chloride (NaCl) was used as a proxy for marine aerosol, while ammonium sulphate ($(NH_4)_2SO_4$) was used a proxy for urban aerosol (Hinds, 1999). Solutions of these salts were made up, at various concentrations, in distilled water. The solutions were made into polydisperse aerosol using a constant output atomiser (TSI: Model 3076). The atomiser operates by flowing a high-velocity jet of air perpendicular to a liquid flow. The high-velocity jet was formed by flowing 3 slm of air through a small orifice (0.0135 inch diameter). The aerosol exited from the top of the atomiser, while any large droplets impacted on the walls of the atomiser and

excess liquid fed back into the liquid feed bottle. This recirculation of liquid ensured that the concentration of liquid in the feed bottle was constant, so the atomiser produced a constant distribution of aerosol over time. Figure 2.6 shows a schematic of the atomiser. Aerosol produced by the atomiser were highly charged so to minimise losses of aerosol anti-static tubing was used for any aerosol flow.

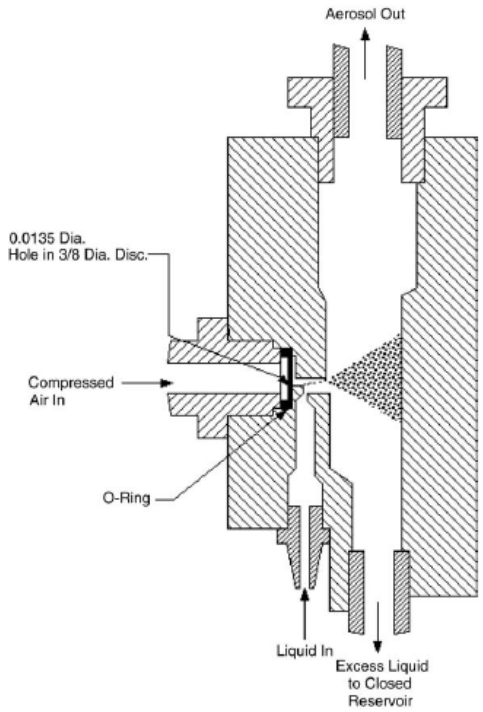

Figure 2.6: A schematic of the atomiser assembly block (TSI, 2008a).

The aerosol was either flowed directly into the main tube for the investigation of radical uptake to 'wet' aerosol or flowed through a diffusion dryer (TSI: Model 3062) prior to entry into the main tube for the investigation of radical uptake to 'dry' aerosol. Whether the aerosol particle is termed as 'wet' or 'dry' depends nominally on the relative humidity of the gas the particles are suspended within; particles suspended in a gas at a low relative humidity will be solid or 'dry' - as the relative humidity increases they will take water into the bulk of the particle, transforming the particle into a droplet or making it 'wet'. The relative humidity at which the droplet is formed is called the deliquescence relative humidity. The same process occurs in reverse - if a particle is suspended in a gas

at a high relative humidity it will be a droplet - as the relative humidity drops it will lose water until it reaches a certain relative humidity, whereupon it crystallises and becomes a solid particle. This relative humidity is called the efflorescence relative humidity. However the system is not as simple as described: a hysteresis effect is present so the deliquescence relative humidity and the efflorescence relative humidity are not the same. If a 'wet' particle is dried out it will not become a 'dry' particle until the efflorescence relative humidity, which is usually lower than the deliquescence relative humidity. Likewise a 'dry' particle will not become a droplet until it has reached the deliquescence relative humidity, which is often higher than the efflorescence relative humidity (Hinds, 1999). This is effect is shown in Figure 2.7. In this study all aerosol was created from solution using an atomiser, meaning that they all started at 100 % relative humidity. If applicable the aerosol was then dried out either by passing through a diffusion dryer or by mixing with dry air.

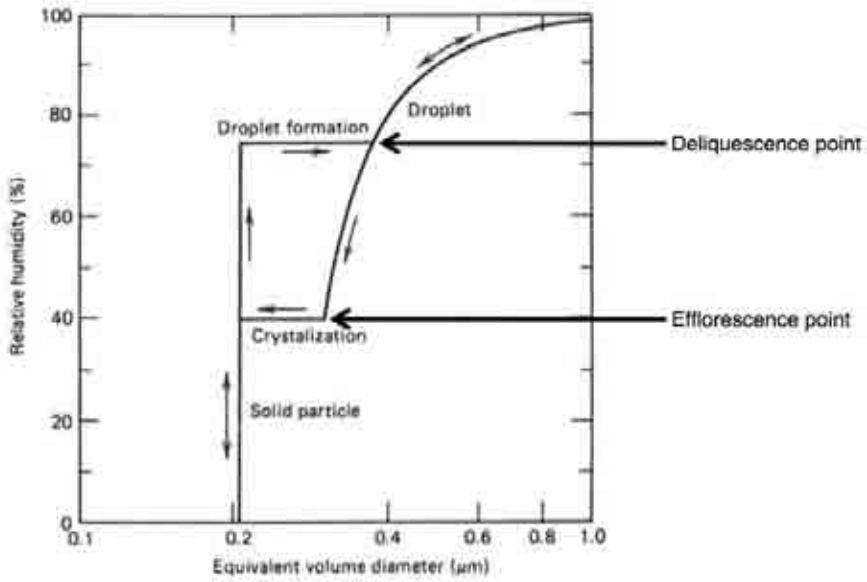

Figure 2.7: Relative humidity versus equivalent volume particle diameter. This shows how the particle grows with increasing relative humidity and shrinks with decreasing relative humidity, it also shows the hysteresis effect that occurs during these processes (Hinds, 1999). The efflorescence and deliquescence points are marked on the diagram.

The concentrations used for the salt solutions were initially based on previous studies. Taketani et al. (2008) used 0.02 to 0.05 M solutions of both $(NH_4)_2SO_4$ and NaCl

while Thornton and Abbatt (2005a) used concentrations of 0.0005 to 0.005 M for their $(NH_4)_2SO_4$ uptake experiments, they did not study the uptake to NaCl. Gershenzon et al. (1995), Remorov et al. (2002) and Loukhovitskaya et al. (2009) have also studied the uptake of HO_2 to NaCl but these studies focused on a thin film coating of the salt on the walls of the reaction vessel, rather than creating particles as was the case in this study. A study by Cooper and Abbatt (1996) looked at the uptake of HO_2 to $(NH_4)_2SO_4$, but again this was to a solid film rather than to aerosol particles. This study used both $(NH_4)_2SO_4$ and NaCl solution concentrations between 0.001 and 0.05 M, which covered the full range of data already studied by Taketani et al. (2008) and Thornton and Abbatt (2005a); the concentration of the salt solution determined the size distribution of the particles produced by the atomiser.

Copper doped aerosol was created in order to determine the mass accommodation coefficient, α. Transition metal chemistry has been discussed in detail in Chapter 1. In short, copper will catalyse the conversion (and thus loss) of HO_2 to H_2O_2 if it is the aqueous phase. α is determined as the probability that a gas molecule will be taken up by the particle if a collision has occurred at the surface of the particle. Compare this to γ, which is the net loss of the gas to the particle; this includes both the gains and losses of the gas molecules with regards to the aerosol particle. This means that the mass accommodation coefficient can be described as the maximum possible loss of the gas molecule to the particle and gives an upper limit to γ. By using copper to catalyse the aqueous reactions within the bulk of the particle an equilibrium is avoided between the particle bulk and the surrounding environment, thus the rate at which the radicals are taken up into the aqueous phase can be measured. In this study $CuSO_4$ was added to the salt solution at a molar ratio of between 1 – 3 %, which is comparable to the study by Taketani et al. (2008), who used a 5 % ratio and Thornton and Abbatt (2005a), who used 2 %.

2.7 Detection of Aerosol

A monodisperse aerosol is described by its particle diameter and the number of particles in a particular volume of gas. Unfortunately most aerosol is polydisperse and thus their size distribution and concentration is described in a statistical manner instead. Empirically it has been seen that most aerosol produced from a single source display a lognormal distribution (see Figure 2.8), which is a skewed distribution, rather than a symmetrical normal distribution seen with monodisperse aerosol (Finlayson-Pitts and Pitts, 2000).

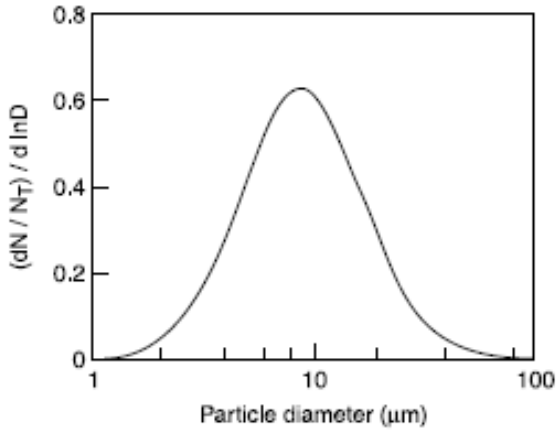

Figure 2.8: A lognormal size distribution. Most polydisperse aerosol coming from a single source can be described statistically using this distribution. (Finlayson-Pitts and Pitts, 2000)

In this study the aerosol distribution was measured using a Scanning Mobility Particle Sizer (SMPS, TSI Inc.: Model 3936). In summary, an SMPS samples a polydisperse aerosol, which is then charged to a known distribution by a neutraliser and passed through a Differential Mobility Analyser (DMA). Within the DMA is an electric field, which is used to obtain only aerosol with a particular charge mobility and results in a monodisperse aerosol from the exit of the DMA. The particles in this monodisperse aerosol are counted by a Condensation Particle Counter (CPC) in order to determine the number of particles of one particular size. The electric field within the DMA varies and the number of particles are counted over a range of electric fields (and thus particle sizes). The output from the SMPS provides a number count of particles over a range of sizes. The surface area or volume of the particles can also be determined from this, but such calculations assume the

particles are spherical, which is not always true - for example NaCl particles are known to be cubic when in crystalline form.

A block diagram of the SMPS is shown in Figure 2.9, the next few sections describe each step in the SMPS in more detail.

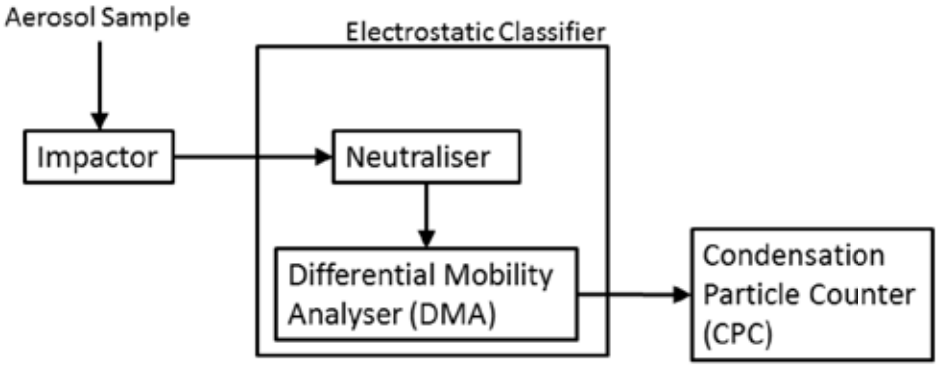

Figure 2.9: A schematic of the Scanning Mobility Particle Sizer (SMPS), consisting of an impactor, an Electrostatic Classifier (EC) and a Condensation Particle Counter (CPC). The SMPS measures the size distribution (number, surface area or density weighted) of aerosol particles. The individual components are controlled by the Aerosol Instrument Management (AIM) software, provided by TSI Inc., which also analyses the raw data and produces corrected size distributions.

Aerosol produced in this study were polydisperse aerosol, so a lognormal distribution was used to characterise them. Determination of γ involves the total surface area available for HO_2 uptake, so the surface area of the aerosol particles was measured. The diameter of particles at the peak of the aerosol particle distribution was also used during the analysis. This, and other statistical parameters (such as the geometric standard deviation), are recorded by the SMPS.

Impactor

The impactor removes large particles from the aerosol flow before it enters the SMPS system. An impactor is a very simple device; it consists of a flow of aerosol through a nozzle set perpendicular to a plate, as shown in Figure 2.10. Particles within the aerosol flow which are small enough to follow the gas streamlines as they curve around the 90° bend will do so and will exit the impactor with the rest of the gaseous flow. Larger

particles will impact at the surface and be lost from the flow. The impactor used in this study had a 0.0508 cm nozzle diameter and so removed particles greater than 1 µm. This is a typical cut-off point for characterising aerosol in the atmosphere and was used in this study as the usual particle diameter of particles produced were less than 400 nm diameter, with a peak diameter of around 100 nm. During the early part of this study the impactor was used at the start of the SMPS; however later in the study it was realised that the impactor could have removed large aerosol particles that had contributed to the uptake of radicals. Experiments were performed measuring the same aerosol with and without the impactor present. No discernible change was seen in the aerosol distribution, which suggested that large particles were not entering the AFT from the atomiser (or if they were they were impacting on the walls of the AFT, as the aerosol flow entered the tube perpendicular to the desired flow direction).

2.7.1 Neutraliser

After the aerosol passes through the impactor it enters the neutraliser. Aerosol exiting the atomiser are highly charged, which is undesirable within the SMPS system because highly charged aerosol is more easily lost to surfaces and is more difficult to characterise as the SMPS system is based on particle mobility in an electric field, which is strongly dependent on the charge of the particle. The neutraliser uses radioactive Krypton-85 to ionise the carrier gas into positive and negative ions. Particles with a high charge lose

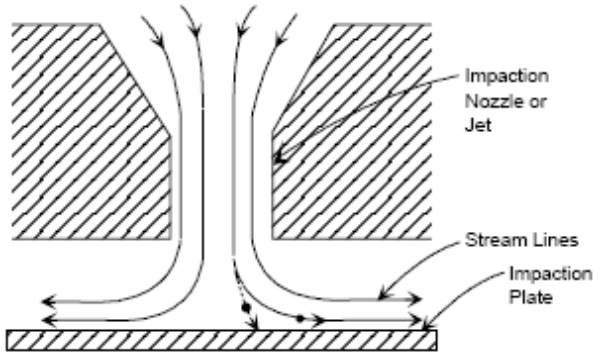

Figure 2.10: A schematic of a conventional impactor. (Hinds, 1999)

their charge by collision with these ions, while particles with a small charge gain charge. After a short period of time ($\approx 2\,\mathrm{s}$ for this neutraliser) equilibrium was achieved and the aerosol distribution was in a known bipolar charge distribution. Wiedensohler (1988) used the theory of Fuchs (1963) (backed up by experimental data (Wiedensohler et al., 1986)) to calculate the fraction of particles in a neutralised distribution that will be charged, and to what degree they will be charged. These calculations account for the small fraction of doubly (or multiply) charged particles found within aerosol distributions.

Differential Mobility Analyser

Once the particles pass through the neutraliser they enter the Differential Mobility Analyser (DMA). The DMA consists of two concentric metal cylinders (see Figure 2.11). The outer cylinder is grounded, while the inner one (the rod) scans through a range of negative voltages from $0\,\mathrm{V}$ to $-10\,000\,\mathrm{V}$. In this way a varying electric field is set up between the two cylinders. The aerosol flow ($0.3\,\mathrm{slm}$) enters the DMA and flows just inside the walls of the outer cylinder. A sheath air flow of $3\,\mathrm{slm}$ is formed by the recirculation of the sample air (filtered to remove any particles) within the SMPS system and the flow is kept constant using a critical orifice. The sheath air flows in the annular space between the rod and aerosol flow; the sheath air and the sample flows are laminar, so they do not mix within the DMA. As the voltage on the rod scans through the negative voltage range different positively charged particles are attracted to it and move through the sheath flow. The particles either impact on the rod (and are lost) or escape through a small slit at the bottom of the rod, forming the monodisperse flow that exits the DMA. Any excess sheath or aerosol flow exits via the bypass flow. The particles attracted to the rod for a particular voltage depend on their electrical mobility, the flow rates within the DMA and geometry of the DMA. For each voltage on the rod only particles within a narrow range of electrical mobilities escape, forming a monodisperse aerosol flow at the exit of the DMA. As the particle diameter is indirectly proportional to the electrical mobility, the DMA scans through a range of particle diameters as the voltage changes. In this

study each scan of the DMA took 120 s. The neutraliser and the DMA are combined as one instrument - the Electrostatic Classifier (TSI Inc., Model 3080).

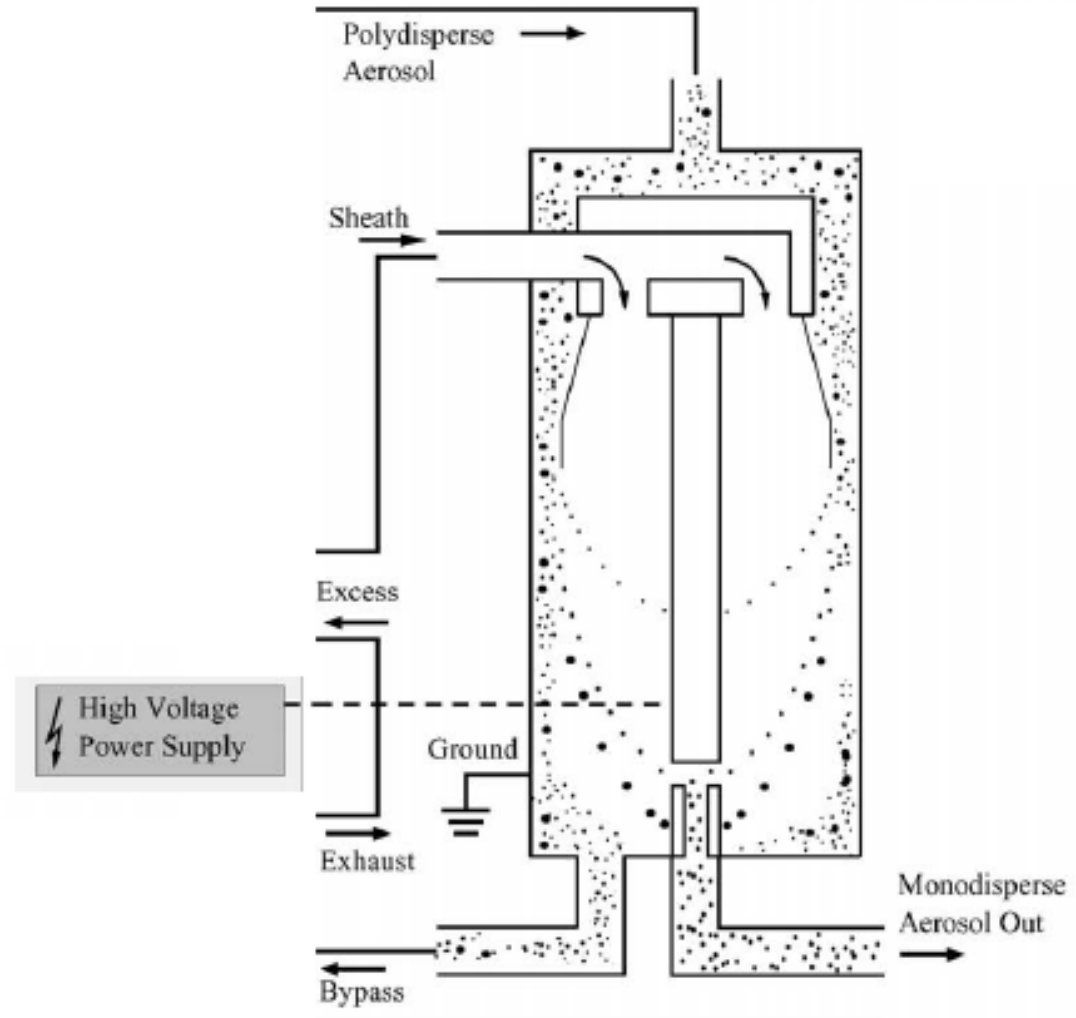

Figure 2.11: A schematic of a Differential Mobility Analyser. Polydisperse aerosol enters at the top. The inner cylinder is negatively charged, so that positively charged particles move towards it, leading to the particles being classified according to their electrical mobility and a monodisperse aerosol being produced. (TSI, 2008b)

Condensation Particle Counter

The monodisperse flow from the DMA enters the Condensation Particle Counter (CPC) where the particles in the flow can be counted. The CPC is an optical counter; particles pass the optical viewing area, an area along the sample line where light from a laser or other source is focused by condenser lenses. When each particle passes this area it

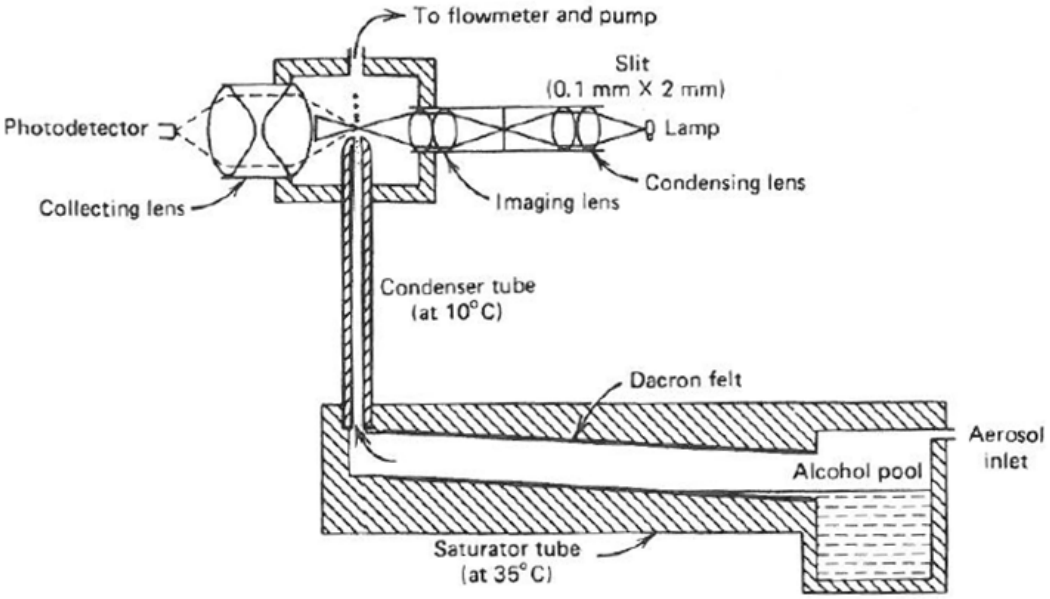

Figure 2.12: A schematic of a Condensation Particle Counter (CPC). Aerosol particles are grown to a optically detectable size by the condensation of butanol. The particles then pass a viewing area, where they scatter light to produce a pulse. The frequency of the pulses can be used to determine the concentration of aerosol particles. (Hinds, 1999)

will produce a pulse due to light scattering. Using the frequency of these pulses the concentration of particles in the sample can be calculated. For an optical counter to be used the particles must be large enough to be detectable by this method ($>\approx 0.11\,\mu m$). A heterogeneous condensation process is used to increase particle size so that optical counting is possible even for the smaller particles. Inside the CPC is a reservoir of butanol (see Figure 2.12 for a schematic), above which the aerosol flow passes. The aerosol plus butanol laden air then flows past a cooling jacket which promotes condensation of butanol onto the particles. Typically particles are expected to grow to a couple of micrometers diameter. In this study a 3022A model (TSI Inc.) CPC was used, the smallest particle it detects is 7 nm.

2.8 Summary

This chapter has described in detail the particular set-up of this aerosol flow tube system. The creation of HO_2 by UV photolysis of water has been discussed, including the discussion of producing HO_2 rather than a mixture of HO_2 and OH. Measurements of HO_2 were made using a custom built PERCA, which is described in detail in the next chapter. The creation of aerosol using an atomiser has been described - characteristics of the aerosol created is described in Chapter 5. The aerosol is characterised using an SMPS system, the theory of which has been described briefly.

CHAPTER 3

PEROXY RADICAL CHEMICAL AMPLIFIER (PERCA)

3.1 Introduction

This chapter describes the development of the PEroxy Radical Chemical Amplifier (PERCA), which was used in this study to measure the concentration of HO_2 within the AFT. A summary of peroxy radical measurement techniques is given, followed by a detailed introduction to the PERCA measurement technique. Next the implementation of the PERCA used within this study is described, along with the calibration technique used for the PERCA. The analysis of the data from the PERCA is shown, with typical data used as an example. Finally the PERCA is characterised in order to obtain the maximum sensitivity from it.

3.2 Peroxy Radical Measurement Techniques

Peroxy radicals (HO_2 and RO_2) are present in the troposphere at low concentration levels (1×10^8 molecules cm^{-3} in a clean environment) and have a short chemical lifetime (a few minutes). This means that measurement of these radicals must be sensitive to low concentrations and short time scales. A number of techniques have been used to determine concentrations of peroxy radicals in the troposphere.

The first estimates of HO_2 were made using an indirect method of measurement (Parrish et al., 1986). A photostationary state is quickly set up in the daytime atmosphere, with the steady state concentration of ozone being determined by the Leighton Equation (Equation 1.1). Tropospheric measurements have shown that the Leighton Equation underestimates the amount of ozone present in the troposphere, implying there must be a missing chemical process. This process could be the transformation of NO to NO_2 by a peroxy radical. If this process is added to the stationary state process, and atmospheric measurements of NO, NO_2 and O_3 are taken, the concentration of peroxy radicals can be determined using Equation 3.1 (where k is defined as the species weighted average rate for either HO_2 or RO_2 with NO). Obviously this technique only gives an estimate of the concentration of peroxy radicals in the atmosphere and does not distinguish between different radicals or other processes which could also be occurring.

$$[\mathrm{O_3}] = \frac{J_{\mathrm{NO_2}}[\mathrm{NO_2}]}{k[NO]} \tag{1.1}$$

$$[RO_2] = \frac{k}{k'}(\frac{J_{NO2}[NO_2]}{k[NO]} - [O_3]) \tag{3.1}$$

To date the only direct measurement of HO_2 is that by Mihelcic et al. (1990) using Matrix Isolation Electron Spin Resonance (MIESR) (Heard et al., 2006). This technique consists of trapping the radical on a cold finger (a solid matrix, such as ice), which is then analysed using ESR. The sample is a direct method, but has long sampling times (approximately 30 min) and the samples must be kept frozen and analysed in a laboratory, making field measurements difficult. The ESR method can be used to determine other species (such as various RO_2) simultaneously. This method detects HO_2 specifically, whereas other techniques discussed determine the sum of HO_2 and RO_2.

Other measurement techniques use chemical conversion methods to detect HO_2. Techniques used to detect OH are often used to detect HO_2 by conversion of HO_2 to OH via reaction by NO ($HO_2 + NO - \quad OH + NO_2$) (Heard and Pilling, 2003). A Laser Induced

Fluorescence (LIF) technique is one which has been used to detect HO_2 (Creasey et al., 1997; Kanaya et al., 2001; Faloona et al., 2004). The LIF technique is a resonance florescence method, with a low pressure optical cell. A tuneable light at a wavelength of 308 nm is used to excite the sample and (typically) a Photo-Multiplier Tube (PMT) is used to detect the florescence.

Chemical amplifier techniques have also been used to detect HO_2. The principle of the method is to convert the HO_2 radical into a species which is more easily detected. The difference between this method and a direct chemical conversion method is that a chain of reactions is set up which reforms HO_2 and amplifies the signal from the HO_2 radical. One technique which uses this amplifying method is the RO_x Mass Spectrometer (ROxMAS). The reactions employed by this instrument are shown in Reaction R 3.1 – R 3.4 and H_2SO_4 is detected using Chemical Ionisation Mass Spectrometry (Hanke et al., 2002).

$$HO_2 + NO - \quad OH + NO_2 \tag{R 3.1}$$

$$OH + SO_2 + M - \quad HOSO_2 + M \tag{R 3.2}$$

$$HOSO_2 + O_2 - \quad SO_3 + HO_2 \tag{R 3.3}$$

$$SO_3 + 2\,H_2O - \quad H_2SO_4 + H_2O \tag{R 3.4}$$

The Peroxy Radical Chemical Amplifier uses a similar chemical conversion and amplification technique as the ROxMAS and has been used to detect the sum of HO_2 and RO_2 on recent field campaigns (e.g. Clemitshaw et al. (1997); Fleming et al. (2006)). This method will be explained in detail in the next section as it is the detection method used in this study. It was chosen due to its high sensitivity yet low complexity compared to other currently established methods of detection.

3.3 PERCA Theory

3.3.1 Introduction to the PERCA System

The PERCA technique is used to detect atmospheric levels of gas-phase peroxy radicals. It was first developed by Cantrell and Stedman (1982) and has been improved by various research groups since then (Cantrell et al., 1984; Hastie et al., 1991; Newman, 1993; Cantrell et al., 1996; Clemitshaw et al., 1997). The PERCA technique has been used in numerous field projects to detect ambient peroxy radicals in the atmosphere (e.g. Cantrell et al. (1984); Arias and Hastie (1996); Carslaw et al. (2002); Green et al. (2003); Fleming et al. (2006)).

The PERCA is an indirect measurement of HO_2; the technique chemically converts HO_2 and RO_2 radicals to NO_2 molecules. NO_2 measurement techniques are well established and there are many readily available instruments to detect NO_2. The PERCA system also amplifies the HO_2 concentration, so although concentrations of atmospheric HO_2 are low (1×10^8 molecules cm^{-3}), the NO_2 signal detected is higher, making measurements easier and more reliable. The measurements are modulated; a background mode measures the background levels of NO_2, while the measurement mode records the additional NO_2 produced by the conversion and amplification of HO_2 as well as the background levels of NO_2. In this way any interferences in the NO_2 measurements (e.g. by ozone) will be accounted for.

3.3.2 Reactions within the PERCA

The methodology of the PERCA is based upon Reactions R 3.5–R 3.7.

$$HO_2 + NO - \quad OH + NO_2 \tag{R 3.5}$$

$$OH + CO - \quad CO_2 + H \tag{R 3.6}$$

$$H + O_2 + M - \quad HO_2 + M \qquad \text{(R 3.7)}$$

HO_2 is sampled and enters a reaction chamber. NO is present in this chamber and is oxidised by HO_2 to form NO_2; OH is also produced by this reaction (R 3.5). OH reacts with CO (also present in the reaction chamber) to produce an H atom, which reacts with O_2 to reform HO_2 (R 3.7). This HO_2 radical can then react with NO (R 3.5) to restart this process and a repeating cycle occurs. Each time Reactions R 3.5 – R 3.7 occur an NO_2 molecule is formed, amplifying the HO_2 signal many times (typically 200 (Clemitshaw et al., 1997)). Measurements of NO_2 are well established (Heard et al., 2006), so the conversion of HO_2 to NO_2 means that indirect measurements of HO_2 can be made using one of the many commercially (or other) available NO_2 detection systems. One example of an NO_2 detection system is a chemiluminescence technique which measures the light produced when an excited NO_2 molecule losses energy to drop to the ground state. This technique is an indirect method, with the conversion of NO_2 to NO needed before the excited NO_2 molecule is produced by reaction with O_3 (Heard et al., 2006).

The PERCA technique uses a modulation method. If CO is present in the reaction chamber the amplification process occurs (measurement mode), but if CO is not present no amplification occurs and a background measurement of NO_2 is recorded. The difference in the NO_2 concentration recorded between the two modes is used to determine the concentration of HO_2. This modulation removes any interference in the NO_2 measurements (for example O_3 interferes with some NO_2 detection techniques). It should also be noted that the OH radical and RO_2 radicals (where R is a hydrocarbon) can also start the chain process, leading to the detection of these radicals as well as HO_2. (It was assumed that neither RO_2 or OH was present in this AFT system, so only HO_2 was detected.)

To determine the concentration of HO_2 from the NO_2 measurement the amount of amplification must be known. The number of times the cycle repeats is known as the Chain Length (CL) and is dependent on the ratio of the rate of the chain reactions (R 3.5 – R 3.6) to the rate of termination reactions within the reaction chamber (R 3.8 – R 3.12) as shown in Equation 3.2. RO_2 losses also occur but as RO_2 is converted to HO_2

after the first step the HO_2 termination reactions dominate.

$$\text{Chain Length} = \frac{\text{Rate of chain process reactions}}{\text{Rate of termination reactions}} \tag{3.2}$$

$$\mathrm{OH + NO + M} - \quad \mathrm{HONO + M} \tag{R 3.8}$$

$$\mathrm{OH + walls} - \quad \mathrm{non{-}radical\ products} \tag{R 3.9}$$

$$\mathrm{HO_2 + NO_2 + M} \rightleftharpoons HO2NO2 + \mathrm{M} \tag{R 3.10}$$

$$\mathrm{HO_2 + walls} - \quad \mathrm{non{-}radical\ products} \tag{R 3.11}$$

$$\mathrm{HO_2 + HO_2} - \quad \mathrm{H_2O_2 + O_2} \tag{R 3.12}$$

Chain lengths as high as 1000 (i.e. the chain process reactions occurred 1000 times for each HO_2 radical present) were recorded by Cantrell et al. (1984) but typical chain lengths for more modern PERCAs (better calibration and modelling comparisons) are around 200 (Clemitshaw et al., 1997; Green et al., 2003, 2006; Arias and Hastie, 1996).

To obtain high chain lengths the balance between the chain process reactions and the terminating reactions must be understood. A comparison of the relative rates of the competing OH reactions (R 3.6 and R 3.8) is needed (these reactions are repeated below for clarity).

$$\mathrm{OH + CO} \quad \mathrm{CO_2 + H} \tag{R 3.6}$$

$$\mathrm{OH + NO + M} \quad \mathrm{HONO + M} \tag{R 3.8}$$

The rate constant for the chain process (OH + CO) is 2.1×10^{-13} cm^3 molecule^{-1} s^{-1} (Atkinson et al., 2004). The competing termination reaction is OH + NO, with a rate constant of 1.4×10^{-11} cm^3 molecule^{-1} s^{-1} (Atkinson et al., 2004). This indicates that the relative rate of reaction of OH with NO is faster than its reaction with CO; however

the reaction of OH with CO will be favoured if the concentration of CO is high compared to that of NO. When this is the case the dominating reaction for OH will be the chain process and the important termination reactions will be the loss of HO_2 radicals (e.g. R 3.10 – R 3.12).

In conditions when HO_2 loss is the dominating termination reaction (which are the desired conditions, with high [CO] and low [NO]) there are three terminating reactions to compare (R 3.10 – R 3.12): the loss of HO_2 to walls, to NO_2 or due to its self-reaction (these reactions are repeated below for clarity).

$$HO_2 + NO_2 + M \rightleftharpoons HO_2NO_2 + M \qquad \text{(R 3.10)}$$

$$HO_2 + \text{walls} \qquad \text{non-radical products} \qquad \text{(R 3.11)}$$

$$HO_2 + HO_2 \qquad H_2O_2 + O_2 \qquad \text{(R 3.12)}$$

Various studies have recorded a rate of wall loss of HO_2 within a PERCA system: Clemitshaw et al. (1997) reported a value of $2.5\,s^{-1}$ for loss of HO_2 to the walls of a glass reactor chamber; Cantrell et al. (1984) reported a rate of $0.35\,s^{-1}$ for loss to a glass surface; Hastie et al. (1991) reported $0.19\,s^{-1}$ and Mihele (1999) reported values between 2 - $8\,s^{-1}$, dependent on the relative humidity.

Concentrations of HO_2 in the study were typically of the order of 1×10^9 molecules cm^{-3}. Assuming this and assuming a high wall loss of $2.5\,s^{-1}$ (Clemitshaw et al., 1997) the lifetime of HO_2 with respect to wall loss is 0.4 s and with respect to its self-reaction is 200 s. At higher HO_2 concentrations the self-reaction will compete with the wall loss (e.g. at $[HO_2] = 1 \times 10^{12}$ molecules cm^{-3} the lifetime of HO_2 due to the self-reaction is 0.19 s). With a lower wall loss the lifetime due to the self reaction will become comparable at lower concentrations (e.g. for the wall loss equal to 0.19 s (Hastie et al., 1991), the lifetime of HO_2 with respect to this is 5 s, which becomes comparable with the self-reaction at $[HO_2]$

$= 1 \times 10^{11}$ molecules cm^{-3}). The loss due to NO_2 is dependent on the chain length: as the chain length increases [NO_2] also increases, leading to this loss becoming more important. For example with a chain length of 100 the lifetime of HO_2 with respect to this loss is 3 s, but with a chain length of 300 the lifetime is 0.19 s which is comparable to that of the lifetime of HO_2 due to walls.

The chain length for a particular PERCA system must be optimised with the above reactions in mind. The chain length varies with relative humidity (Mihele, 1999), so regular calibrations of the PERCA must be performed. Once the chain length has been determined and a measurement of the change in NO_2 between the background and measurement modes ($\Delta[NO_2]$) has been made then the concentration of HO_2 can be determined using Equation 3.3.

$$\text{Chain Length} = \frac{\Delta[NO_2]}{[HO_2]} \tag{3.3}$$

3.4 Implementation of the PERCA Instrument

The PERCA system used in this study is shown in Figure 3.1. The PERCA system was initially set up based on the design by Clemitshaw et al. (1997) and was optimised once the system was initially working.

3.4.1 NO_2 Detector

An LMA-3 Luminox instrument (Scintrex Ltd.) was used to detect NO_2 via a chemiluminescence detection system. This instrument makes a direct measurement of NO_2 unlike other detection techniques that first convert NO_2 to NO (Thermo, 2007). The sample air is drawn into the reaction cell and past a wick wetted with luminol solution (Luminol II Solution, Drummond Technology Inc.). NO_2 within the sample oxidises the luminol and emits light at a wavelength of approximately 425 nm. A window in the reaction cell allows

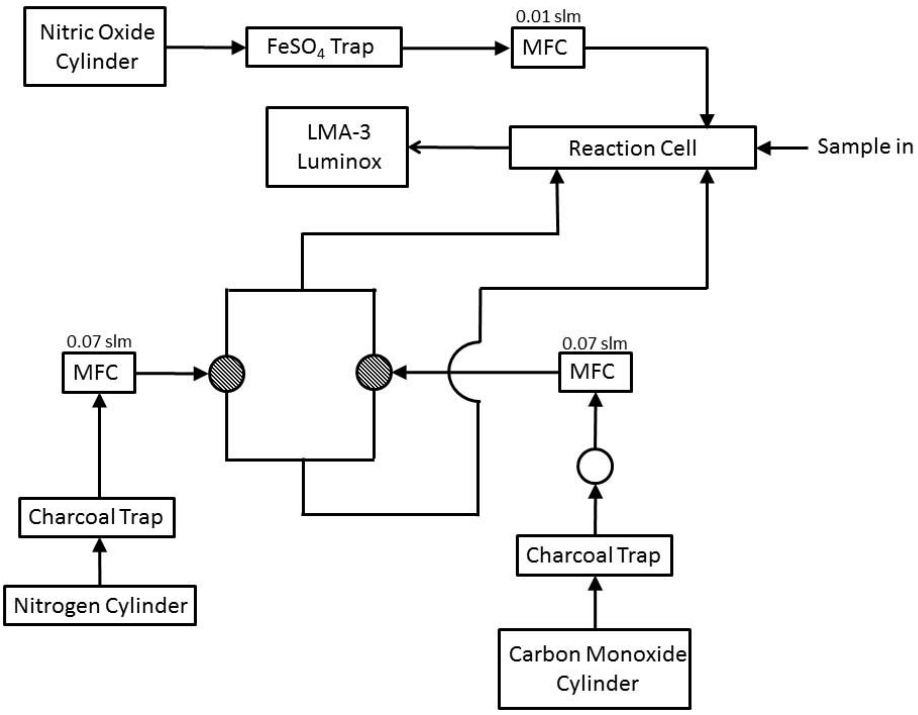

Figure 3.1: A schematic of the PERCA system used in this study. The shaded circles are three way valves and the empty circle is a two way valve.

this chemiluminescence to be detected by a photomultiplier tube. The signal from the photomultiplier tube is directly proportional to the amount of NO_2 present in the sample. A schematic of the LMA-3 is shown in Figure 3.2. (Scintrex, 1987).

The LMA-3 was modified to increase its sensitivity and to allow better user control. The internal air pump, used for drawing the sample flow into the reaction chamber, was replaced with an external pump (KNF Laboport) regulated by a mass flow controller (2 slm, Brooks Instruments). The internal peristaltic pump, used to wet the wick with luminol solution, was replaced with an external one (Masterflex C L) which allowed more precise control over the rate of flow of the solution and was more reliable. The reaction cell and the photomultiplier tube were used as supplied. Data from the analogue output was fed into a computer via an A/D converter (IGI systems) and logged. Calibrations were performed regularly in order to convert the analogue signal recorded into an NO_2 concentration (see Section 3.5.2).

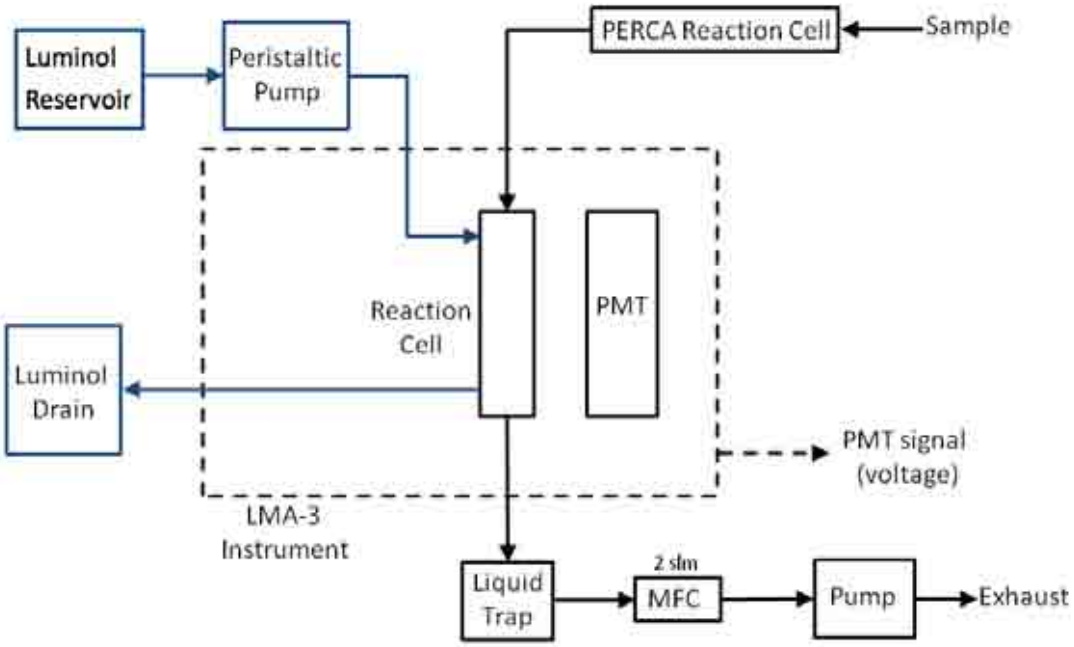

Figure 3.2: A schematic of the LMA-3 Luminox instrument used throughout this study

3.4.2 PERCA Reaction Cell

A cylindrical glass reaction chamber (2 cm diameter, 25 cm length) was used (shown in Figure 3.3). The inlet for the sample into the chamber was a glass cylinder (6 mm diameter, 3.75 cm length). The reactant gases used for the PERCA where injected into the reaction chamber via a glass sleeve, with multiple holes into the chamber, which allowed faster mixing of the reactant gases with the sampled air flow. NO (10 sccm, 600 ppmv) was added at the top of the chamber (Position A), while CO (140 sccm, 99.9 % stated purity) and N_2 were alternately switched between the top and the bottom of the chamber (Positions B and C) for amplification and measurement mode respectively. This maintained a total constant flow through the system when changing from background to measurement mode. Charcoal traps (Grace Discovery Science) were used on the N_2 and CO gas lines to remove hydrocarbon impurities. A ferrous sulphate trap was used on the NO gas line to reduce trace amounts of NO_2 to NO. A total flow of 2 slm was maintained throughout the chamber, which provided a laminar flow with a Reynolds number of 70.

The PERCA was switched between measurement mode and background mode once

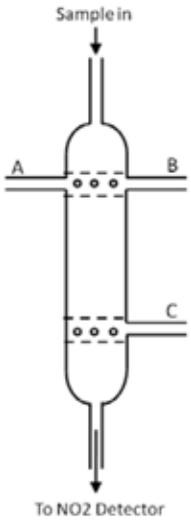

Figure 3.3: The PERCA reaction tube. NO is added at position A; CO and N_2 are added alternately at positions B and C. A glass sleeve with holes is used to help with mixing of the gases before they enter the PERCA tube.

per minute using computer controlled solenoid valves (Entegris). The NO_2 signal from the PERCA was recorded at a sampling rate of 1 s. A typical signal from the NO_2 detector is shown in Figure 3.4.

The PERCA signal shows a clear difference in background and measurement modes, with ΔNO_2 the difference between the two signals. It can be seen in Figure 3.4 that the PERCA signal lags behind the valve signal. This is shown in more detail in Figure 3.5

The valve signal was high when in the measurement mode, with CO being injected at the top of the reaction chamber and N_2 being injected at the bottom. As the PERCA mode changes from the background mode to the measurement mode (a valve change from low to high) there was a time lag from when the valve change occurs to when the amplification occurs. This time lag was approximately 20 seconds. The lag is due to the chemical reactions taking time to reach a steady state. A time lag was also seen when the PERCA changes from measurement mode to background mode (a valve change from high to low). This time lag was slower (approximately 30 seconds) and is due to the time it takes for the reactants to be flushed out of the chamber and a chemical steady state to be reached. When analysing the data from the PERCA only the last 30 s was used for determining ΔNO_2.

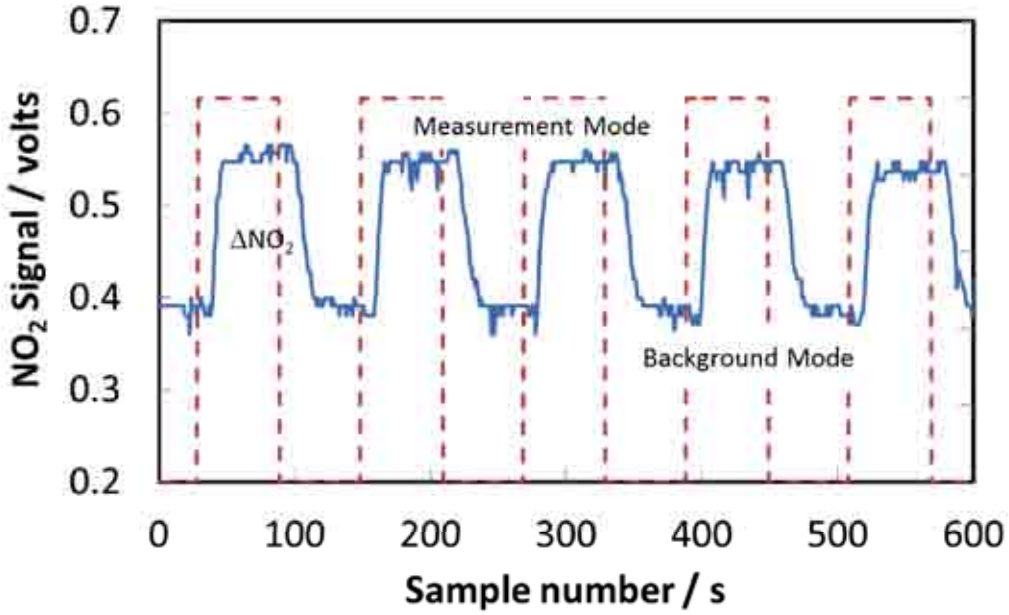

Figure 3.4: A typical PERCA signal. The solid line shows the PERCA signal and the dashed line shows the valves controlling the PERCA. When the valve signal is high the PERCA is in measurement mode, when the valve signal is low the PERCA is in background mode.

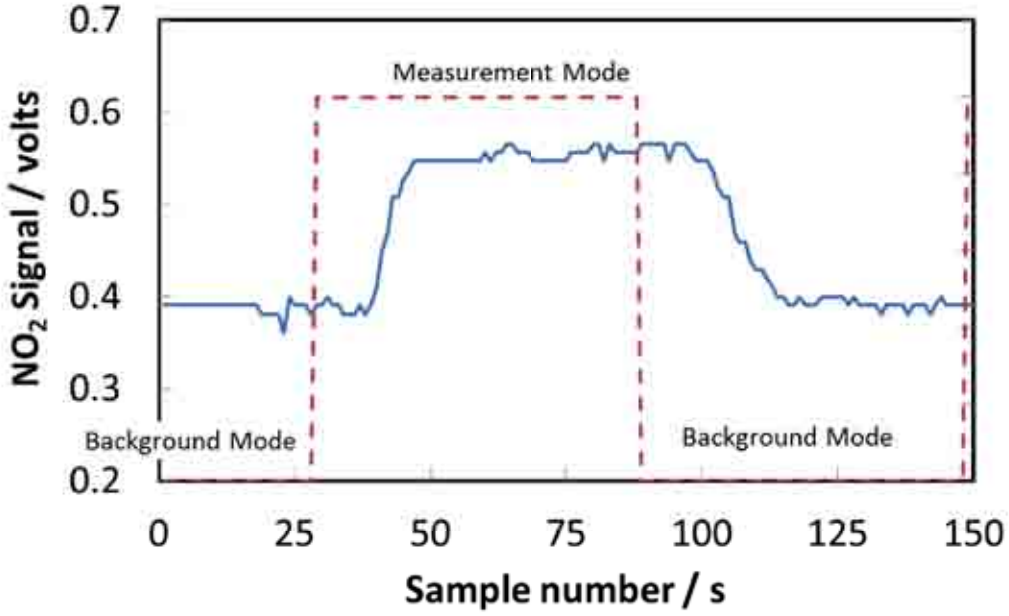

Figure 3.5: The PERCA signal lags behind the valve signal. The lag when changing from the background mode to the measurement mode is smaller than the lag when changing from the measurement mode to the background mode.

3.5 Calibration Techniques

Various calibrations are required before the concentration of HO_2 can be determined using the PERCA. Mass Flow Controllers (MFCs) were used to control the flows within the PERCA instrument, so needed calibrating to ensure the required flows were correct. The NO_2 detector produced a voltage which was directly proportional to the NO_2 signal; to convert from this signal to the NO_2 concentration a calibration curve was regularly produced. Finally the PERCA itself was calibrated, by determining the chain length, in order to determine the concentration of HO_2 from the NO_2 signal recorded.

3.5.1 MFC Calibration

Mass Flow Controllers (MFCs) were used to control all gas flows within the PERCA system. The MFCs were controlled using custom designed software (IGI Systems). The 'set point' was used to set the required flow through the MFC and the actual flow through the MFC was also recorded using the same system. All flows were recorded once a minute throughout experiments.

During a MFC calibration the set point was changed to vary the flow of gas through the MFC. The MFC to be calibrated was set up with another MFC in line with it, which was used to measure the flow through the first one - its set point was set to a higher value than the set point of the MFC being calibrated. A bubble flow meter was attached to the exit of the second MFC to record the actual flow from the MFCs. The MFC software recorded the flows through the two MFCs. The bubble flow meter had a volume of 1 litre and the time it took for a bubble to pass through this volume was recorded to determine the flow rate. A typical calibration graph can be see in Figure 3.6.

The MFCs were new at the start of this study and had been recently calibrated in the factory. The bubble flow readings showed a high correlation to the the set points. Figure 3.6 shows that the line of best fit is y = 1.04, with the R^2 value being 0.94. The MFCs were calibrated periodically for any change and were also calibrated if they were

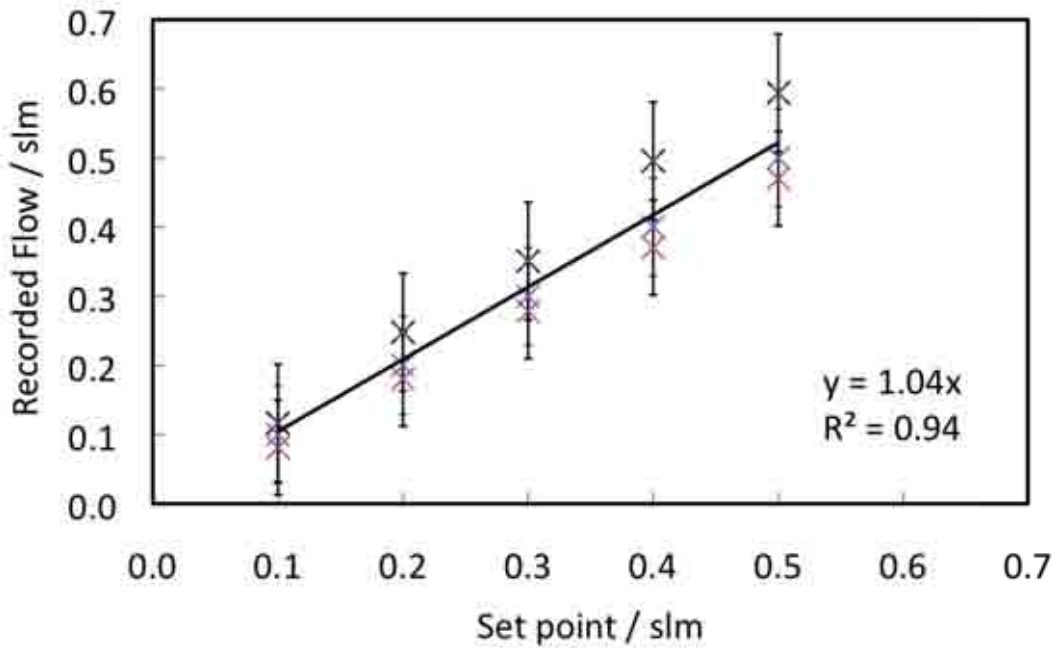

Figure 3.6: A typical MFC calibration plot. The blue crosses show the recorded flow for the MFC being calibrated, the red crosses show the recorded flow for the second measurement MFC and the black crosses show the flow determined using the bubble flow meter.

cleaned, or repaired in any way.

3.5.2 NO_2 Calibration

The signal obtained from the LMA-3 Luminox instrument was the direct output from the photomultiplier tube within the instrument. This signal was in volts and was directly proportional to the NO_2 present in the sample. A calibration curve was used to convert the voltage signal into a concentration of NO_2. Luminol solution was used to produce the chemiluminescence from the NO_2 molecules. Luminol solution degrades over time, unless kept refrigerated, which was not possible when it was in use in the instrument. Luminol solution was typically used for one week before being replaced by fresh solution. Each time a fresh solution of luminol was used a calibration curve was produced.

To perform a calibration a known mixture of NO_2 (BOC, 1.065 ppm) and air (BOC) was sampled by the LMA-3 Luminox instrument. The mixing ratio of the two gases was changed every five minutes to provide various concentrations of NO_2. The voltage output

of the analyser was recorded every second and the average over each five minute sample was found. A typical calibration curve is shown in Figure 3.7. It was noted that the relationship between the NO_2 mixing ratio and the signal from the LMA-3 instrument was not linear below 10 ppb. For all experiments using this PERCA the NO_2 mixing ratio was kept above this level so that a linear calibration curve could be used.

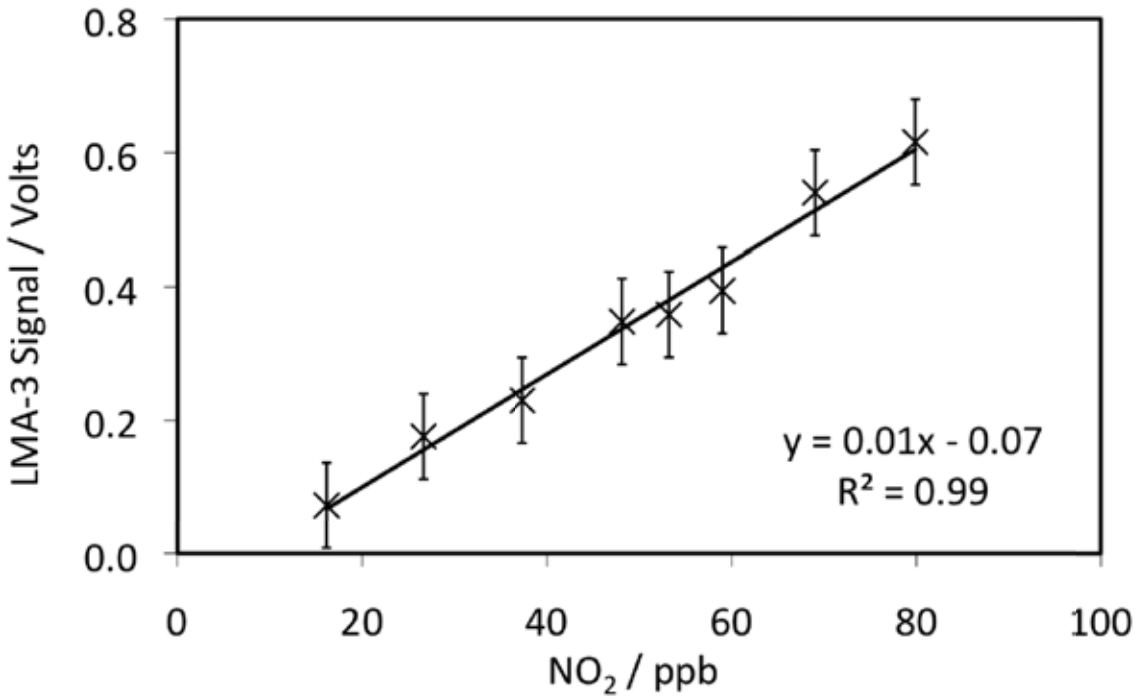

Figure 3.7: A calibration curve for determining NO_2 using the voltage signal recorded from the LMA-3 Luminox instrument.

3.5.3 PERCA calibration

Chemical Actinometry

The PERCA detects the concentration of NO_2 produced due to the amplification of HO_2 within the reaction chamber. To calculate the concentration of HO_2 from this signal the chain length of the PERCA must be known (Equation 3.3).

$$\text{Chain Length} = \frac{\Delta[NO_2]}{[HO_2]} \tag{3.3}$$

In order to determine the chain length during the calibration of the PERCA a known concentration of HO_2 must be sampled by the instrument. A chemical actinometer method is used to produce a known amount of HO_2, a method which has been used for HO_2 calibrations by Schultz et al. (1995), Creasey et al. (2000), Kanaya et al. (2001) and Bloss et al. (2004) amongst others. This technique relies on the simultaneous production of HO_2 and O_3 by photolysis of H_2O and O_2 at 184.9 nm (R 3.13 – R 3.16).

$$H_2O + h\nu - \quad OH + H \tag{R 3.13}$$

$$H + O_2 + M - \quad HO_2 + M \tag{R 3.14}$$

$$O_2 + h\nu - \quad O + O \tag{R 3.15}$$

$$O + O_2 + M - \quad O_3 + M \tag{R 3.16}$$

The rate of production of HO_2 and O_3 is shown in Equations 3.5 and 3.6. It was assumed that O and H were in a steady state due to their short lifetimes with respect to recombination with O_2. J is the photolysis coefficient of a reactant, x, at a particular wavelength, λ, and is calculated using Equation 3.4 (where I is the light flux, σ is the absorption cross-section of x and ϕ is the quantum yield of x).

$$J_{x,\lambda} = I_\lambda \sigma_{x,\lambda} \phi_{x,\lambda} \tag{3.4}$$

$$\frac{d[HO_2]}{dt} = J_{H_2O,184.9nm}[H_2O] = I_{184.9nm}\sigma_{H_2O,184.9nm}\phi_{HO_2,184.9nm}[H_2O] \tag{3.5}$$

$$\frac{d[O_3]}{dt} = J_{O_2,184.9nm}[O_2] = I_{184.9nm}\sigma_{O_2,184.9nm}\phi_{O_3,184.9nm}[O_2] \tag{3.6}$$

Equations 3.5 and 3.6 are integrated and, as the light flux, $I_{184.9nm}$, is the same for both equations and O_2 and H_2O are exposed to the light for the same amount of time,

the equations can be rearranged to give Equation 3.7.

$$[HO_2] = \frac{\sigma_{H_2O,184.9nm}\phi_{HO_2,184.9nm}[H_2O][O_3]}{\sigma_{O_2,184.9nm}\phi_{O_3,184.9nm}[O_2]P} \tag{3.7}$$

The added factor, P, is the profile factor, which arises due to the laminar nature of the flow - the gas in the centre of the calibration tube will flow faster than the gas at the walls of the calibration tube leading to the molecules near the sides of the flow spending more time in the photolysis region than molecules in the centre of the flow. P was initially assumed to be 2 (in a perfectly laminar flow gas at the centre of the tube would move twice as fast as gas at the sides). A value for P was determined experimentally for this system (see Section 3.6.2). Values for σ_{O_2} and σ_{H_2O} were also determined experimentally, as recommended by Creasey et al. (2000), due to the dependence of the optical depth and the lamp flux on σ_{H_2O} (see Section 3.6.1). ϕ_{HO2} is equal to 1 (Atkinson et al., 2004) and ϕ_{O_3} has a value of 2 (Washida et al., 1971). The concentration of H_2O was calculated by recording the relative humidity during a calibration and the concentration of O_2 was calculated as 21% of the molecular concentration of air (i.e. $0.21 \times [M]$). The concentration of O_3 was recorded throughout the calibration.

Implementation of PERCA Calibration

The PERCA calibration experiment was set up as shown in Figure 3.8.

10 slm humidified air was flowed through the calibration tube (fused silica, 60 cm length, 2.5 cm outer diameter), and the relative humidity of the flow was measured just before it entered the calibration tube. The relative humidity of this flow was varied by changing the ratio of wet and dry air entering the calibration tube. The calibration tube was fixed in a metal block which also held a UV mercury lamp (Ultra-Violet Products Ltd., 184.9 nm). The H_2O and O_2 present within the calibration tube were photolysed as the gas flowed past the UV light. The calculated Reynolds number for flow in the calibration tube was 550 and the entry length for the flow to become laminar was 48 cm, so the flow

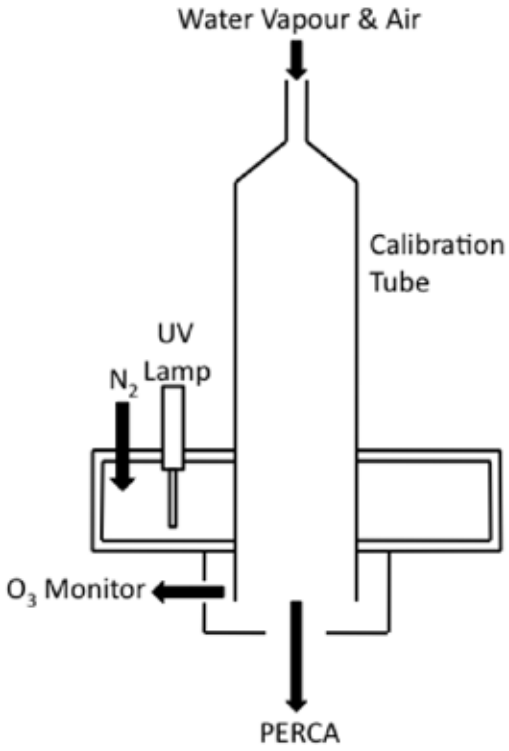

Figure 3.8: The calibration set-up for the PERCA system.

was assumed to be near laminar when it passed the photolysis region (at 50 cm). 1 slm of nitrogen was flowed into the cavity in the metal block that housed the UV lamp. This was to ensure the temperature of the lamp (and thus its output) was constant and to avoid forming O_3 in ambient air. 2 slm of the flow from the calibration tube was sampled by the PERCA, 1.5 slm was sampled by an ozone monitor (2B Technologies, Model 205) and the rest was vented to the exhaust. The PERCA output was recorded as the NO_2 signal from the LMA-3 Luminox instrument.

The ozone monitor (2B Technologies) works by a UV absorption technique. Ozone absorbs ultraviolet light at 254 nm, the intensity of this light is recorded after an air sample passes through an absorption cell. A background light intensity is recorded simultaneously in a second cell, with ozone being scrubbed from the air sample first. Using these two measurements the Beer-Lambert Law is used to determine the concentration of O_3 (Atkins and de Paula, 2006). PERCA calibrations were performed each day at the relevant relative humidity for experiments that were performed on that day as the chain length is known

to be dependent on relative humidity (Reichert et al., 2003).

Table 3.1: Typical flows for a PERCA calibration experiment. MFCs 2 and 3 control the relative humidity within the calibration tube. MFCs 8-11 control the PERCA flows. MFC 7 fills the cavity around the UV lamp.

MFC #	**Flow / slm**	**Gas**
2	3	Dry air
3	7	Wet air
8	0.07	CO
9	0.07	N_2
10	0.01	NO
11	2	PERCA exhaust
7	1	N_2 in light cavity

Analysis of the PERCA Calibration

The data that was recorded from a PERCA calibration was the NO_2 signal, the concentration of O_3, the relative humidity and the flows recorded by the MFCs. The data was recorded over a ten minute sampling period for each relative humidity setting. The chain length was determined for each calibration using Equation 3.3.

$$\text{Chain Length} = \frac{\Delta[NO_2]}{[HO_2]} \tag{3.3}$$

The NO_2 signal was converted from a voltage to a mixing ratio using the relevant NO_2 calibration curve. The PERCA was switched between the background mode and the measurement mode every minute. The first 30 s of measurements made after a mode change was discarded due to the lag in the chemistry after the mode change (see Section 3.4.2). The last 30 s of measurement in each mode was averaged (see Figure 3.9). $\Delta[NO_2]$ was found by subtracting an average for a measurement mode from the average from its two neighbouring background modes. Figure 3.9 shows this clearly. $\Delta[NO_2]_1$ was calculated as $M1 - \frac{B1+B2}{2}$ and $\Delta[NO_2]_2$ is calculated as $M2 - \frac{B2+B3}{2}$ etc.. The calibration was performed over a ten minute period and the average $\Delta[NO_2]$ was calculated over this time.

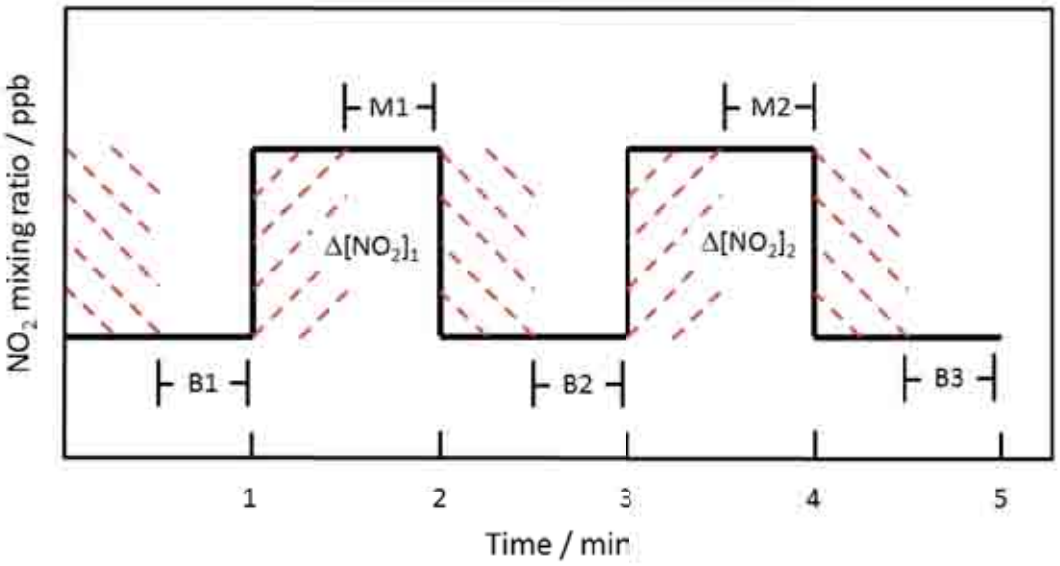

Figure 3.9: Analysis of the PERCA signal. The dashed area of the signal was discarded. M1 and M2 are the calculated average for the measurement mode and B1, B2 and B3 are the calculated averages for the background mode.

The concentration of H_2O was determined from the measurement of relative humidity. The saturated vapour pressure of water was calculated using the Antoine Equation (Equation 3.8) with A = 5.402 21, B = 1838.675 and C = −31.737 for units of bar and Kelvin for H_2O at room temperature (NIST, 2011). The temperature was measured throughout the calibration and the average was used to determine the saturated vapour pressure. The calibration was performed at atmospheric pressure.

$$\log(P) = A - \frac{B}{T + C} \tag{3.8}$$

The partial pressure of water vapour was calculated using the average measured relative humidity (RH %) over the 10 min period of calibration, the saturated vapour pressure of water and the definition of relative humidity (Equation 3.9).

$$\text{Relative Humidity} = \frac{\text{Partial pressure of } H_2O}{\text{Saturated Pressure of } H_2O} \times 100 \tag{3.9}$$

Finally the ideal gas law (Equation 3.10) was used to calculated the concentration ($\frac{N}{V}$) of H_2O from the calculated partial pressure of H_2O, the measured average temperature

(in K) and the Boltzmann constant ($k = 1.38 \times 10^{-23}\,\mathrm{J\,K^{-1}}$).

$$\frac{N}{V} = \frac{p}{kT} \tag{3.10}$$

The ozone concentration recorded throughout the calibration was averaged over the ten minute sample period.

The H_2O concentration was calculated using Equation 3.7; the parameters in orange where measured or calculated for each calibration procedure, the parameters in blue were calculated for this particular PERCA instrument (Section 3.6) and the parameters in green were found in literature (Section 3.5.3).

$$[HO_2] = \frac{\sigma_{H_2O,184.9nm}\phi_{HO_2,184.9nm}[H_2O][O_3]}{\sigma_{O_2,184.9nm}\phi_{O_3,184.9nm}[O_2]P} \tag{3.7}$$

Finally the chain length was calculated using Equation 3.3, the calculated $\Delta[NO_2]$ and the calculated $[HO_2]$.

3.6 PERCA Characterisation

3.6.1 Determination of Absorption Cross Sections

The absorption cross sections of H_2O and O_2 at 184.9 nm must be known in order to use the chemical actinometery calibration method. The values of both σ_{H_2O} and σ_{O_2} have been debated with respect to this calibration method (Lanzendorf et al., 1997; Hofzumahaus et al., 1997). The discussion of the absorption cross section of H_2O at 184.9 nm has now been resolved and the recommended value is $6.78 \times 10^{-20}\,\mathrm{molecule^{-1}cm^2}$ (Atkinson et al., 2004), in agreement with Cantrell et al. (1997), Hofzumahaus et al. (1997) and Creasey et al. (2000), who had all reported a value approximately 30% higher than the recommended value at the time.

Various studies using this calibration technique have shown that the absorption cross

section of O_2 varies with the oxygen column (i.e. the concentration of oxygen over a particular length, l) and with the operating characteristics of the lamp (Creasey et al., 2000; Lanzendorf et al., 1997; Kanaya et al., 2001). The absorption cross section is dependent on the oxygen column because some absorption features of the lamp spectrum will be saturated, but others will not be (Bloss et al., 2004). Figure 3.10 shows the emitted spectrum from a mercury light (in a vacum) and the overlap of that spectrum with the absorption cross section of O_2. Figure 3.10 also shows how the spectrum of the light changes with a change in the optical path of O_2, it can be seen that some parts of the spectrum are saturated.

Lanzendorf et al. (1997) reported a decrease in σ_{O2} if the oxygen column was increased. Creasey et al. (2000) and Lanzendorf et al. (1997) recommend the determination of the O_2 absorption cross section for the lamp used during a calibration and at the same conditions (i.e. oxygen column) used in the calibration procedure. The effective cross-section, rather than the apparent cross-section (which is observed) must be used to determine the actual cross-section for O_2 at the relevant conditions. This section outlines the experimental set up used to determine the cross section for O_2 under operating conditions used during the PERCA calibration. The absorption cross section for H_2O was found using the same experimental set up to determine the accuracy of the experiment.

The absorption cross section experiments were based on the Beer Lambert Law (Equation 3.11), where I_x is the measured intensity of the light with the species of interest, x, present, I_0 is the intensity of the light without species x present, σ_x is the absorption cross section of x, c is the concentration of x and l is the distance the light traveled from its source to the light detector.

$$I_x = I_0 \exp(-\sigma_x c l) \tag{3.11}$$

A cylindrical absorption reaction cell (Pyrex, inner diameter 2 cm; length 10 cm) was used throughout these experiments. The cell was wrapped in black tape in order to prevent any ambient light from contributing to the measured signal of the light of interest.

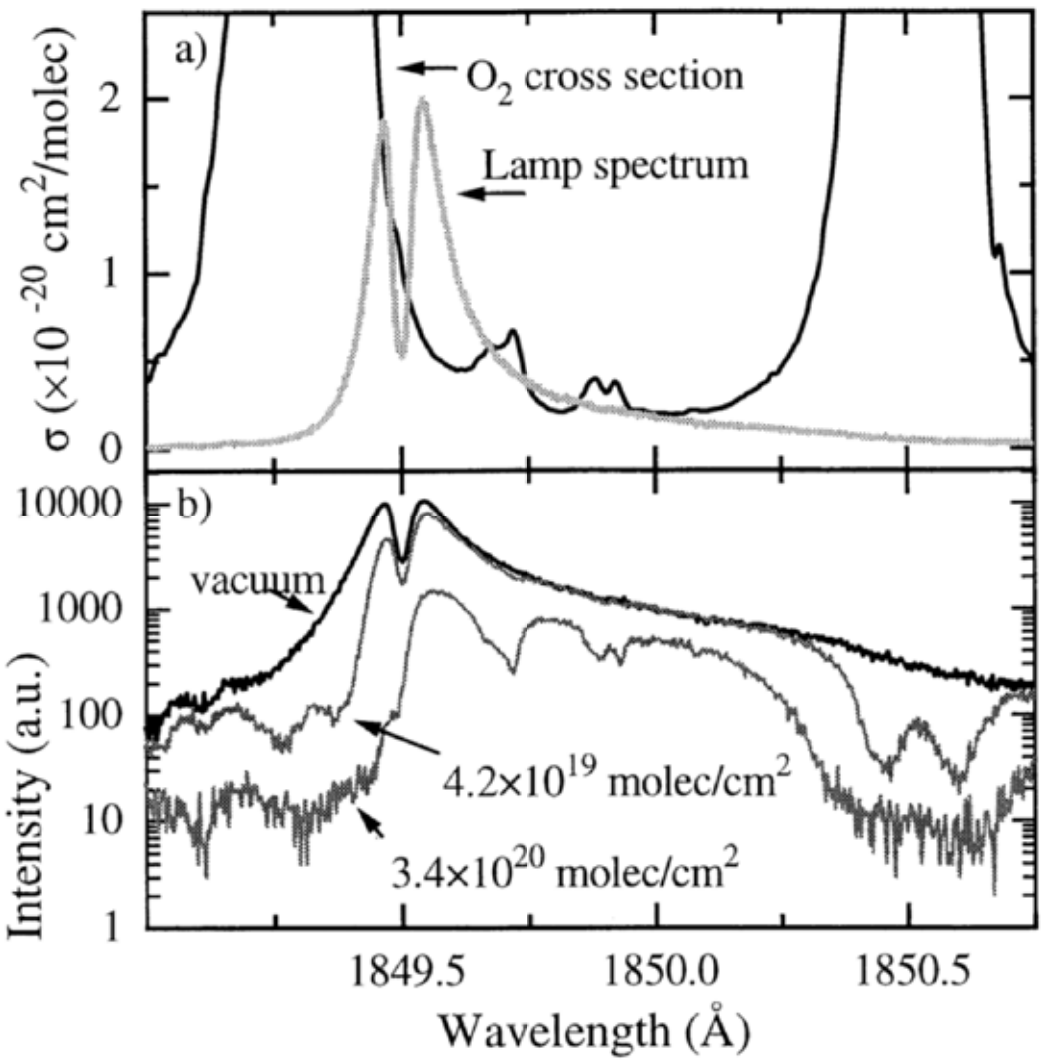

Figure 3.10: (a) Expanded portion of the oxygen absorption cross section superposed with the Hg spectrum measured with the spectrometer evacuated. (b) Spectrum for three different amounts of oxygen added to the spectrometer. The intensity is plotted on a log scale and the O_2 concentration shown as the optical path (molecules cm^{-3}). (Lanzendorf et al., 1997)

Windows (fused silica) were glued to the ends of the cell which allowed the UV light to pass into the cell. The same mercury UV lamp (Ultra-Violet Products Ltd., $\lambda = 184.9\,\text{nm}$) that was used for the calibration experiments was also used for these experiments. The lamp was housed in the same metal block as used for calibrations and the cavity around it was flushed continuously with 1 slm of nitrogen. A bandpass filter (Acton Research; 184.9 nm) was placed between the lamp and the absorption cell. An iris was placed between the filter and the absorption cell in order to allow the transmission of light through only the centre of the absorption cell in order to avoid any potential wall transmission of light around the sample. A photodiode (Thor Labs Inc.; DET25K) was used to detect the intensity of the light after it had passed through the absorption cell. The output from the photodiode was a voltage and was dependent on the intensity of the light detected. The output voltage was recorded using a voltmeter. A pump (KNF Laboport), regulated to a flow of 2 slm by an MFC, was used to draw the gas flow through the absorption cell at ambient pressure.

The absorption cross section of H_2O was determined using this set-up. I_0 was determined by flowing dry nitrogen through the absorption cell; the intensity of the light reaching the detector at the end of the absorption cell was recorded as a voltage from the signal of the photodiode. I_{H_2O} was determined by flowing humidified nitrogen through the absorption cell and the corresponding voltage from the photodiode was recorded. The relative humidity of the flow was measured before it entered the absorption cell. Various values for I_{H_2O} were recorded by changing the relative humidity of the humidified nitrogen flow through the absorption cell (thus changing the total absorbing column of H_2O). Data recorded from these experiments are shown in Figure 3.11.

The value for σ_{H_2O} was determined by regression analysis as $9.35 \times 10^{-20} \pm 2.02 \times 10^{-21}$ molecule^{-1} cm^2. Data below the ozone column of 10×10^{17} molecule^{-1} cm^2 was not used due to the limit of detection of the photodiode used in the experiment. This experimentally determined cross section is 30 % higher than the recommended value of 6.78×10^{-20} molecule^{-1}cm^2 (Atkinson et al., 2004).

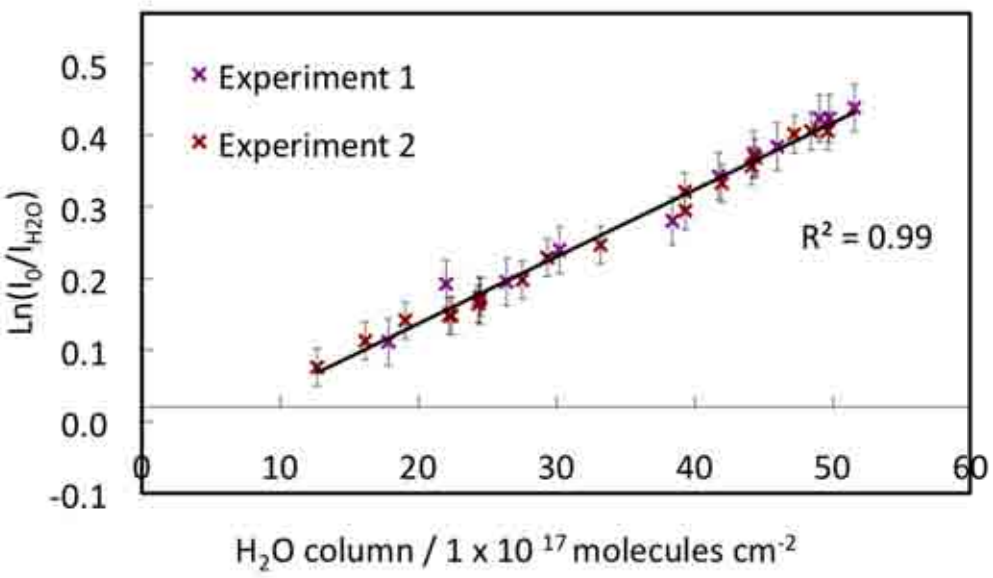

Figure 3.11: Data to determine the absorption cross section of H_2O. Two sets of experimental data is shown. Regression analysis determined σ_{H_2O} as 9.35×10^{-20} molecule^{-1}cm^2.

The absorption cross section of O_2 was determined using the same experimental set up. To determine I_0 dry nitrogen (BOC) was flowed through the absorption cell. To determine I_{O_2} dry air (BOC) was flowed through the absorption cell. The O_2 column was varied by using different ratios of dry N_2 and dry air. Data recorded from these experiments are shown in Figure 3.12. However, as discussed previously it is the apparent and effective cross-sections which are needed to determine the absorption cross-section at the relevant O_2 column.

Figure 3.13 shows how the apparent absorption cross section varies with the oxygen column. The apparent absorption cross section was calculated using Equation 3.12, where y is the O_2 column (Hofzumahaus et al., 1997; Creasey et al., 2000).

$$\sigma_{O_2,app}(y) = \frac{1}{y} \ln \frac{I_0}{I_{O_2}} \tag{3.12}$$

The O_2 column at the centre of the calibration tube was calculated to be 6.56×10^{18} molecules cm^{-2} (i.e. 1.25 cm $\times 0.21[O_2]$). All other paths around the lamp were flushed with nitrogen. Figure 3.14 shows the apparent absorption cross section around the O_2 column of interest.

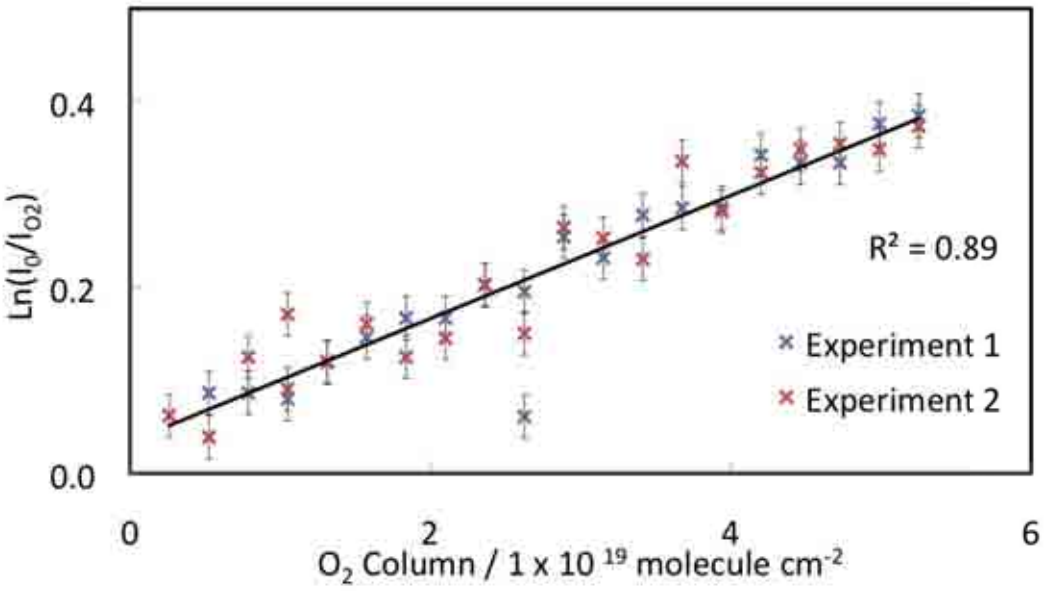

Figure 3.12: A plot showing the relationship between the absorbance ($\ln \frac{I_0}{I_{O_2}}$) and the oxygen column measured for O_2. Two experiments were performed.

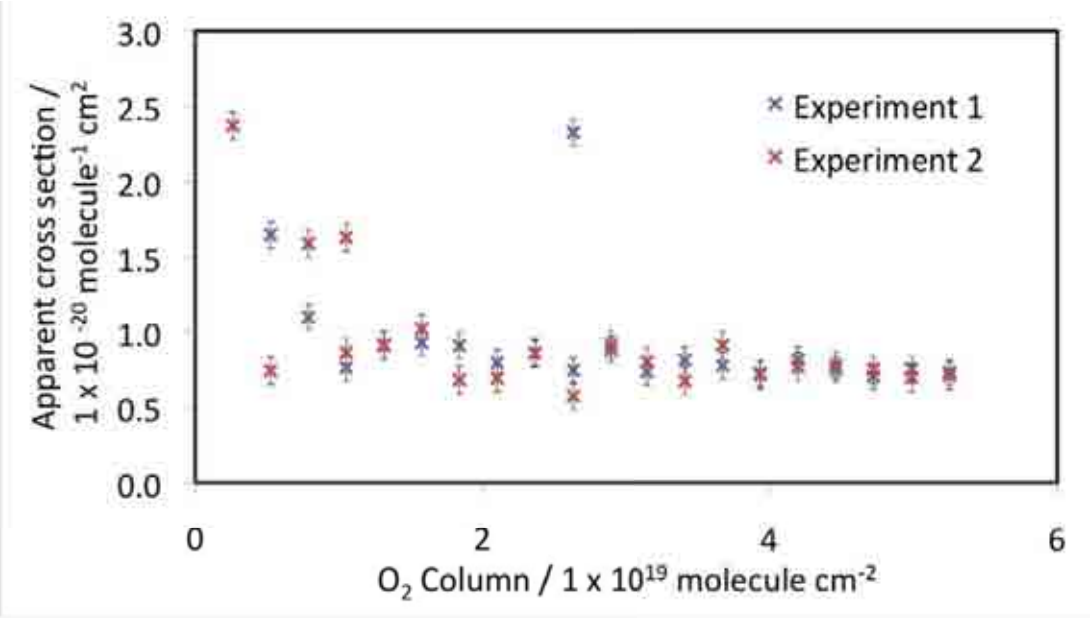

Figure 3.13: The apparent oxygen absorption cross section changes with the absorbance of the light by O_2

The value of the effective absorption cross section of O_2 is determined using Equation 3.13.

$$\sigma_{O_2,eff}(y) = \sigma_{O_2,app}(y) + y\frac{d(\sigma_{O_2,app}(y))}{dy} \tag{3.13}$$

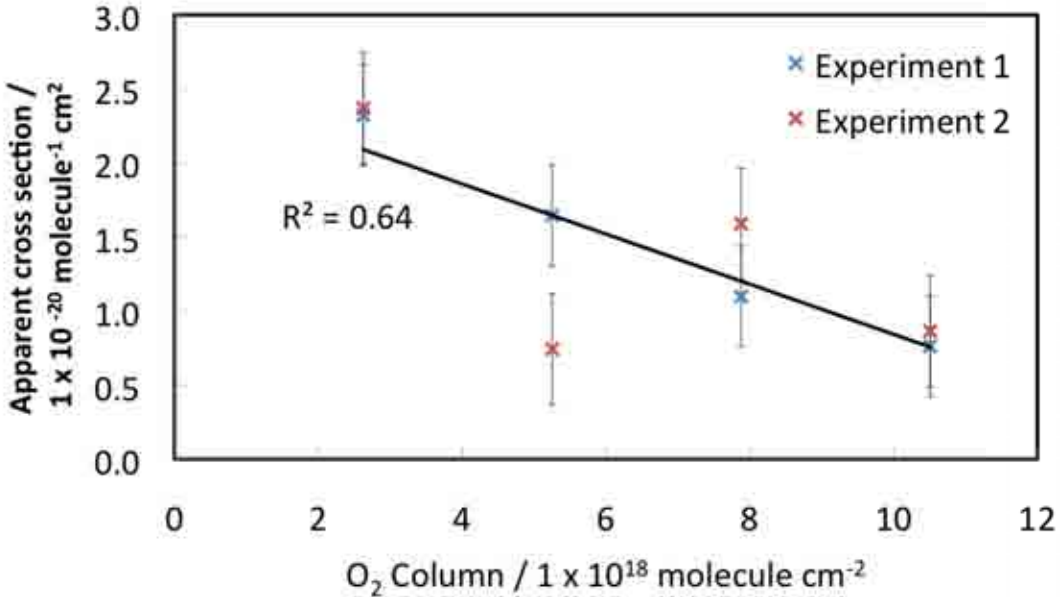

Figure 3.14: The apparent absorption cross section for O_2 around the O_2 column used during calibration of the PERCA.

With an oxygen column of 6.56×10^{18} molecules cm^{-2}, $\sigma_{O_2,app}$ was calculated as 1.46×10^{-20} cm^2 molecule^{-1} and $\sigma_{O_2,eff}$ was calculated as 1.51×10^{-21} cm^2 molecules^{-1} (Equation 3.13). This value of $\sigma_{O_2,eff}$ is approximately one order of magnitude smaller than those determined by Creasey et al. (2000) and Hofzumahaus et al. (1997), however the value obtained for $\sigma_{O_2,app}$ agreed fairly well. Figure 3.15 shows experimental data from Creasey et al. (2000), it can be seen that at an oxygen column of 6.56×10^{18} molecules cm^{-2}, $\sigma_{O_2,app}$ is approximately 1.2×10^{-20} cm^2 molecule^{-1}. However the gradient of the apparent cross section data shown in Figure 3.15 is much shallower than seen in Figure 3.14, leading to a larger difference between the apparent and effective cross sections. The observed difference between the effective cross sections could be due to variations in the lamp used in these determinations, or due to a difference in the sensitivity of the light detector.

3.6.2 Profile Factor

The profile factor, P, arises due to the laminar nature of the flow of gas in the PERCA calibration tube. A laminar flow has a parabolic profile, as shown in Figure 3.16 because

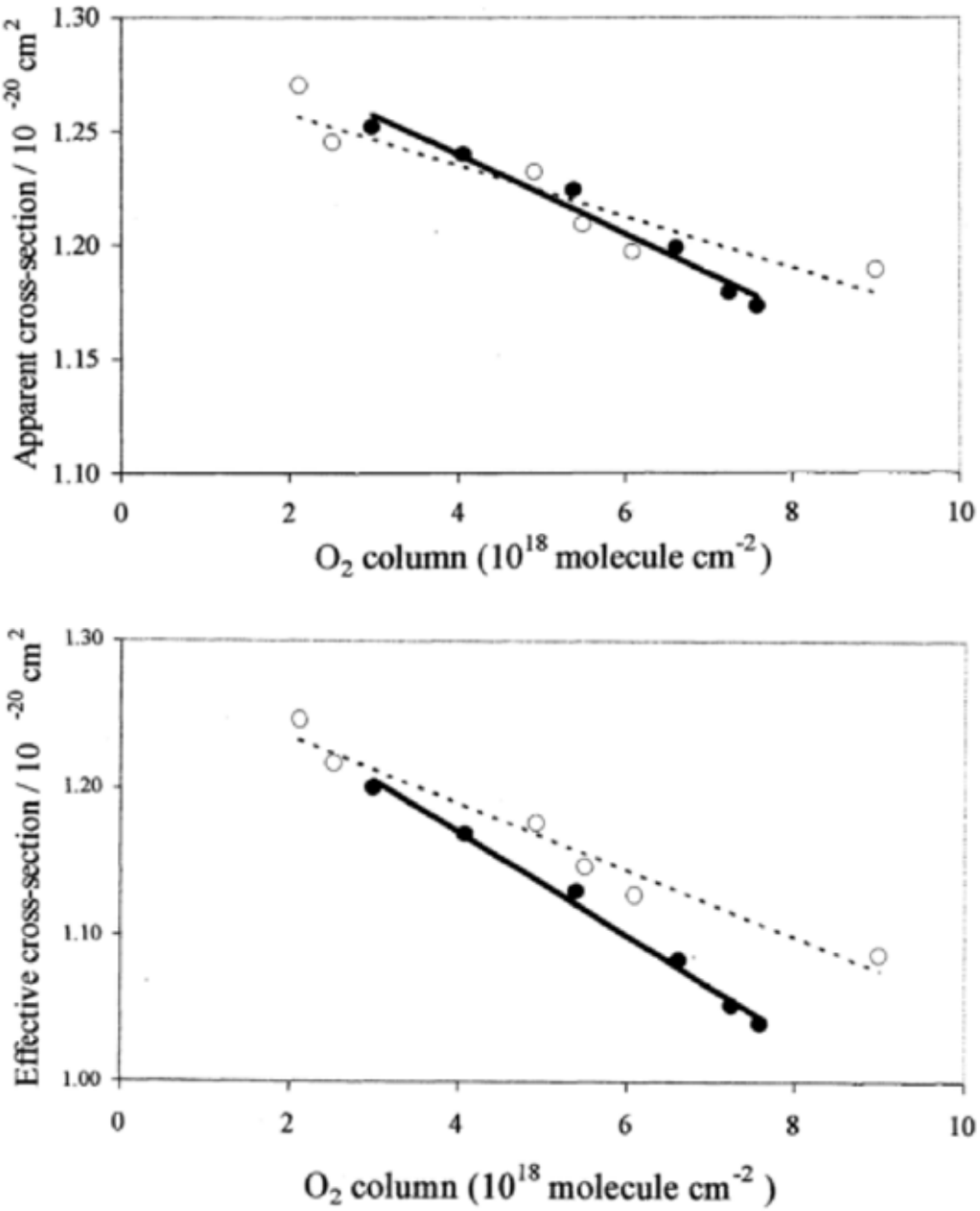

Figure 3.15: (a) Apparent and (b) effective O_2 absorption cross-sections in the vicinity of the O_2 column used in field calibrations, for operation of the Hg pen lamp at currents of 2.5 mA (filled circles) and 10 mA (open circles). The plots are roughly linear in this region and the lines show a least squares fit to the data. (Creasey et al., 2000)

the centre of the gas flow moves faster than the flow in contact with the walls of the tube.

The calibration tube was held close to the UV lamp in order to photolyse H_2O and O_2 within the tube. The gas flow in the centre of the calibration tube spent less time in the photolysis region than the flow in the outer parts of the tube, leading to a gradient in

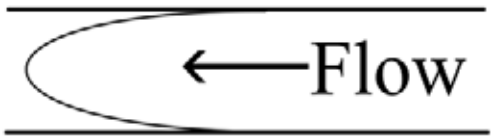

Figure 3.16: The parabolic profile of a laminar flow.

the concentration of the photolysis products across the diameter of the calibration tube. During a calibration the PERCA sampled from the centre of the calibration tube while the ozone was sampled from the remaining part of the calibration tube flow. In an ideal laminar flow the profile factor will be 2 (i.e. the gases at the centre of the tube are moving twice as fast as the gases at the sides of the tube), while in a turbulent flow the profile factor will be 1. Even though a laminar flow is assumed in the calibration tube (see Section 3.5.3) the profile factor for the system was not expected to be exactly 2, as the PERCA and the O_3 monitor withdrew a significant fraction of the flow, and was therefore determined experimentally.

The profile factor was determined by making measurements of ozone concentration throughout the cross-section of the calibration tube. Ozone and hydroperoxy radicals were produced by the same process in the calibration tube, so would have the same production profile. Figure 3.17 shows a cross section of the calibration tube, the crosses show where measurements of ozone were recorded. The shaded area in the centre of the calibration tube indicates the area of the flow that was sampled by the PERCA during a calibration while the unshaded part was sampled by the ozone monitor. The ratio of the average ozone concentration measured in the PERCA sampling area and the average ozone concentration measured in the ozone sampling area gave a value for the profile factor in this calibration set up (Equation 3.14, Heard and Pilling (2003)).

$$P = \frac{[O_3]_{excess}}{[O_3]_{centre}} \tag{3.14}$$

Figure 3.18 shows the ozone profile for the calibration tube cross section; a value of

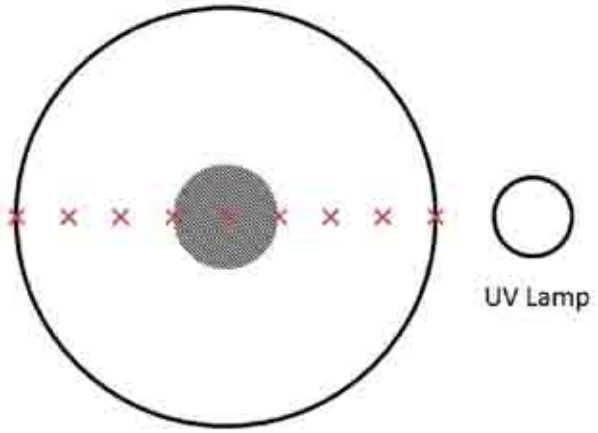

Figure 3.17: A cross section of the PERCA calibration tube. The shaded area was sampled by the PERCA while the unshaded part was sampled by the ozone monitor. The crosses show where ozone measurements were taken to obtain a profile over the cross section of tube.

1.92 was found experimentally for this calibration setup. During these experiments it was noted that the profile of the light from the UV lamp made a difference to the photolysis within the tube. It can be seen in Figure 3.18 that two sets of data are consistently higher than the other two sets of data. The difference in the data recorded was due to the orientation of the light profile directed towards the calibration tube.

The UV light used is a mercury pen-ray lamp. The mercury is held within a tube inside the lamp which leads to a particular shape of the light produced by this lamp. The light profile produced is shown in Figure 3.19; it can be seen that there are two orientations for the lamp output.

During the calibration procedure the lamp can be positioned so that either orientation (or somewhere in between) is directed towards the calibration tube. When the lamp output is as shown in Figure 3.19(a) more UV light is available for the photolysis of O_2 and H_2O, than when the lamp is in the position shown in Figure 3.19(b). Figure 3.18 shows the ozone cross section measured for both orientations of the lamp. It can be seen that slightly higher O_3 levels are recorded when the lamp is in orientation A (pink and blue data points) and lower levels with the lamp in orientation B (red and green data points). The P factor experimentally determined for orientation A was 2.02 ± 0.23, while the P factor experimentally determined for orientation B was 1.85 ± 0.17, where

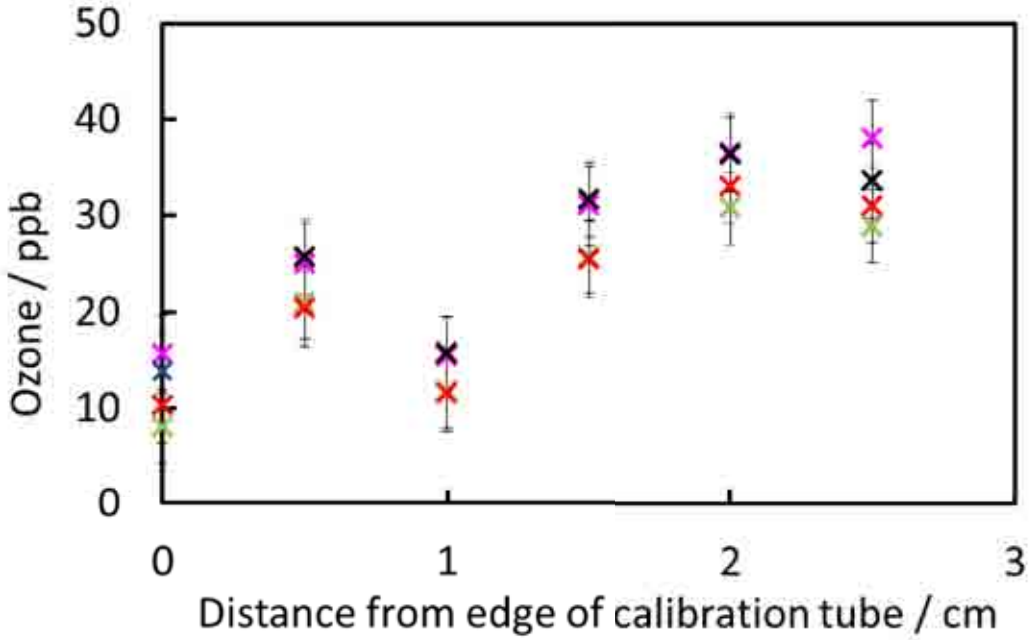

Figure 3.18: The ozone profile at the output of the peroxy radical calibration tube. The red and green crosses show data that was recorded with one orientation (B) of the lamp output while the pink and blue crosses show data that was recorded with the other orientation (A) of the lamp output.

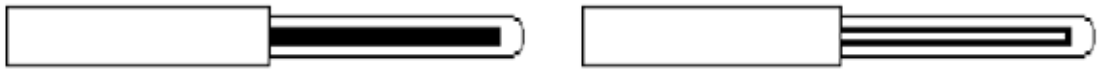

(a) Lamp orientation A

(b) Lamp orientation B

Figure 3.19: The light profiles of the UV lamp.

the uncertainty given is the standard error of the data. When PERCA calibrations were performed the lamp was always in orientation A.

3.6.3 Optimisation of the Chain Length

The number of times the PERCA amplification process repeats is known as the Chain Length (CL). The chain length is dependent on the relative rates of the PERCA chain reaction processes with respect to the relative rates of the termination reactions - this has been discussed in detail in Section 3.3.2.

The PERCA was characterised in order to obtain optimum conditions for the particular

reaction cell used in this study. The variation in chain length due to changing NO and CO concentrations was investigated in order to determine the optimum flows of these gases to use for this PERCA (Figures 3.20 and 3.21).

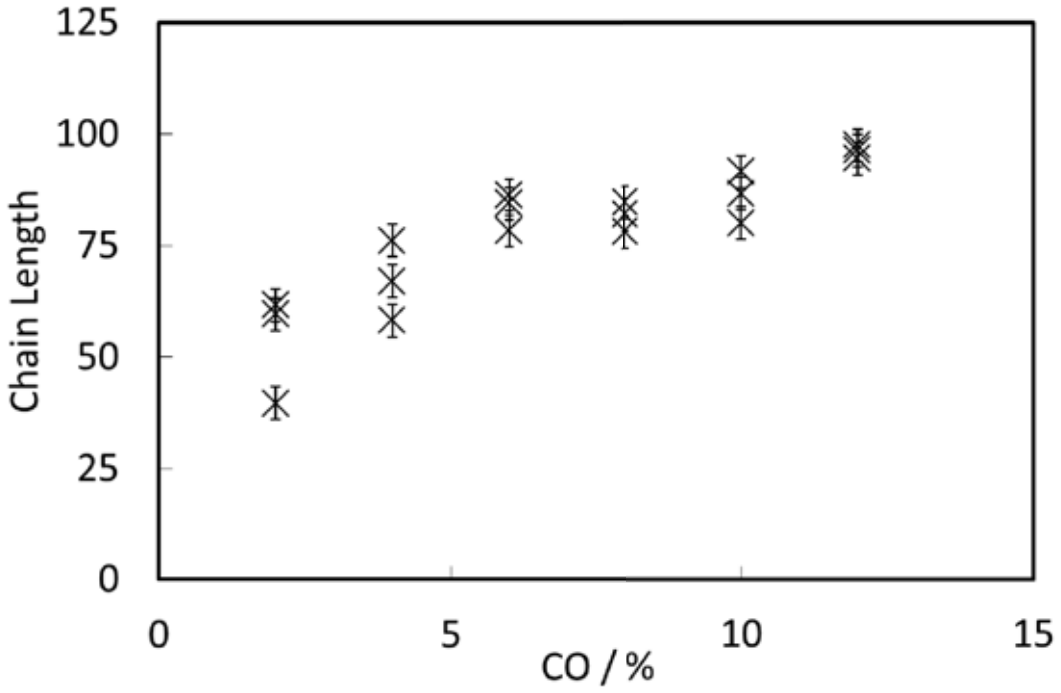

Figure 3.20: Data showing the dependence of the chain length of the PERCA on the CO mixing ratio.

Figure 3.20 shows that as the mixing ratio of CO was increased the chain length initially increased and then started to plateau out. At low CO mixing ratios the conversion of OH to HO_2 was slower than the loss of OH through termination reactions with NO, thus the chain length was low as it was dominated by the loss of OH. At higher CO mixing ratios (greater than approximately 6 %) the conversion of OH to HO_2 was faster than the competing NO termination reaction, thus increasing the chain length. CO mixing ratios needed to be kept as low as possible due to the hazard caused by CO in the laboratory. A CO mixing ratio of 3.5 % was used for this PERCA system, which combined a balance of safety in the laboratory and a high chain length.

Figure 3.21 shows the dependence of the chain length on the mixing ratio of NO. At lower NO mixing ratios the chain length was seen to increase until the mixing ratio of NO

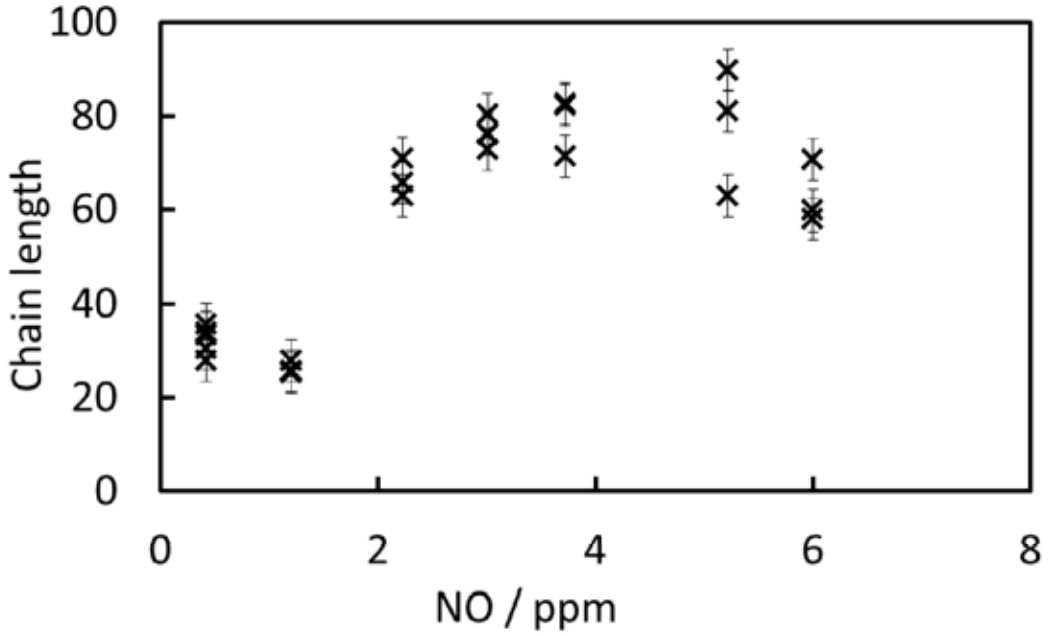

Figure 3.21: Data showing the dependence of the chain length of the PERCA on the NO mixing ratio.

was approximately 4 ppm, then it started to decrease. At low mixing ratios of NO the reaction of HO_2 and NO dominated over the competing NO reaction with OH, increasing the chain length. At higher NO mixing ratios the competing termination reaction of NO with OH dominated over the amplification reaction with CO and led to a decrease in chain length. A NO mixing ratio of 3 ppm was used in this PERCA system - which was slightly smaller than the turning point in the chain length seen with increasing NO mixing ratio.

3.6.4 PERCA Chain Length Characterisation

The PERCA chain length was determined each day before a main tube experiment was performed. The chain length was typically determined at two relative humidities. A calibration at 10 % relative humidity was performed in order to assess the difference in the chain length from day to day. Figure 3.22 shows how the chain length varied over different experiments. All calibrations shown in Figure 3.22 were determined at about 10 % relative humidity. It can be seen that although the chain length varied between 15 and 120 between experiments a typical chain length (at 10 %) was about 80. It was

noted that when the PERCA cell walls were cleaned the chain length increased. It was thought that the very low chain lengths seen in August 2010 (Figure 3.22 was due to this (after being used for this study the PERCA was used for another project and higher chain lengths were seen once the reaction chamber had been cleaned).

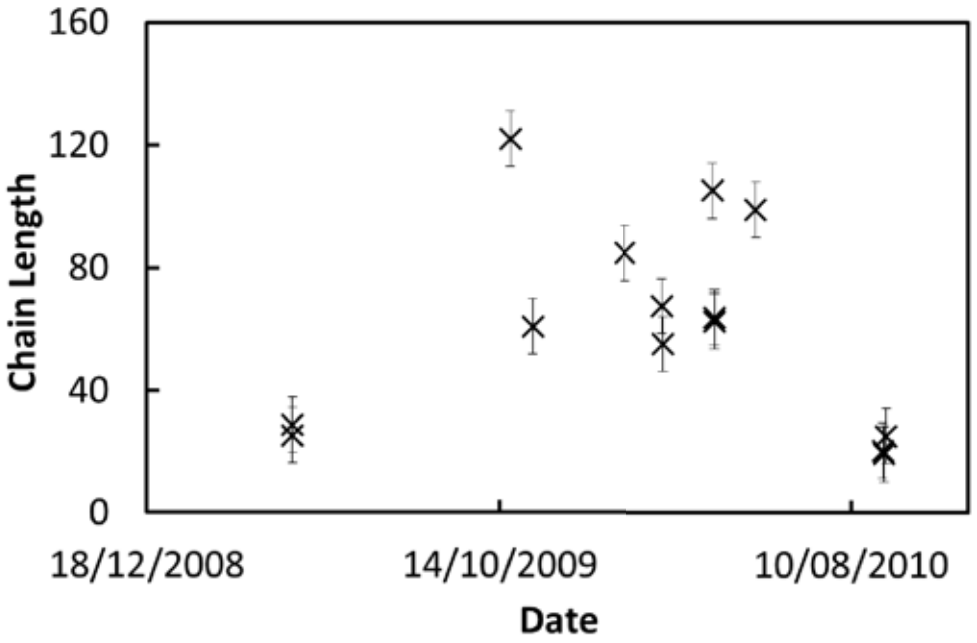

Figure 3.22: Data showing how the PERCA chain length changes with experimental variation. The chain lengths shown here were determined at about 10 % relative humidity.

As mentioned above the PERCA chain length is dependent on the relative humidity. Figure 3.23 shows how the chain length changes with relative humidity. It can be seen that as the relative humidity increases the chain length decreases, as seen by others (Reichert et al., 2003; Mihele, 1999). Low chain lengths at higher relative humidities meant that some wet aerosol experiments could not be performed.

3.7 Summary

This chapter introduced various methods for detecting HO_2 and OH radicals in the atmosphere. The PERCA was chosen for use in this study because it was easier to implement than many other techniques discussed. The theory of the PERCA system has been ex-

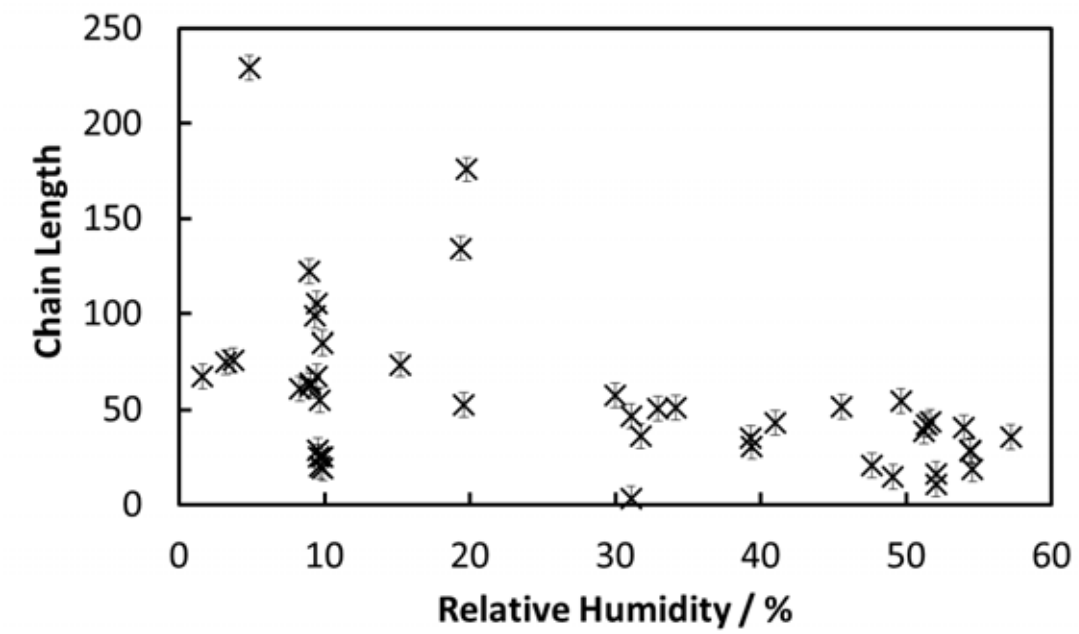

Figure 3.23: Data showing how the PERCA chain length changes with the relative humidity within the PERCA cell.

plained, as has the implementation of the PERCA used in this study. Procedures for the calibration of the PERCA, and the other instruments used within the PERCA system (LMA-3 Luminox, MFCs) have been described, along with the analysis of the data recorded. Finally the PERCA system was characterised.

CHAPTER 4

ANALYSIS

4.1 Introduction

This chapter outlines the analysis of the experimental flow tube data recorded throughout this thesis. Analysis of the PERCA data and various calibration procedures have been covered in Chapter 3. In this chapter the kinetic analysis used to determine the observed rate of loss of HO_2 to the walls of the AFT, k^{obs}_{walls}, and the observed rate of loss of HO_2 to both the walls of the AFT and to aerosol particles, k^{obs}_{total}, is described. Corrections for laminar flow within the AFT are applied to k^{obs}_{walls} and k^{obs}_{total} to determine the corrected loss rate coefficients, k^{*}_{walls} and k^{*}_{aero} (defined in detail later in this chapter). The observed uptake coefficient to aerosol particles, γ_{obs}, is calculated using the determined corrected rate of loss of HO_2 to aerosol, k^{*}_{aero}. Finally a small correction is made to γ_{obs} to account for molecular diffusion within the AFT to obtain the corrected calculated value for the uptake coefficient of HO_2 to aerosols, γ. The uncertainties shown for calculated data are the standard errors unless otherwise stated.

Example data is used throughout this chapter to clearly show each analysis step. The example data shown in this chapter is from an experiment using NaCl doped with $CuSO_4$ as the aerosol. 1.5 g NaCl and 0.08 g $CuSO_4$ were dissolved in 1 L of distilled water to create these aerosols. The experiments were performed at 40 % relative humidity.

A brief summary of the experimental procedure follows; for more detailed information

see Chapter 2.

The aerosol flow tube system was used to determine the rate of loss of HO_2 radicals to aerosol particles. Two types of flow tube experiments were performed. The first was a *wall loss* experiment which was used to determine the rate of loss of radicals to the walls of the AFT; aerosol was not present in the AFT during these experiments. The second type of experiment was an *aerosol loss* experiment, with both aerosols and radicals present within the AFT; this experiment was used to determine the total rate of loss of radicals to the flow tube walls and to aerosol particles. Aerosol was present in the main tube of the AFT and radicals were injected into the centre of the AFT via the injector tube. The injector tube was moved every ten minutes to vary the contact distance and hence the mixing time of the reactants. The concentration of HO_2 was monitored throughout the experiment using the PERCA system and the decay of this reactant was used to determine the rate of loss of the radical.

A summary of the analysis for the flow tube data is shown in Figure 4.1, each term used will be defined and described within this chapter.

4.2 Flow Tube Data Analysis

4.2.1 Raw Data

Throughout each flow tube experiment the relative humidity, temperature, ozone concentration, MFC flows, aerosol distribution and PERCA signal (NO_2 mixing ratio) were recorded. Table 4.1 shows a summary of the data recorded throughout the flow tube experiments. Table 4.1 also shows the frequency at which these data points were recorded and how these data were initially analysed.

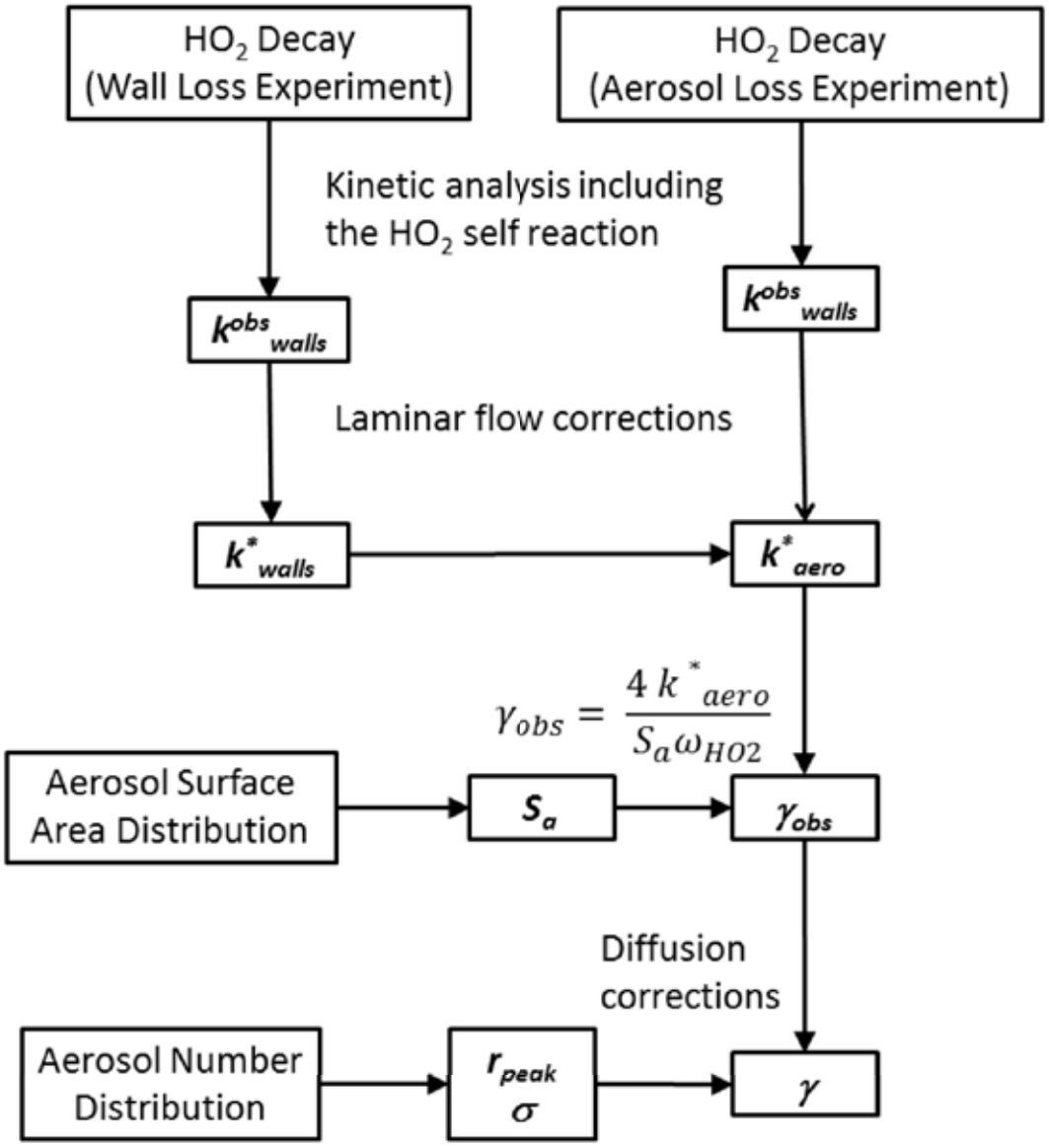

Figure 4.1: A summary of the analysis carried out on the flow tube data in order to determine the uptake coefficient, γ. Details of each step of the analysis is described in the text.

Table 4.1: A summary of the data recorded throughout each experiment and a brief explanation of how they were analysed.

Data Recorded	**Instrument**	**Measurement**	**Period / s**	**Data Handling**
MFC flow	IGI controller	Flow Rate	60	Monitor for abnormal flow rates throughout length of experiment
Ozone	2B Technologies ozone monitor	Mixing ratio	10	Average over 10 minutes
Temperature	Hygropalm	Temperature	10	Average over 10 minutes
Relative Humidity	Hygropalm	% Relative Humidity	10	Average over 10 minutes
Aerosol distribution	SMPS	Number & surface area	340	Average total surface area and peak diameter over the whole flow tube experiment
NO_2 Signal	LMA-3 Luminox	Voltage	1	Convert to HO_2 concentration using the relevant PERCA chain length

MFC Flows

The MFC flows were recorded in order to ensure that all flows were as set throughout each experiment. The flow rates for all gases throughout flow tube experiments were constant, so any change in flow rates (e.g. due to broken MFCs or empty gas cylinders) were easily spotted and the data was not used. Typical flows recorded for an aerosol loss experiment are shown in Table 4.2.

Table 4.2: Typical flows recorded during an aerosol loss experiment. The flow shown is an average over the whole flow tube experiment.

MFC Number	Average Flow / slm	Reagent
2	3.00	Dry air in main tube
3	3.99	Wet air in main tube
4	2.99	Wet N_2 in injector tube
5	1.00	Dry N_2 in injector tube
8	0.07	PERCA CO
9	0.07	PERCA N_2
10	0.01	PERCA NO
11	2.00	PERCA exhaust

Ozone Mixing Ratio

The ozone mixing ratio was monitored to check for any abnormalities throughout the flow tube experiments. Ozone mixing ratios were recorded using a 2B Technologies: Model 205 ozone monitor. There should be little ozone present in the main tube (less than $\approx$ 3 ppb); if a higher ozone mixing ratio was recorded it was usually due to photolysis of O_2. The injector tube was set up (see Chapter 2) so that the UV light from the lamp inside the injector tube did not penetrate to the main tube. If UV light did penetrate into the main tube O_2 could be photolysed to produce O_3. Alternatively if air was present in the injector tube it would be photolysed by the UV light to produce O_3. If a high ozone mixing ratio was detected the experimental set up was investigated for leaks of light into the main tube or leaks of air into the injector tube. The ozone mixing ratio was recorded throughout a flow tube experiment and the average over each ten minute

sample was calculated. Table 4.3 shows typical mixing ratios of O_3 recorded during a flow tube experiment. The mean for the ozone mixing ratio for the experimental data shown in Table 4.3 was 0.7 ppb, with a standard deviation of 0.2 ppb, showing that the variation of ozone values over the whole flow tube experiment was small. The limit of detection for the Model 205 ozone monitor is 2 ppb, indicating that the ozone levels measured below this level are not reliable.

Table 4.3: Typical O_3 mixing ratios recorded throughout a flow tube experiment. The mixing ratios shown are averages over a ten minute period.

Mixing Distance / cm	**O_3 / ppb**
20	0.4
30	0.9
60	1.0
90	1.1
50	0.5
80	0.7
10	0.5
5	0.3
40	0.8
25	1.0
15	0.8
70	0.4
10	0.9
0	0.5

Temperature and Relative Humidity

The temperature and relative humidity were recorded in order to determine the correct chain length to use for the PERCA and to determine whether the aerosol particles were 'wet' or 'dry' (see Chapter 2). The data were recorded throughout the flow tube experiment and the average for both were found over a ten minute period. Table 4.4 shows typical data for the relative humidity and temperature within the flow tube system. All flow tube experiments were conducted at room temperature. The relative humidity varied between experiments depending on which aerosols were being investigated. For the data shown in Table 4.4 the mean relative humidity recorded was 38.18 % with a standard

deviation of 2.01 % and the mean temperature was 22.42 °C with a standard deviation of 0.45 °C. Both values show that the spread of these variables over the whole experiment was small.

Table 4.4: Typical ten minute averages for the temperature and relative humidity recorded throughout a flow tube experiment.

Mixing Distance / cm	**Relative Humidity / %**	**Temperature** / °C
20	36.51	22.52
30	36.93	22.29
60	37.86	22.11
90	35.85	21.89
50	42.24	21.83
80	41.18	21.61
10	38.96	22.12
5	37.84	22.47
40	38.99	22.63
25	39.14	22.70
15	37.89	22.77
70	38.79	22.83
10	37.91	22.97
0	34.41	23.14

Aerosol Distribution

The aerosol distribution was recorded using a Scanning Mobility Particle Sizer (SMPS) with samples taken every five minutes (see Chapter 2 for more information). The total surface area, the peak diameter and the standard deviation of the aerosol distribution was needed to determine γ, so average values over each flow tube experiment were calculated for these values. A ten minute average was also calculated for these parameters to check that there was no significant difference in the aerosol distribution throughout the experiment.

The aerosol number distribution and the aerosol surface area distribution were needed in order to calculate γ; both distributions were exported directly from the SMPS Aerosol Instrument Manager (AIM) Software. The number distribution was used to determine the peak diameter, r_{peak}, and the geometric standard deviation, σ, for each aerosol sample.

These values were calculated automatically by the AIM software for each aerosol sample run through the SMPS. The surface area distribution was used to determine the total surface area, S_a, which was also calculated by the AIM software for each aerosol sample. Table 4.5 and Figure 4.2 show the data extracted from the aerosol distributions recorded by the SMPS. The data is averaged over two five minute samples. The experimental average (averaged over the whole experiment) for each value was used to determine γ. No significant change was seen in the aerosol distribution throughout the experiment, although there is some variation in the data which will translate into scatter on further analysis plots. During a *wall loss* experiment the SMPS data was also recorded, but minimal (less than 1×10^{-8} $cm^2\,cm^{-3}$) aerosol particles were detected.

Table 4.5: Typical data extracted from the AIM software exports for the number and surface area distribution of an aerosol. The data shown here are ten minute averages.

Mixing Distance / cm	S_a / $cm^2\,cm^{-3}$	r_{peak} / **nm**	σ
20	9.28×10^{-4}	69.8	1.71
30	1.02×10^{-3}	73.9	1.70
60	8.30×10^{-4}	72.5	1.74
90	7.78×10^{-4}	66.6	1.68
50	8.40×10^{-4}	69.7	1.72
80	9.52×10^{-4}	65.6	1.71
10	8.33×10^{-4}	63.7	1.74
5	1.03×10^{-3}	69.8	1.69
40	8.95×10^{-4}	73.1	1.72
25	9.80×10^{-4}	69.2	1.70
15	1.02×10^{-3}	67.9	1.69
70	1.03×10^{-3}	65.3	1.71
10	8.86×10^{-4}	78.6	1.73
0	9.12×10^{-4}	69.9	1.70
Experimental Average	9.24×10^{-4}	69.7	1.71
Standard deviation	8.44×10^{-5}	3.9	0.02

PERCA Signal

The PERCA signal was recorded as an NO_2 mixing ratio, which was converted to an HO_2 concentration as described in Chapter 3. The data recorded for a HO_2 decay throughout a flow tube experiment is shown in Figure 4.3.

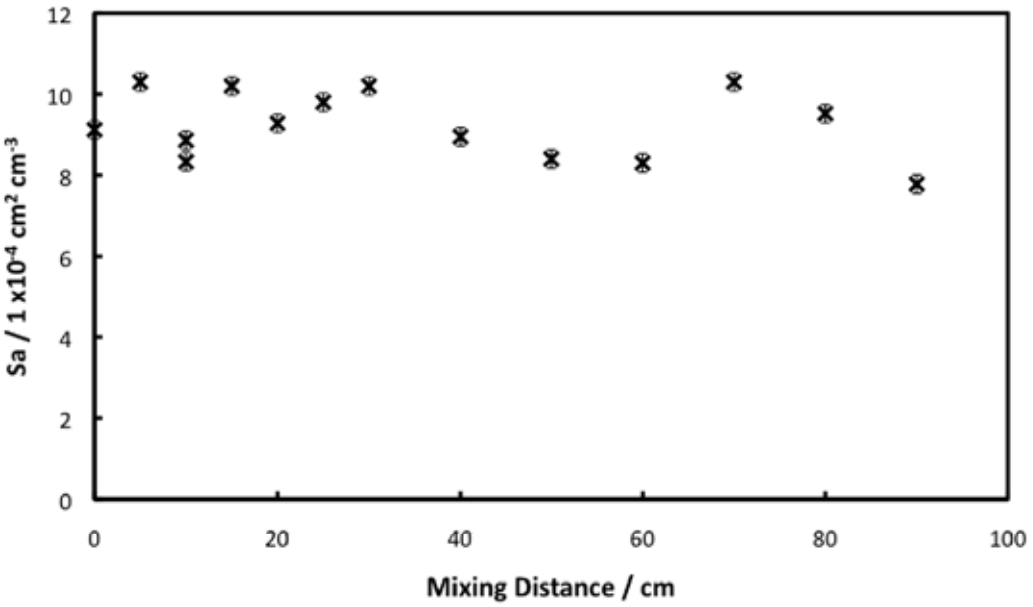

(a) Surface area

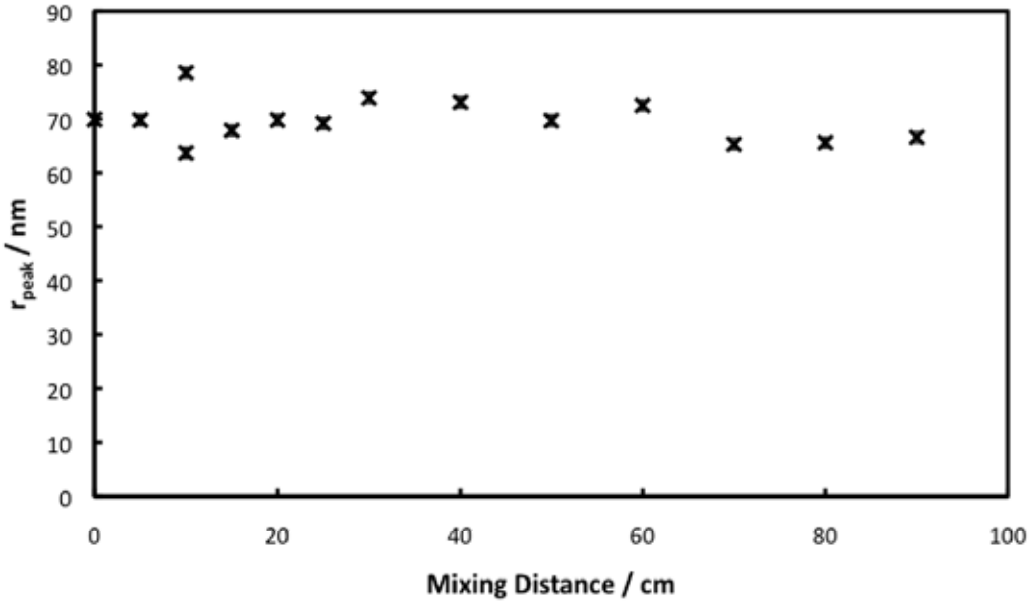

(b) Peak radius

Figure 4.2: A plot showing the variation in total surface area and peak radius of the aerosol distribution throughout an *aerosol loss* experiment. It can be seen that there is little variation throughout the experiment.

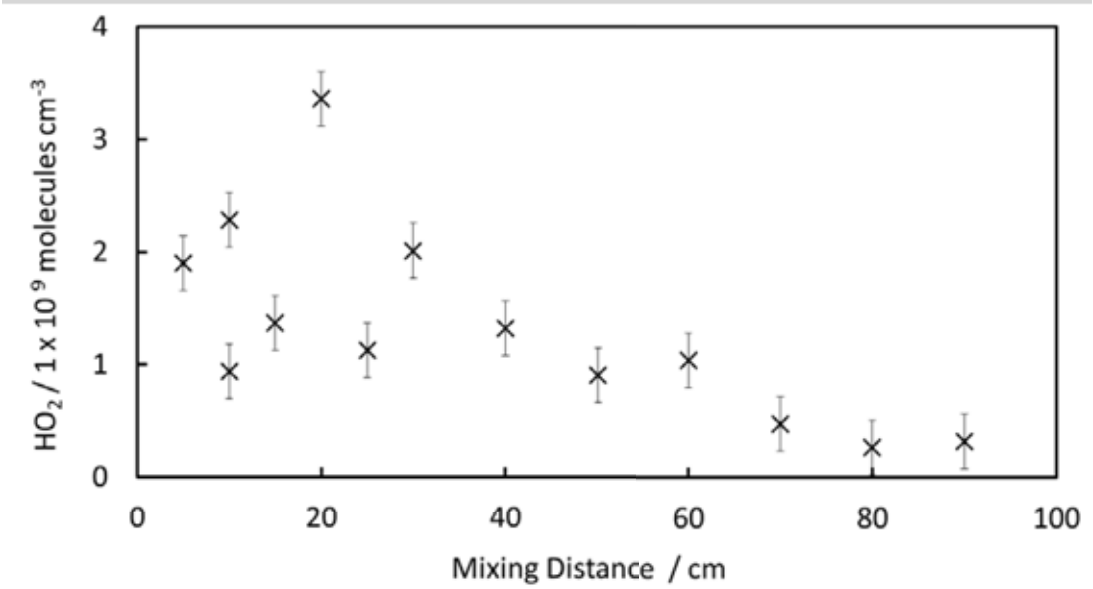

Figure 4.3: The raw data recorded for a HO_2 decay within the flow tube. This is data for a *aerosol loss* experiment.

Figure 4.3 shows a typical decay of HO_2 radicals. All data points recorded for this experiment are shown, although only the data points between 25 cm and 90 cm were used for the analysis. A few points should be noted regarding it:

- The scatter of the data points before 25 cm is large. This is due to the reactants not being fully mixed before this point (See below and Chapter 2 for more details).
- The maximum mixing distance is 90 cm due to the length of the flow tube used in this study. However at 80 cm and 90 cm the concentration of HO_2 is very low and at the limit of detection, so usable data would not be produced if a longer flow tube was used.
- The concentration is approximately one order of magnitude higher than ambient HO_2 concentrations ($\approx 1 \times 10^8$ molecules cm^{-3}).
- The data points after 25 cm appear to show an exponential decay (indicating a first order reaction - see next section for more details.).

The mixing distance shown in Figure 4.3 was converted to reaction time by using Equation 4.1.

$$\text{Reaction Time} = \frac{\text{Mixing Distance}}{\text{Velocity of Main Flow}} \tag{4.1}$$

This calculation assumes plug flow within the AFT, however this was not the case as the flow in the AFT will be laminar, as discussed in Chapter 2. Corrections by Brown (1978) are described later which account for the laminar flow within the tube. Further analysis of this data was performed to determine the loss rate of HO_2 to the walls of the AFT and to aerosols, which is discussed in the next section.

4.2.2 Determination of k_{walls}^{obs}

Flow tube experiments are designed in such a way that a first order decay can be assumed. A flow tube system studies the reaction between two species, by ensuring the concentration of one species, aerosol particles in this study, is in substantial excess of the other species, the HO_2 radicals. It can then be assumed that the species in excess is at an effectively constant concentration throughout the experiment, while the decay of the other species is assumed to be a pseudo first order decay.

The loss of HO_2 to the walls of the AFT was determined by performing a kinetic analysis on the HO_2 decay recorded during a *wall loss* experiment. A typical decay is shown in Figure 4.4, this figure shows that an exponential curve fits the decay reasonably well ($R^2 = 0.75$), indicating that the loss of HO_2 to the walls of the AFT could be described as first order. However this was not the case in this study (see next section).

First Order Kinetic Analysis

A first order rate decay of the reactant, HO_2, can be described by Equation 4.2 (Atkins and de Paula, 2006).

$$\frac{d[HO_2]}{dt} = -k[HO_2] \tag{4.2}$$

Integrating Equation 2.1 gives Equation 4.3, where $[HO_2]_0$ is the initial concentration

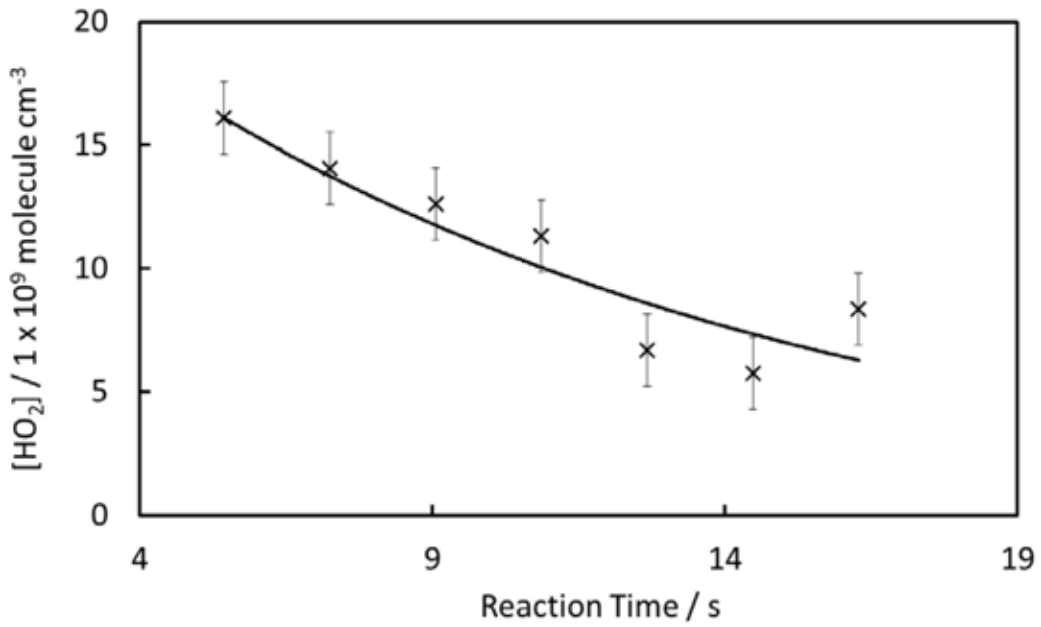

Figure 4.4: Data recorded for an HO_2 decay within the flow tube. This is data for a *wall loss* experiment - no aerosols were present in the flow tube. An exponential curve fits the data reasonably well ($R^2 = 0.75$).

of HO_2.

$$[HO_2] = [HO_2]_0 \exp(-kt) \tag{4.3}$$

A plot of $\ln(\frac{[HO_2]_0}{[HO_2]})$ against the reaction time, t, should be well described by a straight line, the gradient of which is the rate constant, k^{obs}_{walls}. k^{obs}_{walls} is defined as the observed experimental wall loss with no corrections.

This first order kinetic analysis neglects the flow profile, mixing limitations and diffusion within the flow tube. Corrections for these can be made (see Sections 4.2.4 and 4.3.1).

However this analysis also neglects other gas-phase reaction processes which could occur within the AFT. At ambient HO_2 concentrations the self-reaction of HO_2 is small compared to the total loss of HO_2 (i.e. loss to walls and to aerosol), so the loss of HO_2 due to the self reaction of HO_2 within the AFT can be neglected (see Chapter 2). This study uses initial HO_2 concentrations of approximately 1×10^9 molecules cm^{-3} (for *aerosol loss* experiments) and 1×10^{10} molecules cm^{-3}(for *wall loss* experiments) so the rate of loss of

HO_2 due to the self-reaction was investigated with respect to the rate of loss of HO_2 to the walls of the AFT and to aerosol.

Figure 4.5 shows the rate of loss of HO_2 due to its self-reaction, loss to the walls of the AFT (various wall loss rates have been used) and aerosol loss (calculated from the currently recommended value for γ), each considered in isolation. It can be seen from Figure 4.5 that for wall loss rates below and including $k_{walls} = 0.06\,s^{-1}$ the loss of HO_2 to its self-reaction dominates over its loss to walls; once the wall loss is higher than $k_{walls} = 0.02\,s^{-1}$ it becomes the dominant reaction. The rate of loss of HO_2 to aerosol is faster than both the loss to walls and to the self-reaction. These rate calculations indicate that the self-reaction of HO_2 must be taken into account during the analysis of the flow tube data, especially for *wall loss* experiments, where the self-reaction will be the dominating loss of HO_2.

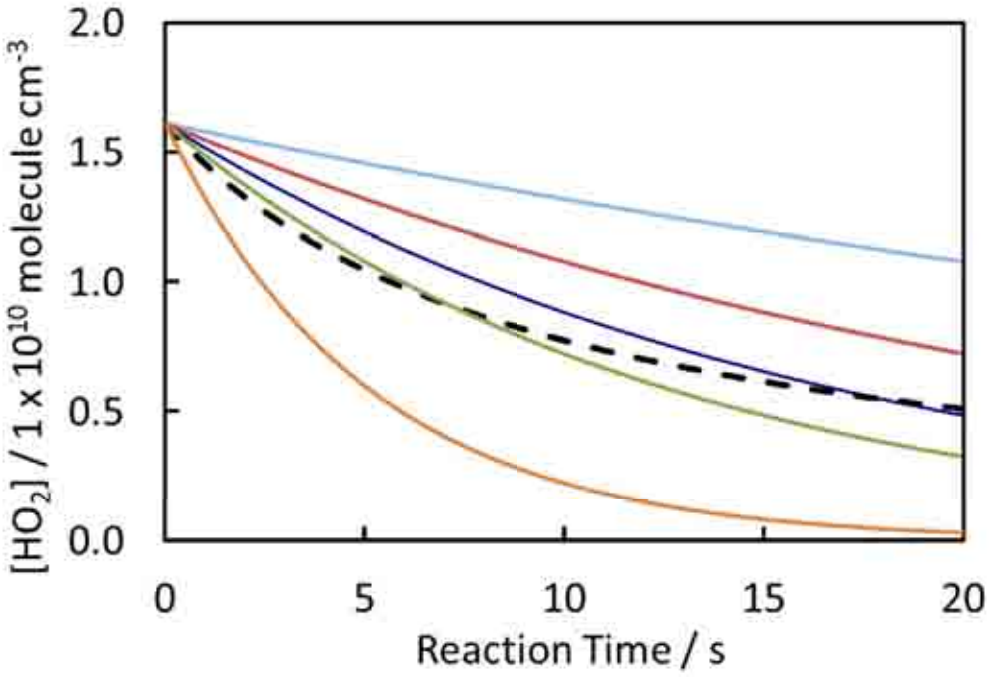

Figure 4.5: Rate loss curves for the self-reaction of HO_2 (dashed line, $k_{self} = 3.35 \times 10^{-12}\,cm^3$ molecule^{-1} s^{-1} at 40 %) and the loss of HO_2 to walls (light blue line, $k_{walls} = 0.02\,s^{-1}$; red line, $k_{walls} = 0.04\,s^{-1}$, dark blue line, $k_{walls} = 0.06\,s^{-1}$; green line, $k_{walls} = 0.08\,s^{-1}$). The orange line shows the loss rate due to aerosol (assuming $k_{aero} = 0.1980\,s^{-1}$, calculated using γ= 0.02 recommended literature value) and a representative total surface area of aerosol particles, $S_a = 9 \times 10^{-4}\,cm^2\,cm^{-3}$).

Mixed Order Kinetic Analysis

A mixed order kinetic analysis was needed in order to determine of the loss of HO_2 within the AFT, taking into account both the loss of HO_2 to walls and to the HO_2 self-reaction. During a *wall loss* experiment Reactions R 4.1 and R 4.2 occurred within the AFT.

$$HO_2 + HO_2 \xrightarrow{M} H_2O_2 + O_2 \quad \text{(R 4.1)}$$

$$HO_2 + \text{wall} - \quad \text{products} \quad \text{(R 4.2)}$$

The rate of loss of HO_2 during a *wall loss* experiment is shown in Equation 4.4, which can be solved, as shown in Equation 4.5 (Pilling and Smith, 1987), to determine the concentration of HO_2 at time t.

$$\frac{d[HO_2]}{dt} = -k_{walls}[HO_2] - 2k_{self}[HO_2]^2 \quad (4.4)$$

$$[HO_2]_t = \left\{ \left([HO_2]_0^{-1} + \frac{2k_{self}}{k_{walls}} \right) \exp(k_{walls}t) - \frac{2k_{self}}{k_{walls}} \right\}^{-1} \quad (4.5)$$

The rate of self-reaction of HO_2, k_{self}, has a dependency on the concentration of water vapour (see Chapter 2). The relative humidity within the AFT was recorded for all flow tube experiments, so the rate of the self-reaction of HO_2 corrected for the presence of water, was calculated for each experiment. This corrected rate constant was used in the analysis to determine k_{walls}^{obs}. In order to determine k_{walls}^{obs} a curve, based on Equation 4.5, was fitted to the data produced from each *wall loss* experiment. The curve fitting program Origin 8.5 was used to fit the curve to the data and to determine k_{walls}^{obs}.

Figure 4.6 shows the wall loss decay data with both the first order (exponential) and mixed order (Equation 4.5) best fit curves. The curve based on Equation 4.5 fitted the data better than the exponential curve fitted (R^2 for the mixed order fit was 0.82 compared to an R^2 value of 0.75 for exponential fit). Although the best fit lines were similar, using them to determine the rate of loss of HO_2 to the walls gives significantly different values

with the example data used in this chapter. The observed rate of loss of HO_2 to the walls of the AFT k^{obs}_{walls} was determined as 0.0867 ± 0.0222 s^{-1} using the first order analysis and as 0.0122 ± 0.01814 s^{-1}, when the self-reaction of HO_2 is accounted for. k^{obs}_{walls} decreased by 86 % once the self reaction of HO_2 had been taken into account.

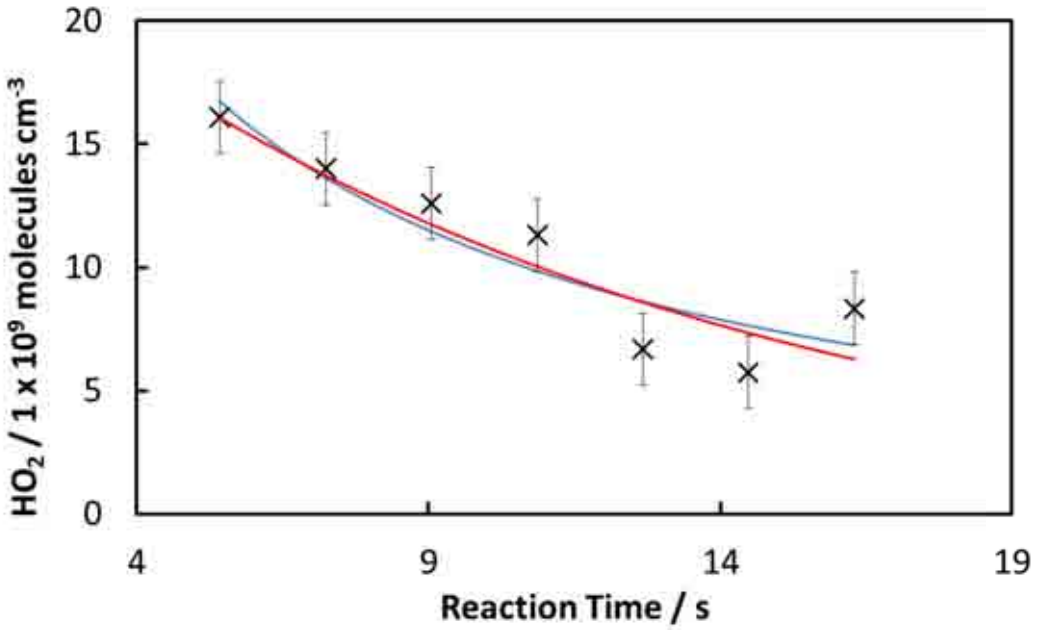

Figure 4.6: Data from a *wall loss* experiment. The red curve shows an exponential curve fitted to the data and the blue line shows the curve fitted using Origin and based on Equation 4.5.

4.2.3 Determination of k^{obs}_{total}

The observed rate of loss of HO_2 to the walls of the flow tube and to aerosol particles, k^{obs}_{total}, was determined by an *aerosol loss* experiment. Chapter 2 gives details of the experimental set up. For an *aerosol loss* experiment data was recorded as described in Section 4.2.1. The HO_2 decay recorded during an *aerosol loss* experiment was analysed in the same way as described for a *wall loss* experiment in the last section. Figure 4.7 shows a typical HO_2 decay for an *aerosol loss* experiment. It can be seen from Figure 4.7 that the first order curve fit and the mixed order curve fit are very similar ($R^2 = 0.91$ and 0.93 respectively), however k^{obs}_{total} determined from the first order analysis was 0.1850 ± 0.0254 s^{-1}, while k^{obs}_{total} was determined as 0.1692 ± 0.0244 s^{-1} when the self-reaction was

taken into account. Taking the self-reaction of HO_2 into account decreased the observed total rate loss by 9 %, this decrease in the observed rate constant was smaller than that seen with the observed rate constant for k^{obs}_{walls}. The reason the self-reaction analysis was smaller was due to the lower concentration of HO_2 used in the *aerosol loss* experiment, which in this example was one order of magnitude less than in the *wall loss* experiment. At higher HO_2 concentrations the self-reaction of HO_2 is a more dominant reaction as its rate depends on the square of the concentration of HO_2.

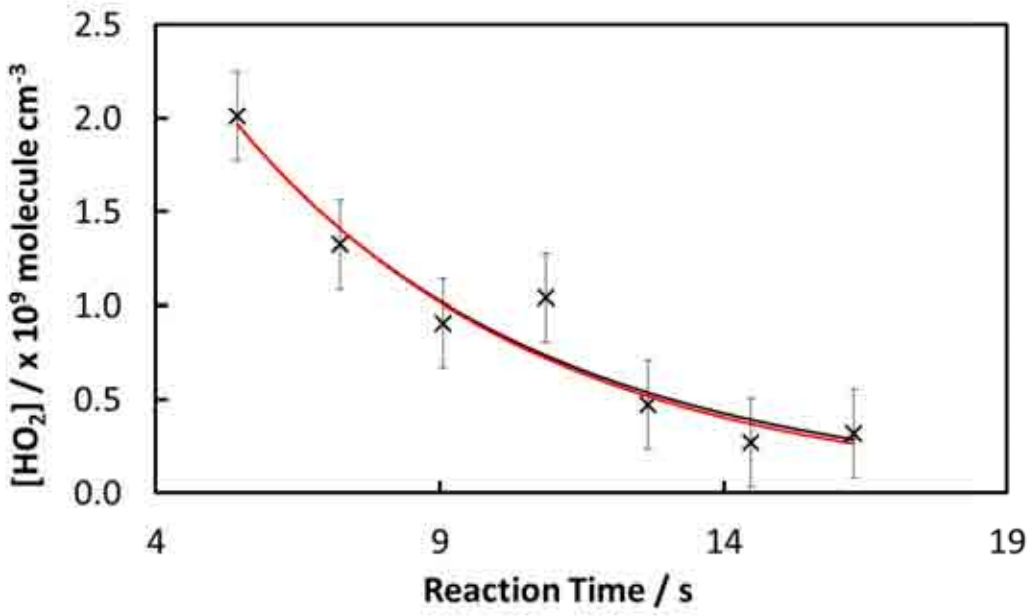

Figure 4.7: A typical HO_2 decay recorded from an *aerosol loss* experiment. The red line shows a first order exponential curve, while the black line shows the mixed order curve defined in Section 4.2.2.

4.2.4 Laminar Flow Corrections

Laminar flow was assumed within the AFT (see Chapter 2), however the analysis presented in Sections 4.2.2 and 4.2.3 to determine k^{obs}_{walls} and k^{obs}_{total} did not take this into account. The observed rate constants (k^{obs}_{walls} and k^{obs}_{total}) were corrected for laminar flow using the methods of Brown (1978). This method includes a correction for the parabolic flow profile across the radial axis of the tube and for the diffusion gradient created when gas molecules are lost to the walls of the tube. A web-based application (*The Brown*

Program: http://www.pouvesle.eu/brown/index.html) was used to implement these corrections. The program is a direct implementation of the Fortran program described by Brown (1978) and was checked against the example presented in that paper.

Variables to describe the AFT used in this study were input into *The Brown Program*: the radius of the flow tube was 3.25 cm; the velocity of the flow within the AFT was 5.52 cm s^{-1}; the diffusion constant, D_g for HO_2 is 0.25 cm^2 s^{-1} (Mozurkewich et al., 1987). Figure 4.8 shows calculated values of k^*_{walls} plotted against k^{obs}_{walls}. It can be seen that as k^{obs}_{walls} gets larger it starts to deviate further from k^*_{walls}. This is expected because as the wall loss gets greater the diffusion gradient created across the flow tube will be more significant, so a greater correction will be applied. The deviation between k^{obs}_{walls} and k^*_{walls} starts with k^{obs}_{walls} values greater than approximately 0.06 s^{-1}, once k^{obs}_{walls} is about 0.08 s^{-1} the correction is too large to be reliably applied. This indicates that observed wall loss rates in this study need to be smaller than 0.08 s^{-1}.

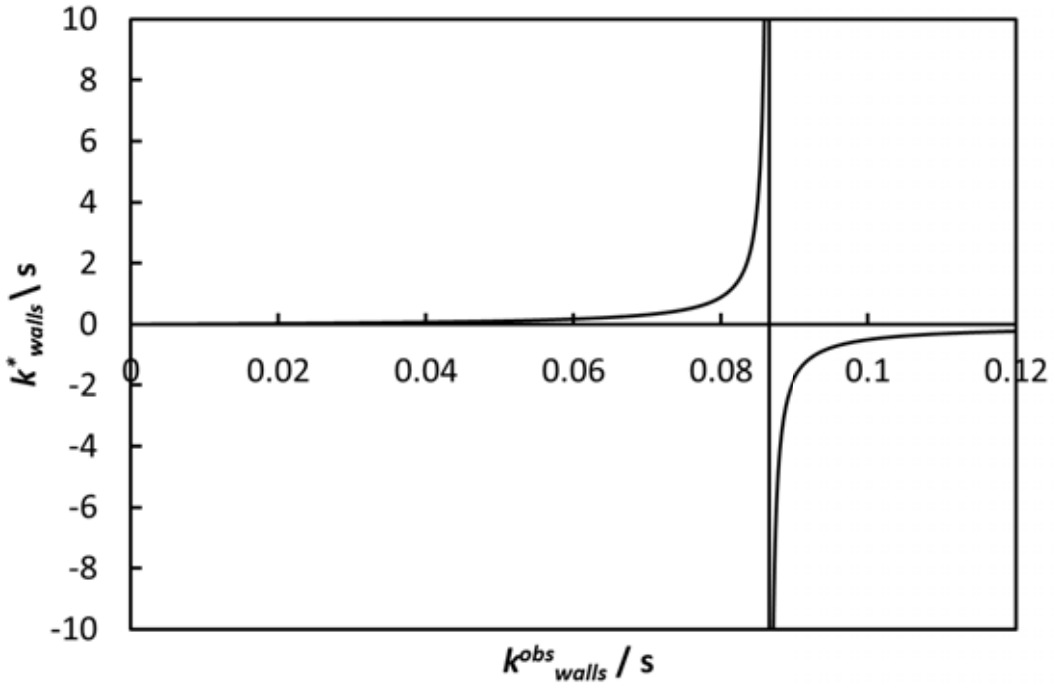

Figure 4.8: Calculated data to show how k^*_{walls} changed with k^{obs}_{walls}.

The laminar flow correction was first applied to k^{obs}_{walls} to determine a corrected value for the rate of loss of HO_2 to the walls of the AFT, k^*_{walls}. This corrected rate loss, k^*_{walls},

and the observed total loss of HO_2 to aerosols and to the AFT walls, k^{obs}_{total}, were used as an input into *The Brown Program* in order to determine a laminar flow corrected value of the rate of loss of HO_2 to aerosols only, k^*_{aero}. Note that *The Brown Program* uses the corrected k^*_{walls} to directly determine a value for k^*_{aero}. The laminar flow correction process is summarised (with values for all rate constants) in Table 4.6.

Table 4.6: Example inputs and outputs for *The Brown Program*, which was used to correct the observed rate constants for effects caused by laminar flow within the AFT.

	Inputs / s^{-1}	**Output** / s^{-1}
First Correction	k^{obs}_{walls}= 0.012 ± 0.018	k^*_{walls}= 0.014 ± 0.021
Second Correction	k^*_{walls}= 0.014 ± 0.021; k^{obs}_{total}= 0.17 ± 0.024	k^*_{aero}= 0.19 ± 0.03

The laminar flow correction increased the determined rate constant for loss of HO_2 to the walls of the AFT by 12 %. The rate of loss of HO_2 to aerosols only was determined directly with the laminar flow correction included.

4.3 Determination of γ

The observed uptake co-efficient, γ_{obs}, was determined using Equation 4.6 (Kolb et al., 2010).

$$\gamma_{obs} = \frac{4k^*_{aero}}{S_a \omega_{HO_2}} \tag{4.6}$$

k^*_{aero} and S_a were determined from experimental data (as described in Section 4.2) and ω_{HO_2} is the mean molecular speed of HO_2 (calculated as 43 724 cm s^{-1} at an average temperature of 298 K using $\sqrt{\frac{8RT}{\pi M_{HO_2}}}$) (Atkins and de Paula, 2006). Following the example used throughout this chapter γ_{obs} was determined as 0.0192 ± 0.0032, with S_a = 9.06 ± 0.03 × 10^{-4} cm^2 cm^{-3} and k^*_{aero}= 0.1904 ± 0.0304 s^{-1}.

A value for γ_{obs} can be found more rigorously over a number of flow tube experiments. If k^*_{aero} is experimentally determined for various values of the total surface area of an aerosol distribution then a plot of k^*_{aero} against S_a should fit a straight line, with the

gradient equal to $\frac{\gamma_{obs}\omega}{4}$.

4.3.1 Diffusion Corrections

The analysis of the flow tube data so far has not included the effect of gas-phase diffusion of the gas to the particle, which will occur within the AFT system. As gas molecules are taken up by the particle the concentration of these molecules decreases close to the particle. The low concentration of molecules near the particle will lead to a measured γ value lower than the actual rate of uptake. A correction can be used to account for this and in this case is expected to be small (due to the small radii of the particles). Taketani et al. (2008) and Thornton and Abbatt (2005a) describe the procedure for correction for the gas-phase diffusion, which is based on techniques by Fuchs and Sutugin (1970) and Fried et al. (1994).

The correction for gas phase diffusion was made to the observed uptake coefficient, γ_{obs}, which was determined in the previous section. Equation 4.7 (Fuchs and Sutugin, 1970; Taketani et al., 2008; Thornton and Abbatt, 2005a) was used to determine the diffusion correction. $\lambda(r_s)$ is calculated as shown in Equation 4.8.

r_s is the mean surface-area weighted radius of the aerosol particles. The mean surface-area weighted radius is used for these calculations because of the dispersed nature of the aerosol distribution. In theory an integration of Equation 4.7 should be performed over the particle size represented in the aerosol distribution, but if the aerosol distribution is log-normal then r_s can be used instead. r_s is calculated using Equation 4.10 from the peak radius of the experimental number distribution and the geometric standard deviation of the same distribution. The aerosol distributions used throughout this study were log-normal distributions (see Chapter 5), so this simplification was valid.

K_n is the Knudsen number and is defined as the ratio of the mean free path of the gas molecule to the radius of the particle. If the Knudsen number is large (i.e. the particle radius is much smaller than the mean free path) the concentration gradient near the particles will be negligible. If the Knudsen number is small (i.e. the particle radius is much

larger than the mean free path) the concentration gradient near the particles will be important. Mathematical terms have been derived by Fuchs and Sutugin (1970) to describe both extremes for the Knudsen number. For intermediate Knudsen numbers an exact mathematical treatment is not readily carried out; for these Knudsen numbers an approximation is suggested by Fuchs and Sutugin (1970). The Knudsen number is calculated using Equation 4.9, where D_g is the gas-phase diffusion constant for HO_2 ($0.25\,cm^2\,s^{-1}$). If the Knudsen number is much larger than the reaction probability then diffusion will not limit the reaction (Lovejoy and Hanson, 1995). In this case the reaction probability, γ, must be less than 1 by definition; K_n was calculated to be 1.16 for the example data used in this chapter, therefore diffusion is not expected to limit the reaction but as the Knudsen number is not very much greater than the maximum reaction probability a correction for diffusion should be applied (but is expected to be small).

$$\gamma_{corr} = \frac{\gamma_{obs}}{(1 - \gamma_{obs}\lambda(r_s))} \tag{4.7}$$

$$\lambda(r_s) = \frac{0.75 + 0.283K_n}{K_n(1 + K_n)} \tag{4.8}$$

$$K_n = \frac{3D_g}{\omega_{HO_2} r_s} \tag{4.9}$$

$$r_s = r_{peak} \exp(2.5(\ln \sigma)^2) \tag{4.10}$$

For the example used in this chapter r_{peak} was determined as 69.7 ± 1.05 nm and the geometric standard deviation of the particle distribution was determined as 1.71 ± 0.0050.

Table 4.7 shows example calculations used to determine the diffusion corrected value of γ.

The diffusion corrected uptake coefficient, γ, was less than 1 % higher than the uncorrected uptake coefficient, γ_{obs}, for the example used in this analysis. This was expected

Table 4.7: Calculations used to determine γ

Variable	Equation	Experimentally determined inputs	Calculated inputs	Calculated Value
r_s	4.10	$r_{peak} = 69.7\,\text{nm}$; $\sigma = 1.71$		$1.47 \times 10^{-5}\,\text{cm}$
K_n	4.9	$r_s = 1.47 \times 10^{-5}\,\text{cm}$	$D_g = 0.25\,\text{cm}^2\,\text{s}^{-1}$ $\omega_{\text{HO}_2} = 43\,724\,\text{cm}\,\text{s}^{-1}$	1.20
$\lambda(r_s)$	4.8	$K_n = 1.2013$		0.3917
γ	4.7	γ_{obs}= 0.0192 $\lambda(r_s) = 0.3917$		0.0194

due to the large Knudsen number of the particles with respect to the reaction probability.

4.4 Summary

This chapter outlines the analysis performed on the data recorded during a flow tube experiment (both *wall loss* and *aerosol loss* experiments). Background data were averaged over the whole experiment in order to check for any abnormalities and to characterise each flow tube experiment. In particular the relative humidity was recorded in order to ensure the relevant chain length was used for the PERCA data and to determine what phase the aerosol particles were in. The aerosol distribution was recorded in order to determine the total surface area of the particles, which was needed to determine γ.

The HO_2 decay, with respect to the reaction time, was recorded during flow tube experiments. The decay was analysed using a mixed order kinetic analysis, which included the rate of the self-reaction of HO_2 at the relevant relative humidity, to determine the rate of loss of HO_2. A *wall loss* experiment determined the observed rate of loss of HO_2 to the walls of the AFT, k^{obs}_{walls}. An *aerosol loss* experiment determined the observed rate of loss of HO_2 to both the walls of the AFT and to aerosol particles, k^{obs}_{total}. Originally a first order decay was assumed for the analysis process, but it was realised that the self-reaction of HO_2 needed to be accounted for. The percentage decrease of k^{obs}_{walls} due to including the self-reaction rather than not including it was 86 %, while the equivalent percentage

decrease was 9 % for k_{total}^{obs}. The large difference in the decrease of the observed rate constants due to including analysis for the self reaction was due to two factors. The first was a difference in the two experiments - the initial HO_2 concentration was an order of magnitude greater for the *wall loss* experiment compared to the *aerosol loss* experiment, due to losses in the mixing stage with the latter, a greater correction is expected for larger HO_2 concentrations. The second difference in the two experiments was the relative rates of the reactions occurring during the experiments. In a *wall loss* experiment two reactions occur with respect to HO_2 - its loss to the walls of the AFT and its loss due to its self-reaction. The AFT was coated with halocarbon wax to keep wall losses low, so the self reaction was the most dominating loss reaction unless the loss to wall was greater than around $0.06\,s^{-1}$ (see Section 4.2.2). During an *aerosol loss* experiment the rate of loss of HO_2 to aerosols was the dominating reaction (assuming a low enough HO_2 concentration - see Chapter 5).

To date no other studies investigating the loss of HO_2 to aerosols have been analysed including the self-reaction of HO_2. Taketani et al. (2008) used ambient concentrations of HO_2 (approximate initial HO_2 concentrations were 1×10^8 molecules cm^{-3} with no aerosol present and 3×10^7 molecules cm^{-3} with aerosol present); the study assumed the self-reaction of HO_2 to be negligible. Thornton and Abbatt (2005a) used initial concentrations of HO_2 of 2.5×10^{10} molecules cm^{-3} (no aerosol present) in their experiments. Thornton and Abbatt indicated that their non-aerosol losses fitted a mixed order kinetic analysis better than a first order kinetic analysis and attributed it to the self-reaction of HO_2. Their HO_2 decays due to aerosol loss HO_2 fitted a first order kinetic analysis well. To aid with analysis Thornton and Abbatt assumed a first order decay for non-aerosol losses as well as for aerosol losses despite the mixed order rate loss seen, however they only used the parts of the non-aerosol decay that fitted a first order analysis well (as the concentration of HO_2 reduced during a reaction the self-reaction would have become less important with respect to other losses).

In order to determine the actual rate of loss of HO_2 to aerosol, corrections for laminar

flow were made to the observed rate losses for the HO_2 decays. k^{obs}_{walls} was corrected for laminar flow to determine the actual rate loss to walls, k^{*}_{walls}. The laminar flow correction increased the rate loss of HO_2 to the walls by 12 % for the example data used in this chapter. This correction is in agreement with Taketani et al. and Thornton and Abbatt, whose observed rate constants increased by 10 – 20 % and 20 % respectively. The rate of loss to aerosols was determined directly using the laminar corrected values.

Once the true values of k^{*}_{walls} and k^{*}_{aero} were determined γ_{obs} was found using the experimentally determined averages of the total surface area of aerosol particles. Finally, γ_{obs} was corrected for gas phase diffusion to determine γ. The gas phase diffusion correction was small (less than 1 %).

CHAPTER 5

CHARACTERISATION OF THE FLOW TUBE SYSTEM

5.1 Introduction

This chapter describes the characterisation of the flow tube system. The first half of this chapter describes the characterisation of the aerosol used throughout this study, while the second half characterises the various factors which affect the loss of HO_2 to the walls of the AFT.

The aerosol used in this study was created using an atomiser (see Chapter 2 for details) which was filled with a salt solution of the desired composition. The aerosol distribution produced by the atomiser depends on the concentration of the salt solution and the flows employed in the atomiser. This dependency was characterised and the results are shown in this chapter for the aerosol types used in this study (sodium chloride and ammonium sulphate).

Aerosol particles can be termed as 'wet' or 'dry' depending on the amount of water within the bulk of the particle. Aqueous (wet) and solid (dry) particles are present in the atmosphere so both phases of aerosols were used in this study (Kolb et al., 2010). Some aerosols were created from just the salt, while others were doped with copper (II) sulphate ($CuSO_4$). The Cu(II) ion acted as a catalyst for the HO_2 termination reactions within the aqueous bulk of an aerosol particle and therefore these Cu(II) doped aerosol were used

to determine α, the mass accommodation coefficient, (see Chapter 1 for details). This chapter also looks at the loss of aerosols within the experimental apparatus, including loss to the walls of the aerosol flow tube as well as other possible losses within the apparatus.

The second half of this chapter characterises the loss of HO_2 to the walls of the AFT, k^*_{walls}, by discussion of how it was affected by:

- halocarbon wax coating on the flow tube walls
- variation between experiments
- relative humidity
- initial HO_2 concentration

k^*_{walls} was calculated from wall loss experiments using a mixed order rate analysis as described in Chapter 4. The mixed order rate analysis accounted for both the second order rate of reaction for the self-reaction of HO_2 and the first order rate of reaction for loss of HO_2 to the walls of the AFT. Values of k^*_{walls} shown in this chapter have also been corrected for both laminar flow (Brown, 1978) and gas phase diffusion (Fuchs and Sutugin, 1970), unless otherwise stated. For all data shown within this chapter the uncertainty shown is the standard error of the data.

5.2 Characterisation of the Production of Aerosols

The number and surface area distribution are used in the analysis of the AFT data to determine γ (see Chapter 4). A typical number distribution for an *aerosol loss* experiment is shown in Figure 5.1(a) and the corresponding surface area distribution is shown in Figure 5.1(b).

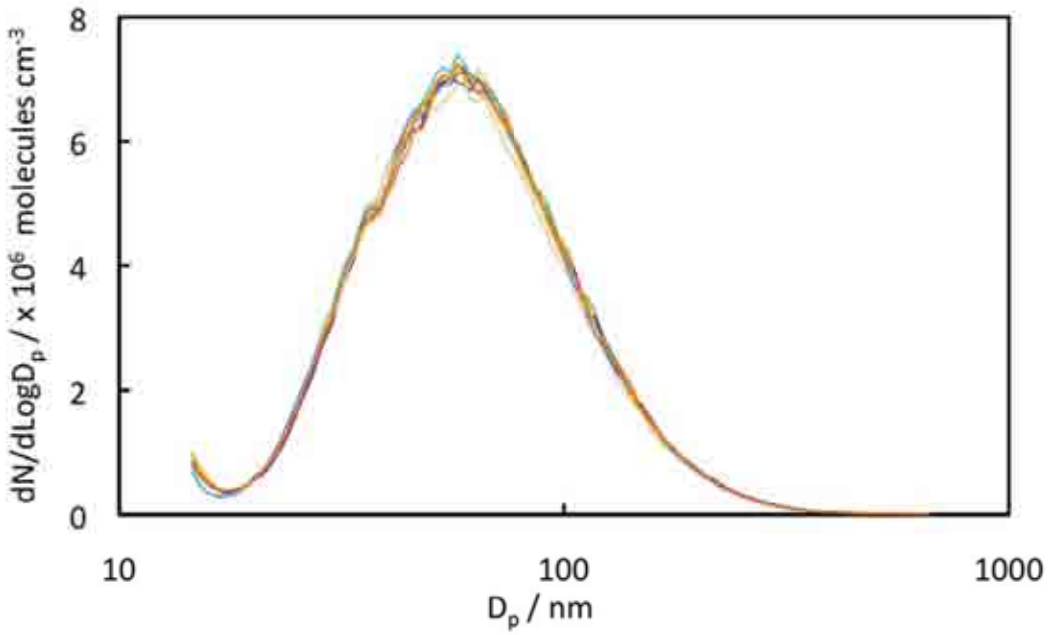

(a) Number Distribution

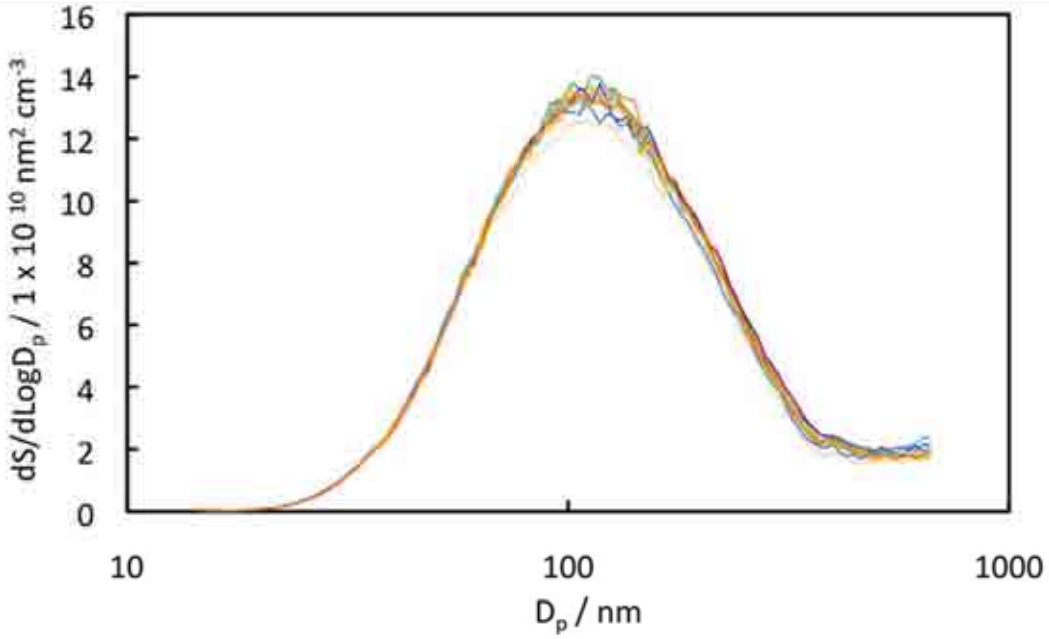

(b) Surface Area Distribution

Figure 5.1: A typical aerosol distribution for an *aerosol loss* experiment. The aerosol was generated by an atomiser from a 0.01 M sodium chloride solution and the data was recorded using an SMPS. Each line represents a five minute sample of the aerosol.

5.2.1 Aerosol Distribution Dependency on Solution Concentration

The concentration of the salt solution used in the atomiser determines the size distribution of the aerosol particles produced (see Chapter 2). Experiments were performed to determine the optimum concentration of salt solution to use for creating particles of the size distribution required in this study. Various concentrations of salt solutions were made up and the size distribution was recorded by the SMPS for each solution. The total surface area of the aerosol distribution and the total number of particles within the aerosol distribution were recorded. Figures 5.2 and 5.3 show that as the concentration of the salt solution was increased both the total surface area and the total number of particles in the aerosol distribution increased.

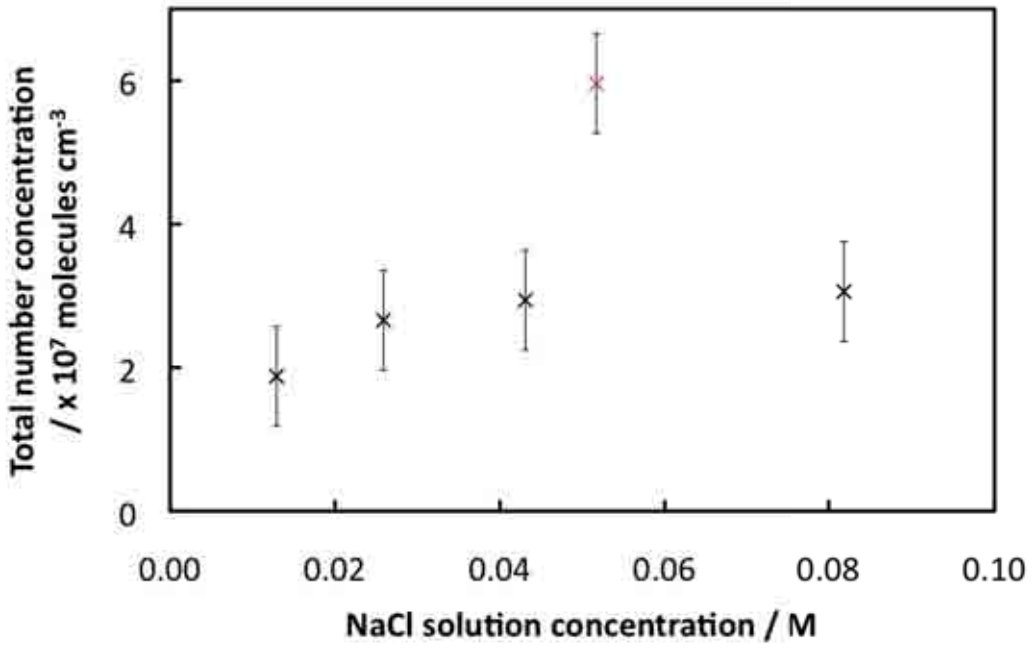

Figure 5.2: Data showing how the total number concentration of a aerosol distribution varies with the concentration of the salt solution from which the aerosol is atomised. The red point is an outlying point.

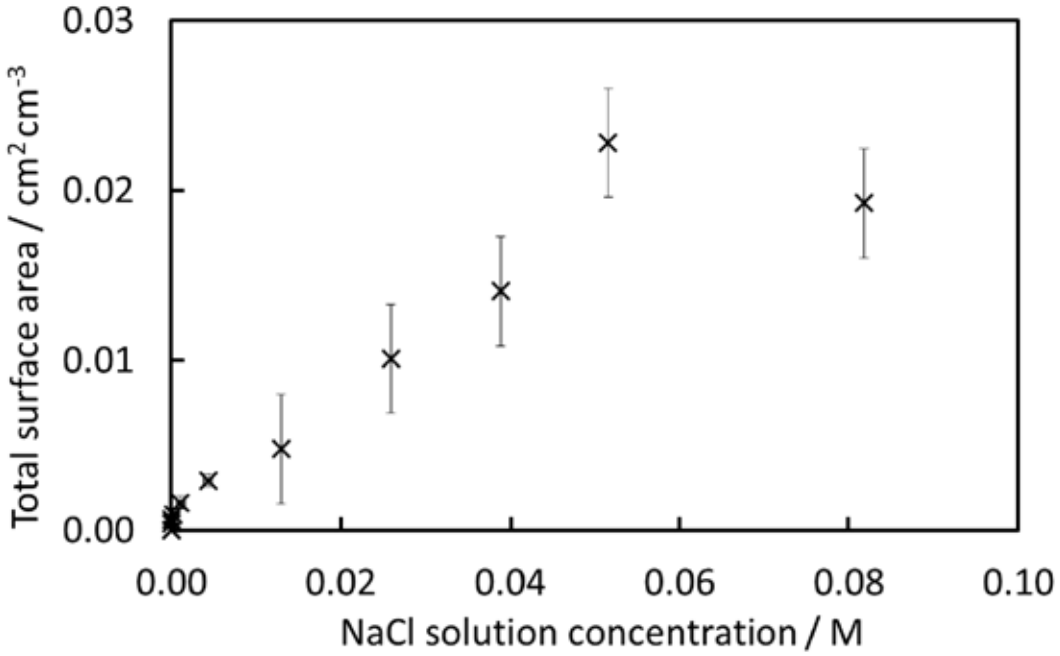

Figure 5.3: Data showing how the total surface area of an aerosol distribution varies with the concentration of the salt solution from which the aerosol is atomised.

5.2.2 Wet and Dry Aerosols

Aerosol particles can be termed as 'wet' or 'dry' depending on the amount of water within their bulk (see Chapter 2). Wet particles are defined as particles present in a gas which has a relative humidity greater than that particle's deliquescence relative humidity. Dry particles are defined as particles present in a gas which has a relative humidity less than that particle's efflorescence relative humidity. It should be noted that care must be taken over the relative humidity history of the particle due to a hysteresis effect on the water uptake to the particle (see Chapter 2). This section characterises the efflorescence relative humidity for NaCl and $(NH_4)_2SO_4$ aerosols used in this study.

Sodium Chloride Aerosols

Martin (2000) reports values of the deliquescence relative humidity of NaCl to be 75 % and the efflorescence relative humidity to be between 40 – 50 % (see Table 5.1). The variation in the recorded efflorescence relative humidity is considered to be due to impurities in the NaCl which will cause nucleation, and thus crystallisation, to occur at a higher relative

humidity than expected.

Table 5.1: Literature values recorded for the efflorescence and deliquescence relative humidities. This data has been taken from a review by Martin (2000). All data is for NaCl at 298 K except the studies by Cohen et al. (1987b,a), which were performed at 293 K.

Study	**Deliquescence RH / %**	**Efflorescence RH / %**
Cziczo et al. (1997)	75 ± 1	43 ± 2
Tang (1980)	75.7	43
Richardson and Snyder (1994)	75.3	45.5 ± 0.6
Cohen et al. (1987b) and Cohen et al. (1987a)	75 ± 1	44
Cziczo and Abbatt (2000)	75 ± 2	40 ± 2
Weis and Ewing (1999)		50 ± 15

The efflorescence relative humidity for NaCl aerosol, doped with Cu(II) was determined for this AFT system. Cu(II) doped aerosol could have a higher efflorescence relative humidity than pure NaCl due to potential nucleation by Cu(II). The aerosol particles were produced by the atomiser (so were at a high relative humidity) and then flowed through the AFT. The aerosol was dried out to obtain various relative humidities either by passing it through a diffusion dryer (TSI, Model 3062) and then diluting with the bulk air (of controlled relative humidity) in the AFT or by simply diluting it with the bulk air in the AFT. The aerosol in the AFT was sampled by the SMPS and the number distribution obtained was recorded. By assuming that the particles are larger in size when they contain water (Martin, 2000) the efflorescence relative humidity was determined by determining the mean particle diameter at various relative humidities. The efflorescence relative humidity, rather than the deliquescence relative humidity, was determined because the aerosol particles were dried out from a high relative humidity. The number distribution was used to determine the mean particle diameter at each relative humidity - this is shown in Figure 5.4 for NaCl particles doped with $CuSO_4$.

The step change in the mean diameter indicates the change in phase of the particle from an aqueous to a solid phase, indicating the efflorescence point. Figure 5.4 shows the step change in particle diameter, and thus the efflorescence relative humidity for NaCl doped with Cu(II), is around 50 %. This efflorescence relative humidity is in agreement

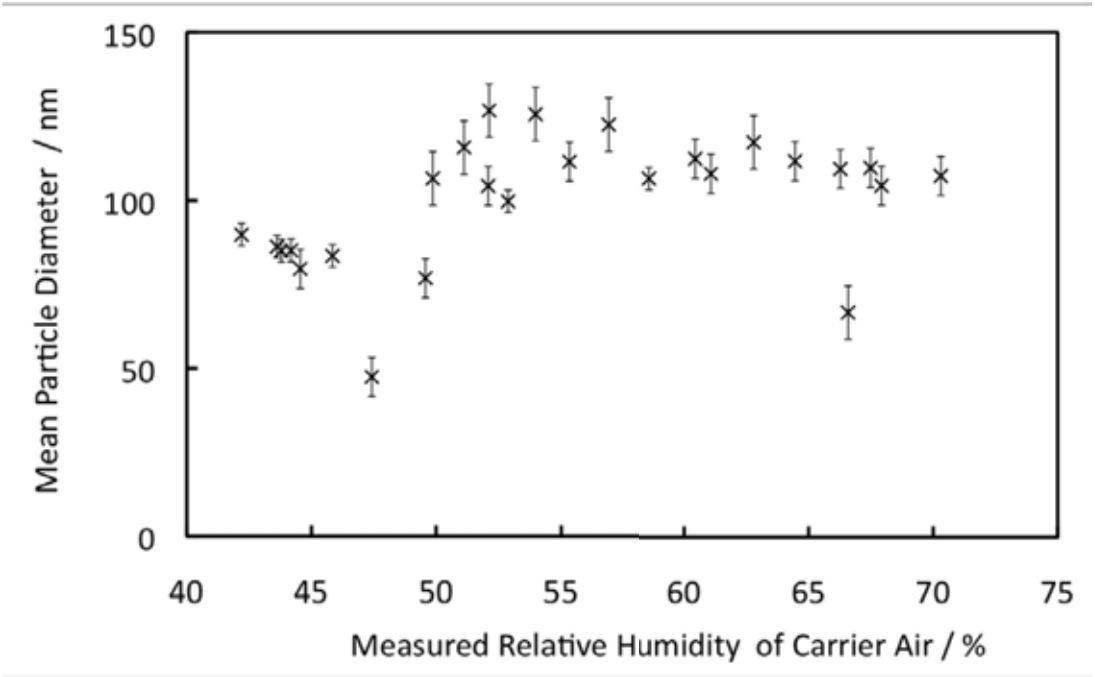

Figure 5.4: This plot shows the mean particle diameter of the number distribution for NaCl aerosols doped with Cu(II) plotted against the relative humidity of the bulk air flow which the particles are suspended in. The increase in the mean diameter occurs at approximately 50 %.

with the measurement of impure NaCl by Weis and Ewing (1999), but between 6 – 10 % higher than other literature values (Cziczo et al., 1997; Tang, 1980; Richardson and Snyder, 1994; Cohen et al., 1987b,a; Cziczo and Abbatt, 2000).

Ammonium Sulphate Aerosols

Martin (2000) reports values of the deliquescence relative humidity of $(NH_4)_2SO_4$ to be between 79 – 81 % and the efflorescence relative humidity to be between 33 – 48 % (see Table 5.2). As with the efflorescence relative humidity point for NaCl aerosol the variation in the recorded efflorescence relative humidity is considered to be due to impurities in the salt.

The efflorescence relative humidity for $(NH_4)_2SO_4$ aerosols doped with Cu(II) was determined experimentally in the same way as the NaCl efflorescence relative humidity described previously. Figure 5.5 shows the step change in the mean particle diameter occurs at approximately 45 %. This value is in agreement with the upper values given by

Table 5.2: Literature values recorded for the efflorescence and deliquescence relative humidities. This data has been taken from a review by Martin (2000). All data is for $(NH_4)_2SO_4$ at 298 K except the studies by Cohen et al. (1987b,a), which was at 293 K.

Study	Deliquescence RH / %	Efflorescence RH / %
Cziczo et al. (1997)	79 ± 1	33 ± 2
Han and Martin (1999)	79 ± 2	35 ± 2
Tang (1980)	79.5	36
Richardson and Snyder (1994)	80.0 ± 1.2	34.7 ± 0.4
Cohen et al. (1987b) and Cohen et al. (1987a)	81	48
Dougle et al. (1998)	80	42

literature (Dougle et al., 1998; Cohen et al., 1987a,b), but between 9 – 12 % higher than other literature values (Cziczo et al., 1997; Han and Martin, 1999; Tang, 1980; Richardson and Snyder, 1994).

5.3 Characterising Aerosol Flow and Aerosol Loss Within the Experimental Apparatus

Aerosol particles created by the atomiser were expected to be highly charged due to the nature of the atomiser (TSI, 2008a). Highly charged particles are easily lost to surfaces they encounter, in this case the walls of the aerosol flow tube or any other part of the apparatus. Losses were minimised by using conductive tubing wherever aerosol was present. In some cases this was not possible (such as within the aerosol flow tube). This section investigates those losses to determine their magnitude.

5.3.1 Aerosol Flow Tube Losses

Aerosol will be lost to the walls of the experimental apparatus - to determine the magnitude of loss the aerosol number distribution was measured directly exiting the atomiser and then a distribution for the same aerosol was measured once the flow has passed through the set-up (i.e. from the atomiser into the AFT; from the AFT into the SMPS).

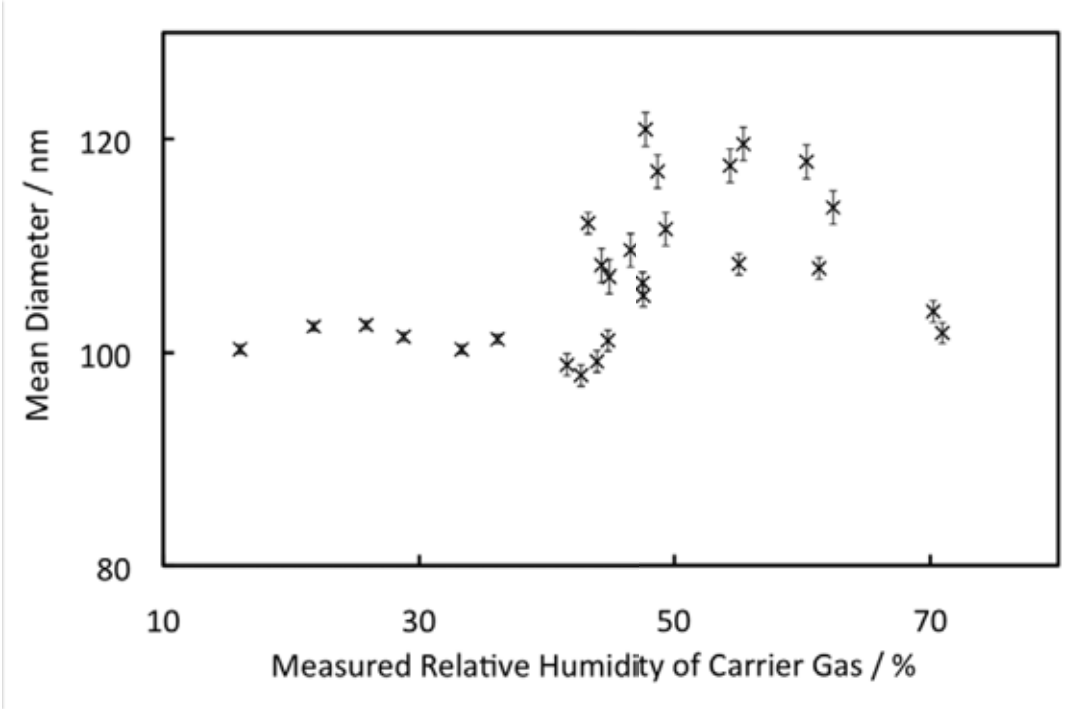

Figure 5.5: This plot shows the average particle diameter of the number distribution for $(NH_4)_2SO_4$ aerosols doped with Cu(II) plotted against the relative humidity of the bulk air flow which the particles are suspended in. The increase in the mean diameter occurs at approximately 45 %.

Figure 5.6 shows the comparison of these measurements, indicating that approximately half the aerosol was lost within the AFT system.

The losses due to the experimental apparatus was investigated further to ensure the flow was uniform along the tube, which was desired in order to accurately measure the uptake of HO_2 to the aerosol particles. The aerosol profile along the AFT was investigated by employing the AFT in a 'reverse configuration' as shown in Figure 5.7. In the 'reverse configuration' the AFT was turned around within the set-up so that the injector tube carried the flow out of the system, rather injecting a flow into the system. The injector tube was connected to the SMPS via anti-static tubing. The SMPS sampled flow, through the injector tube, from the main tube. The injector was moved in order to sample the aerosol at various points along the AFT and the SMPS was used to record the number distribution of each aerosol sample. Aerosol was flowed into the AFT in the normal way and was diluted with the carrier air. The flows used were the same as those used for

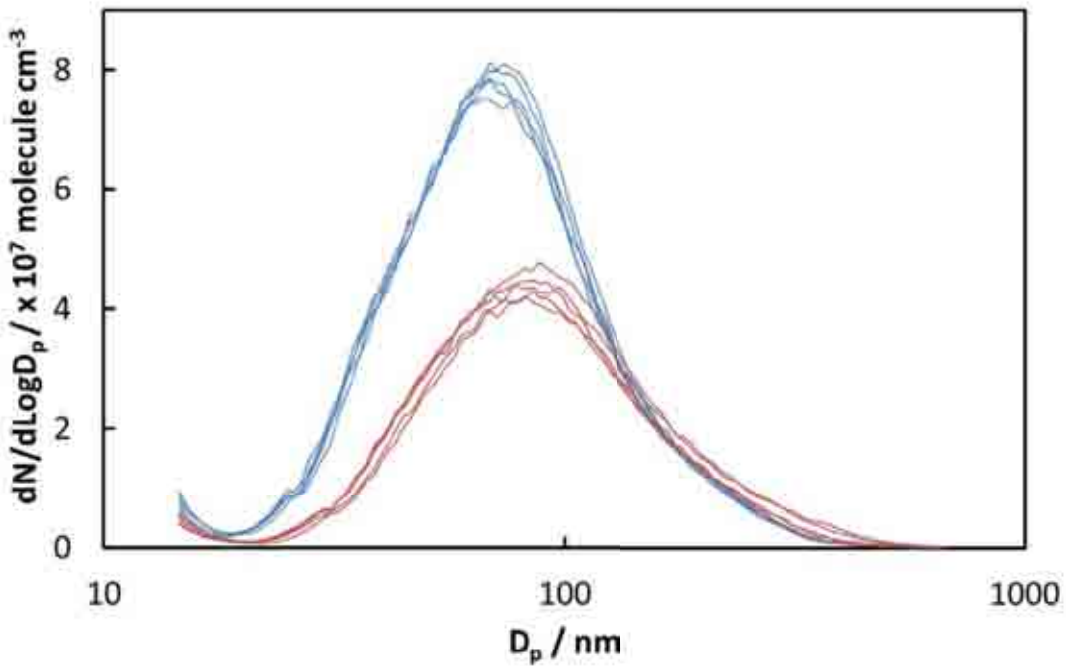

Figure 5.6: The aerosol number distribution was measured directly from the atomiser (blue lines) and also once it had passed through the aerosol flow tube (red lines).

a typical *aerosol loss* experiment. Radicals were not present in the AFT during these measurements.

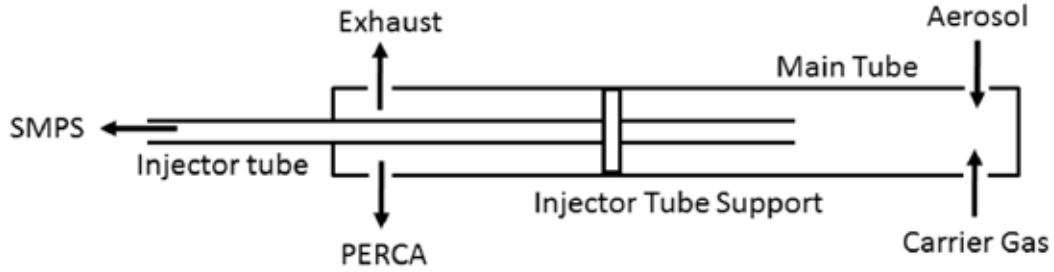

Figure 5.7: The experimental set up to investigate the aerosol profile along the AFT.

Figure 5.8 shows the total number concentration for each sample plotted against the distance along the AFT from the aerosol entry point. There was no significant variation in the total number concentration along the AFT, indicating that most of the aerosols were lost on entry to the flow tube rather than along the length of the flow tube (i.e. to the walls). The aerosol entered the AFT perpendicular to the carrier flow; this connection may have acted as an impactor, leading to the loss of larger particles.

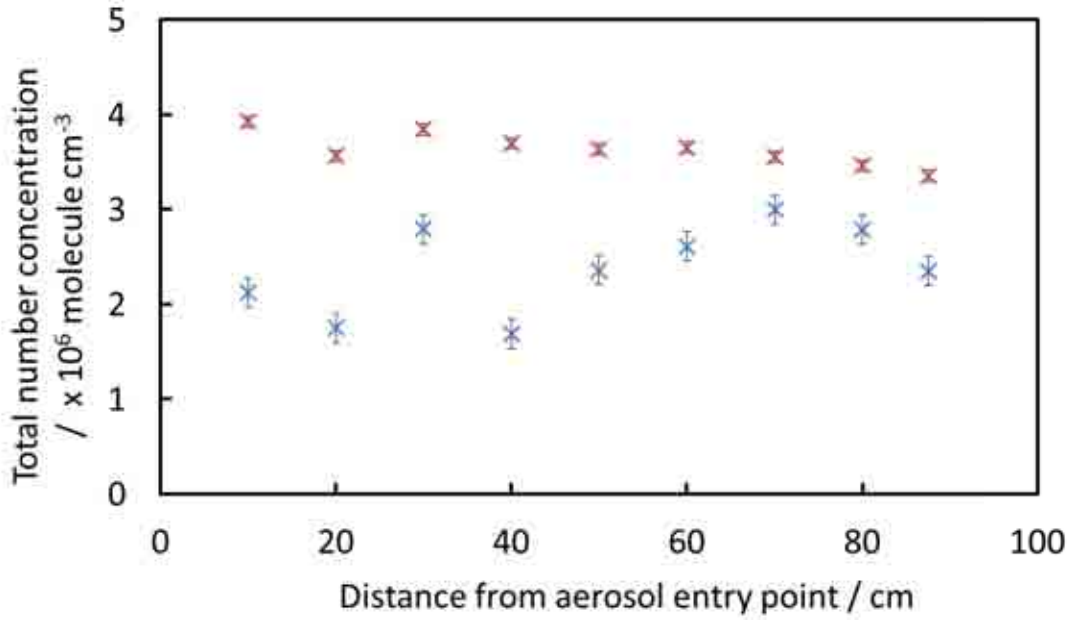

Figure 5.8: This plot shows how the total number concentration of aerosol particles changes along the length of the AFT. The red crosses show data for wet NaCl aerosols doped with Cu(II) and the blue crosses show the same aerosol passed through the diffusion dryer.

Aerosol loss was also found to depend on the cleanliness of the AFT. Figure 5.9 shows how the total number concentration changed over time when aerosol was flowed into a freshly washed and dried tube. The aerosols were added after 5 min, but it took a further 20 min until the aerosol total number concentration was stable.

Figure 5.10 shows data from a similar experiment, this experiment was performed twenty three days after the corresponding experiment with the clean tube. The flow tube had not been cleaned between the two experiments, although other aerosol experiments had been performed in the intervening time. The aerosol was added to the tube after 5 min and the total number concentration was at a stable value within 5 min of the aerosols being added.

The fact that the total aerosol number concentration reached a stable point more quickly when the tube was 'dirty' indicates that the aerosols were lost more easily to the clean tube. This effect was also encountered when determining the loss of HO_2 to the walls of the tube - a faster loss was recorded if the tube was clean (see later in this chapter). In order to accurately determine the loss of HO_2 to the walls of the AFT the walls must

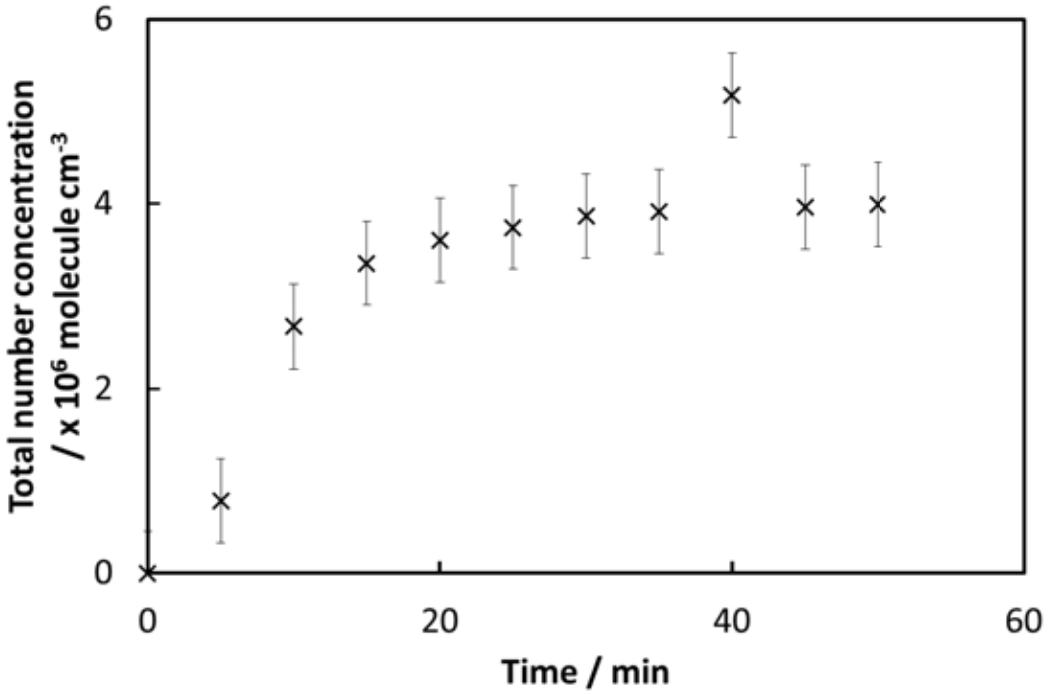

Figure 5.9: A plot showing how the total number concentration of NaCl aerosol doped with Cu(II) changes with the time it is present in the AFT. The AFT was washed and dried before the aerosols were added.

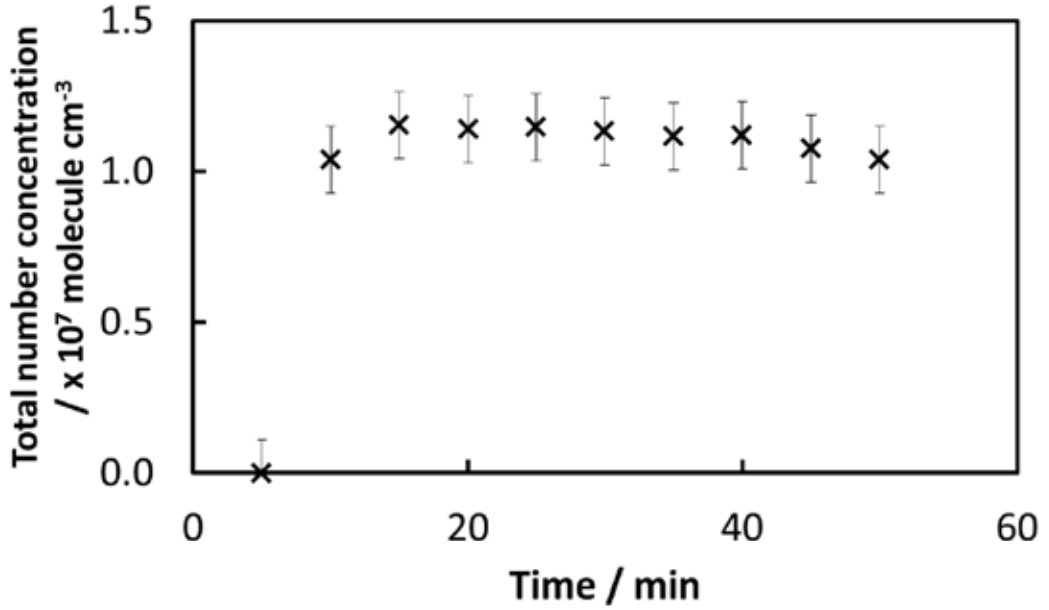

Figure 5.10: A plot showing how the total number concentration of NaCl aerosol doped with Cu(II) changes with the time it is present in the AFT. The AFT had not been recently cleaned.

be conditioned so that the rate of loss to the walls during a *wall loss* experiment was the same as the rate of loss to the walls during an *aerosol loss* experiment. If a clean tube was used for a *wall loss* experiment and an *aerosol loss* experiment was then performed the rate of loss of HO_2 to the walls of the tube would be rapidly changing during the start of the *aerosol loss* experiment and the rate of wall loss found in the *wall loss* experiment would not be valid for the *aerosol loss* experiment. To ensure that the rate of loss of HO_2 to the walls of the AFT was constant for the *wall loss* experiment and the *aerosol loss* experiment the walls of the AFT were conditioned by flowing aerosol for at least 20 min through the flow tube before any flow tube experiments were performed.

5.3.2 Aerosol Loss over Time

Each experiment undertaken to determine the uptake co-efficient of HO_2 to aerosol took about two hours. Experiments were undertaken to investigate the stability of the aerosol distribution throughout this time. Aerosol was added to the tube, without any radicals present, and the number distribution of the aerosol was recorded every five minutes over a three hour period of time. The total number concentration for each sample was recorded and the change in the concentration over time can be seen in Figure 5.11.

The data show a steady decline in the total number concentration over time, which appears to level slightly after about an hour. As a constant output atomiser was used (see Chapter 2) it is unclear what this decline is due to. The decline was possibly due to a measurement issue with the SMPS. The SMPS has two air flows within it (the sheath flow and the sample flow) if these flows are not at the same relative humidity then measurement errors could occur. The sheath air flow is recirculated and mixed with the sample air, so over time the sheath air will be the same relative humidity as the sample flow, thus reducing any measurement errors.

Figure 5.11 shows a decrease in the total number concentration over time, however this shows the measurements of aerosol over time for just one experiment. Figure 5.12 combines the measurements from a number of experiments showing how the total aerosol

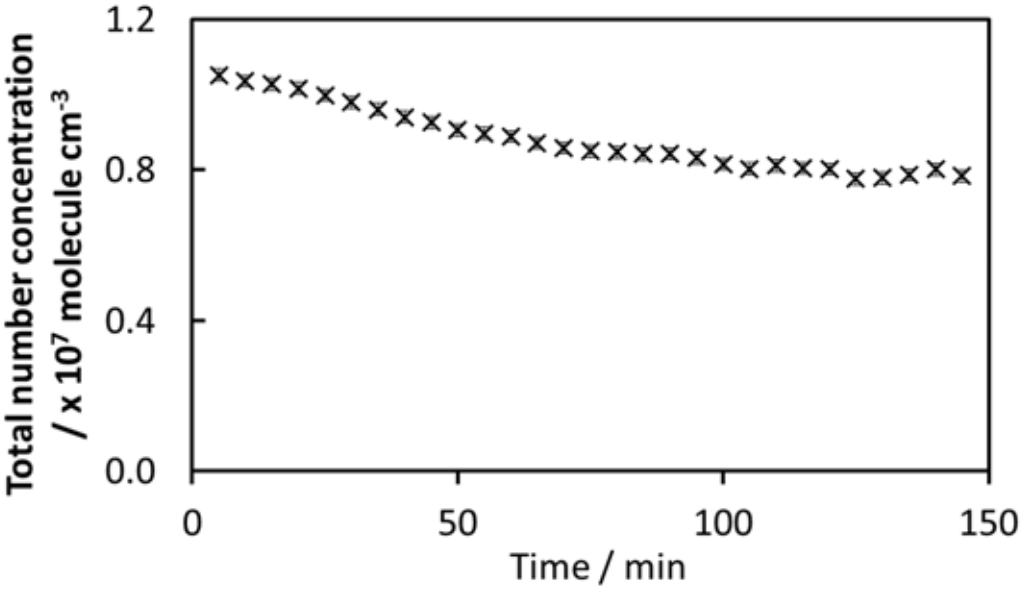

Figure 5.11: Aerosols were added to the flow tube and the number distribution was measured by the SMPS every five minutes. A drop in the total number concentration of a NaCl aerosol is seen over time. The total number concentration drops by 25 % over a period of 2.5 hours. The errors shown are the standard error of the data.

number concentration varies over the time of the experiment (this data was recorded as part of the experiments to determine the uptake co-efficient so radicals are present in the tube as well as the aerosol).

After initial stabilisation no trend is apparent within each experiment. If there is a change in aerosol over time it would affect the determination of the uptake coefficient. In order to eliminate systematic impact from any changes (e.g. in aerosol, temperature, relative humidity etc.) during the length of each flow tube experiment the injector tube position (and thus the reaction time) was varied randomly (rather than systematically) throughout the experiment. By varying the reaction time in this way if there was any gradual change in conditions during a flow tube experiment it would not affect the analysis of the rate constants (and thus the uptake coefficient). The effect of moving the reaction tube randomly can be seen in Figure 5.13, which shows that no trend can be seen in the total number concentration of aerosols with a change in reaction time.

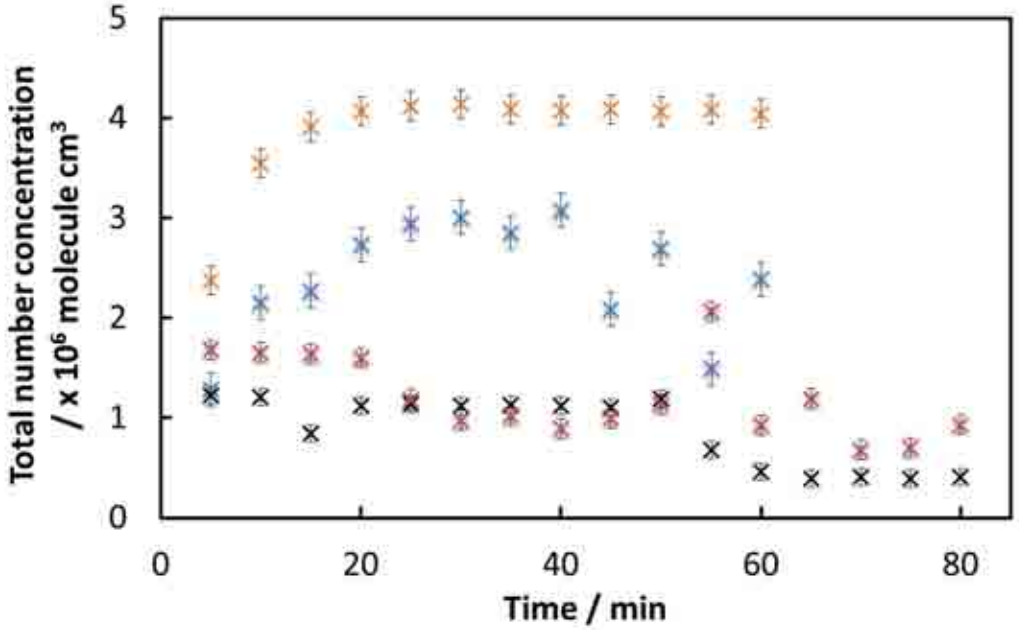

Figure 5.12: A plot showing how the total number concentrations of aerosols vary over time. The different colour crosses show data from different experiments. The errors shown are the stand error of the data.

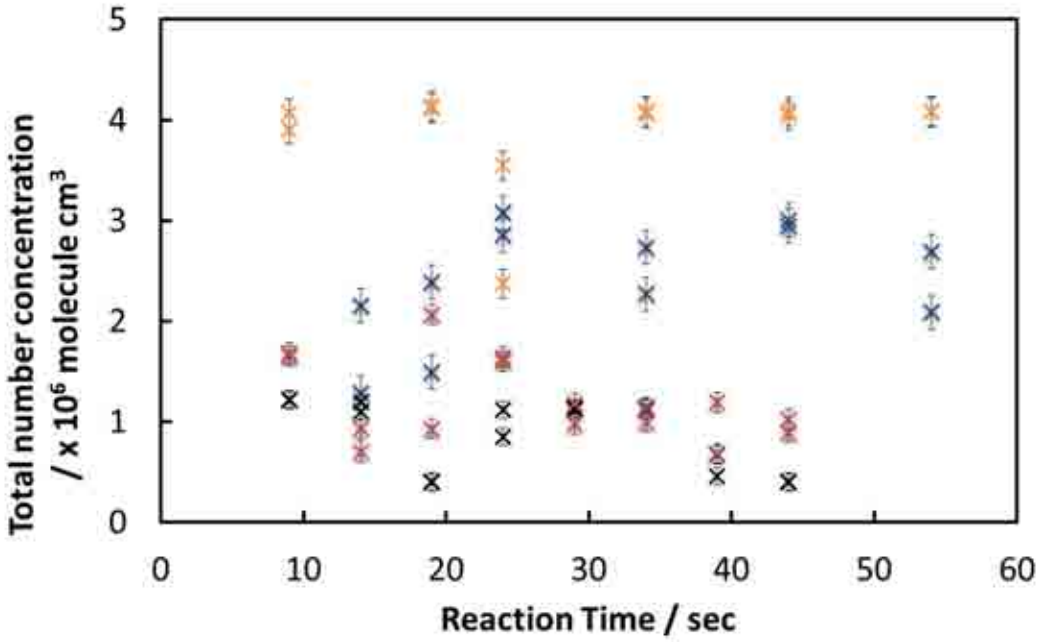

Figure 5.13: A plot showing how the total number concentrations of the aerosol varies with the reaction time between aerosol and the HO_2 radicals in the AFT. The different colour crosses show data from different experiments. The errors shown are the stand error of the data.

5.4 Characterising the Loss of HO_2 to the Walls of the AFT

During an *aerosol loss* experiment HO_2 was lost to both the walls of the AFT and to aerosol particles. *Wall loss* experiments were performed to determine the rate of loss of HO_2 to the walls of the AFT, k^*_{walls}. Once k^*_{walls} was determined the rate of loss to aerosol particles was obtained (see Chapter 4 for details). In principle k^*_{walls} could be a constant for the walls of a particular AFT, however in practise this was not the case. k^*_{walls} was found to vary due to various factors which are discussed in detail in this section.

5.4.1 Effect of the halocarbon wax coating on k^*_{walls}

A halocarbon wax coating was applied to the walls of the AFT (see Chapter 2) for experiments performed during the later part of this study. During earlier experiments no coating was applied to the walls of the AFT.

Figure 5.14(a) shows values of k^{obs}_{walls} determined from various experiments throughout this study (note that the observed rate loss to the walls is shown with no correction for gas phase diffusion or laminar flow).

Figure 5.14(a) shows that when the halocarbon wax coating was used on the walls of the AFT k^{obs}_{walls} was, in general, lower than k^{obs}_{walls} determined with no coating on the walls. Values for k^{obs}_{walls} determined from the first two experiments performed with the halocarbon wax coating were significantly higher than the future experiments. These higher values could be due to an improved application of the halocarbon wax after the initial experiments. The mean k^{obs}_{walls} determined without a coating on the AFT was 0.11 $\pm$ 0.017 s^{-1}, while the mean for k^{obs}_{walls} determined with the halocarbon wax coating on the AFT was 0.016 $\pm$ 0.015 s^{-1}. The lower mean value of k^{obs}_{walls} confirms the expected effect of the halocarbon wax on the rate of loss of HO_2 to the walls of the AFT: the halocarbon wax lowers the rate of loss of HO_2.

It can be seen from Figure 5.14(a) that some values of k^{obs}_{walls} were found to be negative

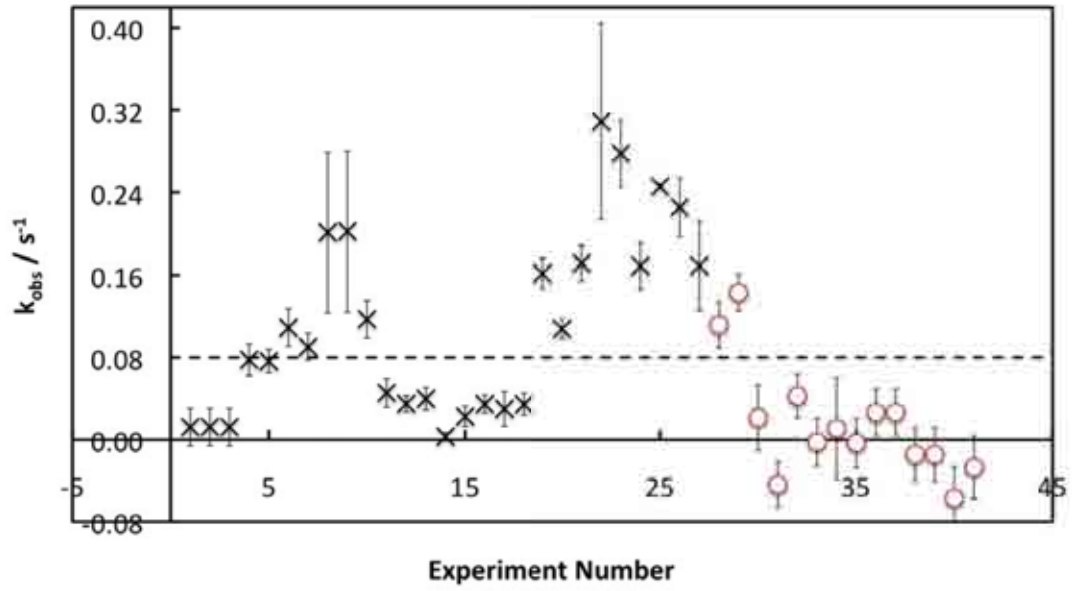

(a) These data have not been corrected for either laminar flow or gas phase diffusion. The dashed line is at $k^{obs}_{walls} = 0.08\,s^{-1}$.

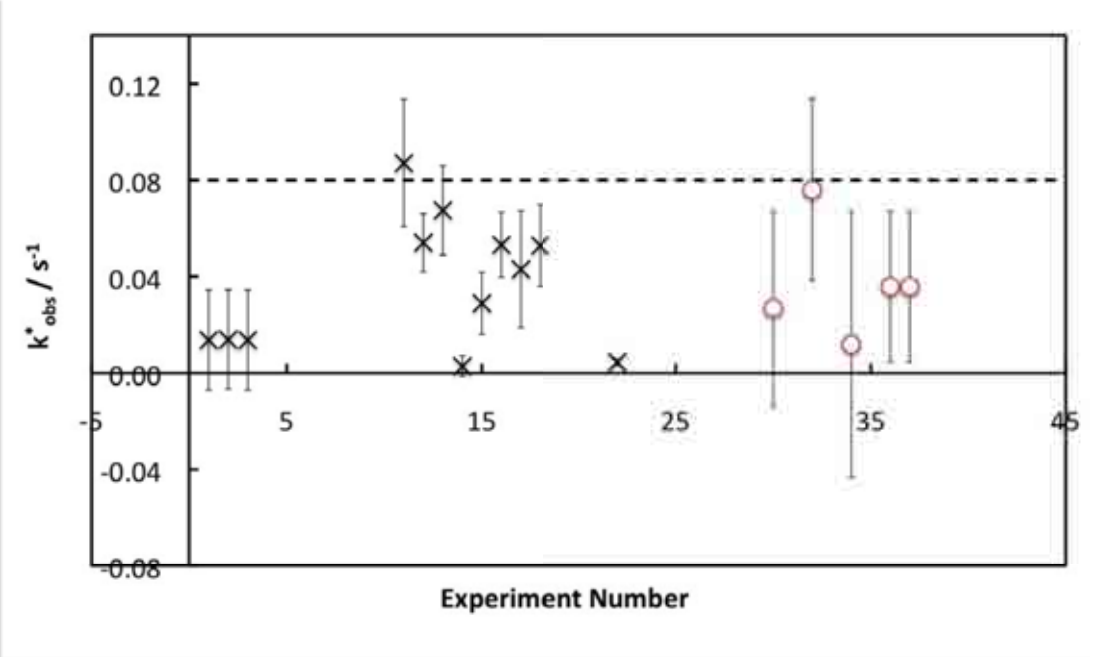

(b) These data have been corrected for both laminar flow and gas phase diffusion.

Figure 5.14: Data from various experiments determining the rate of loss of HO_2 to the walls of the AFT. The crosses show data that was recorded with no coating on the walls of the AFT and the circles show data that was recorded with halocarbon wax coating on the walls of the AFT.

when the mixed order kinetic analysis was applied to the HO_2 decay. These negative values occurred more often with the halocarbon wax on the walls of the AFT than with no coating present. Values for k^{obs}_{walls} determined with halocarbon wax on the tube were small values with a large uncertainty. It can be seen in Figure 5.14(a) that all but two of the negative values of k^{obs}_{walls} would be positive within the range of uncertainty shown.

The halocarbon wax coating was applied to the tube walls so that k^{obs}_{walls} was low enough (i.e. less than $0.08\,s^{-1}$) for the laminar flow correction to be valid (see Chapter 4). The laminar flow correction assumes a fully laminar flow within the AFT, however the flow within the AFT will not be completely laminar due to the mixing of the injector flow into the main flow and also due to the time it will take for the laminar flow to build up (see Chapter 2). When the correction for laminar flow was applied to a value of k^{obs}_{walls} that was greater than about $0.08\,s^{-1}$ the resulting k^{*}_{walls} returned was negative.

Figure 5.14(b) shows values for k^{*}_{walls} (i.e. k^{obs}_{walls} corrected for laminar flow and gas phase diffusion) determined throughout this study. It can be seen that many experiments shown in Figure 5.14(a) are missing in Figure 5.14(b) - this is because many values of k^{obs}_{walls} were too high to correct for laminar flow, so had to be discounted. Other values for k^{obs}_{walls} were discounted because they were determined as negative values, as discussed previously.

5.4.2 Variation of k^{*}_{walls} between experiments

It was seen that k^{*}_{walls} was not consistent between *wall loss* experiments. The variation of k^{*}_{walls} between experiments was investigated to determine how often it was necessary to determine k^{*}_{walls}.

Table 5.3 shows values for k^{*}_{walls} determined on various days throughout this study, this table shows the variation of k^{*}_{walls} throughout this study. There was no coating on the walls of the AFT for the first eight experiments (07/12/09 - 28/01/10), while in the the next four (23/07/10 - 07/09/10) there was a halocarbon wax coating on the tube walls.

Figure 5.15 shows data for k^{*}_{walls} determined from *wall loss* experiments performed

Date of Experiment	$k^*_{walls}(s^{-1})$
07/12/2009	0.0870 ± 0.0264
15/12/2009	0.0541 ± 0.0121
16/12/2009	0.0675 ± 0.0185
14/01/2010	0.0028 ± 0.0043
26/01/2010	0.0289 ± 0.0129
27/01/2010	0.0532 ± 0.0134
29/01/2010	0.0529 ± 0.0169
28/01/2010	0.0430 ± 0.0243
23/07/2010[a]	0.0268 ± 0.0405
26/07/2010[a]	0.0759 ± 0.0377
27/07/2010[a]	0.0119 ± 0.0552
07/09/2010[a]	0.0358 ± 0.0312

Table 5.3: k^*_{walls} determined on different dates throughout the study. [a] indicates halocarbon wax was coating the walls of the tube during this experiment. The errors given are the standard error of the data.

without any coating on the walls of the AFT.

The data in Figure 5.15 shows a general downward trend in k^*_{walls} over time between experiments performed sequentially in time. This trend could be caused by the conditioning of the tube by the reactants over time, as discussed earlier in this chapter: when a clean tube (i.e. a new tube, or one that had been washed and dried) was used to determined k^*_{walls} then the radical loss was due to interactions between HO_2 and the glass walls of the tube. Once a tube had been used for aerosol experiments the walls had some deposits of aerosol on them. This was seen in the extreme when using $(NH_4)_2SO_4$ aerosols at high relative humidities - during these experiments the AFT became visibly misty, indicating that aerosols were depositing on the AFT walls. These deposits would probably be expected to occur during other experiments although visually nothing was seen. When k^*_{walls} was determined using this conditioned (i.e. exposed to aerosols) tube then the radical loss would be due to aerosol (and radical) deposits on the tube walls as well as the loss to the glass walls of the tube. In effect this conditioning coats the wall with aerosols, making a *wall loss* experiment similar to a coated wall flow tube system.

As k^*_{walls} was used to calculate k^*_{aero} it was important to ensure that k^*_{walls} was the same during a *wall loss* experiment and the corresponding *aerosol loss* experiment. If a

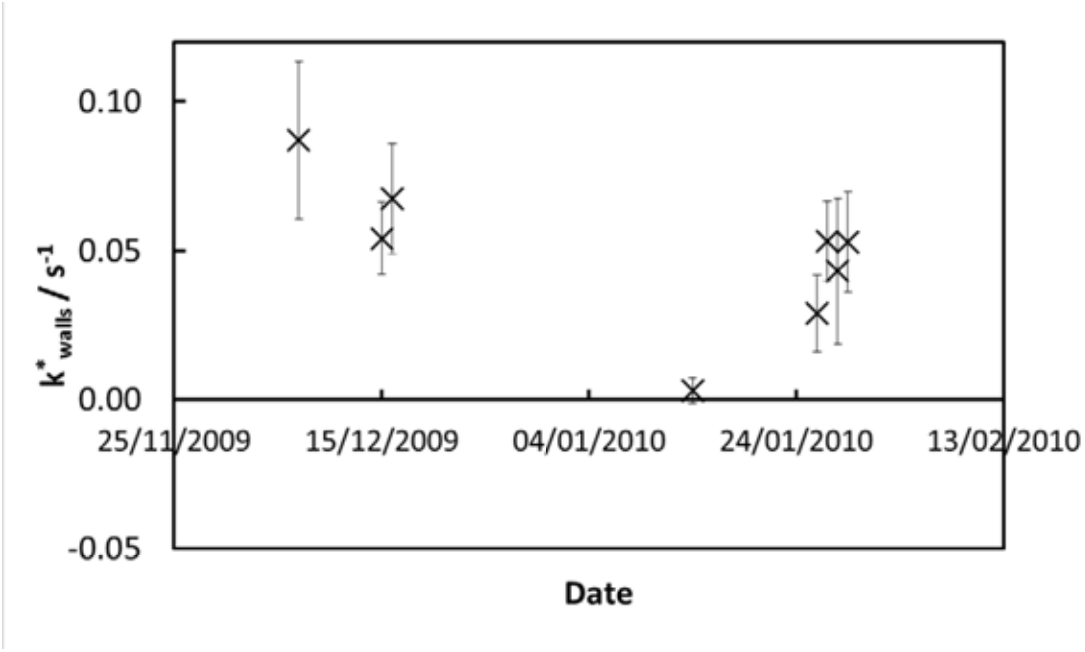

Figure 5.15: k^*_{walls} determined from various experiments on different days. This data was obtained from *wall loss* experiments without any halocarbon wax coating the walls of the AFT.

clean tube was used to determine k^*_{walls} and then used for the corresponding *aerosol loss* experiment then aerosol would be deposited to the walls of the clean AFT, thus changing the effective wall loss between the two experiments. Therefore all flow tube experiments were performed once the AFT had been conditioned by aerosols. *Wall loss* experiments were also performed just before or just after a *aerosol loss* experiment and on the same day to ensure that the conditions in both experiments were the same.

When halocarbon wax was present on the tube no significant trend was seen in the day to day variation of k^*_{walls} (Figure 5.16). Any variation that was seen was due to normal experimental variation as the data points are in agreement if the uncertainties are taken into account. The conditioning of the tube was no longer an issue as the halocarbon wax is a very unreactive material - as well as lowering the loss of HO_2 to the walls of the AFT it also lowered the deposition of aerosols to the walls. Thus the rate of loss of HO_2 to the walls of the AFT did not change as rapidly due to conditioning by reagents when halocarbon wax was applied to the AFT as it did when no coating was applied to the AFT.

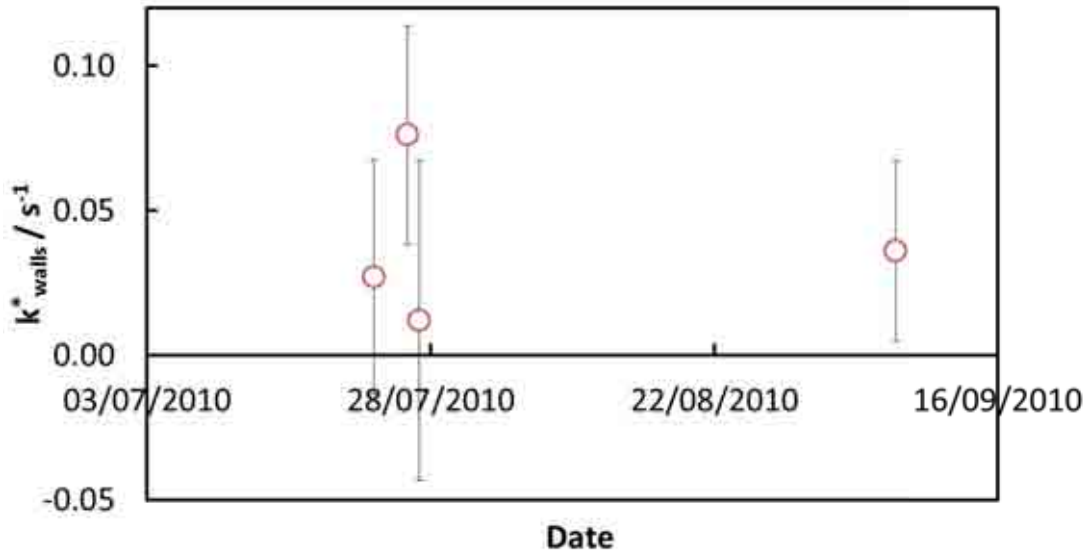

Figure 5.16: k^*_{walls} determined from various experiments on different days. This data was obtained from *wall loss* experiments with halocarbon wax coating the walls of the AFT.

5.4.3 Effect of the relative humidity on k^*_{walls}

The uptake coefficient depends on the phase of the aerosol particle (i.e. if the particle is in the aqueous phase or the solid phase). In order to obtain particles in the different phases the relative humidity of the aerosol was changed, meaning that *aerosol loss* experiments were performed at various relative humidities. To ensure that the conditions of an *aerosol loss* experiment were the same as the conditions for the corresponding *wall loss* experiment the *wall loss* experiments were also performed at various relative humidities. This section describes an investigation into how the rate of loss of HO_2 to the walls of the AFT changed with relative humidity within the AFT. Figure 5.17 shows that if there is no coating on the walls of the AFT k^*_{walls} increases with relative humidity.

The rate of the self-reaction of HO_2 has a dependence on relative humidity (see Chapter 4), but this was taken into account during the analysis of k^*_{walls}, so the trend seen here is in addition to this effect. The HO_2-H_2O complex which causes the HO_2 self-reaction relative humidity dependency will also form within this AFT system and may affect the interaction between HO_2 and the walls of the AFT. During the self-reaction of HO_2 the HO_2-H_2O complex stabilises the intermediate formed, allowing the reaction to occur faster

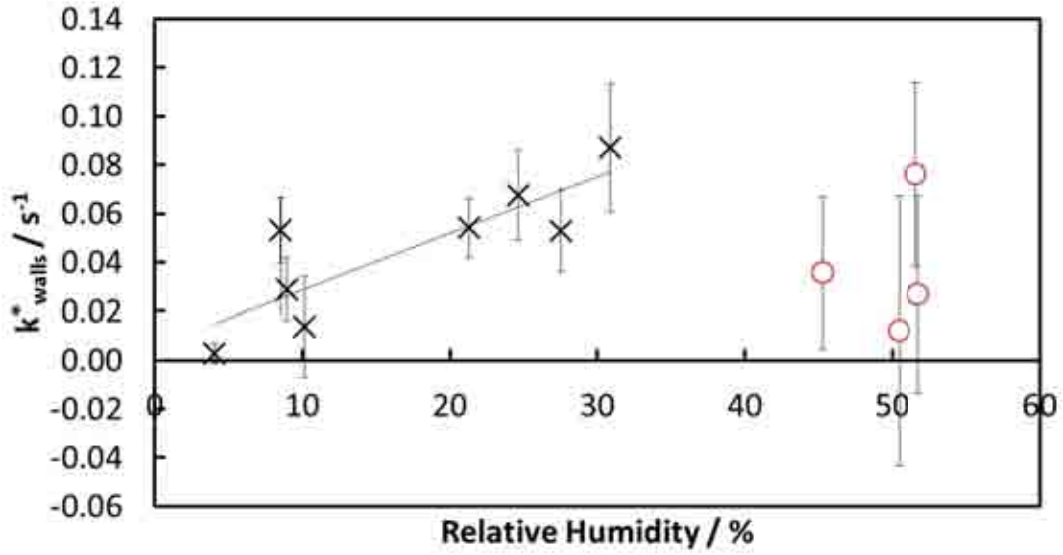

Figure 5.17: This plot shows how k^*_{walls} changes due to the relative humidity of the AFT. The crosses are values determined with no coating on the AFT, the circles are values determined with the halocarbon wax coating.

than without the complex being formed. The same process could be occurring here with the complex stabilising the intermediate in the reaction between the radicals and the walls. As the relative humidity increases the partitioning between the radical and the complex will be towards the complex. k^*_{walls} was seen to increase with increasing relative humidity, which would make sense with a higher levels of the complex and the stabilisation of the intermediate.

Figure 5.17 also shows data for k^*_{walls} obtained when the halocarbon wax coating was applied to the AFT. These experiments were performed at similar relative humidities so it is not possible to determine if there is a dependancy of k^*_{walls} on the relative humidity.

5.4.4 Effect of the Initial Concentration of HO_2 on k^*_{walls}

The initial concentration of HO_2 in a *wall loss* experiment varied from 1×10^9 molecules cm^{-3} to 9×10^9 molecules cm^{-3} throughout this study. This concentration is approximately one order of magnitude higher than atmospheric boundary layer concentrations (see Chapter 2). The higher concentration used was due to the measurement sensitiv-

ity of the PERCA, especially at higher relative humidities (see Chapter 3). The higher concentration also meant that the self-reaction of HO_2 had to be taken into account when k^*_{walls} was determined (see Chapter 4). Figure 5.18 shows the determined values of k^*_{walls} with respect to the initial concentration of HO_2 in the AFT - no trend can be seen in this data. This data gives confidence in the accuracy of the mixed order kinetic analysis which was used to account for the impact of the HO_2 self-reaction.

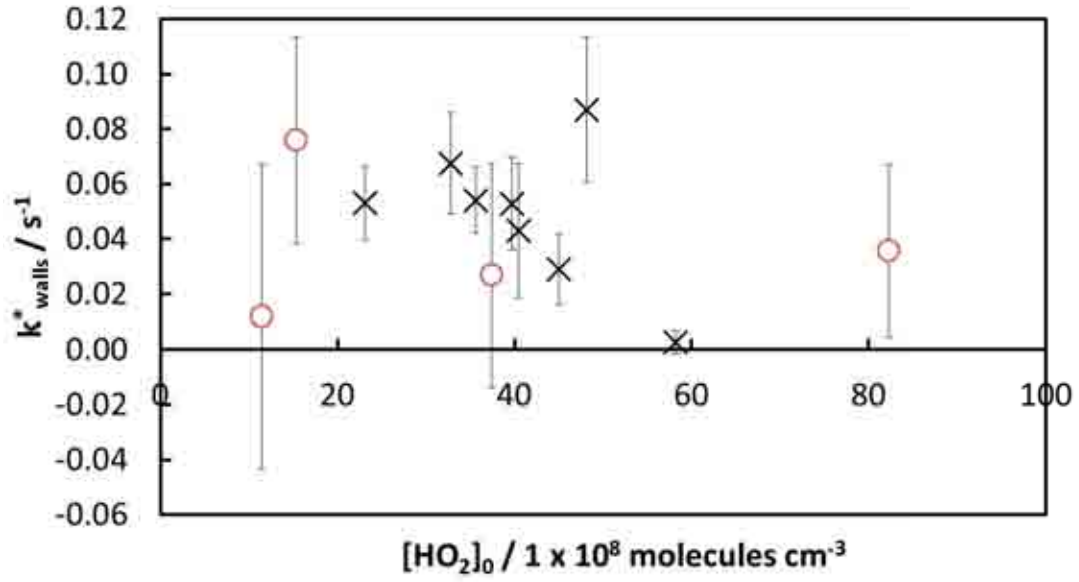

Figure 5.18: There is no discernible trend in k_{walls} with a change in the initial concentration of HO_2.

5.5 Summary

The aerosol produced during this study was characterised. In general the more concentrated the salt solution used to make the aerosol the larger the particles produced. Once it was decided which aerosol size distribution was needed the salt solution to make that size could be determined from relationships such as those plotted in Figures 5.2 and 5.3.

Experiments were performed to determine the efflorescence relative humidity of the aerosol used in this study. To obtain wet Cu(II) doped NaCl aerosol the relative humidity

must be greater than 50 %. To obtain wet Cu(II) doped $(NH_4)_2SO_4$ aerosol the relative humidity must be greater than 45 %. These values are slightly higher than the literature values, indicating that some experiments performed which were thought to be for wet aerosol were actually dry aerosol. The PERCA used in this study had a low sensitivity above approximately 40 % relative humidity (see Chapter 3) making it more challenging to obtain results for uptake of HO_2 to wet aerosols.

The loss of aerosol particles to the apparatus was investigated. Although particles were lost due to the apparatus no change in the total number distribution was seen along the length of the flow tube once the flow tube had been conditioned by aerosol flowing through it. This indicates that the majority of losses were on entry to the apparatus rather than within the AFT system.

k^*_{aero} (and thus γ) was calculated using k^*_{walls}, therefore in order for the calculation of γ to be valid, the conditions (e.g. relative humidity, conditioning of the AFT etc.) of a *wall loss* experiment were kept the same as for the corresponding *aerosol loss* experiment. The corresponding flow tube experiments were performed sequentially in order to ensure the conditions were similar in the two experiments. Experimental variation, associated with ageing of aerosols and the conditioning of the AFT was minimised by performing *wall loss* experiments on the same day as the corresponding *aerosol loss* experiment.

The biggest factors that affected k^*_{walls} were the presence or absence of the halocarbon wax coating on the walls of the AFT and the relative humidity of the flow tube experiment. Halocarbon wax was used on the walls of the AFT in order to minimise the loss of reactants to the walls and hence to keep values sufficiently low for the laminar flow correction to be applied. The relative humidity affected k^*_{walls} significantly when there was no halocarbon wax coating the walls of the AFT, but there was limited evidence to determine if there was an affect on k^*_{walls} when there was halocarbon wax present on the walls. k^*_{walls} and k^*_{aero} were typically determined at similar relative humidities. The initial concentration of HO_2 had no effect on k^*_{walls}, so although it was kept as close to atmospheric conditions as possible there was no need (in principle) to ensure that similar concentrations were used

for aerosol and wall loss experiments.

CHAPTER 6

HO_2 UPTAKE TO SODIUM CHLORIDE AND AMMONIUM SULPHATE AEROSOLS

6.1 Introduction

This chapter presents measured values for the uptake of HO_2 radicals to dry sodium chloride and ammonium sulphate aerosol particles. Values for uptake to wet particles of sodium chloride are also shown, but due to experimental issues the data are limited. The data shown in this chapter were obtained from multiple *wall loss* and *aerosol loss* flow tube experiments. All data shown in this chapter has been analysed using a mixed order rate analysis and has been corrected for both laminar flow and gas phase diffusion, unless otherwise stated. Full details of the analysis procedure is shown in Chapter 4. For all values given within this chapter the uncertainty shown is the standard error of the data. Many more flow tube experiments were performed than those shown by the data in this chapter, but the data from many experiments were discarded for one of a number of reasons:

- a high rate of loss of HO_2 to the walls of the uncoated AFT to which the laminar flow corrections could not be reliably applied (see Chapter 5)
- a high uncertainty in the rate of loss of HO_2 to the walls of the AFT when the rate of loss was very low (see Chapter 5)

- the low sensitivity of the PERCA when used at relative humidities above about 40 % (see Chapter 3)

This chapter also shows data obtained from a zero-dimensional photochemical box model. The model was run using conditions for the marine boundary layer, with the assumption that sea-salt particles make up the majority of the surface area for aerosol within the marine boundary layer. The model was run with no loss to aerosol, with the new uptake coefficient determined, and with the currently recommended value for γ. The model was used to investigate how the concentration of ambient HO_2 and ambient OH was affected by the change in γ. The resulting change in the chemical production of ozone in the marine boundary layer, depending on the value of γ, was also investigated using the model, as was the change in the percentage of HO_2 lost due to uptake with respect to other loss processes.

6.2 Dry Aerosol Particles

Dry aerosol particles are those which are suspended in a gas at a relative humidity lower than the particles' efflorescent relative humidity (see Chapter 2 for details). The efflorescence relative humidity for both sodium chloride and ammonium sulphate aerosols (both doped with $CuSO_4$) were determined in this study (Chapter 5) to be 50 % and 45 % respectively. *Aerosol loss* experiments which were performed below the relevant efflorescence relative humidity were used to determine γ for dry aerosol, while *aerosol loss* experiments performed above this relative humidity were used to determine γ for wet aerosol.

Aerosol loss experiments performed with wet Cu(II) doped aerosols were used to determine the mass accommodation coefficient, α. Cu(II) acts as a catalyst for the destruction of HO_2 within the aqueous phase, so provides an efficient sink for HO_2 within the aqueous phase. The rate of loss of HO_2 to the aerosol could therefore be attributed to the rate of uptake of HO_2 to the aqueous phase of the particle (i.e. mass accommodation). *Aerosol loss* experiments were performed with Cu(II) doped aerosol which were below the efflo-

rescence relative humidity - in this case the aerosol particles would be dry so the aqueous processes for which Cu(II) acts as a catalyst would not occur. *Aerosol loss* experiments which were performed using dry Cu(II) doped aerosol were therefore considered equivalent to the undoped aerosol. Dry aerosol (whether doped with Cu(II) or not) were used to determine γ (data shown in this section), while wet Cu(II) doped aerosols were used to determine α (see next section).

6.2.1 Sodium Chloride Aerosol

The uptake of HO_2 to sodium chloride aerosol was investigated as a proxy for uptake to sea-salt aerosol. The uptake coefficient, γ, for HO_2 uptake to dry NaCl was determined using data obtained from *aerosol loss* (and corresponding *wall loss*) experiments using dry NaCl and dry NaCl doped with Cu(II) aerosols.

Table 6.1 shows a summary of data obtained from dry NaCl and dry NaCl doped with Cu(II) *aerosol loss* experiments and the corresponding *wall loss* experiments. Table 6.1 shows the calculated rate of loss of HO_2 to the walls of the AFT (k^*_{walls}), the calculated rate of loss of HO_2 to the aerosol (k^*_{aero}), the mean total surface area of the aerosol during the *aerosol loss* experiment and the relative humidity of the *aerosol loss* experiment. γ is also shown in Table 6.1, which was calculated using Equation 4.6 (reproduced below for clarity). Chapter 4 gives details of the full analysis procedure.

$$\gamma_{obs} = \frac{4k^*_{aero}}{S_a \omega_{HO_2}} \tag{4.6}$$

The γ values shown in Table 6.1 are shown plotted against relative humidity in Figure 6.1; one extra point, for a wet NaCl doped with Cu(II), is also shown and is discussed in more detail later in this section. Figure 6.1 shows no significant trend in γ with relative humidity. The mean value of the γ values shown in Table 6.1 for the uptake of HO_2 to dry NaCl aerosol was determined as $2.1 \pm 0.56 \times 10^{-2}$.

γ can be determined more rigorously by plotting a graph of k^*_{aero} against S_a; a re-

Table 6.1: Data determined from *aerosol loss* experiments and *wall loss* experiments which were used to calculate values for γ for each set of experiments. The first set of data is for NaCl aerosol and the rest are for NaCl doped with Cu(II) aerosols. The relative humidity refers to the relative humidity of the *aerosol loss* experiment. All of these experiments were performed below the efflorescence relative humidity so the aerosol particles were dry. The uncertainty of the data is the standard error of the values for each experiment.

k^*_{walls} / s^{-1}	k^*_{aero} / s^{-1}	S_a / $cm^2\,cm^{-3}$	RH / %	γ
0.014 ± 0.021	0.17 ± 0.032	$6.3 \pm 0.053 \times 10^{-4}$	35	$2.6 \pm 0.52 \times 10^{-2}$
0.64 ± 0.13	0.18 ± 0.015	$1.1 \pm 0.047 \times 10^{-3}$	22	$1.6 \pm 0.15 \times 10^{-2}$
0.068 ± 0.019	0.07 ± 0.023	$2.8 \pm 0.039 \times 10^{-4}$	36	$2.3 \pm 0.73 \times 10^{-2}$
0.053 ± 0.017	0.19 ± 0.10	$1.7 \pm 0.042 \times 10^{-3}$	38	$1.1 \pm 0.56 \times 10^{-2}$
0.014 ± 0.021	0.19 ± 0.028	$9.1 \pm 0.17 \times 10^{-4}$	39	$2.0 \pm 0.28 \times 10^{-2}$
0.036 ± 0.031	0.050 ± 0.014	$3.6 \pm 0.19 \times 10^{-4}$	48	$1.3 \pm 0.37 \times 10^{-2}$
0.054 ± 0.012	0.061 ± 0.036	$1.7 \pm 0.017 \times 10^{-3}$	38	$3.2 \pm 1.9 \times 10^{-3}$
0.014 ± 0.021	0.40 ± 0.16	$6.9 \pm 0.28 \times 10^{-4}$	35	$5.6 \pm 0.22 \times 10^{-2}$

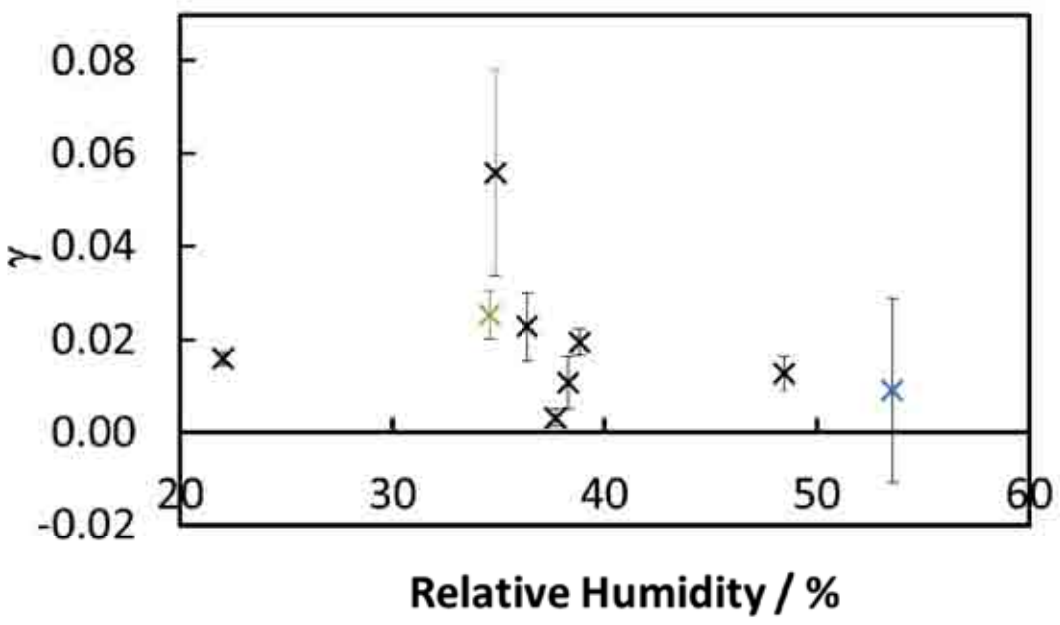

Figure 6.1: The data shows values determined for γ for various relative humidities. The black crosses are data for uptake to solid NaCl doped with Cu(II) aerosols, the blue cross is datum for uptake to aqueous NaCl doped with Cu(II) aerosols. The green cross is datum for uptake to solid NaCl aerosol.

gression analysis for this plot can then be used to determine γ. However, as shown in Figure 6.2, the data obtained for a plot of k^*_{aero} against S_a during experiments in this study did not have a good fit to a straight line. More data needs to be produced in order to use this method to determine the uptake coefficient.

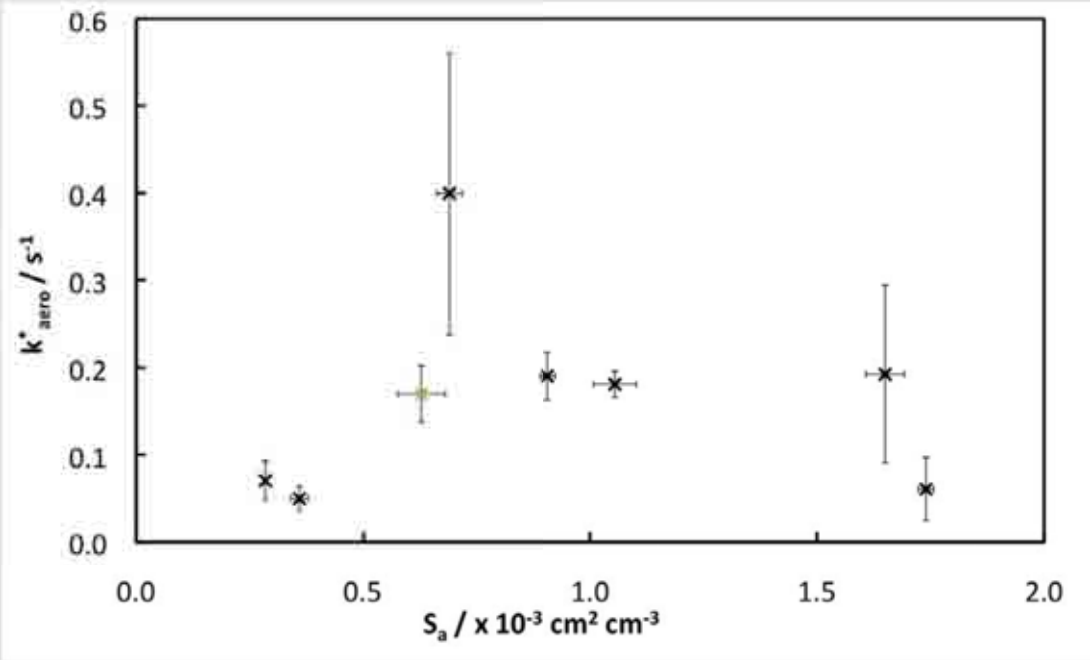

Figure 6.2: This data shows values determined for k^*_{aero} for various total surface area concentrations of NaCl (green cross) and NaCl doped with Cu(II) (black crosses) dry aerosol particles. The red crosses show outlying points which have not been included in the regression analysis.

6.2.2 Ammonium Sulphate Aerosol

Uptake of HO_2 to ammonium sulphate aerosol was investigated as a proxy for uptake to urban aerosol. Data for uptake to $(NH_4)_2SO_4$ doped with Cu(II) was obtained in order to determine α, however, the relative humidity at which experiments were performed was lower than the efflorescence relative humidity (45 %). The low relative humidity meant that uptake was to dry particles, rather than aqueous particles, and so γ was obtained from these experiments rather than α. Only one experiment was successfully carried out and analysed to determine γ for $(NH_4)_2SO_4$ aerosols. γ was determined as 0.047 ± 0.015 at 36 % relative humidity (see Figure 6.3).

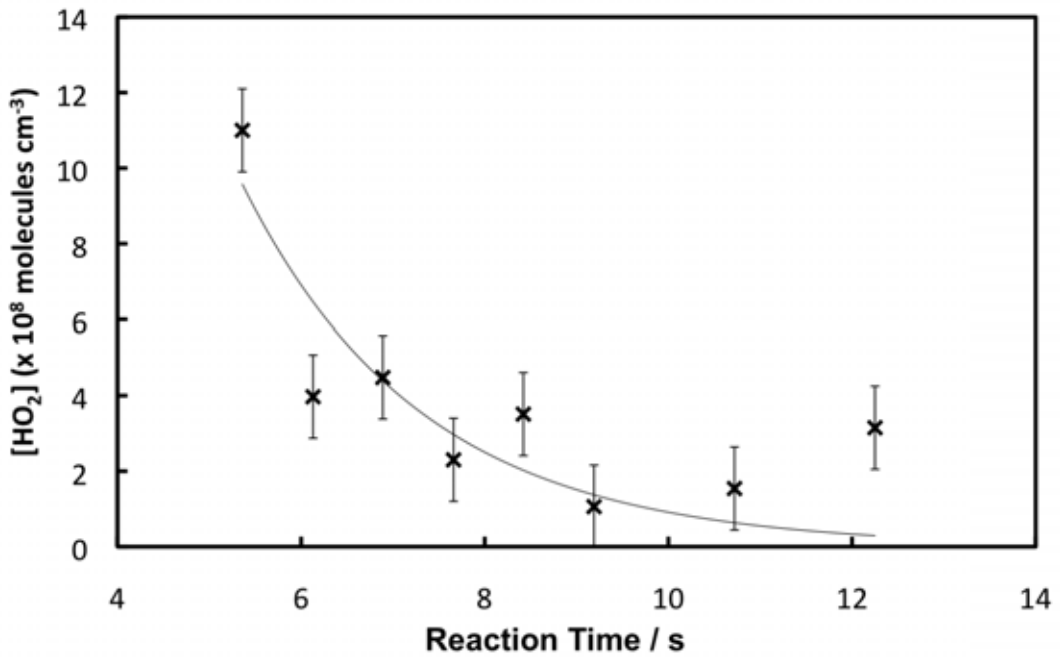

Figure 6.3: This data shows the HO_2 decay measured during a 'dry' *aerosol loss* experiment with $(NH_4)_2SO_4$ doped with Cu(II). The errors shown are the standard error.

6.3 Wet Aerosol Particles

Wet aerosol particles are those which are suspended in a gas at a relative humidity greater than the aerosol particles' deliquescence relative humidity. However a hysteresis effect on the particle water uptake occurs (see Chapter 2 for details), so the history of the relative humidity of the particle must be known to determine if the particle is wet or dry. The aerosol particles produced in this study are produced from a wet solution - this means that they will contain water until they reach the efflorescence relative humidity, whereupon they will crystallise and become solid particles. Therefore for *aerosol loss* experiments in this study the particles will be wet if they are suspended in a gas which has maintained a relative humidity greater than the particles' efflorescence relative humidity.

In the case of NaCl doped with Cu(II) the efflorescence relative humidity was found to be 50 % and in the case of $(NH_4)_2SO_4$ doped with Cu(II) the efflorescence relative humidity was found to be 45 % (see Chapter 5 for details).

Wet aerosol particles, doped with Cu(II) can be used to determine α, while wet un-

doped aerosols can be used to determine γ for aqueous aerosols.

Few wet *aerosol loss* experiments were successfully performed, because of a number of issues with the experimental setup at high relative humidity. The biggest problem was due to the lack of sensitivity of the PERCA at high relative humidity - the chain length of the PERCA decreases with increasing relative humidity (see Chapter 3), reaching a lower limit around 40 %. The low PERCA sensitivity problem was compounded during a wet *aerosol loss* experiment as the concentration of HO_2 was low (approximately 1×10^9 molecules cm^{-3}) compared to that for a *wall loss* experiment (approximately 1×10^{10} molecules cm^{-3}) which could successfully be performed at higher relative humidities. The initial concentration was measured at a reaction time of 4.5 s, with aerosol present in the AFT loss of HO_2 prior to this measurement increased.

Another issue with wet *aerosol loss* experiments was that originally the efflorescence relative humidities for both NaCl and $(NH_4)_2SO_4$ were taken from literature to be 45 % and 35 % respectively; these values were then determined within this system and were found to be be higher. Prior to determining the efflorescence relative humidities for NaCl and $(NH_4)_2SO_4$ many *aerosol loss* experiments were performed at relative humidities which were thought to produce wet particles but actually produced dry particles.

6.3.1 Sodium Chloride Aerosol

The rate of loss of HO_2 to sodium chloride aerosol doped with copper sulphate was studied in order to determine the mass accommodation coefficient, α. As discussed previously there were issues obtaining HO_2 decays with wet aerosol, which meant that only one *aerosol loss* experiment with aqueous NaCl doped with Cu(II) was successfully performed and analysed (Figure 6.4).

The value of α determined from this experiment was 0.0090 ± 0.020. This experiment was carried out at 53 % relative humidity. This value of α is shown in Figure 6.1 (blue cross) - it can be seen from this figure that there is no significant difference between the value of α and the values determined for γ for uptake to NaCl. The measured relative

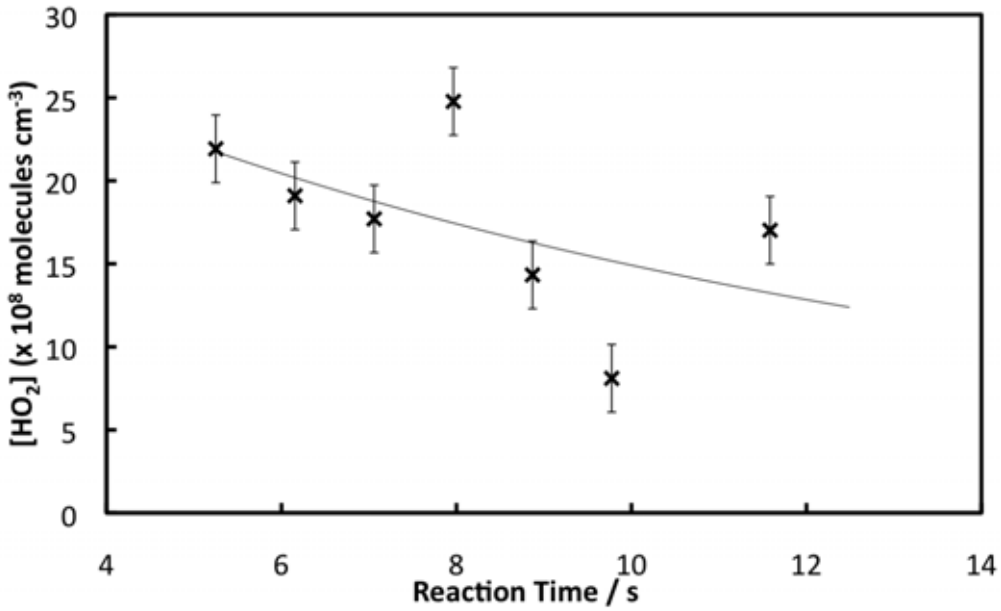

Figure 6.4: This data shows the HO_2 decay measured during a 'wet' *aerosol loss* experiment with NaCl doped with Cu(II). The errors shown are the standard error.

humidity for the wet experiment was 53 %, which is only just above the measured efflorescence relative humidity for NaCl doped with Cu(II). The relative humidity was measured using a HygroPalm relative humidity monitor, which has a stated accuracy of ± (0.5 % + 1.5 % of reading), which gives an error of ± 1 % on the relative humidity of 53 % measured during the aqueous aerosol experiment. This proximity of the measured relative humidity to the efflorescence relative humidity and the fact that the determined value of α shows no significant difference from γ values suggests that the 'wet' aerosol may not have actually been wet, despite the measured relative humidity being above the efflorescence relative humidity.

6.4 Comparison of Experimental Data with Literature Data

6.4.1 Sodium Chloride Aerosol

The new data obtained in this study for α for NaCl particles and γ for dry NaCl particles are shown in Table 6.2. For comparison data determined for α and γ from other studies are also shown in Table 6.2.

Table 6.2: A summary of the NaCl uptake coefficient data obtained in this study, along with comparisons of values from other studies. In this study α was determined using aqueous aerosols, but all other aerosols were dry. Values shown in this table are valid for 298 K. AFT: Aerosol Flow Tube, CC: Chemical Conversion, LIF: Laser Induced Fluorescence, EPR: Electron Paramagnetic Resonance, FAGE: Fluorescence Assay by Gas Expansion

α	RH / %	Method	Reference
0.0090 ± 0.020	53	AFT PERCA	This study
0.65 ± 0.17	53	AFT CC LIF	Taketani et al. (2008)
γ			
0.021 ± 0.006	22 – 48	AFT PERCA	This study
< 0.01	20	AFT CC LIF	Taketani et al. (2008)
0.02 ± 0.01	53	AFT CC LIF	Taketani et al. (2008)
		Solid film reactor	
0.015		EPR	Gershenzon et al. (1995)
0.016 ± 0.003		Solid film reactor	Gershenzon et al. (1995)
		Matrix isolation with EPR	
0.012 ± 0.002		EPR	Remorov et al. (2002)
0.0018		Discharge flow reactor MS	Loukhovitskaya et al. (2009)
< 0.002	7 – 50	AFT CC FAGE	George et al. (2010)

The value determined in this study for uptake to dry NaCl aerosol particles (γ = 0.021 ± 0.006) is similar to studies by Taketani et al. (2008), Gershenzon et al. (1995) and Remorov et al. (2002). Taketani et al. (2008) determined a value of 0.02 ± 0.01 (at 53 % relative humidity), which is in good agreement with the value found in this study. Taketani et al. used a similar experimental system as this study - they used an aerosol flow tube with an atomiser to create aerosol and the photolysis of H_2O to produce HO_2 radicals. A Chemical Conversion (CC) technique followed by Laser Induced Fluorescence (LIF) was used to detect the HO_2 radicals. The CC LIF detection technique has a lower

detection limit than the PERCA used in this study, which enabled Taketani et al. to use a lower initial concentration of HO_2 (approximately 1×10^8 molecules cm^{-3}); this study accounted for the higher concentrations of HO_2 radicals by using a mixed order kinetic analysis. The agreement between the values found in this study and that by Taketani et al. could be due to the similar experimental apparatus. However the value determined by Gershenzon et al. (1995) ($\gamma = 0.015$ & 0.016) also shows good agreement with the values found in this study and that by Taketani et al. Gershenzon et al. used a low pressure coaxial reactor, with the central rod coated with NaCl salt, coupled to a matrix isolation electron paramagnetic resonance detector to detect the HO_2 radicals. This technique is different to that used in this study and that used by Taketani et al., so independently confirms the results determined.

Remorov et al. (2002), whose study used the same experimental apparatus as Gershenzon et al. (1995), determined a slightly lower value for γ of 0.012 ± 0.002. They used high concentrations of HO_2 radicals (4×10^{10} – 5×10^{11} molecules cm^{-3}), but considered the rate of the self reaction negligible with respect to the rate of the heterogeneous reaction. This lower value for γ agrees with the value determined by Taketani et al. (2008) at 20 % relative humidity (< 0.01). Remorov et al. (2002) investigated the change in γ with water vapour present in the flow tube. The rate of loss of HO_2 was seen to decrease in the presence of water vapour, which was attributed to the adsorption of water to the salt surface and reduced the number of active sites for HO_2 reactions. This decrease in dependency is the opposite to that seen by Taketani et al., who recorded an increase in γ with an increase in relative humidity. The concentration of H_2O, in the form of vapour, added by Remorov et al. was two orders of magnitude smaller than that added by Taketani et al. A study of the uptake of HNO_3 to NaCl surfaces by Davies and Cox (1998) investigated the dependency of the uptake coefficient on water vapour. They suggest that with low concentrations of H_2O present a number of defect sites are produced, but as the water vapour pressure increases more defect sites become reactive because the water making them inactive sites can start to participate in the surface reactions.

Values of γ determined by George et al. (2010) and Loukhovitskaya et al. (2009) are significantly lower than the other values shown in Table 6.2. It is not clear why the values determined by George et al. are so low. The system used for their study was an aerosol flow tube experiment, with similar creation of HO_2 and aerosol as used in both this study and the study by Taketani et al.. A CC LIF instrument, similar to that used by Taketani et al., was used to detect HO_2 radicals and low initial concentrations of HO_2 (1×10^8 – 2×10^9 molecules cm^{-3}) were used. A journal publication by George et al. has yet to be published, which could give more details as to why the data disagrees with other values. Loukhovitskaya et al. (2009) used a low pressure coaxial flow tube for their experiments with the injector tube coated with NaCl salt. A mass spectrometer was used to detect the HO_2 radicals, either directly or by chemical conversion. High initial concentrations of HO_2 were created either by reactions including Cl atoms (Reactions R 6.1 and R 6.2) or F atoms (Reaction R 6.3). The Cl and F atoms were created by microwave discharge.

$$Cl + CH_3OH - \quad CH_2OH + HCl \tag{R 6.1}$$

$$CH_2OH + O_2 - \quad HO_2 + CH_2O \tag{R 6.2}$$

$$F + H_2O_2 - \quad HO_2 + HF \tag{R 6.3}$$

During experiments by Loukhovitskaya et al. the loss of HO_2 to salt was seen to continuously decrease with exposure time and did not reach a steady state even after three hours of exposure. This decrease in uptake rate was attributed to the deactivation of the salt sample by the intermediates formed during the formation of the HO_2 radicals (in particular HF, created in Reaction R 6.3). The low pressure system did not allow for the creation of HO_2 radicals by the photolysis of H_2O which involves a termolecular step, which would have been a purer source of radicals and caused less deactivation of the salt samples (as mentioned above H_2O at low concentrations also deactivates the salt samples). In order to determine values of γ for HO_2 uptake to salts Loukhovitskaya et al. (2009) used only the initial rate of uptake. The deactivation of the salt in this system

could account for the low values of uptake determined using this experimental set up.

Only one previous value of α for NaCl has been determined (Taketani et al., 2008). Taketani et al. determined a value for α nearly two orders of magnitude greater than the value of α determined in this study. As discussed previously, the value determined in this study may have actually been for uptake to dry aerosol, which could explain the difference between the value of α determined in this study and that determined by Taketani et al.

6.4.2 Ammonium Sulphate Aerosol

Table 6.3 gives a summary of γ for uptake to dry $(NH_4)_2SO_4$ particles determined in this and other studies.

Table 6.3: A summary of the $(NH_4)_2SO_4$ data obtained in this study, along with comparisons from other studies. In this study all aerosols were dry.

γ	RH / %	Method	Reference
0.047 ± 0.015	36	AFT PERCA	This study
0.04 ± 0.02	20	AFT CC LIF	Taketani et al. (2008)
0.05 ± 0.02	45	AFT CC LIF	Taketani et al. (2008)
0.011		EPR	Gershenzon et al. (1995)
< 0.002	15 – 60	CC FAGE	George et al. (2010)

The value of γ (0.047 ± 0.015) for HO_2 uptake to $(NH_4)_2SO_4$ particles is in agreement with other studies - values of γ determined by Taketani et al. (2008) agree well (0.04 – 0.05 ± 0.02), while the value determined by Gershenzon et al. (1995) is slightly lower. The lower value obtained by Gershenzon et al. could be due to the different experimental set-up used with respect to this study and the one by Taketani et al. This study and the study by Taketani et al. used an aerosol flow tube approach, while Gershenzon et al. used a solid film coaxial reactor rather than aerosol particles, which could explain some of the difference in the determined values. The value of γ determined recently by George et al. is one order of magnitude smaller than other values of uptake to $(NH_4)_2SO_4$. It is not clear what this difference is due to.

6.5 Implications for the atmosphere

The heterogeneous loss of HO_2 to aerosol particles has been shown to be an important sink for HO_2 in the troposphere (Jacob, 2000; Martin et al., 2003; Kolb et al., 2010; Macintyre and Evans, 2011). The loss of HO_2 radicals to aerosol particles affects the chemistry of HO_x species in the troposphere as discussed in detail in Chapter 1. A summary diagram (Figure 6.5) showing the main reactions of OH and HO_2 in the troposphere has been reproduced in this chapter for clarity. This thesis aimed to quantify the rate of loss of HO_2 to aerosol (reaction (2) in Figure 6.5) as the magnitude of γ directly affects the concentration of HO_2 in the troposphere. The loss of HO_2 to aerosol particles will reduce the total concentration of HO_2 in the troposphere and will therefore also reduce the total concentration of OH. The concentration of OH is an indicator of the oxidising capacity of the atmosphere - a reduction in OH means a reduction in the oxidising capacity.

At present the recommended value for use in models for uptake of HO_2, to any aerosol is 0.2 (Jacob, 2000). A recent modelling study by Macintyre and Evans (2011) uses a new parameterisation for uptake to HO_2, which takes into account relative humidity and temperature dependence determined in various laboratory studies for various aerosols. Macintyre and Evans (2011) determined the global mean for HO_2 uptake to aerosols as 0.028 - significantly lower than the current recommended value, but in agreement with recent laboratory values. The study described in this thesis determined uptake coefficients for dry sodium chloride and ammonium sulphate aerosols to be 0.021 $\pm$ 0.006 and 0.047 $\pm$ 0.015 respectively. This section describes the use of a zero dimensional model to investigate the implications to ambient tropospheric HO_x chemistry of the various values determined for HO_2 uptake to aerosol.

6.5.1 Model Initialisation

The model used during this investigation is a zero dimensional box model which used inorganic and organic reaction schemes from the Master Chemical Mechanism V. 3.1

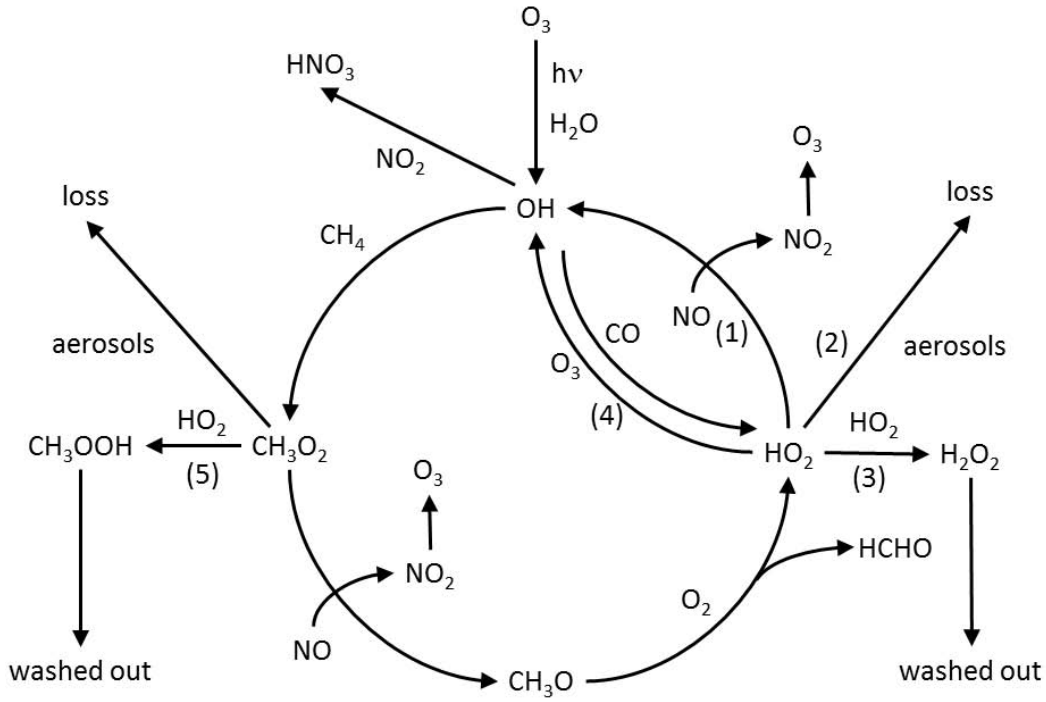

Figure 6.5: The main reactions of HO_x chemistry in the troposphere.

(Bloss et al., 2005a). The model is described in detail in the paper by Bloss et al. (2010). Initialisation conditions used for the model were for a marine boundary layer and assumed that the dominant aerosol was sea-spray (O'Dowd et al., 1997; Rinaldi et al., 2009). Solid NaCl will be present in a marine environment because sea-spray produces liquid droplets containing NaCl; winds then evaporate the liquid leaving the solid particle behind (Remorov et al., 2002), so the new uptake coefficient, $\gamma = 0.021$, for uptake to solid NaCl is pertinent for use in a marine boundary layer model. The model was initialised with concentrations of long lived chemicals and aerosol surface areas (shown in Table 6.4) obtained from observed measurements from the North Atlantic Marine Boundary Layer Experiment (NAMBLEX) campaign at Mace Head Atmospheric Research Station on the west coast of Ireland in 2002 (Heard et al., 2006; Fleming et al., 2006; Still et al., 2006; Coe et al., 2006; Smith et al., 2006).

The photolysis rates were calculated within the model with respect to the solar zenith

Table 6.4: Values used for initialising the model for a marine boundary layer based on observations during the NAMBLEX campaign in 2002. The average temperature throughout the campaign was 288 K and the average relative humidity was 85 %. The model was run in steps of 30 seconds from 6am to 6pm during a summer day.

Species	**Mixing Ratio**	**Reference**
CH_4	1800 ppb	Heard et al. (2006)
O_3	30 ppb	Heard et al. (2006)
NO_2	40 ppt	Heard et al. (2006)
CO	80 ppt	Heard et al. (2006)
NO	15 ppt	Heard et al. (2006)
CH_3CHO	0.5 ppb	Still et al. (2006)
HCHO	0.69 ppb	Still et al. (2006)
CH_3OH	1.16 ppb	Lewis et al. (2005)
DMS	150 ppt	Heard et al. (2006)
Total aerosol surface area	1.5×10^8 $nm^2\,cm^{-3}$	Coe et al. (2006)

angle which was dependent on the location (53.32 N, 9.90 W) and the time (the model was run from 06:00 - 18:00 for the 18th August 2002). It was assumed that there were clear sky conditions for the photolysis calculations. After initialisation all species within the model evolved freely as there were no external source terms (e.g. advection or mixing from the troposphere). Therefore the concentration of the precursor species gradually declined throughout the model run which limited the useful simulation duration to only a few hours. For HO_x species this time scale is satisfactory as their lifetime in the troposphere is a few seconds.

The model was run four times - with varying values for γ of HO_2 uptake to aerosols (Table 6.5).

Table 6.5: Values used for γ for HO_2 uptake to aerosols during the four runs of the model.

γ	Reference
0	N/A
0.021	This study
0.028	Macintyre and Evans (2011)
0.2	Jacob (2000)

6.5.2 Modelled Changes in the Concentration of OH and HO_2

The concentration of HO_2 was modelled over a daylight period using four different values for γ. The model results are shown in Figure 6.6.

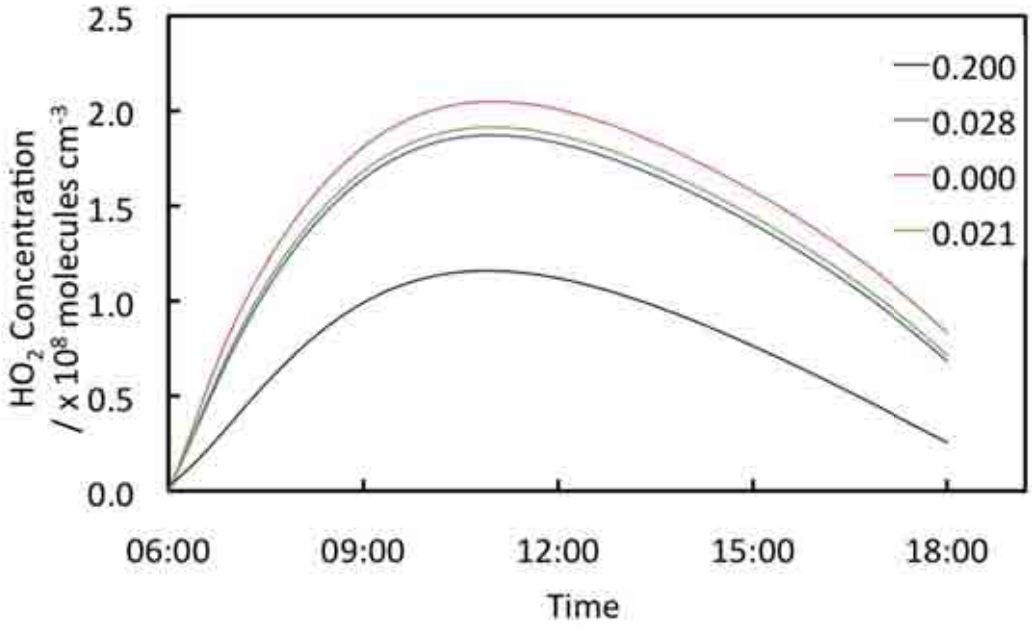

Figure 6.6: This modelled data shows how the concentration of HO_2 varies between 06:00 and 18:00 for four values of γ for HO_2.

The blue line in Figure 6.6 shows the HO_2 concentration when there was no loss of HO_2 to aerosol (i.e. $\gamma = 0$). The percentage decrease (with respect to no loss of HO_2 to aerosol) of the maximum HO_2 concentration for $\gamma = 0.021$, 0.028 and 0.2 is 7 %, 9 % and 43 % respectively. This shows that using the recommended value of $\gamma = 0.2$ in models will predict a HO_2 concentration 38 % lower than using the new $\gamma = 0.021$ value determined in this study (a similar reduction is seen when using the new parameterisation by Macintyre and Evans (2011)).

The concentration of HO_2 has a direct effect on the concentration of OH (see Figure 6.5), meaning that this concentration will also be affected by the changes in γ. The concentration of OH was been modelled for the four γ values, the results of which can be seen in Figure 6.7.

From a comparison between Figures 6.6 and 6.7 it can be seen that γ has a greater

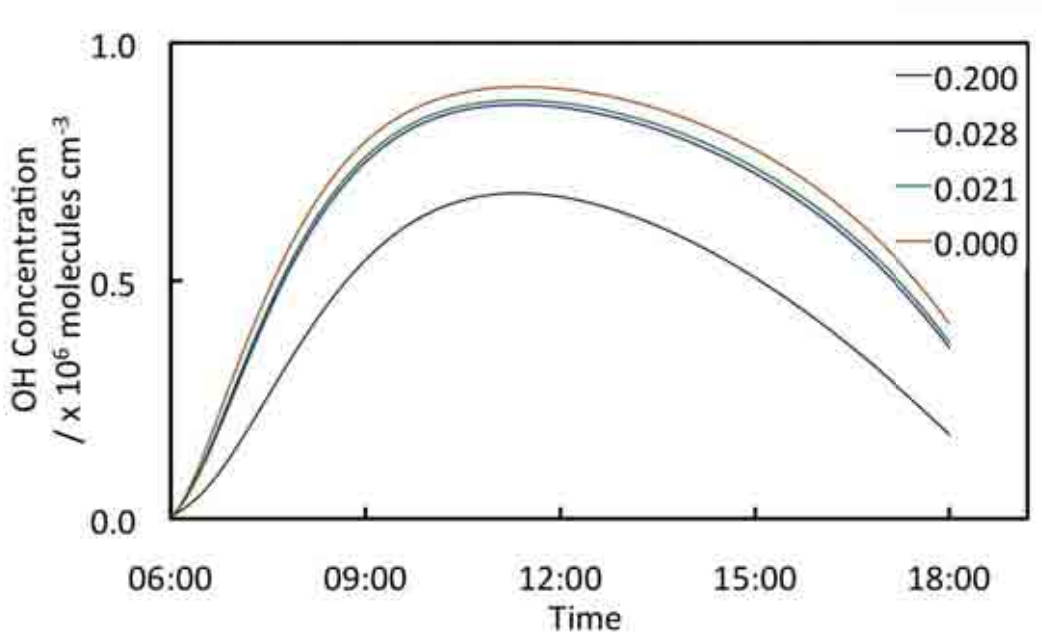

Figure 6.7: This modelled data shows how the concentration of OH varies between 06:00 and 18:00 for four values of γ for HO_2.

effect on HO_2 concentration that on OH concentration, as expected. The smaller effect on the OH concentration compared to the HO_2 concentration is due to the low level of NO_x used in these model runs. The low NO_x level means that the HO_x chemistry is NO_x limited, therefore conversion of HO_2 to OH via the $HO_2 + NO$ will be low. At higher NO_x levels the coupling between HO_2 and OH will be closer, resulting in an increased loss of OH due to aerosol loss. The percentage decrease (with respect to no loss of HO_2 to aerosol) of the maximum OH concentration for $\gamma = 0.021$, 0.028 and 0.2 is 2 %, 4 % and 25 %. Models using the recommended value of $\gamma = 0.2$ will under-predict the concentration of OH by 23 %, which could lead to further consequences within the model (e.g. the rate of loss of pollutants).

6.5.3 Modelled Changes in HO_2 Loss

There are five main net loss processes for HO_2 in the troposphere - by reaction of HO_2 with NO, aerosol particles, HO_2, O_3 and RO_2; these are labelled (1) to (5) in Figure 6.5. In the marine environment an extra loss of HO_2 is seen - the reaction with halogen oxides (e.g. IO

or BrO, Bloss et al. (2005c)). Throughout this modelling reactions of HO_2 with halogens have not been considered; this was because the interaction of HO_x and halogen species is complex and beyond the scope of this modelling, which concentrated on the relative loss of HO_2 to aerosols with respect to well understood HO_2 losses in the troposphere. It should be noted that loss of HO_2 to halogen species should be considered in more rigorous modelling scenarios, if it is atmospherically relevant to the chosen environment (e.g. a marine environment). The percentage loss of HO_2 due to each loss reaction ((1) to (5) as shown in Figure 6.5) is shown in Figure 6.8.

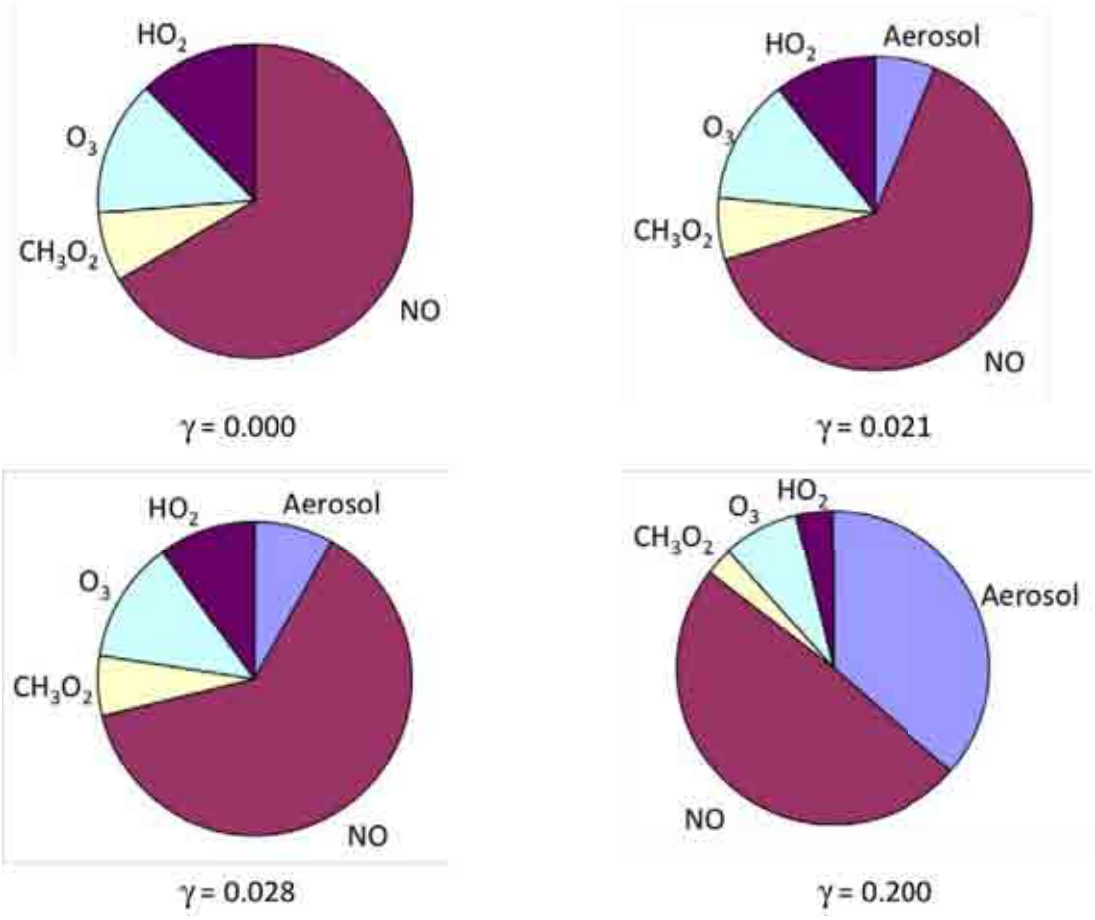

Figure 6.8: This modelled data shows the percentage loss of HO_2 due to its various loss processes in the troposphere. The fractional loss is shown for four values of γ: 0, 0.021, 0.028 and 0.2.

For all values of γ the largest loss of HO_2 was due to its reaction with NO. For $\gamma = 0.2$ the next largest loss of HO_2 is uptake to aerosol (35 %). For smaller values of γ (0.021 and 0.028) the second largest loss of HO_2 was its reaction with O_3 (both 14 %), with the loss

to aerosols being 5 % and 8 % respectively. These differences in the relative importance of the percentage of loss of HO_2 to aerosol shows the need to quantitatively understand this loss process.

6.5.4 Modelled Changes in Ozone Production

The model was initialised with an NO mixing ratio of 15 ppt. This mixing ratio of NO is high enough for the HO_x chemistry to be in the ozone production regime (see Chapter 1 for a full discussion). Ozone is produced via the conversion of NO into NO_2 and the subsequent photolysis of NO_2. Figure 6.5 shows that a reduction in HO_2 concentration (i.e. by loss to aerosol) could reduce the rate at which reaction (1) occurs and therefore reduce the amount of O_3 produced from that reaction. The rate of O_3 production was investigated rather than the absolute concentration of O_3 due to the limited duration of the modelled simulations, over which time a change in O_3 is not seen due to its long lifetime.

During the model runs the production of O_3 from the conversion of NO to NO_2 was recorded to investigate how the change in γ would affect the production of O_3. The production of O_3 was determined for $\gamma = 0$, 0.021, 0.028 and 0.2. The percentage decrease in O_3 production, with respect to the O_3 production determined for $\gamma = 0$, was calculated for $\gamma = 0.021$, 0.028 and 0.2, the result of which is shown in Figure 6.9.

It can be seen from Figure 6.9 that when $\gamma = 0.2$ there is a 25 % reduction in O_3 production, while when $\gamma = 0.028$ and 0.021 the percentage decrease in O_3 production is much less (4 % and 2 % respectively). The percentage decrease in the ozone production rate will be highly dependent upon the initial conditions in the model, particularly the NO_x mixing ratio, but the values illustrate the change in the O_3 production rate. The change in the O_3 production rate in the troposphere has global implications because O_3 is a greenhouse gas. Understanding the rate of O_3 production in the troposphere is key to predicting the radiative forcing of O_3.

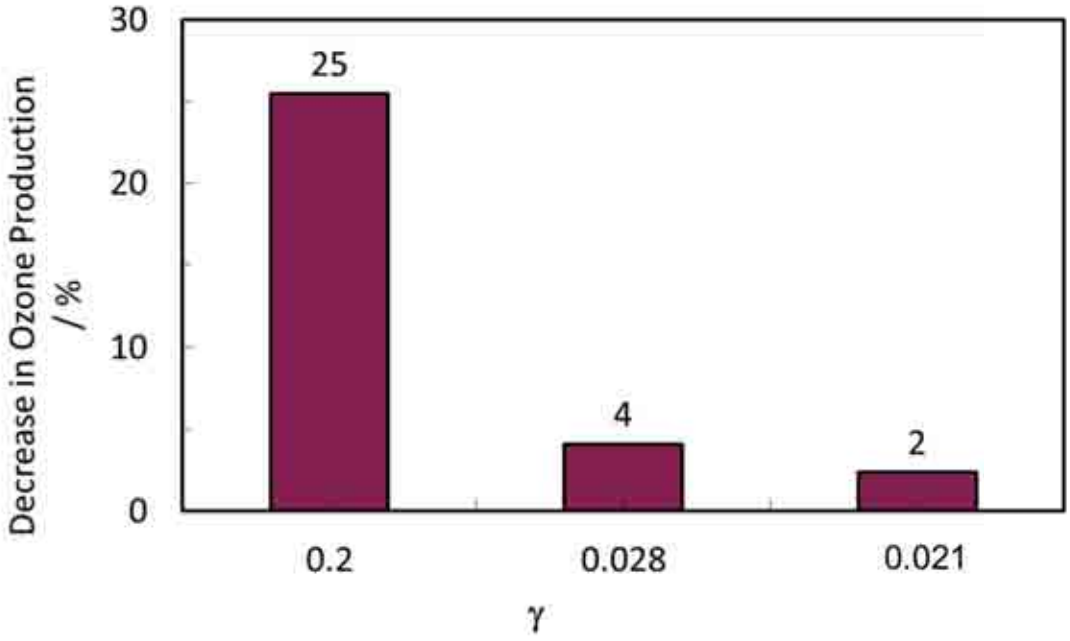

Figure 6.9: This modelled data shows the percentage loss of O_3 production by the conversion of NO to NO_2. The loss is compared to the ozone produced with $\gamma = 0$.

6.6 Summary

Values for HO_2 uptake to dry NaCl (0.021 $\pm$ 0.006) and $(NH_4)_2SO_4$ (0.047 $\pm$ 0.015) were determined and are in good agreement with values from other studies. A value of α determined for HO_2 to NaCl aerosol was also determined. However there is a large difference between the value determined in this study and the only other value of α (0.009 $\pm$ 0.002) for HO_2 to NaCl, determined by Taketani et al. (2008). The discrepancy could be that the particles used in this study were not actually aqueous particles, despite being suspended in a gas above the efflorescence relative humidity determined for these aerosols.

A box model was used in order to investigate changes in tropospheric HO_x chemistry due to the new γ values for NaCl with respect to the currently recommended value of γ for marine boundary layer conditions. The model was used to investigate the concentration of HO_2 and OH, the change in the percentage loss of HO_2 to its loss reactions and the change in the O_3 production within the troposphere. The model showed significant changes in HO_x tropospheric chemistry due to a change in the heterogeneous uptake coefficient.

CHAPTER 7

CONCLUSION

This thesis described the design, construction and characterisation of an aerosol flow tube system used to investigate the heterogeneous loss of HO_2 to aerosol. A PERCA was also developed to monitor the concentration of HO_2 within the AFT. The PERCA was calibrated using a chemical actinometer technique in order to determine the absolute concentration of peroxy radicals within the system. The AFT was used to determine new coefficients for the uptake of HO_2 to dry NaCl and $(NH_4)_2SO_4$ aerosol and the mass accommodation for NaCl aerosol.

The γ values determined in this system are in agreement with other studies (Gershenzon et al., 1995; Taketani et al., 2008). Only one other value for α had previously been determined for NaCl aerosol (Taketani et al., 2008) but does not agree with the value determined in this study. This disagreement could be due to issues producing aqueous aerosol during this study. Literature values for the efflorescence relative humidity values for the aerosol used in this study were lower than actual values measured during this study. α was determined in this system at 53 % relative humidity, which is only 3 % higher than the determined efflorescence relative humidity, leading to the possibility that the aerosol was already dry at this relative humidity.

Another issue with the aqueous aerosol experiments was the sensitivity of the PERCA at high relative humidity. The chain length of the PERCA dropped significantly once the relative humidity was above approximately 40 %, making measurements challenging

above this. To aid in these measurements the initial concentration of HO_2 within the AFT was increased by an order of magnitude to approximately 1×10^9 molecules cm^{-3}. Many experiments were therefore performed at concentrations one order of magnitude higher than ambient concentrations (1×10^8 molecules cm^{-3}). The increase from ambient concentrations meant that a new analysis was needed to account for the self-reaction of HO_2, which is significant at the concentrations used here.

A mixed order kinetic analysis was performed which accounted for both the loss of HO_2 due to its self reaction and due to its loss to the walls of the AFT and to aerosol. No other studies have accounted for the self-reaction of HO_2 in their analysis. Taketani et al. (2008) assumed that their initial concentrations of HO_2 were low enough to neglect the self reaction, which was consistent with their observed decays of HO_2 to the walls of the AFT being first order. The equivalent observed decays in this study also seemed to be first order, but calculations indicated that the self-reaction would be important at the concentrations used. Thornton and Abbatt (2005a) observed second order rate decays for non-aerosol loss. They approximated a first order decay to aid in the analysis of the data, but were careful to use data at the point in the HO_2 decay which fitted a first order decay well. The new analysis used in this data rigorously deals with the non-aerosol loss of HO_2 due to both the self-reaction and the loss to the AFT.

A box model was used to show the implications that the new measured values for γ have on tropospheric HO_x chemistry. The box model was set up for a clean marine environment, with the new γ determined for uptake onto dry NaCl used for the relevant uptake to aerosol. The model was also run with no loss of HO_2 to aerosol and with the currently recommended value γ of 0.2. Significant changes were seen in the concentration of HO_2 and OH and in the production of O_3 within the troposphere.

7.1 Further Work

The successful determination of γ for uptake to dry NaCl particles, in agreement with other studies, indicates that the new system is suitable for measurements of heterogeneous uptake coefficients. Further studies investigating wet NaCl aerosol should be performed in order to determine the mass accommodation coefficient. Once α has been determined γ should also be determined for wet NaCl aerosol. Only one experiment for dry $(NH_4)_2SO_4$ aerosol was performed during this study. Further work should be undertaken to determine the uptake to both wet and dry $(NH_4)_2SO_4$.

Other atmospherically relevant aerosols should also be investigated - for example sea water could be used to produce aerosol, which would give a direct representation of the main source of aerosol particles in the marine environment. Nitrates, sulphates and organics form the majority of urban aerosols (Allan et al., 2003), so solutions which could be atomised which would act as a proxy for these (e.g. ammonium nitrate), could be used to determine the uptake to urban aerosols.

When performing experiments with wet aerosol particles, care should be taken to ensure that the particles are actually aqueous. Experiments could be performed to determine the average size of the dry aerosol particle under investigation and the average size of the same wet aerosol particle. The average size of the particle during an *aerosol loss* experiment would then be indicative of the phase of the particle.

In order to make future measurements of uptake of HO_2 to wet aerosol, the sensitivity of the PERCA needs to be improved for relative humidities greater than 30 %. The chain length could be improved by repeating experiments used to find the optimum flows of nitrogen oxide and carbon monoxide used within the PERCA reaction chamber, at various relative humidities (see Section 3.6.3 for more details on these experiments). The optimum flows could change due to the relative humidity of the system, which is controlled during these laboratory experiments. It was also noted that the chain length improved when the PERCA reaction chamber was clean, so regular cleaning of this could improve the chain length of the instrument.

The system could be modified in order to control the temperature within the AFT. A new AFT could be made which incorporates a 'glass jacket' into the design. Fluid at a constant temperature could be pumped through this 'jacket' to ensure the AFT was kept at a constant temperature. Once the AFT had been modified in this way the temperature dependancy of uptake of HO_2 to aerosol could be investigated.

The product of HO_2 loss to aerosol should be investigated. The mechanism of uptake of HO_2 to aerosol is unknown at present, although suggestions have been made for possible reactions. Only one study (Loukhovitskaya et al., 2009) has, to date, investigated the product of these uptake reactions - they observed H_2O_2 to be a product. An instrument, such as a mass spectrometer, could be coupled to the aerosol flow tube in order to detect the chemical species produced during an *aerosol loss* experiment.

Finally the system could also be used to look at the loss of RO_2 radicals to aerosol, which is thought to happen in a similar way to the HO_2 radical loss. CH_3O_2 radicals, for example, could be made via the reaction of methane with OH in the injector tube (see Chapter 1 for reaction details). The PERCA can detect RO_2 radicals, so the same detection method could be used to investigate the uptake of these radicals.

REFERENCES

Allan, J. D., Alfarra, M. R., Bower, K. N., Williams, P. I., Gallagher, M. W., Jimenez, J. L., McDonald, A. G., Nemitz, E., Canagaratna, M. R., Jayne, J. T., Coe, H., and Worsnop, D. R. (2003). Quantitative Sampling Using an Aerodyne Aerosol Mass Spectrometer 2. Measurements of Fine Particulate Chemical Composition in Two U.K. Cities. *Journal of Geophysical Research*, 108(D3):4091.

Arias, M. C. and Hastie, D. R. (1996). Radical Chemistry at the SONTOS Site in Rural Ontario. *Atmospheric Environment*, 30(12):2167–2175.

Atkins, P. W. and de Paula, J. (2006). *Atkins' Physical Chemistry*. 7th edition.

Atkinson, R., Baulch, D. L., Cox, R. A., Crowley, J. N., Hampson, R. F., Hynes, R. G., Jenkin, M. E., and Rossi, M. J. (2004). Evaluated Kinetic and Photochemical Data for Atmospheric Chemistry : Volume I - Gas Phase Reactions of O_x, HO_x, NO_x and SO_x species. *Atmospheric Chemistry and Physics*, 4:1461–1738.

Badger, C. L., Griffiths, P. T., George, I., Abbatt, J. P. D., and Cox, R. A. (2006). Reactive Uptake of N_2O_5 by Aerosol Particles Containing Mixtures of Humic Acid and Ammonium Sulfate. *The Journal of Physical Chemistry A*, 110(21):6986–94.

Baron, P. A. and Willeke, K., editors (2001). *Aerosol Measurement: Principles, Techniques and Applications*. John Wiley & Sons Inc., 2nd edition.

Bird, R. B., Stewart, W. E., and Lightfoot, E. N. (2002). *Transport Phenomena*. John Wiley & Sons Inc.

Bloss, C., Wagner, V., Jenkin, M. E., Volkamer, R., Bloss, W. J., Lee, J. D., Heard, D. E., Wirtz, K., Martin-Reviejo, M., Rea, G., Wenger, J. C., and Pilling, M. J. (2005a). Development of a Detailed Chemical Mechanism (MCMv3.1) for the Atmospheric Oxidation of Aromatic Hydrocarbons. *Atmospheric Chemistry and Physics*, 5(3):641–664.

Bloss, W. J., Camredon, M., Lee, J. D., Heard, D. E., Plane, J. M. C., Saiz-Lopez, A., Bauguitte, S. J.-B., Salmon, R. A., and Jones, A. E. (2010). Coupling of HO_x, NO_x and Halogen Chemistry in the Antarctic Boundary Layer. *Atmospheric Chemistry and Physics*, 10(21):10187–10209.

Bloss, W. J., Evans, M. J., Lee, J. D., Sommariva, R., Heard, D. E., and Pilling, M. J. (2005b). The Oxidative Capacity of the Troposphere: Coupling of Field Measurements of OH and a Global Chemistry Transport Model. *Faraday Discussions*, 130:425.

Bloss, W. J., Lee, J. D., Bloss, C., Heard, D. E., Pilling, M. J., Wirtz, K., Martin-Reviejo, M., and Siese, M. (2004). Validation of the Calibration of a Laser-Induced Fluorescence Instrument for the Measurement of OH Radicals in the Atmosphere. *Atmospheric Chemistry and Physics*, 4(2):571–583.

Bloss, W. J., Lee, J. D., Johnson, G. P., Sommariva, R., Heard, D. E., Saiz-Lopez, A., Plane, J. M. C., McFiggans, G., Coe, H., Flynn, M., Williams, P., Rickard, A. R., and Fleming, Z. L. (2005c). Impact of halogen monoxide chemistry upon boundary layer OH and HO_2 concentrations at a coastal site. *Geophysical Research Letters*, 32(6):3–6.

Brown, R. L. (1978). Tubular Flow Reactors with First-Order Kinetics. *Journal of Research of the National Bureau of Standards*, 83(1):1 – 9.

Cantrell, C., Zimmer, A., and Tyndall, G. (1997). Absorption Cross Sections for Water Vapor from 183 nm to 193 nm. *Geophysical Research Letters*, 24(17):2195–2198.

Cantrell, C. A., Shetter, R. E., and Calvert, J. C. (1996). Dual-Inlet Chemical Amplifier for Atmospheric Peroxy Radical Measurements. *Analytical Chemistry*, 68:4194–4199.

Cantrell, C. A. and Stedman, D. H. (1982). A Possible Technique for the Measurement of Atmospheric Peroxy Radicals. *Geophysical Research Letters*, 9(8):846–849.

Cantrell, C. A., Stedman, D. H., and Wendel, G. J. (1984). Measurement of Atmospheric Peroxy Radicals by Chemical Amplification. *Analytical Chemistry*, 56:1496–1502.

Carslaw, N., Creasey, D. J., Heard, D. E., Jacobs, D. J., Lee, J. D., Lewis, A. C., McQuaid, J. B., Pilling, M. J., Bauguitte, S., Penkett, S. A., Monks, P., and Salisbury, G. (2002). Eastern Atlantic Spring Experiment 1997 (EASE97) 2. Comparisons of Model Concentrations of OH, HO_2, and RO_2 with Measurements. *Journal of Geophysical Research*, 107(D14):1–16.

Clemitshaw, K. C., Carpenter, L. J., Penkett, S. A., and Jenkin, M. E. (1997). A Calibrated Peroxy Radical Chemical Amplifier for Ground-Based Tropospheric Measurements. *Journal of Geophysical Research*, 102:25405 – 25416.

Coe, H., Allan, J. D., Alfarra, M. R., Bower, K. N., Flynn, M. J., McFiggans, G. B., Topping, D. O., Williams, P. I., O'Dowd, C. D., Dall'Osto, M., Beddows, D. C. S., and Harrison, R. M. (2006). Chemical and Physical Characteristics of Aerosol Particles at a Remote Coastal Location, Mace Head, Ireland, during NAMBLEX. *Atmospheric Chemistry and Physics*, 6(11):3289–3301.

Cohen, M. D., Flagan, R. C., and Seinfeld, J. H. (1987a). Studies of Concentrated Electrolyte Solutions Using the Electrodynamic Balance. 1. Water Activities for Single-Electrolyte Solutions. *Journal of Physical Chemistry*, 91:4563 – 4574.

Cohen, M. D., Flagan, R. C., and Seinfeld, J. H. (1987b). Studies of Concentrated Electrolyte Solutions Using the Electrodynamic Balance. 3. Solute Nucleation. *Journal of Physical Chemistry*, 91(17):4583–4590.

Cooper, P. L. and Abbatt, J. P. D. (1996). Heterogeneous Interactions of OH and HO_2 Radicals with Surfaces Characteristic of Atmospheric Particulate Matter. *Journal of Physical Chemistry*, 100:2249–2254.

Cox, R. A. and Burrows, J. P. (1979). Kinetics and Mechanism of the Disproportionation of HO_2 in the Gas Phase. *Journal of Physical Chemistry A*, 83(20):2560–2568.

Creasey, D. J., Halford-Maw, P. A., Heard, D. E., Pilling, M. J., and Whitaker, B. J. (1997). Implementation and Initial Deployment of a Field Instrument for Measurement of OH and HO_2 in the Troposphere by Laser-Induced Fluorescence. *Journal of the Chemical Society, Faraday Transactions*, 93(16):2907–2913.

Creasey, D. J., Heard, D. E., and Lee, J. D. (2000). Absorption Cross-section Measurements of Water Vapour and Oxygen at 185 nm. Implications for the Calibration of Field Instruments to Measure OH, HO_2 and RO_2 Radicals. *Geophysical Research Letters*, 27:1651–1654.

Crowley, J. N., Ammann, M., Cox, R. A., Hynes, R. G., Jenkin, M. E., Mellouki, A., Rossi, M. J., Troe, J., and Wallington, T. J. (2010). Evaluated Kinetic and Photochemical Data for Atmospheric Chemistry: Volume V - Heterogeneous Reactions on Solid Substrates. *Atmospheric Chemistry and Physics*, 10(18):9059–9223.

Cziczo, D. J. and Abbatt, J. P. D. (2000). Infrared Observations of the Response of NaCl, $MgCl_2$, NH_4HSO_4 and NH_4NO_3 Aerosols to Changes in Relative Humidity from 298 to 238 K. *Journal of Physical Chemistry*, 104:2038–2047.

Cziczo, D. J., Nowak, J. B., Hu, J. H., and Abbatt, J. P. D. (1997). Infrared Spectroscopy of Model Tropospheric Aerosols as a Function of Relative Humidity: Observation of Deliquescence and Crystallisation. *Journal of Geophysical Research*, 102(D15):18843–18850.

Davies, J. A. and Cox, R. A. (1998). Kinetics of the Heterogeneous Reaction of HNO_3 with NaCl: Effect of Water Vapor. *The Journal of Physical Chemistry A*, 102(39):7631–7642.

Dougle, P. G., Veefkind, J., and ten Brink, H. M. (1998). Crystallisation of Mixtures of Ammonium Nitrate, Ammonium Sulphate and Soot. *Journal of Aerosol Science*, 29(3):375–386.

Faloona, I. C., Tan, D., Lesher, R. L., Hazen, N. L., Frame, C. L., Simpas, J. B., Harder, H., Martinez, M., Di Carlo, P., Ren, X., and Brune, W. H. (2004). A Laser-induced Fluorescence Instrument for Detecting Tropospheric OH and HO_2: Characteristics and Calibration. *Journal of Atmospheric Chemistry*, 47(2):139–167.

Finlayson-Pitts, B. J. and Pitts, J. N. (2000). *Chemistry of the Upper and Lower Atmosphere*. Academic Press.

Fleming, Z. L., Monks, P. S., Rickard, A. R., Heard, D. E., Bloss, W. J., Seakins, P. W., Still, T. J., Sommariva, R., Pilling, M. J., Morgan, R., Green, T. J., Brough, N., Mills, G. P., Penkett, S. A., Lewis, A. C., Lee, J. D., Saiz-Lopez, A., and Plane, J. M. C. (2006). Peroxy Radical Chemistry and the Control of Ozone Photochemistry at Mace Head, Ireland During the Summer of 2002. *Atmospheric Chemistry and Physics*, 6(8):2193–2214.

Forster, P., Ramaswamy, V., Artaxo, P., Bertsen, T., Betts, R., Fahey, D., Haywood, J., Lean, J., Lowe, D., Myhre, G., Nganga, J., Prinn, R., Raga, G., Schulz, M., and Van Dorland, R. (2007). Changes in atmospheric constituents and in radiative forcing. In Solomon, S., Qin, D., Manning, M., Chen, Z., Maquis, M., Averyt, K. B., Tignor, M., and Miller, H., editors, *Climate Change 2007: The Physical Science Basis. Contribution of Working Group 1 to the Fourth Assessment Report of the Intergovermental Panal on Climate Change*. Cambridge University Press, Cambridge UK & New York USA.

Fried, A., Henry, B. E., and Calvert, J. G. (1994). The Reaction Probability of N_2O_5 With Sulfuric Acid Aerosols at Stratospheric Temperatures and Compositions. *Journal of Geophysical Research*, 99:3517–3532.

Fuchs, N. and Sutugin, A. (1970). *Highly Dispersed Aerosols*. Ann Arbor Science Publishers Ltd., London.

Fuchs, N. a. (1963). On the Stationary Charge Distribution of Aerosol Particles in a Bipolar Ionic Atmosphere. *Geofisica Pura e Applicata*, 92(1):144–193.

George, I., Whalley, L., Matthews, P., Brooks, B., Goddard, A., Baeza-Romero, M. T., and Heard, D. (2010). Heterogeneous Uptake of HO_2 Radicals onto Atmospheric Aerosols. In *2010 Fall Meeting, AGU, San Franciso, California: 13-17th December 2010*.

Gershenzon, Y. M., Grigorieva, V. M., Ivanov, A. V., and Remorov, R. G. (1995). O_3 and OH Sensitivity to Heterogeneous Sinks of HO_x and CH_3O_2 on Aerosol Particles. *Faraday Discussions*, 100:83–100.

Green, T. J., Reeves, C. E., Brough, N., Edwards, G. D., Monks, P. S., and Penkett, S. A. (2003). Airborne Measurements of Peroxy Radicals Using the PERCA Technique. *Journal of Environmental Monitoring*, 83(1):75–83.

Green, T. J., Reeves, C. E., Fleming, Z. L., Brough, N., Rickard, A. R., Bandy, B. J., Monks, P. S., and Penkett, S. A. (2006). An Improved Dual Channel PERCA Instrument for Atmospheric Measurements of Peroxy Radicals. *Journal of Environmental Monitoring*, 8(5):530–6.

Han, J.-h. and Martin, S. T. (1999). Heterogeneous Nucleation of the Efflorescence of $(NH_4)_2SO_4$ Particles Internally Mixed with Al_2O_3, TiO_2 and ZrO_2. *Journal of Geophysical Research*, 104:3543–3553.

Hanke, M., Uecker, J., Reiner, T., and Arnold, F. (2002). Atmospheric Peroxy Radicals: ROXMAS, a New Mass-Spectrometric Methodology for Speciated Measurements of HO_2 and ΣRO_2 and First Results. *International Journal of Mass Spectrometry*, 213(2-3):91–99.

Hanson, D. R. and Ravishankara, A. E. L. (1991). The Reaction Probabilities of $ClONO_2$ and N_2O_5 on 40 to 75 % Sulfuric Acid Solutions. *Journal of Geophysical Research*, 96:17307 – 17314.

Hastie, D. R., Weissemayer, M., Burrows, J. P., and Harris, G. W. (1991). Cali-

brated Chemical Amplifier for Atmospheric RO_x Measurements. *Analytical Chemistry*, 63(18):2048–2057.

Heard, D. E. and Pilling, M. J. (2003). Measurement of OH and HO_2 in the Troposphere. *Chemical Reviews*, 103:5163–98.

Heard, D. E., Read, K. a., Methven, J., Al-Haider, S., Bloss, W. J., Johnson, G. P., Pilling, M. J., Seakins, P. W., Smith, S. C., Sommariva, R., Stanton, J. C., Still, T. J., Ingham, T., Brooks, B., De Leeuw, G., Jackson, a. V., McQuaid, J. B., Morgan, R., Smith, M. H., Carpenter, L. J., Carslaw, N., Hamilton, J., Hopkins, J. R., Lee, J. D., Lewis, a. C., Purvis, R. M., Wevill, D. J., Brough, N., Green, T., Mills, G., Penkett, S. a., Plane, J. M. C., Saiz-Lopez, A., Worton, D., Monks, P. S., Fleming, Z., Rickard, a. R., Alfarra, M. R., Allan, J. D., Bower, K., Coe, H., Cubison, M., Flynn, M., McFiggans, G., Gallagher, M., Norton, E. G., O'Dowd, C. D., Shillito, J., Topping, D., Vaughan, G., Williams, P., Bitter, M., Ball, S. M., Jones, R. L., Povey, I. M., O'Doherty, S., Simmonds, P. G., Allen, A., Kinnersley, R. P., Beddows, D. C. S., Dall'Osto, M., Harrison, R. M., Donovan, R. J., Heal, M. R., Jennings, S. G., Noone, C., and Spain, G. (2006). The North Atlantic Marine Boundary Layer Experiment (NAMBLEX). Overview of the Campaign Held at Mace Head, Ireland, in Summer 2002. *Atmospheric Chemistry and Physics*, 6(8):2241–2272.

Hinds, W. C. (1999). *Aerosol Technology: Properties, Behaviour and Measurement of Airborne Particles*. John Wiley & Sons Inc., 2nd edition.

Hofzumahaus, A., Brauers, T., Aschmutat, U., Brandenburger, U., Dorn, H.-P., Hausmann, M., Hessling, M., Holland, F., Plass-Dulmer, C., Sedlacck, M., Weber, M., and Ehhalt, D. (1997). Reply. *Geophysical Research Letters*, 24:2039–3040.

Howard, C. J. (1979). Kinetic Measurements Using Flow Tubes. *The Journal of Physical Chemistry*, 83(1):3–9.

Jacob, D. (2000). Heterogeneous Chemistry and Tropospheric Ozone. *Atmospheric Environment*, 34(12-14):2131–2159.

Jacob, D. J. (1999). Oxidizing Power of the Troposphere. In *Introduction to Atmospheric Chemistry*. Princeton University Press, Princeton, New Jersey.

Jenkin, M. E. and Clemitshaw, K. C. (2000). Ozone and Other Secondary Photochemical Pollutants: Chemical Processes Governing their Formation in the Planetary Boundary Layer. *Atmospheric Environment*, 34(16):2499–2527.

Kanaya, Y., Cao, R., Kato, S., Miyakawa, Y., Kajii, Y., Tanimoto, H., Yokouchi, Y., Mochida, M., Kawamura, K., and Akimoto, H. (2007). Chemistry of OH and HO_2 Radicals Observed at Rishiri Island, Japan, in September 2003: Missing Daytime Sink of HO_2 and Positive Nighttime Correlations with Monoterpenes. *Journal of Geophysical Research*, 112(D11):1–17.

Kanaya, Y., Sadanaga, Y., Hirokawa, J. U. N., Kajii, Y., and Akimoto, H. (2001). Development of a Ground-Based LIF Instrument for Measuring HO_x Radicals: Instrumentation and Calibrations. *Journal of Atmospheric Chemistry*, pages 73–110.

Kaye, G. W. C. and Laby, T. H. (1986). *Tables of Physical and Chemical Constants*. Longman Group Limited, 15 edition.

Keyser, L. F. (1984). High-Pressure Flow Kinetics. A Study of the OH + HCl Reaction from 2 to 100 Torr. *Journal of Physical Chemistry*, pages 4750–4758.

Kircher, C. C. and Sander, S. P. (1984). Kinetics and Mechanism of HO_2 and DO_2 Disproportionations. *Journal of Physical Chemistry*, 33(1979):2082–2091.

Kolb, C. E. (2002). Iodine's Air of Importance. *Nature*, 417(6889):597–8.

Kolb, C. E., Cox, R. A., Abbatt, J. P. D., Ammann, M., Davis, E. J., Donaldson, D. J., Garrett, B. C., George, C., Griffiths, P. T., Hanson, D. R., Kulmala, M., McFiggans, G., Poschl, U., Riipinen, I., Rossi, M. J., Rudich, Y., Wagner, P. E., Winkler, P. M.,

Worsnop, D. R., and O'Dowd, C. D. (2010). An Overview of Current Issues in the Uptake of Atmospheric Trace Gases by Aerosols and Clouds. *Atmospheric Chemistry and Physics*, pages 10561–10605.

Lanzendorf, E. J., F., H. T., Donahue, N. M., and Wennberg, P. O. (1997). Comment on: "The Measurement of Tropospheric OH Radicals by Laser-Induced Fluorescence Spectroscopy During the POPCORN Field Campaign" by Hofzumahaus et al. and "Inter-comparison of Tropospheric OH Radical Measurements by Multiple Folded Long-Path Laser Absorption and Laser Induced Fluorescence" by Brauers et al. *Geophysical Research Letters*, pages 3037–3038.

Lewis, A. C., Hopkins, J. R., Carpenter, L. J., Stanton, J., Read, K. a., and Pilling, M. J. (2005). Sources and Sinks of Acetone, Methanol, and Acetaldehyde in North Atlantic Marine Air. *Atmospheric Chemistry and Physics*, 5(7):1963–1974.

Lii, R.-R., Sauer, M. C., and Gordon, S. (1981). Temperature Dependence of the Gas-Phase Self-Reaction of HO_2 in the Presence of H_2O. *Journal of Physical Chemistry*, 85:2833–2834.

Loukhovitskaya, E., Bedjanian, Y., Morozov, I., and Le Bras, G. (2009). Laboratory Study of the Interaction of HO_2 with NaCl, NaBr, $MgCl_2 \cdot 6\,H_2O$ and Sea Salt Surfaces. *Physical chemistry chemical physics : PCCP*, 11:7896–7905.

Lovejoy, E. R. and Hanson, D. R. (1995). Measurement of the Kinetics of Reactive Uptake by Submicron Sulfuric Acid Particles. *The Journal of Physical Chemistry*, 99(7):2080–2087.

Macintyre, H. L. and Evans, M. J. (2011). Parameterisation and Impact of Aerosol Uptake of HO_2 on a Global Tropospheric Model. *Atmospheric Chemistry and Physics Discussions*, 11(6):16311–16334.

Mao, J., Jacob, D. J., Evans, M. J., Olson, J. R., Ren, X., Brune, W. H., Clair, J. M. S., Crounse, J. D., Spencer, K. M., Beaver, M. R., Wennberg, P. O., Cubison,

M. J., Jimenez, J. L., Fried, a., Weibring, P., Walega, J. G., Hall, S. R., Weinheimer, a. J., Cohen, R. C., Chen, G., Crawford, J. H., McNaughton, C., Clarke, a. D., Jaeglé, L., Fisher, J. a., Yantosca, R. M., Le Sager, P., and Carouge, C. (2010). Chemistry of Hydrogen Oxide Radicals HO_x in the Arctic Troposphere in Spring. *Atmospheric Chemistry and Physics*, 10(13):5823–5838.

Martin, R. V., Jacob, D. J., Yantosca, R. M., Chin, M., and Ginoux, P. (2003). Global and Regional Decreases in Tropospheric Oxidants from Photochemical Effects of Aerosols. *Journal of Geophysical Research*, 108(D3).

Martin, S. T. (2000). Phase Transitions of Aqueous Atmospheric Particles. *Chemical Reviews*, 100(9):3403–3454.

McMurry, P. H., Takano, H., and Anderson, G. R. (1983). Study of the Ammonia (Gas) - Sulfuric Acid (Aerosol) Reaction Rate. *Environmental Science & Technology*, 17(6):347–352.

Mihelcic, D., Volzthomas, A., Patz, H., and Kley, D. (1990). Numerical-Analysis of ESR-Spectra from Atmospheric Samples. *Journal of Atmospheric Chemistry*, 11(3):271–297.

Mihele, C. M. (1999). Radical Loss in a Chain Reaction of CO and NO in the Presence of Water: Implications for the Radical Amplifier and Atmospheric Chemistry. *International Journal of Chemical Kinetics*, 47(2):524–152.

Moore, J., Davis, C., and Coplan, M. (2003). *Building Scientific Apparatus*. Westview Press, 3rd edition.

Mozurkewich, M., McMurry, P. H., Gupta, A., and Calvert, J. G. (1987). Mass Accommodation Coefficient for HO_2 Radicals on Aqueous Particles. *Journal of Geophysical Research*, 92(7):4163–4170.

Newman, L. (1993). *Measurement Challenges in Atmospheric Chemistry*. Washington, D. C.: American Chemical Society.

NIST (2011). NIST Chemistry Web Book.

O'Dowd, C. D., Smith, M. H., Consterdine, I. E., and Lowe, J. A. (1997). Marine Aerosol, Sea-Salt, and the Marine Sulphur Cycle: A Short Review. *Atmospheric Environment*, 31(1):73–80.

Parrish, D. D., Trainer, M., Williams, E. J., Fahey, D. W., Hubler, G., Eubank, C., Liu, S. C., Murphy, P. C., Albritton, D. L., and Fehsenfeld, F. C. (1986). Measurements of the NO_x-O_3 Photostationary State at Niwot Ridge, Colorado. *Journal of Geophysical Research*, 91(5):5361–5370.

Pilling, M. and Smith, I. (1987). *Modern Gas Kinetics: Theory, Experiment and Application*. Oxford: Blackwell Scientific.

Reichert, L., Andres Hernandez, M. D., Stobener, D., Burkert, J., and Burrows, J. P. (2003). Investigation of the Effect of Water Complexes in the Determination of Peroxy Radical Ambient Concentrations: Implications for the Atmosphere. *Journal of Geophysical Research*, 108:4017.

Remorov, R. G., Gershenzon, Y. M., Molina, L. T., and Molina, M. J. (2002). Kinetics and Mechanism of HO_2 Uptake on Solid NaCl. *Journal of Physical Chemistry*, 2:4558–4565.

Richardson, C. B. and Snyder, T. D. (1994). A Study of Heterogeneous Nucleation in Aqueous Solutions. *Langmuir*, 10(7):2462–2465.

Rinaldi, M., Facchini, M. C., Decesari, S., Carbone, C., Finessi, E., Mircea, M., Fuzzi, S., Ceburnis, D., Ehn, M., Kulmala, M., de Leeuw, G., and O'Dowd, C. D. (2009). On the Representativeness of Coastal Aerosol Studies to Open Ocean Studies: Mace Head - A Case Study. *Atmospheric Chemistry and Physics*, 9(24):9635–9646.

Salisbury, G., Monks, P. S., Bauguitte, S., Bandy, B. J., and Penkett, S. A. (2002). A Seasonal Comparison of the Ozone Photochemistry in Clean and Polluted Air Masses at Mace Head, Ireland. *Journal of Atmospheric Chemistry*, 41:163–187.

Sander, S. P., Friedl, R. R., Golden, D. M., Kurylo, M. J., Moortgat, G. K., Wine, P. H., Ravishankara, A. R., Kolb, C. E., Molina, M. J., Diego, S., Jolla, L., Huie, R. E., and Orkin, V. L. (2006). Chemical Kinetics and Photochemical Data for Use in Atmospheric Studies Evaluation Number 15. *Cross Sections*, (15).

Schultz, M., Heitlinger, M., Mihelcic, D., and Volz-thomas, A. (1995). Calibration Source for Peroxy Radicals with Built-in Actinometry Using H_2O and O_2 Photolysis at 185 nm. *Journal of Geophysical Research*, 100(95):18811 – 18816.

Scintrex (1987). LMA-3 Luminox Operation Manual. Technical report.

Seinfeld, J. H. and Pandis, S. N. (1998). *Atmospheric Chemistry and Physics: From Air Pollution to Climate Change*. John Wiley & Sons Inc.

Sillman, S. (1999). The Relation Between Ozone, NOx and Hydrocarbons in Urban and Polluted Rural Environments. *Atmospheric Environment*, 33(12):1821–1845.

Smith, S. C., Lee, J. D., Bloss, W. J., Johnson, G. P., Ingham, T., and Heard, D. E. (2006). Concentrations of OH and HO_2 Radicals During NAMBLEX: Measurements and Steady State Analysis. *Atmospheric Chemistry and Physics*, pages 1435–1453.

Sommariva, R., Bloss, W. J., Brough, N., Carslaw, N., Flynn, M., Haggerstone, A., Heard, D. E., and Hopkins, J. R. (2006). OH and HO_2 Chemistry During NAMBLEX: Roles of Oxygenates, Halogen Oxides and Heterogeneous Uptake. *Atmospheric Chemistry and Physics*, pages 1135–1153.

Stedman, J. (2004). The Predicted Number of Air Pollution Related Deaths in the UK During the August 2003 Heatwave. *Atmospheric Environment*, 38(8):1087–1090.

Still, T. J., Al-Haider, S., Seakins, P. W., Sommariva, R., Stanton, J. C., Mills, G., and Penkett, S. A. (2006). Ambient formaldehyde measurements made at a remote marine boundary layer site during the NAMBLEX campaign a comparison of data

from chromatographic and modified Hantzsch techniques. *Atmospheric Chemistry and Physics*, 6(9):2711–2726.

Taketani, F., Kanaya, Y., and Akimoto, H. (2008). Kinetics of Heterogeneous Reactions of HO_2 Radical at Ambient Concentration Levels with $(NH_4)_2SO_4$ and NaCl Aerosol Particles. *Journal of Physical Chemistry*, 112:2370–2377.

Tang, I. N. (1980). *Generation of Aerosols and Facilities for Exposure Experiments*. Ann Arbor Science Publishers Ltd.

Thermo (2007). Model 42i: Instruction Manual. Technical report.

Thornton, J. and Abbatt, J. P. D. (2005a). Measurements of HO_2 Uptake to Aqueous Aerosol: Mass Accommodation Coefficients and Net Reactive Loss. *Journal of Geophysical Research*, 110(D8):1–12.

Thornton, J. and Abbatt, J. P. D. (2005b). N_2O_5 Reaction on Submicron Sea Salt Aerosol: Kinetics, Products, and the Effect of Surface Active Organics. *The Journal of Physical Chemistry A*, 109(44):10004–12.

Thornton, J., Jaeglé, L., and McNeill, V. F. (2008). Assessing Known Pathways for HO_2 Loss in Aqueous Atmospheric Aerosols: Regional and Global Impacts on Tropospheric Oxidants. *Journal of Geophysical Research*, 113(D5):1–15.

TSI (2008a). Model 3076: Constant Output Atomizer. Technical report.

TSI (2008b). Model 3936, Scanning Mobility Particle Sizer Spectrometer. Technical report.

Washida, N., Mori, Y., and Tanaka, I. (1971). Quantum Yield of Ozone Formation from Photolysis of the Oxygen Molecule at 1849 and 1931 Å. *The Journal of Chemical Physics*, 54:1119 – 1122.

Wayne, R. P. (2002). *Chemistry of Atmospheres*. Oxford University Press, 3rd edition.

Weis, D. D. and Ewing, G. E. (1999). Water Content and Morphology of Sodium Chloride Aerosol Particles. *Journal of Geophysical Research*, 104:275–285.

Wiedensohler, A. (1988). An Approximation of the Bipolar Charge Distribution for Particles in the Submicron Size Range. *Journal of Aerosol Science*, 19(3):387–389.

Wiedensohler, A., Lutkemeier, E., Feldpausch, M., and Helsper, C. (1986). Investigation of the Bipolar Charge Distribution at Various Gas Conditions. *Journal of Aerosol Science*, 17(3):413–416.